NATURAL RESOURCES

# Geologic Map and Interpreted Geologic History of the Bow and Alger 7.5-minute Quadrangles, Western Skagit County, Washington

by Joe D. Dragovich,
David K. Norman,
Carly L. Grisamer,
Robert L. Logan,
and Garth Anderson

*Geochronology analysts*
*S. A. Bowring, K. Davidek, C. D. Blome, and K. M. Reed*

*Geochemical analysts*
*C. M. Knaack and D. M. Johnson*

WASHINGTON
DIVISION OF GEOLOGY
AND EARTH RESOURCES

Open File Report 98-5
September 1998

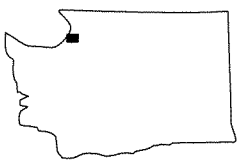

Location of quadrangles

WASHINGTON STATE DEPARTMENT OF
**Natural Resources**
**Jennifer M. Belcher** - Commissioner of Public Lands

# Geologic Map and Interpreted Geologic History of the Bow and Alger 7.5-minute Quadrangles, Western Skagit County, Washington

by Joe D. Dragovich,
David K. Norman,
Carly L. Grisamer,
Robert L. Logan,
and Garth Anderson

WASHINGTON
DIVISION OF GEOLOGY
AND EARTH RESOURCES

Open File Report 98-5
September 1998

*Produced in cooperation with the U.S. Geological Survey*
*National Cooperative Geologic Mapping Program*
*Agreement Number 1434-HQ-97-AG-01809*

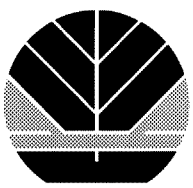

WASHINGTON STATE DEPARTMENT OF
**Natural Resources**
**Jennifer M. Belcher** - Commissioner of Public Lands

# Contents



## APPENDICES



## ILLUSTRATIONS

**PLATES** *(accompany text)*

# Geologic Map and Interpreted Geologic History of the Bow and Alger 7.5-minute Quadrangles, Western Skagit County, Washington

Joe D. Dragovich, David K. Norman, Carly L. Grisamer, Robert L. Logan, and Garth Anderson
Washington Department of Natural Resources
Division of Geology and Earth Resources
PO Box 47007, Olympia, WA 98504-7007

## ABSTRACT

This report consists of geologic maps and cross sections (Plates 1, 2, 3) and an interpretation of the geologic history of the Bow and Alger 7.5-minute quadrangles in the Bellingham 30-minute by 60-minute quadrangle (Fig. 1). Geologic units in the quadrangles are broadly grouped into Quaternary surficial deposits, Eocene sedimentary rocks, and pre-Tertiary metamorphic rocks consisting of the Easton Metamorphic Suite of Tabor and others (1994)(hereafter Easton suite) and overlying Helena–Haystack mélange (Fig. 2).

The Bow and Alger quadrangles are in the western portion of the Northwest Cascades system (Brown and others, 1987; Misch, 1966)(Fig. 2) and contain a diversity of pre-Tertiary lithologic packages that are bounded by thrust faults. These packages were emplaced as nappes[1] in the mid-Cretaceous. Nappe-bounding thrust faults are locally associated with tight to isoclinal folding, mylonitization, and cataclasis. We correlate the assemblage of ultramafite, metabasalt, and metagabbro and locally associated metasedimentary rocks with the Helena–Haystack mélange (HH) of Tabor (1994). The HH of Tabor (1994) is structurally and lithologically similar to the Haystack terrane of Whetten and others (1980a, 1988) but is of a more limited map extent. Our interpretation is that the HH was thrust over the Easton suite (Shuksan nappe) in the study area during the widespread nappe development that affected the Northwest Cascades system (Brown, 1987; Misch, 1966) in the mid-Cretaceous. We present evidence that thrusting and mylonitic structure developed during the late-metamorphic stage. The low degree of recrystallization and the probable lower temperature of metamorphism that affected rocks of the HH nappe contrast with the high degree of recrystallization of underlying Shuksan nappe rock types and suggest a different metamorphic history for the two nappes. Eocene to Oligocene orogeny involving regional dip-slip and strike-slip faulting accompanied the deposition of the Chuckanut Formation. Tertiary faulting and folding dissected and complicated the thrust stratigraphy, leading to the cross-faulted and broken appearance of the rock units and thrusts on Plates 1 and 2.

Late Pleistocene (Fraser age) glacial deposits mantle the mountains and partly fill the Skagit and Samish River valleys. Advance of the Puget lobe of the last (Vashon) glaciation resulted in deposition of basal or lodgment till over much of the area. During Puget lobe advance, subglacial meltwater (Booth, 1987, 1994) excavated the Samish River valley in the study area, as evidenced by the draping of Vashon till along the Samish valley walls. During the Everson Interstade, the lobe wasted back through the northern half of the Puget Lowland as marine waters entered the depressed Puget Sound basin and buoyed the rapidly retreating and thinning ice. Marine and estuarine conditions then prevailed in the study area, resulting in a blanket of glaciomarine drift that is now mapped up to an altitude of 350 ft; isostatic uplift of the deposits was due to rebound of the depressed crust. Complex interfingering of outwash deposits of Everson age indicates a mix of marine, estuarine, deltaic, and fluvial depositional environments. Facies vary both vertically and horizontally from fine distal marine deposits to coarse proximal outwash deposits.

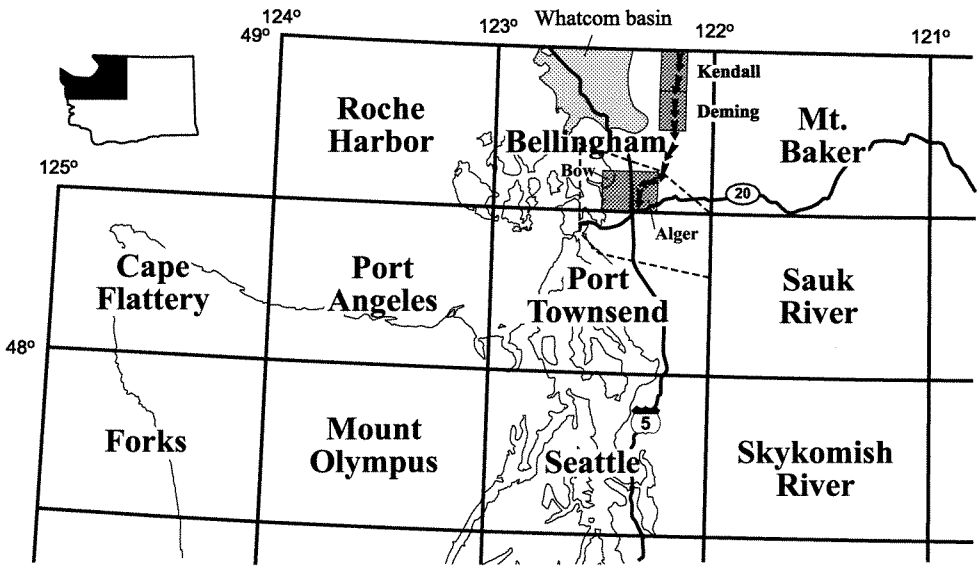


**Figure 1.** Locations of 1:100,000-scale quadrangles and past and current STATEMAP 7.5-minute mapping projects, northwestern Washington. See Dragovich and others (1997d) for the geologic maps and interpreted geologic history of the Kendall and Deming 1:24,000-scale quadrangles. Shaded polygon shows the location of "Whatcom basin" discussed in text. Arrows shows the Sumas Stade outwash path through the foothills of the northwestern Cascade mountains of Easterbrook (1979); the Sumas ice front near Canada fed a braided river system that followed major south-trending valleys. This outwash valley train may have terminated as a deltaic system in the Alger quadrangle.

[1] A nappe is a large body of rock that has moved forward more than one mile from its original position, either by overthrusting or by recumbent folding. We infer overthrusting in our subsequent usage.

A minor southward re-advance of Cordilleran ice back into Whatcom County from Canada is termed the Sumas Stade (for example, Armstrong and others, 1965). North of the study area, Sumas Stade glacial re-advance into the Sumas and Columbia valleys (Easterbrook, 1962; Armstrong and others, 1965) resulted in local deposition of moraines, ice-contact sediments, and outwash over older Everson and Vashon glacial sediments (Easterbrook, 1962, 1966a,b, 1969, 1976a,b). In the study area, terraces and perched valley-train Sumas outwash deposits define an incised fluvial-deltaic system that is consistent with mean sea level at about 100 ft above present sea level (apsl). Our Quaternary subsurface analysis and field mapping indicate that pre-Fraser glacial and nonglacial deposits locally lie under a relatively thin mantle of till and (or) Everson deposits.

Postglacial filling of the Skagit River valley via fluvial, estuarine, and deltaic processes was substantially aided by volcanic sediments and lahars from Glacier Peak. This resulted in rapid Holocene progradation of the Skagit River delta front(s) across the southern part of the study area. In fact, much of the older alluvium mapped in the southeastern part of the Alger quadrangle is probably lahar runout deposit(s) (hyperconcentrated flood deposits) dating from a late Holocene Glacier Peak eruption.

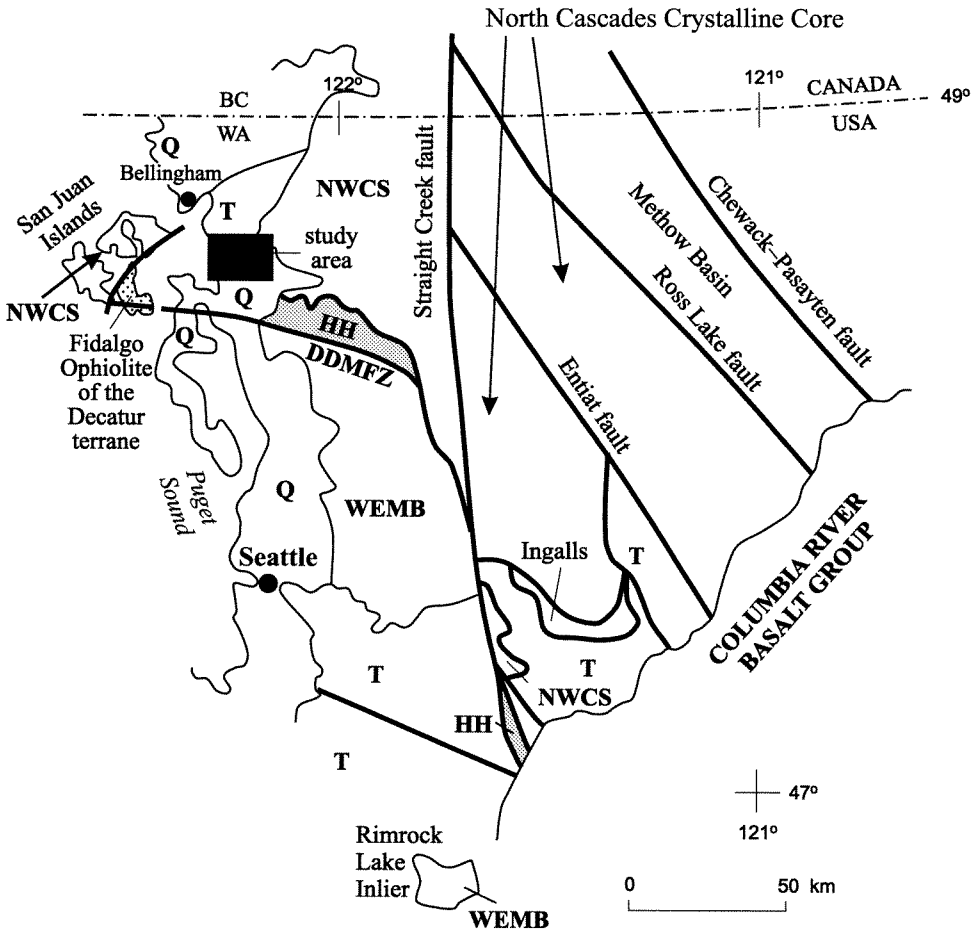


**Figure 2.** Generalized map showing location of the Bow and Alger 7.5-minute quadrangles (study area) and the major geologic domains of the north and central Cascades and southernmost British Columbia (modified from Tabor, 1994). These domains contain contrasting lithologies, metamorphisms, and (or) structural styles. Q, Quaternary deposits; T, Tertiary continental sedimentary and associated volcanic rocks; DDMFZ, Darrington–Devils Mountain fault zone; WEMB, western and eastern mélange belts; HH, Helena–Haystack mélange; NWCS, Northwest Cascades system; Ingalls, Ingalls Tectonic Complex. We correlate the greenstone-ultramafite-metasedimentary package overlying the Easton Metamorphic Suite in the study area with the Helena–Haystack mélange of Tabor (1994). (Also see Fig. 13.) The HH may be lithologically correlative with the Fidalgo ophiolite of the Decatur terrane west of the study area. The Northwest Cascades system (NWCS) is bounded on the east by the Straight Creek fault, on the southwest by the Darrington–Devils Mountain fault zone, and on the northwest by the lower Fraser River, which roughly follows inferred faults of the Vedder discontinuity that separates the metamorphic and plutonic rocks of the Coast Belt of British Columbia. Note the location of the San Juan Islands west of the study area. Pre-Tertiary structural stacking observed in the islands (for example, Brandon and others, 1988) is similar to the structural stacking in the Northwest Cascades system.

## METHODS, PREVIOUS WORK, AND RELATED STUDIES

Our mapping and interpretations are based on field work in 1997 and 1998. This work supplements ongoing field work by R. A. Haugerud as part of the current geologic mapping effort by the U.S. Geological Survey (USGS) in the Bellingham 1:100,000-scale quadrangle.

Mapping by Schmidt (1972)(Chuckanut Mountain), Bechtel, Inc. (1979), Gallagher (1986), Gallagher and others (1988)(Chuckanut Mountain and Blanchard hill), and Cruver (1983)(Butler and Sterling Hills) provided helpful information about the pre-Tertiary bedrock geology and structure. The Bechtel map provides a regional perspective and is the only previous map to cover the entire study area in substantial detail or at a scale less than 1:250,000. Johnson (1982) mapped the Chuckanut Formation along the northernmost portion of the study area. The geologic maps (Plates 1 and 2) incorporate significant amounts of these workers' mapping.

Previous geologic mapping and topical studies in and adjacent to the Bow and Alger quadrangles are documented in Figure 3 or cited in the text. Important 1:100,000-scale geologic studies to the south include Whetten and others (1980a, 1988) and Pessl and others (1989). Adjoining 7.5-minute geologic maps south of the study area were mapped by Dethier and Whetten (1980, 1981) and Whetten and others (1980b). Some of the important regional studies of bedrock and structures to the east of the area are Brown (1987), Brown and others (1987), Misch (1966), Tabor and others (1994), and Tabor (1994). In the San Juan Islands to the west, Brandon and others (1988 and references therein) map a thrust-bounded stratigraphy similar to the stacking observed in the Northwest Cascades system. (See Tabor and others, 1994.)

Siegfried (1978) studied the glacial stratigraphy of Bay View Ridge in the southwestern part of the Bow quadrangle. Easterbrook (1979) made reconnaissance maps of areas around the Samish valley and generally described Everson Interstade

deposits, strandlines, and the relative age relations between the Everson and Sumas deposits in the study area.

Easterbrook (1976a) mapped Quaternary units north of the quadrangles. Kovanen (1996) and Easterbrook and Kovanen (1996a) studied and locally mapped surficial deposits, including Sumas-correlative(?) alpine glacial drifts along the middle and north forks of the Nooksack River directly north of the Alger quadrangle. A few of the important regional Fraser glacial studies are Armstrong and others (1965), Easterbrook (1962, 1969, 1979), and Dethier and others (1995). Sceva (1950) studied the regional geohydrology of the western Skagit River valley. Beale (1990) investigated beach and estuarine sediments west of Bay View Ridge and their potential relation to neotectonics.

A companion study consists of our compiled data from water wells and geotechnical borings in and adjacent to the Bow and Alger quadrangles (Dragovich and Grisamer, in press). We examined more than 1,400 water-well logs and about 80 geotechnical borings logs (Fig. 4) in order to evaluate the Pleistocene stratigraphy of the uplands and Pleistocene to Holocene valley fill stratigraphy of the Samish and Skagit valleys. Quaternary unit thickness values provided in this report have been derived from our analysis of logs of water wells and geotechnical borings (Dragovich and Grisamer, in press) and supporting field observations.

Data and interpretations are presented as a series of cross sections (Plate 3) showing Quaternary materials described in the logs and actual and inferred Quaternary unit contacts. An ongoing study examines compiled regional geochemical data obtained from several of the Northwest Cascades system thrust nappes, including the Decatur terrane of the San Juan thrust system, and further tests the hypothesis that Helena–Haystack mélange meta-igneous rocks structurally overlie the Shuksan nappe (Dragovich and Norman, unpub. data).

Referenced geographic mountain names in the Bow quadrangle are mostly informal. (See Fig. 3 and inset.) Chuckanut Mountain is formally named. The portion of Chuckanut Mountain southeast of Oyster Creek is informally called "south" Chuckanut Mountain in some literature. Colony and Blanchard mountains are not formally named on the topographic map. We use these mountain names to facilitate our discussion.

Formally and informally named and unnamed geologic units are shown on Plates 1, 2, and 3. Unit symbols provide information about the age, lithology, and name (if any) of the units: upper-case letters indicate protolith age, lower-case letters indicate lithology, and subscripts identify named units. For example, Jurassic Darrington Phyllite is shown with the symbol $Jph_d$. We used the geologic time scale devised for the "Correlation of Stratigraphic Units of North America (COSUNA)" project of the American Association of Petroleum Geologists (Salvador, 1985). Absolute ages of Cretaceous stage boundaries are from Obradovich (1994).

Plutonic rocks are named according to their modal compositions using the International Union of Geological Sciences rock classification (Streckeisen, 1973). Some of the volcanic rocks are named using whole-rock geochemistry and the total alkali silica diagram (Zanettin, 1984; Le Bas and others, 1986). Sandstones are named using the classification scheme of Folk (1980) or Dickinson (1970). The term medium-grade metamorphic rocks refers to rocks of amphibolite facies (for example, amphibolite or schist); the term low-grade refers to rocks of greenschist facies. Low-grade rocks, including blueschist metamorphic facies rocks, are described as metasedimentary or metavolcanic rocks (for example, metasiltstone or metamorphosed siltstone); rocks metamorphosed to less than greenschist facies are included in sedimentary, volcanic, or intrusive rock units (for example, siltstone or basalt). Landslides are classified using the terminology developed by Varnes (1958, 1978).

Radiocarbon age analyses for this and other studies and selected water-well, geochemical, and U-Pb data and analyses for this study are given in the appendices. All $^{14}C$ ages provided in this document are uncalibrated. Sample locations are in Figure 3. Quantitative and semiquantitative mineral and clast abundance data from this study (112 thin sections from the various bedrock units) and other studies are incorporated into the text; thin section locations are also shown on Figure 3.

We supplemented our field mapping by inspecting Washington Department of Natural Resources (DNR) color 1:24,000-scale (1976) and black and white ~1:13,600-scale (1994) aerial photographs. We also used 1991 DNR 1:12,000-scale orthophotographs and 1941 U.S. Army 1:20,000 aerial photographs (archived at DNR) to map surficial deposits, bedrock contacts, terraces, strand lines, channel morphology, and lineaments.

# DESCRIPTIONS OF MAP UNITS

## Sedimentary and Volcanic Rocks and Deposits

### QUATERNARY SEDIMENTARY DEPOSITS

#### Nonglacial Deposits

Qb **Beach deposits (Holocene)**—Moderately to well-sorted sand and gravel along shorelines; typically well-rounded; locally includes wave-worn shell fragments; locally includes tidal flat deposits composed of fine sand, silt, and clay. The unit is mapped along the southwestern part of the Bow quadrangle. See Beale (1990) for a discussion of the tidal flat and beach deposits along Padilla Bay.

Qa **Alluvium of the Skagit River valley, undivided (Holocene)**—Generally well stratified and well-sorted deposits of cobbly gravel, gravel, sandy gravel, gravelly sand, sand with overbank flood-generated silt, clay, and locally peat (see unit Qp); clasts rounded to subrounded and derived from volcanic, metamorphic, and plutonic rocks found mostly in the upper part of the Skagit drainage basin and reworked glacial deposits; sands are distinctly micaceous (~1–5%); black or brown to gray, depending on oxidation state and composition; contains minor lacustrine sediments.

This alluvium typically displays fining-upward sequences 20 to 40 ft thick (Appendix 3, for example, wells 41, 45, 142, and 368) that probably are the result of lateral migration of point bars leaving vertical sequences that range from coarse channel deposits to fine overbank deposits. These fluvial deposits overlie Holocene deltaic and estuarine deposits of ancient Samish Bay that locally contain marine shells (Appendix 3, for example, wells 41 and 368). Alluvium near Samish Bay interfingers with estuarine and beach deposits locally containing shells and shell fragments.

Abandoned channels in the Skagit River valley appear as distinct to faint (as a result of land modifications or age differences) traces on aerial photographs. (See Plates 1 and 2.) These channels are commonly associated with arcuate traces of lateral accretion surfaces formed along meander bends of ancient streams. Some

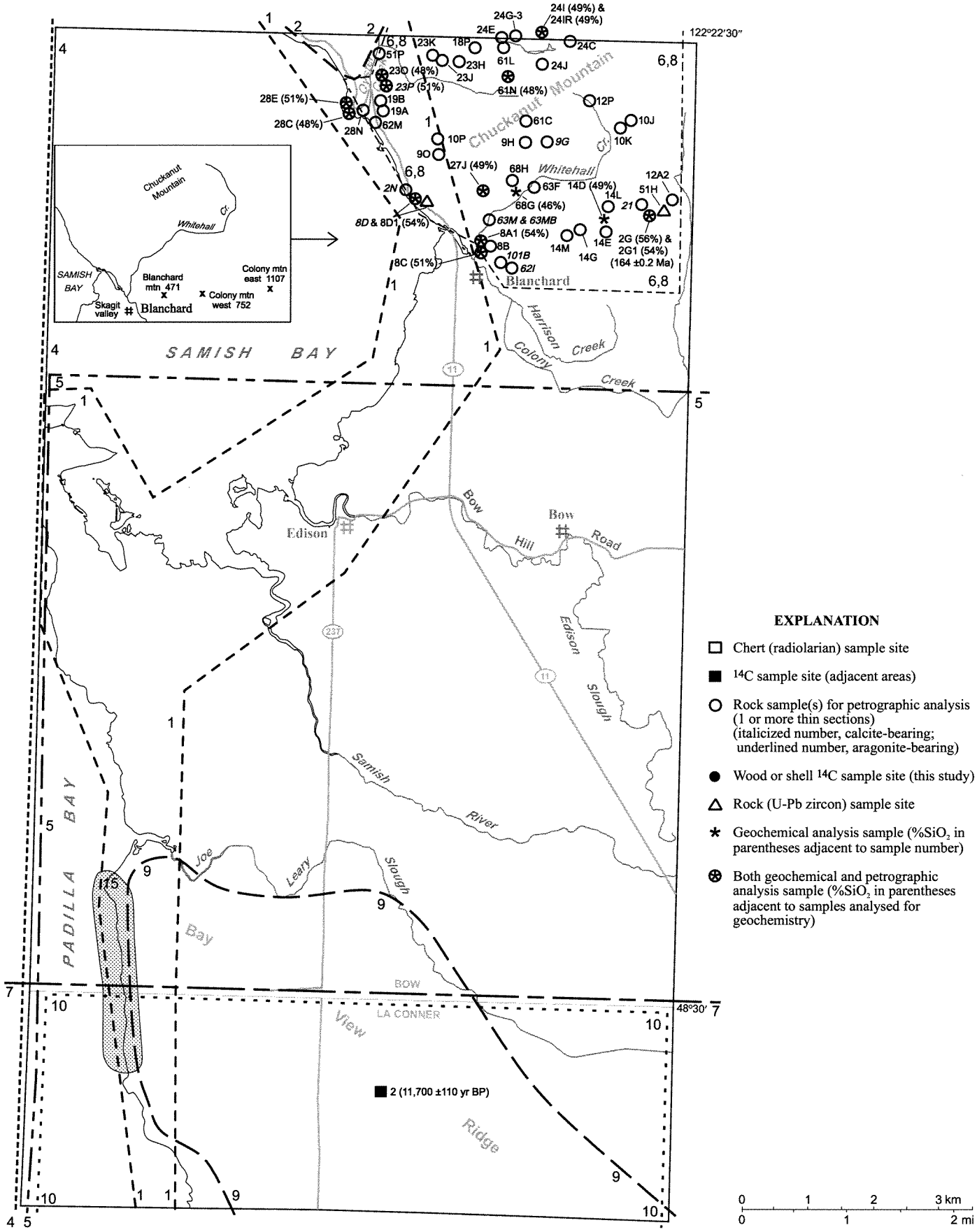


**Figure 3.** Locations of previous geologic map studies and sample locations (this study) in and adjacent to the Bow *(this page)* and Alger *(next page)* quadrangles. "Blanchard mountain, Colony mountain east and Colony mountain west" are informal geographic names used for location purposes in this report (see inset). 1, Washington Department of Ecology (1978): coastal zone atlas, Skagit County, 1:24,000; 2, Johnson (1982), 1:50,000; 3, Easterbrook (1976a), 1:62,500; 4, Bechtel, Inc. (1979), 1:63,360; 5, Sceva (1950), 1:100,000; 6, Gallagher and others (1988) and Gallagher (1986), 1:80,000; 7, Pessl and others (1989) and Whetten and others (1988), 1:100,000; 8, Schmidt (1972), 1:12,000; 9, Siegfried (1978),

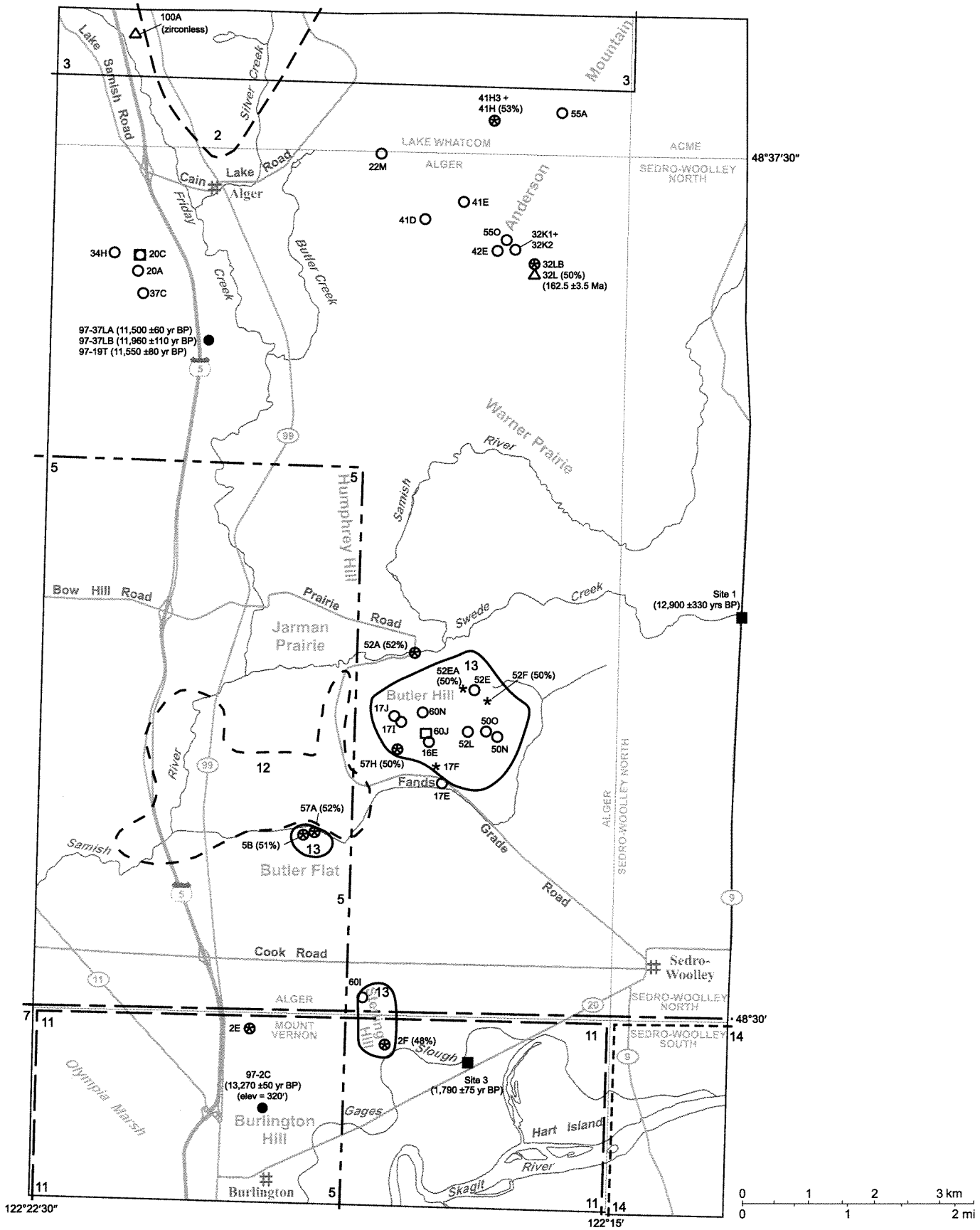


1:12,000; 10, Artim and Wunder (1976), 1:24,000; 11, Dethier and Whetten (1981), 1:24,000; 12, Easterbrook (1979), 1:24,000; 13, Cruver (1983), 1:63,360; 14, Dethier and Whetten (1980), Whetten and others (1979, 1980), Dethier and others (1980) 1:24,000; 15. Beale (1990), approx. 1:12,000. Other important regional studies include a 1:250,000-scale geologic compilation of the Helena–Haystack mélange and adjacent units by Tabor (1994) and the 1:24,000-scale soil survey of Skagit County (Klungland and McArthur, 1989) by the Soil Conservation Service. Greenschist samples 100A (top left) and 8D1 (near Windy Point) contained no zircon, thus no age estimate is available.

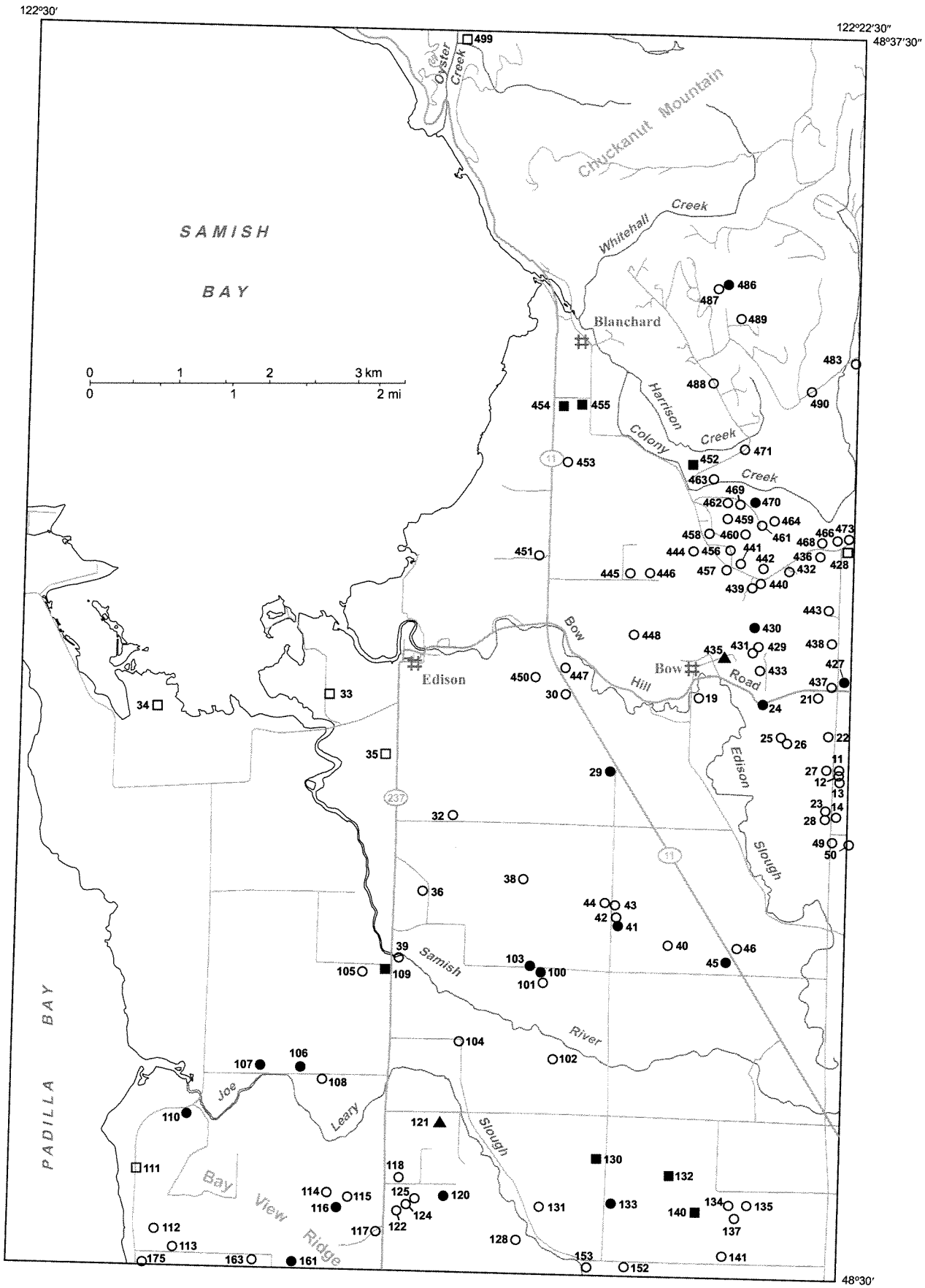


**Figure 4.** Location of selected water wells and geotechnical borings for which logs were analyzed in the Bow *(this page)* and Alger *(next page)* quadrangles. We also analyzed, but do not show here, the logs of wells and borings within a mile of the north, south, and east borders of the study area. See page 8 for an explanation of symbols. See Appendix 3 and Plate 3, cross sections E–G, for illustrations of some of the water-well data.

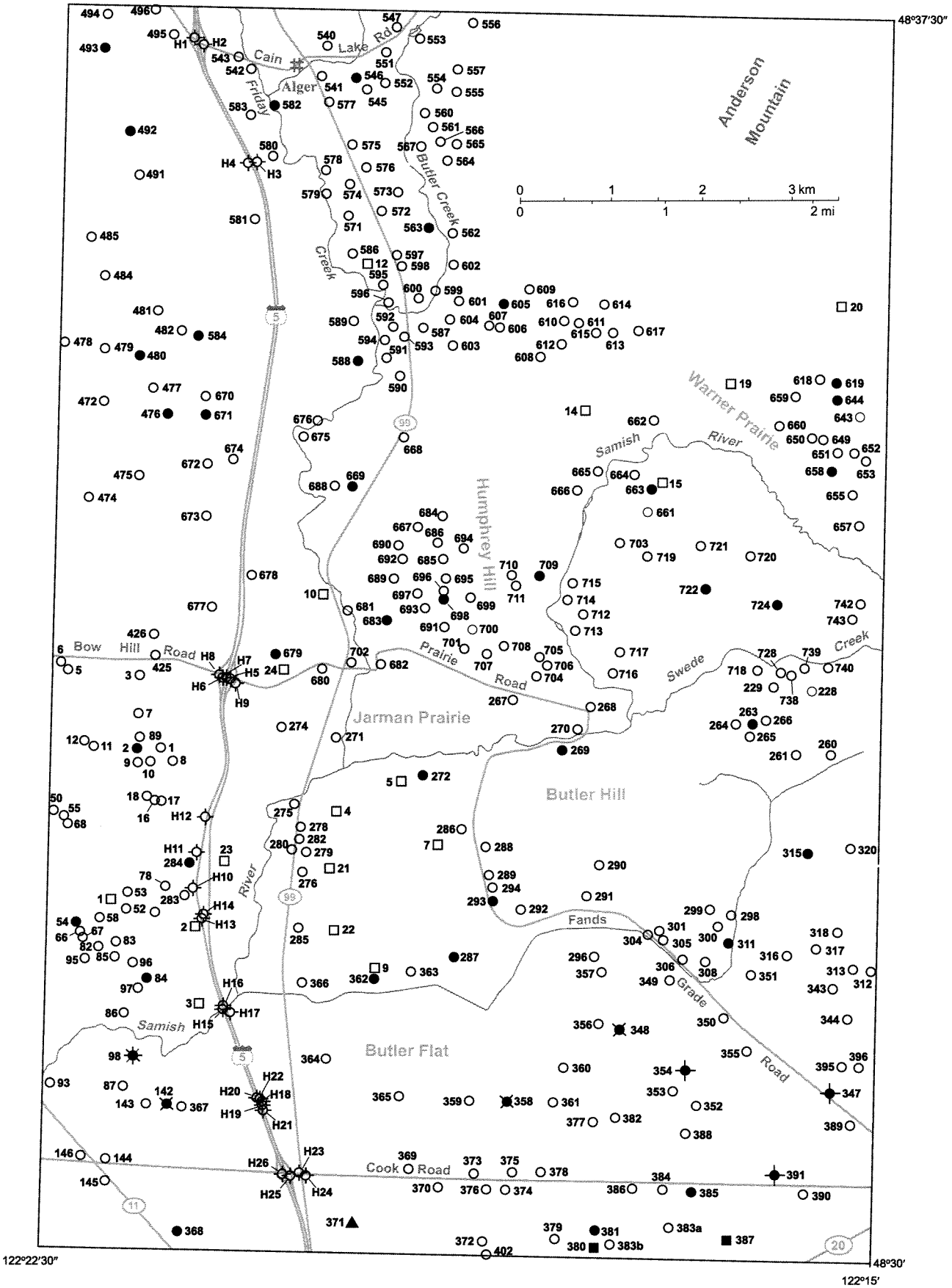
48°37′30″
122°22′30″
48°30′
122°15′
0 1 2 3 km
0 1 2 mi
Anderson Mountain
Warner Prairie
Humphrey Hill
Butler Hill
Jarman Prairie
Butler Flat
Bow Hill Road
Lake Road
Cain Road
Friday Creek
Alger
Butler Creek
Samish River
Prairie Road
Swede Creek
Fands Grade
Cook Road

of these abandoned channels are filled with lacustrine or peat deposits. The abandoned channels we mapped using aerial photographs show a fair to excellent correlation with soil unit boundaries mapped by the Soil Conservation Service (Klungland and McArthur, 1989).

Alluvium thickness ranges from a 20- to 30-ft veneer on shallowly buried glacial paleotopography near the intersection of Cook Road and Interstate 5 to more than 250 ft elsewhere in lower Skagit valley.

$Qa_S$ **Alluvium of the Samish River valley, undivided (Holocene)**—Generally well stratified and well-sorted deposits of clay, silt, and silty sand and, locally, peat (see unit Qp) with lesser sandy gravel and sand; gravel and sand generally rounded to subrounded; derived from local metamorphic rocks and reworked glacial deposits; brown to gray, depending on oxidation state and composition; dominated by fine overbank deposits containing lenses of fluvial channel sand and gravel that probably are the result of lateral migration of point bars and overbank deposits; commonly interlayered with alluvial fan deposits; overlies Sumas Stade and Everson Interstade glacial deposits commonly at a fairly shallow depth (Appendix 3, for example, well 709; Plate 3, cross sections F, G); ranges from a 4-ft veneer to a maximum thickness of 63 ft (avg. 24 ft) (Dragovich and Grisamer, in press).

Abandoned channels in the Samish River valley appear as fairly distinct traces on aerial photographs. (See Plates 1 and 2.) Some of the depressions formed by these ancient abandoned channels are filled with peat deposits.

Qoa **Older alluvium and overbank deposits, undivided (Holocene)**—Locally pumiceous and (or) dacite clast-bearing, moderately to well-sorted and stratified sand, silt, and gravel; brown to gray, depending on oxidation state and composition (pumice-rich sand is tannish white); moderately well bedded to nonbedded (massive); at a depth of about 30 to 50 ft overlies typical nonvolcanogenic alluvium and commonly fines upward from gravels to sands and rarely silts (Appendix 3, wells 348, 354, and 385).

On aerial photographs unit Qoa has a "smooth", dark, homogeneous appearance, in contrast to the uneven, light-gray, and inhomogeneous channeled appearance of unit Qa. The unit is mapped on the basis of (1) geomorphology, composition, as well as soils data from the Soil Conservation Service (Klungland and McArthur, 1989), which recognized the volcanogenic nature of some of the parent materials in the valley, and (2) relative stratigraphic position deduced from water wells. Thickness is about 30 to 50 ft.

The unit is best exposed in erosional river terraces directly south of the Alger quadrangle, where a distinct, 10- to 30-ft-high erosional river terrace separates unit Qoa from the modern Skagit River channel and flood plain. Less distinct changes in altitude separate units Qa and Qoa elsewhere (for example, Fig. 5, loc. 3). The unit overlies more typical Skagit River alluvium containing a mixture of clasts types reflective of the upvalley geology. Locally, the terrace is mantled by Qa overbank deposits composed of fine sand, silt, and clay.

Unit Qoa silts, sands, and gravels commonly contain fresh dacite clasts and pumice derived from a Glacier Peak lahar (Dethier and Whetten, 1981; this study). We interpret unit Qoa as one or more large hyperconcentrated flood deposits resulting from the attenuation of a large noncohesive lahar about ~1,800 $^{14}$C yr B.P. (See Scott and others, 1992, for description of volcanic debris flow types.) The overall fining-upward nature of the unit is consistent with the overall fining-upward characteristic of hyperconcentrated flood deposits (Appendix 3). Derivation of unit Qoa from a Glacier Peak lahar is indicated by (1) local abundance of volcanic clasts (particularly pumiceous concentrations that imply significant hydrodynamic sorting) and (2) the similar ages of unit Qoa and a lahar deposit near Glacier Peak (Beget 1981, 1982). Dethier and Whetten (1981) report that charcoal in alluvium directly under the laharic deposits near Sterling Hill (see Fig. 3, site 3) yields a $^{14}$C age of 1,790 ±75 yr B.P. This is similar to a 1,750 yr B.P. assemblage of lahars along White Chuck River, a tributary to the Skagit River that drains Glacier Peak. Beget "tentatively correlated [the] similar-age terrace deposit of dacite rich alluvium which underlies the town of Burlington [unit Qoa]" with the lahar assemblage observed along the White Chuck River (D. Dethier, oral commun., 1980, to Beget)(Beget, 1982).

Qp **Peat (Holocene)**—Poorly stratified to massive, brown to black, fibrous to woody peat and muck of bogs and swamps in abandoned channels or former oxbow lakes. Other locally organic-rich areas are found in the Skagit River valley alluvium but are too small to map at this scale; they include large areas of pre-agricultural marsh (mapped during initial State land surveys in the 1800s) and shallow oxbow lakes or depressions.

Qaf **Alluvial fan deposits (Holocene and latest Pleistocene)**—Poorly sorted, massive to rarely stratified diamicton consisting of clayey silty sandy gravel and gravelly sandy silt; angular to rounded clasts; mostly of debris-flow or debris-torrent origin and locally modified by stream processes. Clast composition reflects source area; thickness varies from an average of about

**EXPLANATION**

- Department of Transportation geotechnical boring
- "Synthetic" well (shallow strip logs of surficial deposits constructed on the basis of surface exposures)
- Valley well penetrating diamicton (lahar?) or volcanic sediment (for example, black sand or pumice-rich sand or gravel)
- Valley well penetrating glacial deposits below alluvium or other valley sediments
- Water well
- Water well with strip log of stratigraphy shown in Appendix 3
- Water well with strip log of stratigraphy shown in Appendix 3; valley well containing diamicton (lahar?) or volcanic sediment (for example, black sand or pumice-rich sand or gravel)
- Water well with strip log of stratigraphy shown in Appendix 3; valley well containing glacial deposits below alluvium or other valley sediments
- Water well with strip log of stratigraphy shown in Appendix 3; valley well containing *both* diamicton (lahar?) or volcanic sediment (for example, black sand or pumice-rich sand or gravel) *and* glacial deposits below alluvium or other valley sediments

24 ft to a maximum interpreted thickness of 63 ft. Unit Qaf disconformably overlies glacial deposits and disconformably overlies or interfingers with alluvium (units Qa and $Qa_s$) and thus is mostly Holocene in age (Plate 3, cross sections F, G). However, portions of the alluvial fans could be latest Pleistocene.

Qls **Landslide deposits, undivided (Holocene to Pleistocene)**—Poorly sorted, unstratified diamicton consisting of angular to rounded boulders, cobbles, and gravel in a sand, silt, and (or) clay matrix; clast composition reflects source area; largely originating as deep-seated failures (slump-earthflow, debris slump, or rock slump), rarely as rock avalanche, fall, topple and slab failures. Deep-seated landslides are locally associated with younger and smaller, superimposed debris flow and slide deposits emanating from unstable portions of the landslide scarp, flanks, body, or toe. (See unit Qaf.) Although their thickness is highly varied, deep-seated landslide deposits are typically about 30 ft thick; they unconformably overlie bedrock and Quaternary geologic units.

The geomorphology of most of unit Qls suggests a Holocene age. However, the lack of direct dates and the probability that unvegetated and locally steep slopes of unconsolidated glacial deposits were exposed during Everson deglaciation suggest that some of the landslide deposits may have been initiated in the late Pleistocene and may interfinger with late glacial materials at depth. Thus, thicker deposits are likely the result of slope instability and mass wastage immediately following the Fraser glaciation; some mass wastage may be seismically induced. See Heller (1981) for a discussion of the landslide types and controls in the lower Skagit River area.

## Glacial Deposits

Glacial deposits are here generally divided into the Vashon Stade, Everson Interstade, and Sumas Stade categories (Armstrong and others, 1965).

### *Deposits of the Fraser Glaciation, Sumas Stade*

Depositional environments for the Sumas deposits range from braided streams in the northern half of the Bow quadrangle to marine deltas at the junction of the Skagit valley and Sumas outwash valley train deposits (Fig. 1, arrows). (See Fig. 5, locs. 5, 6, 7.) We speculate that the moderate sorting and occurrence of cobbles and boulders in some of the gravelly glacial outwash deposits may be indicative of outburst flood deposition along the Samish River glacial valley train.

Sumas ice re-advanced only into Whatcom County north of the study area. Re-advance occurred after significant isostatic recovery (resulting in a regional land-level rise or sea-level fall). (See, for example, Easterbrook, 1962, 1966b, 1969, 1979; see Armstrong and others, 1965, for an overview of the Fraser glaciation in northern Puget Sound basin.) The latest Pleistocene lower Skagit valley appears to have been a marine embayment whose outline shifted as the crust rebounded from the Vashon Stade ice load (this study; Dragovich and Grisamer, in press). Sumas-time sea level is approximated by the altitude of the Sumas deltaic topset beds (now about 100 ft apsl) along the northern part of the Skagit valley (Easterbrook, 1979). (See unit $Qgod_s$.) (See Discussion.)

The end of the Sumas Stade is approximately dated by $^{14}C$ ages of about 10,000 years (lowermost stratum of peat in abandoned Sumas outwash channels north of the study area; Easterbrook, 1962, 1969, 1971, 1976a,b). Wood from Sumas till in southwesternmost British Columbia yields $^{14}C$ ages of 11,600 ±280, 11,500 ±1,100, 11,400 ±170, and 11,300 ±100 yr B.P. (Armstrong and others, 1965; Armstrong, 1981; Clague, 1980, 1981).

$Qgo_s$ **Fluvial outwash (Pleistocene)**—Loose, moderately to well-sorted, subrounded to rounded sandy cobbly gravel; locally with boulders, sandy gravel, and minor gravelly medium to coarse sand, rare silty sand, sandy silt, and silt; typically brown to gray, depending on oxidation state; massive or moderately to well-bedded; commonly crudely bedded on a scale of centimeters to, more commonly, a few meters as defined by cobble, gravel, and sand content; locally contains lenticular interbeds of sand and (or) rare silty sand or silt. Plane bedded to rarely internally cross-stratified beds in a few meter-thick sets indicate downvalley south to southwest to west sediment transport; clast composition and other provenance data indicate derivation from the Coast Plutonic Complex of British Columbia. The unit includes about 15 percent dunite of probable Twin Sisters Dunite origin, about 0 to 5 percent of Mount Baker andesite, and about 0 to 15 percent phyllite and vein quartz of Darrington Phyllite origin. The unit thickness is 5 to 62 ft (avg. 27 ft).

Sumas outwash overlies older glacial deposits (Appendix 3, wells 287, 558; Plate 3, cross sections E–G; also see Dragovich and others, 1997b,c,d.) Boulder-size rip-up clasts of clay or clayey diamicton derived from underlying Fraser-age glaciomarine drift or till in the outwash (see Fig. 5, loc. 8; this study) and deposition of Sumas outwash on Everson beach strand lines (Easterbrook, 1979) best demonstrate the relative ages of unit $Qgo_s$ and the older glacial deposits.

$Qgod_s$ **Deltaic outwash (Pleistocene)**—Loose, moderately to well-sorted, subrounded to rounded sandy cobbly gravel, locally with boulders; also contains sandy gravel, gravelly medium to coarse sand, lesser sandy silt, silt, silty clay, and clay; typically brown to gray, depending on oxidation state; well-bedded, rarely massive; commonly thickly to thinly bedded. Topset beds are crudely horizontal bedded gravels with interbeds of sand and (or) rare silty sand or silt. Large foreset beds (10–60 ft high) typically dip 15° to 35° southeast to southwest and display numerous truncation surfaces indicative of rapidly changing delta-front positions and generally southward sediment transport into the open Skagit River valley. Bottomset beds are composed of massive to laminated silty clay and clay exposed in the southwest corner of the Concrete Northwest Butler Hill gravel pit (see Fig. 5, loc. 5). The bottomset beds are overlain by gravelly sand foreset beds suggestive of southerly deltaic progradation toward the adjacent Skagit valley. Clast composition and other provenance data indicate derivation mostly from the Coast Plutonic Complex of British Columbia; this unit includes about 2 to 10 percent dunite of probable Twin Sister Dunite origin, about 0 to 3 percent of Mount Baker andesite, and about 0 to 10 percent phyllite and vein quartz of Darrington Phyllite origin. The deltaic deposits coarsen

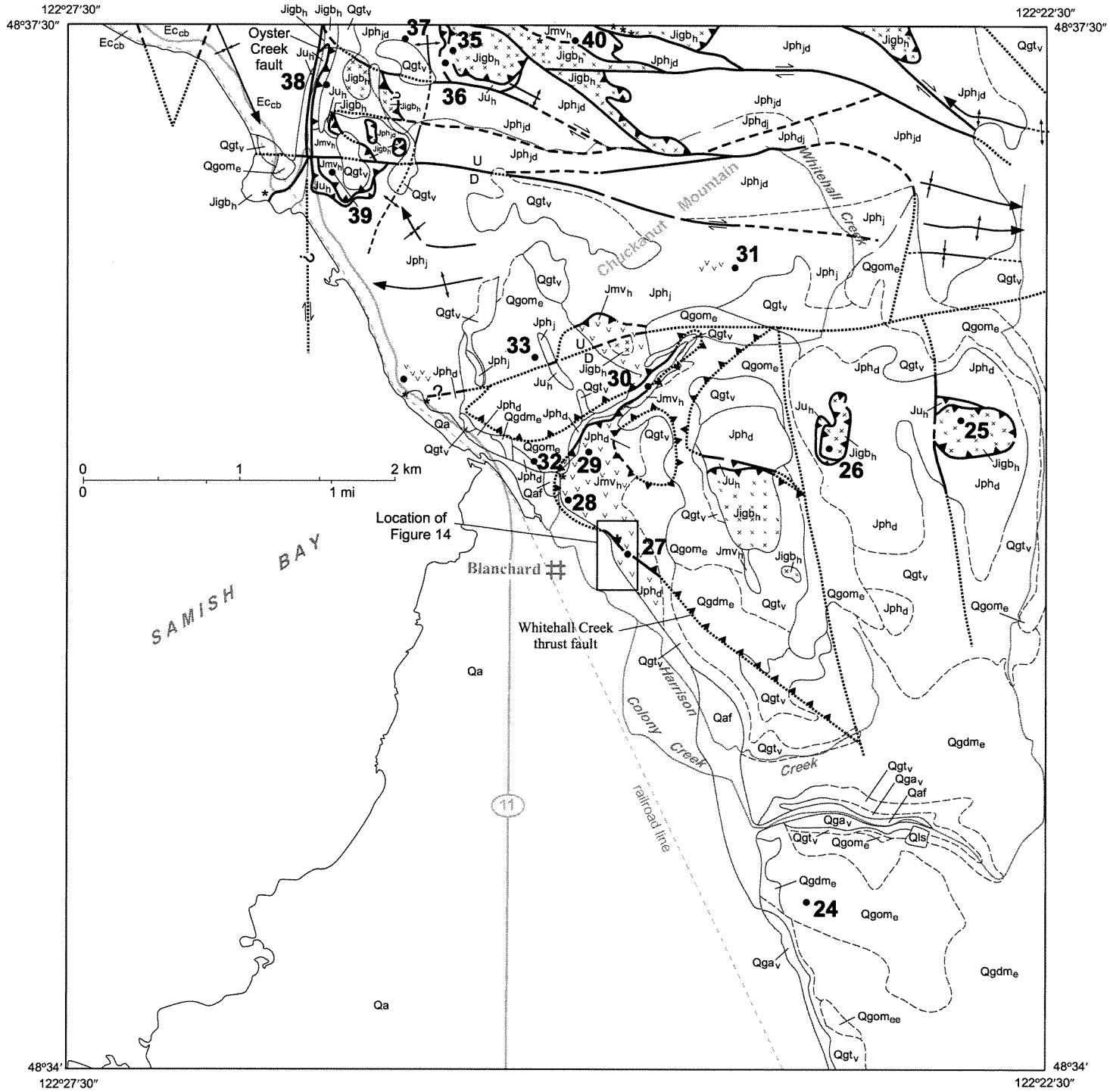


**Figure 5.** Geologic maps of the northeastern portion of the Bow quadrangle *(this page)* and the Alger 7.5-minute quadrangle *(next page)*. (Skagit valley portion of the Bow quadrangle is not shown.) Explanation on page 12. Dots, location of critical geologic features referenced in the text.

upward from generally clayey bottomset beds to sandy gravel topset beds locally containing cobbles. Unit thickness is 23 to 81 ft (avg. 49 ft).

### *Deposits of the Fraser Glaciation, Everson Interstade*

The period of ablation of the Puget lobe during the Fraser Glaciation is termed the Everson Interstade (Armstrong and others, 1965). Ice removal and related isostatic rebound of the crust raised these deposits relative to their original depositional altitude during and immediately after the Everson Interstade. The waning Puget ice lobe was partly buoyed by marine water, and thus a majority of the Everson deposits are glaciomarine in origin.

Earlier studies of Everson Interstade deposits emphasized low-density, fossiliferous diamictons as the dominant marine strata deposited during deglaciation (Easterbrook 1962, 1963a,b; Armstrong and Brown, 1954). Similarly, Easterbrook (1992) uses the model of a floating, rapidly thinning ice sheet

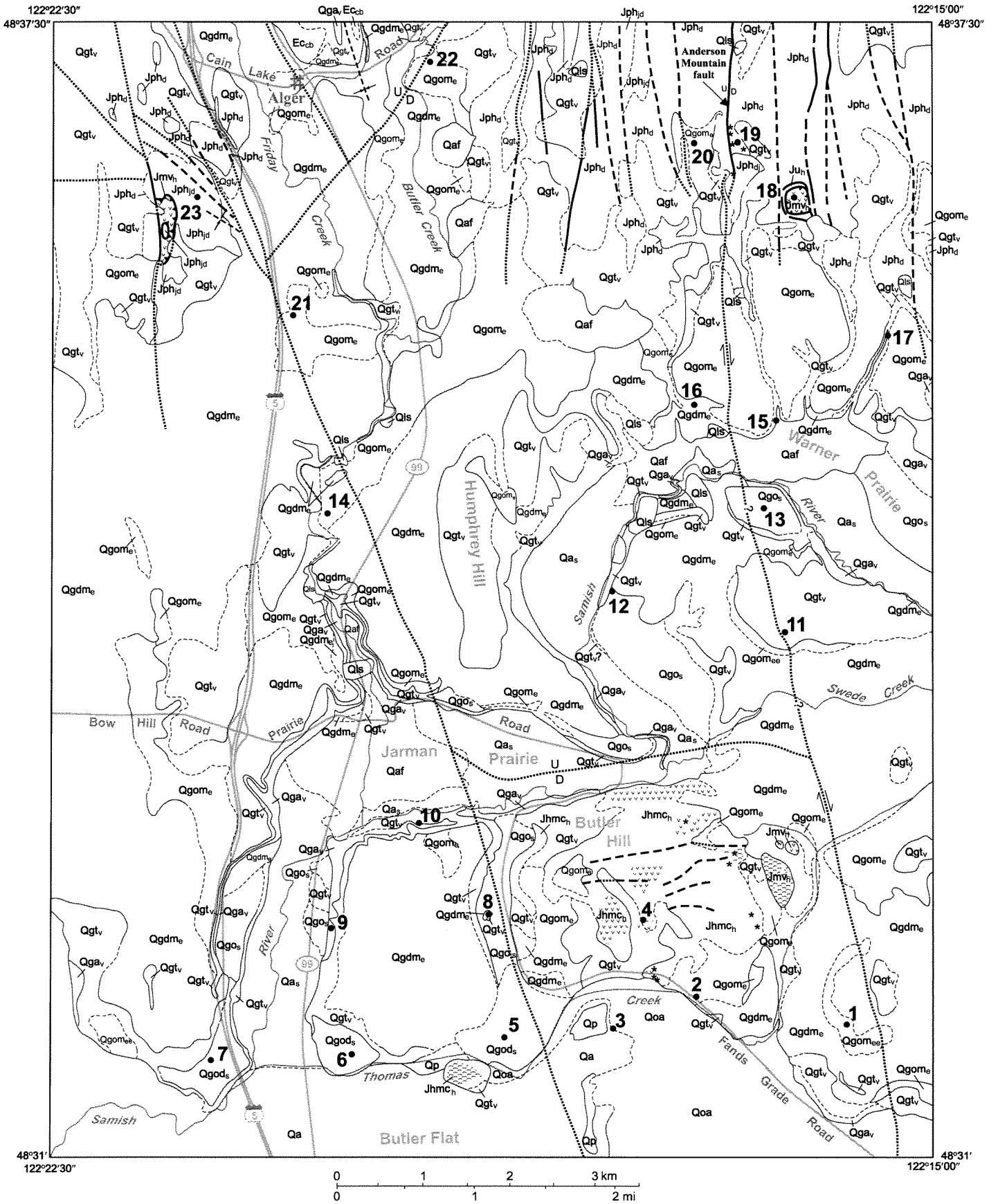
122°22′30″
48°37′30″
122°15′00″
48°37′30″
48°31′
122°22′30″
48°31′
122°15′00″
Cain Lake
Alger
Road
Finney Creek
Butler Creek
Anderson Mountain fault
Humphrey Hill
Warner Prairie
Samish River
Swede Creek
Bow Hill Road
Jarman Prairie
Butler Hill
Thomas Creek
Fands Grade Road
Samish
Butler Flat
0 1 2 3 km
0 1 2 mi

## EXPLANATION

### Geologic Units

**SEDIMENTARY AND VOLCANIC DEPOSITS AND ROCKS**

**Quaternary Sedimentary Deposits**

**Nonglacial Deposits**

Qb Beach deposits (Holocene)

Qa Alluvium of the Skagit River valley (Holocene)

Qoa Older alluvium and lahar run-out deposits of the Skagit River valley (Holocene)

$Qa_s$ Alluvium of the Samish River valley (Holocene)

Qp Peat (Holocene)

Qaf Alluvial fan deposits (Holocene and Pleistocene?)

Qls Landslide deposits (Holocene and Pleistocene?)

**Glacial Deposits, Fraser Glaciation of Armstrong and others (1965) (Pleistocene)**

**Sumas Stade**—Generally low-density (ice-free) outwash deposited during the Sumas re-advance north of the study area

$Qgod_s$ Deltaic glacial outwash deposits

$Qgo_s$ Outwash

**Everson Interstade**—Generally low-density glaciomarine deposits

$Qgdm_e$ Glaciomarine drift

$Qgom_e$ Fluvial deposits

$Qgom_{ee}$ Emergence (beach) deposits

**Vashon Stade**—Moderate- to high-density glacial deposits

$Qgt_v$ Till

$Qga_v$ Advance outwash

**Tertiary Sedimentary Rocks**

$Ec_{cb}$ Bellingham Bay Member of the Chuckanut Formation (Oligocene? to Eocene)

**LOW-GRADE LAYERED METAMORPHIC ROCKS OF THE NORTHWEST CASCADE SYSTEM**

**Mesozoic Metamorphic Rocks of the Shuksan Nappe of Tabor and others (1994)**

**Easton Metamorphic Suite of Misch (1966)(Jurassic)**

Divided into:

$Jph_d$ Darrington Phyllite (0–10% interlayered semischistose metasandstone)

$Jph_{dj}$ Darrington Phyllite (10–50% interlayered semischistose metasandstone)

$Jph_{jd}$ Semischist of Mount Josephine (0–10% interlayered Darrington Phyllite)

$Jph_j$ Semischist of Mount Josephine (10–50% interlayered Darrington Phyllite)

Basaltic to basaltic andesite metatuff interlayers

**Mesozoic Metamorphic Rocks of the Haystack Thrust Nappe of Whetten and others (1988) and the Helena–Haystack Mélange of Tabor (1994)(Jurassic)**

Generally, blocks in a serpentinite-matrix mélange overlying the Easton Metamorphic Suite in the study area

$Jhmc_h$ Heterogeneous metamorphic rocks of Butler Hill

Outcrops dominated by metabasalt

$Jmv_h$ Metabasalt

Pillow metabasalts Metabasalts

$Jigb_h$ Augite-bearing metagabbro

$Ju_h$ Serpentinite with lesser talc schist, talc-tremolite schist, and tremolite schist with rare diopside-bearing clinopyroxenites

* Serpentinite pods and outcroppings too small to show at map scale

### Geologic Map Symbols

Contact – Dashed where inferred; dotted where concealed

High-angle fault – Dashed where inferred; dotted where concealed; U, upthrown block; D, downthrown block; half arrows indicate relative apparent strike-slip motion

Thrust fault – Dashed where inferred; dotted where concealed; sawteeth on upper plate

Antiform – Dashed where inferred; dotted where concealed; arrow indicates direction of plunge

Synform – Dashed where inferred; dotted where concealed; arrow indicates direction of plunge

with abundant icebergs and contends that submarine outwash along a stranded ice shelf is a rare Everson phenomenon in the northern Puget Sound that is not replicated elsewhere.

A different model (for example, Domack 1982, 1983, 1984) emphasizes the diversity of Everson deposits. The sediment types include moderately to well-sorted gravels, sands, silts, and clays as well as poorly sorted deposits such as diamicton. These sediments were formed by proximal and transitional to distal ice-marginal glaciomarine processes in fluvial-deltaic, turbidite fan, estuarine, lagoon, and open-marine basin settings. Shallow marine and estuarine facies in this model are thin-bedded to laminated sandy silt, silt, and clay; proximal facies contain gravel and gravelly diamicton, whereas distal facies consist of interbedded to laminated silt and clay and massive silt containing sparse pebbles and local sandy partings (Dethier and others, 1995). (See Figs. 6, 7; also see Dragovich and Grisamer, in press; Croll, 1980; Balzarini, 1981, 1983). Receding Everson glacial ice stagnated on the bedrock promontory bordering the northern part of the study area. Glacial ice meltwater deposited terrestrial outwash deposits above the glaciomarine limit of 350 ft[1]. These deposits were laid down concurrently with marine outwash deposits (for example, deltaic and turbidite deposits) below the maximum glaciomarine altitude as evidenced by the outwash map pattern (Plate 1) and three-dimensional geometry (Plates 1 and 3, cross sections E–G). (See Discussion.)

We have grouped the diverse sediment types associated with the various Everson Interstade facies (see Figs. 5–7) into generally fine and coarse map units. The units are (1) proximal to distal deposits of glaciomarine drift (GMD)(unit $Qgdm_e$) that include both a clayey diamicton *and* clay (clay that typically overlies the clayey diamicton), (2) proximal glaciomarine and terrestrial deposits (unit $Qgom_e$) that are predominantly outwash sand and (or) gravel; and (3) sand and gravel emergence (beach) deposits along wave-cut terraces (unit $Qgom_{ee}$).

Significant glacial rebound occurred prior to Sumas Stade glacial re-advance north of the study area. The uplift resulted in erosion and fluvial incision of the glaciomarine deposits before deposition of the younger Sumas Stade glacial outwash valley trains in the Samish River valley (Plate 3, cross sections E–G). Glaciomarine and terrestrial outwash deposits of the Everson Interstade unconformably overlie mostly Vashon till and less commonly overlie older Quaternary deposits and bedrock.

We believe the Everson glaciomarine blanket below the glaciomarine limit was more extensive than what is now preserved on the glaciated uplands of the study area, because late Pleistocene and Holocene erosion has locally reduced the extent and thickness of these uncompacted sediments on all but the most gentle slopes. (See Discussion.)

[1] A maximum glaciomarine limit is herein defined as the highest altitude of Everson Interstade marine sediments mapped in the study area. In the study area, this limit is consistently about 350 ft and defines the uppermost limit of glaciomarine diamicton. (See unit $Qgdm_e$.)

$Qgdm_e$ **Everson Glaciomarine Drift and undifferentiated glacial diamicton (Pleistocene)**—Poorly sorted, poorly compacted, silty sandy gravelly clay, silty sandy clayey gravel, clayey gravel diamicton, and moderately sorted sandy silt, sandy clay, clayey silt, and clay with scattered lenses or layers of sand and gravel of submarine outwash origin; massive to thinly bedded, rarely varved or laminated; brown to blue-gray to gray-blue depending on oxidation state; north derivation from the Coast Plutonic Complex of British Columbia; locally phyllite- and vein-quartz-rich as a result of local derivation from bedrock in the northern portion of the study area; marine fossils very rare; thickness 4 to 312 ft (avg. 66 ft). ($Qgdm_e$ includes units $gmd_c$ and $gmd_d$ on Plate 3, cross sections E–G.)

We obtained one radiocarbon date (Appendix 1) of 13,270 ± 50 yr B.P. from shell fragments in glaciomarine gravelly clay exposed at an altitude of about 340 ft along a logging road on Burlington Hill south of the study area (Fig. 3, sample site 97-2C). Subtraction of the marine water reservoir effect (for example, Dethier and others, 1995) gives an approximate age of 12,470 ± 50 yr B.P. and allows for a comparison of $^{14}C$ shell ages with $^{14}C$ ages of woody organics. (See unit $Qgom_e$ for a comparison with $^{14}C$ wood ages in the study area.) This age is consistent with local and regional ages of the Everson Interstade GMD and other deposits. For example, Dethier and others (1995 and references therein) report 17 shell $^{14}C$ ages from west-southwest to south of the study area that range from 13,650 to 11,330 yr B.P. (avg. 12,899 $^{14}C$ yr B.P.). Other selected $^{14}C$ regional Everson Interstade ages are provided in Appendix 2. Easterbrook (1963a) radiocarbon-dated marine shells from western Whatcom County at between 11,000 and 12,900 yr B.P. Shells in GMD from the Deming quadrangle (Fig. 1) yielded $^{14}C$ ages of 12,970 ± 380 yr (location described as 3.7 mi east of the type section of the Everson GMD near Cedarville) and 12,900 ±280 yr (Easterbrook, 1962, 1992; Armstrong and others, 1965). Wood in the basal part of the peat at the Deming Sand type locality (48°49.87′N, 122°55.69′W; sec. 34, T39N, R4E) in glaciomarine drift north of the Alger quadrangle gives $^{14}C$ ages of 11,500 ±200 and 11,455 ±125 yr B.P. (Easterbrook, 1962, 1963a, 1992; Armstrong and others, 1965). Dragovich and others (1997a) relate the terrestrial (fluvial) evidence, composition, and geographic position of the Deming Sand *at the type section* (Fig. 1; directly west of the Deming quadrangle and east of the Whatcom basin) to Quaternary uplift along the Macaulay Creek thrust and suggest that coarse deposits in glaciomarine drift to the west are submarine in origin.

$Qgom_e$ **Fluvial-deltaic-turbiditic glaciomarine outwash (Pleistocene)**—Loose sand and gravel with minor interlayered silts and silty sands; includes two distinct sedimentary assemblages interpreted to represent separable but gradational sedimentary facies. Facies groups are distinguished on the basis of sedimentary structures, textures, altitude relative to the glaciomarine limit, relation to GMD deposits, and internal stratigraphy. The composite thickness ranges from 2 to 266 ft (avg. 42 ft).

We have informally divided unit $Qgom_e$ into two subunits. The first subunit consists of angular to subrounded phyllite- and vein-quartz-rich sands, pebbly sands, sandy gravel, and cobbly gravel with lesser sandy silt of fluvial-alluvial fan and deltaic origins. The unit displays local small-amplitude foreset or trough cross-bedding and is mapped on the southern slopes of Chuckanut and Anderson Mountains. The unit occurs above the glaciomarine limit of about 350 ft, is interlayered with or overlies GMD near the glaciomarine limit, and grades southward into the second marine outwash subunit.

The second subunit consists of subangular to subrounded to locally rounded gravel and sand with lesser sandy silt and silt of fluvial-deltaic-turbidite origin. The unit typically contains significant amounts of phyllite and vein-quartz clasts of local derivation. This subunit occurs below the glaciomarine limit of 350 ft and displays various sedimentary structures and interlayering relations consistent with its complex ice-marginal sedimentary setting. More distal deposits are thinly laminated to varved (silt to sandy silt or silty sand couplets) or distinctly plane laminated to horizontally stratified with crudely bedded sands and gravels; rare dewatering structures or soft-sediment deformation structures locally observed; more proximal deposits elsewhere are moderately thick to thick-bedded gravels that display large foreset beds indicative of deltaic deposition (see Fig. 8). The unit generally grades from sandy gravels and gravels on the north to dominantly sands and silty sands on the south (see "fining" symbol on Plates 1 and 2); interbedded clays or clayey diamicts (unit $Qgdm_e$) attest to cyclic deltaic-turbiditic deposition along a shifting delta front with glaciomarine deposition from iceberg melting and more distal marine suspended-load deposition. The unit overlies thick clayey GMD near Anderson Mountain but generally underlies a thick GMD section elsewhere, defining an overall fining-upward sequence and a waning or northward receding sediment source. (See also Discussion.)

Three dates from this unit (Appendix 1; see Fig. 8) indicate a minimum age of about 11,900 $^{14}C$ yr B.P.

$Qgom_{ee}$ **Emergence (beach) deposits (Pleistocene)**—Loose sand and gravel; massive, laminated, or rarely ripple cross-bedded; occurs as topographic benches interpreted as wave-cut terraces (strandlines); typically reworked glaciomarine drift (unit $Qgdm_e$)(Appendix 3, well 120). Extensive well-sorted and well-rounded coarse sand and gravel overlying GMD and till on northern and northeastern Bay View Ridge are interstratified with and overlie laminated medium sand (Siegfried, 1978).

Many outcrops of Vashon till or Everson glaciomarine deposits have at least a veneer (a meter or less) of emergence sands or gravels, indicating temporary beach reworking of the substrate during isostatic emergence (land rise and sea-level fall). Longer sea-level stillstands produce distinctive geomorphic features termed strandlines (Plate 1). Strandlines were compiled from previous studies (Easterbrook, 1979; Siegfried, 1978) or mapped during this study. Strandlines form moderately to well-defined linear features that parallel

the topographic contours and are commonly associated with well-sorted sand and gravel deposits (for example, see Fig. 5, loc. 1). (See Siegfried, 1978, for a discussion of the stratigraphy of raised marine terraces on Bay View Ridge.) Suburban development and forested areas typically prevent continuous tracing of individual strandlines across the terraced glacial ridges in the study area. The maximum glaciomarine limit of about 350 ft (107 m) in the study area is clearly defined by the altitude of glaciomarine clays and diamictons as well as wave-cut terraces and associated beach deposits.

### *Deposits of the Fraser Glaciation, Vashon Stade*

$Qgt_v$ **Till (Pleistocene)**—Unstratified, dense to very dense diamicton consisting of clay, silt, sand, and gravel in various proportions with scattered cobbles and boulders; dense to very dense lenses of sand or gravel (informally termed dynamic till) that indicate subglacial meltwater processes (Plate 1); dark yellowish brown to brownish gray; clast derivation from the Coast Plutonic Complex of British Columbia (for example, Easterbrook, 1962); locally phyllite-rich; 3 to 280 ft thick (avg. 46 ft).

Till unconformably overlies bedrock and advance outwash and is inferred to rarely overlie older glacial units (Plate 3, cross sections E–G). Below the 350 ft elevation, till commonly underlies glaciomarine drift (for example, unit $Qgdm_e$)(Appendix 3, for example, wells 709 and 722). Differentiating between till and dried, clay-rich GMD is locally difficult because dried clays impart an apparent density to the typically moist and soft GMD. However, dried GMD typically contains desiccation cracks and is distinctly matrix supported with a significant amount of fines in the matrix producing a bimodal clast distribution of fines (silt and clay) and gravel with lesser sand. (Also see Easterbrook, 1962, for differences between till and GMD.)

Limiting radiocarbon dates from other areas (for example, Appendix 2) indicate an age between about 18,000 and 13,600 yr B.P. See Heller (1981) for pebble count diagrams and Vashon Stade ice-flow directions in the lower Skagit River area.

$Qga_v$ **Advance outwash (Pleistocene)**—Moderately to well-sorted, stratified, highly compacted medium to coarse sand, pebbly sand, and sandy gravel with minor amounts of fine silty sand or sandy silt and clay interbeds and with scattered lenses and layers of pebble-cobble gravel; light-gray to tan; thin to very thickly bedded with horizontal and generally south-dipping cross-stratification (Plates 1, 2) with cut and fill structures. Local high-amplitude foreset bedding suggests deltaic deposition into proglacial lakes. The unit forms an overall coarsening-upward sequence from sand, silt, and clay at the base (noted only in well logs) to sand and gravel with locally cobbly gravels at the top (Dragovich and Grisamer, in press; Pessl and others, 1989).

The thickness ranges from 2 to 172 ft (avg. 46 ft). The unit buries a pre-Fraser topography (see Figs. 6, 7) and, as also observed by Pessl and others (1989) south of the study area, overlies "transitional beds" that consist of undifferentiated early Vashon advance outwash and late pre-Vashon nonglacial deposits (Plate 3, cross sections E–G).

## TERTIARY SEDIMENTARY ROCKS

**Chuckanut Formation (Oligocene to Eocene?)**—Johnson (1982, 1984b) divided the formation into the Bellingham Bay and Slide Members. Mustoe and Gannaway (1997) and Dragovich and others (1997d) include the Bellingham Bay and Slide Members in the informally named lower Chuckanut Formation. Johnson also named the Padden, Maple Falls, and Governors Point Members of the informally named upper Chuckanut Formation. Mustoe and Gannaway (1997) examined the flora of the Chuckanut Formation and proposed different ages for the upper part of the formation than those of Johnson (1982). The Bellingham Bay Member crops out in the northernmost part of the Bow and Alger quadrangles.

$Ec_{cb}$ **Bellingham Bay Member (Eocene)**—Thick- to very thinly bedded, well-sorted, rounded to subrounded micaceous medium- to coarse-grained feldspathic sandstone and minor polymictic conglomerate (coarse-grained intervals) alternating with abundant mudstone and lesser fine-grained feldspathic sandstone, siltstone, and minor coal (fine-grained intervals); coarse- and fine-grained intervals organized into fining-upward cycle. Sandstone is yellowish gray, gray, or dark gray with a salt and pepper appearance. Coarse-grained interval sedimentary structures include trough cross-bedding, ripple lamination, or flat lamination; conglomerates are massive to crudely stratified. Fine-grained sedimentary intervals include mostly massive or laminated mudstone; structures include ripples, rootlets, burrows, mottled horizons, and plant fossils (Johnson, 1982, 1984b,c).

Feldspathic sandstones consist dominantly of monocrystalline quartz, plagioclase, potassium feldspar, and biotite, lesser muscovite and lithic fragments, and minor polycrystalline quartz and chert. Accessories include opaque minerals and zircon (Johnson, 1982, 1984b).

The contact between the Chuckanut and the pre-Tertiary bedrock in the study area is exposed on the valley wall northwest of Oyster Creek. We did not examine the contact relations in detail. However, Schmidt (1972) observed that serpentinite (unit $Ju_h$) and the Bellingham Bay Member are locally separated by a laterite, indicating that an Eocene erosional surface or unconformity exists between the units. A high-angle fault probably exists along Oyster Creek, east of the contact with the Chuckanut, and in the Helena–Haystack mélange serpentinite unit.

A fission-track age of 49.9 ±1.2 Ma was obtained from zircon in a dacite lithic-tuff bed close to the top of the Bellingham Bay Member (Johnson, 1982, 1984b) north of the study area. Reiswig (1982) assigned early middle to late Eocene ages to pollen collected from laterally correlative strata. On the basis of the approximate source-terrane uplift ages implied by several detrital zircon fission-track ages from the base of the Bellingham Bay Member, Johnson (1982, 1984b) and Johnson and others (1983) suggest that the base of the Bellingham Bay Member could not be older than about 55 Ma and is probably younger. The lowermost part of the Chuckanut may include late Paleocene strata (for example, Mustard and Rouse, 1994; G. Mustoe, Western Washington Univ., written commun., 1996, 1997; Reiswig, 1982). An Eocene age for most of the Chuck-

anut lithostratigraphic equivalents in western Washington and the central Cascades is consistent with radiometric ages of interbedded volcanic rocks (Mustoe and Gannaway, 1997; Johnson, 1984b; Evans and Ristow, 1994).

Sedimentary cycle thickness, structures, and other criteria indicate a meandering river and adjacent flood-plain depositional environment for the Bellingham Bay Member, with overall west-northwest- to west-directed sediment transport (Johnson, 1982, 1984b). Paleocurrent, fission-track, and provenance data suggest that the potassium-feldspar-rich feldspathic sandstones were derived from uplifted crystalline basement rocks east of the Crystalline Core (Fig. 2), possibly derived from rapidly uplifted and eroded Omineca Crystalline Complex basement in north-central Washington (Johnson, 1982).

## Low-Grade Layered Metamorphic Rocks of the Northwest Cascades System

We divide the pre-Tertiary rocks of the Northwest Cascades system (Fig. 2) in the study area into two "nappe" units that are separated by a mid-Cretaceous thrust fault: the Shuksan nappe and the overlying ophiolitic Helena–Haystack mélange (HH) of Tabor (1994) or Haystack nappe of Whetten and others (1980a). (See Figs. 9, 10.)

The Shuksan nappe (see Fig. 10) includes the Easton Metamorphic Suite, which includes the Darrington Phyllite of Misch (1966) and metasedimentary and metavolcanic facies variants. (The Easton suite corresponds to the Shuksan Metamorphic Suite of Misch, 1966, and Brown, 1987.) The informally named Whitehall Creek thrust fault separates the Shuksan and HH nappes on Chuckanut, Colony, and Blanchard mountains. Evidence for a thrust fault includes metamorphic as well as lithologic and structural discontinuities across the fault contact and the spatial association of the thrust-fault zone with protomylonites and mylonites. See Discussion for the structural evidence for a significant thrust fault between the nappes and an examination of the correlations of the meta-igneous rocks in the study area with the HH. Figures 11 and 12 (see Discussion) schematically show the dominant structural features of the study area.

Our mapping is consistent with that of Tabor (1994) and Whetten and others (1988)(see Fig. 13) south and southwest of the study area and differs from mapping of Gallagher (1986) and Gallagher and others (1988), who include meta-igneous rocks in the study area with the Shuksan nappe. Our thrust-bounded lithologic packages are largely consistent with Northwest Cascades system thrust stratigraphy of Tabor (1994)(see Fig. 9) and Brown and others (1987)(Deer Peak unit shown in Fig. 10).

### MESOZOIC METAMORPHIC ROCKS OF THE SHUKSAN NAPPE OF TABOR AND OTHERS (1994)

Regionally, the Easton Metamorphic Suite (Easton suite) of Tabor and others (1993) includes the Darrington Phyllite (unit $Jph_d$), the semischist of Mount Josephine (unit $Jph_j$), as well as the Shuksan Greenschist. Phyllite and semischist occur widely in both the Bow and Alger quadrangles. The Shuksan Greenschist is sparse in the study area; we tentatively correlate well-recrystallized greenschist underlain by ultramafite in the imbricate zone separating the Shuksan and HH nappes on Anderson Mountain with the Shuksan Greenschist of the Easton Metamorphic Suite. (See unit $Jmv_h$.) This structural-lithologic correlation is consistent with the definition of the HH by Tabor (1994), who also observed imbrication of units into the HH from the structurally lower Shuksan nappe near the thrust contact.

U-Pb zircon, Rb-Sr , and various K-Ar age estimates for the Easton suite indicate a pre-Cretaceous or Jurassic protolith or depositional age for the suite. Armstrong (1980) and Brown and others (1982) proposed that the age of the oceanic protolith of the Easton suite was Jurassic, possibly Late Jurassic. A probable Middle Jurassic protolith age for the Easton is indicated by a zircon age of 163 Ma from diorite on Bowman Mountain, northeast of the Alger quadrangle, that is interpreted by Gallagher and others (1988) to form basement and subarc plumbing to the volcanic-clast-bearing semischist of Mount Josephine. (See also Brown, 1986.) We obtained a concordant zircon age of 163 ±2 Ma from the greenschist klippe on Anderson Mountain that supports a Jurassic protolith age for these oceanic units.

The Easton suite was metamorphosed in the blueschist facies at about 110 to 130 Ma (Brown and others, 1982), possibly into the Late Jurassic (Armstrong and Misch, 1987), and after an early seafloor metamorphism (Haugerud, 1980) or hydrothermal alteration event. These metamorphic events occurred prior to syn- to late-metamorphic thrust emplacement of San Juan–Northwest Cascades system nappes around 88 to 100 Ma (Brandon and others, 1988; Brown, 1987). The resultant recrystallization of the Mount Josephine and Darrington siltstone, shale, and sandstone (Tabor and others, 1994) and rare tuffs and conglomerate is consistent with geothermobarometry (400°C, 7–9 kb) by Haugerud and others (1981), Brown and others (1981), and Brown (1986). (See also Discussion.)

The first deformation (D1) fabric elements in the Easton suite include a distinct and pervasive "first" foliation (S1), a "first" lineation (L1) on the S1 surface, and rarely observed first folds (F1) of the bedding. S1 cleavage parallels bedding structures as a result of transposition of primary layering during syn-D1 blueschist-facies metamorphism. (See Fig. 12.) Easton suite rocks typically consist of granoblastic quartzose matrix with a distinct lepidioblastic S1 quartz and mica segregation layering (0.5–3 mm thick) with one (for example, Chuckanut Mountain) or locally more crenulations (typical of Anderson Mountain) of the S1 cleavage. Tight folding of S1 cleavages is locally associated with an incipient micaceous S2 foliation. Phyllites are mylonitized near the thrust contact with the overlying HH or near high-angle Tertiary faults. At outcrop scale, semischist is characterized by a strong S1 homoclinal cleavage, a strong L1 clast stretching lineation, and typically L2 crenulation lineations (F2 microfolds), but it lacks the macroscopic F2 folding of the S1 foliation that is characteristic of the phyllite. (See Discussion.)

Regionally, manganese-rich pelitic protoliths of the Easton suite reflect deep-basin (locally cherty) sedimentation on Shuksan Greenschist mid-ocean ridge basaltic crust. Areas rich in semischistose metasandstone with lesser metaconglomerate probably represent sedimentation near an island or continental arc. Units composed almost exclusively of fine- to coarse-grained semischistose metasandstone (unit $Jph_j$) with some pebble conglomerate may represent proximal (submarine fan turbidite?) facies, and phyllite-rich units may represent more distal (submarine fan?) facies. Chert (polycrystalline quartz) and lesser volcanic detritus provided much of the clastic material for the Easton suite metasandstones. Therefore, we concur with Gallagher and others (1988) that the metasedimentary portion of the Easton suite should be viewed as a complex sedimentary sequence resulting from various original sedimentary facies, not a simple accumulation of deep-water metapelite and graphitic quartz arenite. However, evidence for near-arc sedimentation

and volcanism as forwarded by Gallagher and others (1988) is restricted by our inclusion of metavolcanic greenstones and ultramafite with the overlying HH plate. Correlation of these meta-igneous units with the HH limits evidence for Easton suite near-arc deposition to relatively rare tuffaceous greenschist layers in the semischist as well as volcanic clasts in the semischistose metasandstone. Our observation that relict chert clasts, not volcanic clasts, are the dominant detrital clast component of the semischistose metasandstones makes the provenance for these metasandstones more complex. (See Discussion.)

$Jph_d$, $Jph_{dj}$, $Jph_{jd}$, $Jph_j$ **Easton Metamorphic Suite of Tabor and others (1993)(Jurassic)**—The suite in the study area includes clastic rocks and rare tuffaceous metavolcanic rocks. (See unit $Jmv_h$, p. 18, for Shuksan Greenschist.) End-member metasedimentary compositions are metapelite (shale) to siliceous argillite (Darrington Phyllite), which grades to the semischist of the semischist of Mount Josephine metagraywacke and metasandstone with increasing relict sand and gravel content. The suite is divided into:

| | |
|---|---|
| $Jph_d$ | Darrington Phyllite (<10% semischist) |
| $Jph_{dj}$ | Darrington Phyllite (10–50% interlayered semischist) |
| $Jph_{jd}$ | Semischist of Mount Josephine (10–50% interlayered phyllite) |
| $Jph_j$ | Semischist of Mount Josephine (<10% interlayered phyllite) |
| v v v | Basaltic to basaltic andesite metatuff greenschist interlayers in unit $Jph_j$ |

The Darrington Phyllite and semischist of Mount Josephine are not strictly separate rock units. Our separation of the Darrington Phyllite of Misch (1966) into fine-grained (Darrington) and coarse-grained (Mount Josephine) rock unit protoliths reflects our semiquantitative field effort to map the proportion of phyllite/semischistose metasandstone in different parts of the study area. We retain the rock unit names of previous mapping (for example, Misch, 1966; Tabor and others, 1993) but emphasize, as did Gallagher (1986), that a continuum of protolith textural types that were deposited in the same basin is represented by the general phyllite and semischist metamorphic rock designations. We observed metapelite and meta-argillite (Darrington) interlayered with semischistose metasandstone (and lesser Mount Josephine metaconglomerate) at thin-section, outcrop, and mountain scales. We divided units on the basis of outcrop-scale proportions of semischistose sandstone–metaconglomerate and of phyllite. Subsequent petrographic examination of our protolith classifications supports our field interpretations. Contacts between the Darrington and Mount Josephine subunits are gradational in the field, as reflected by the dashed contacts. However, distinct primary textural changes occur across many Tertiary high-angle faults where mostly phyllite is exposed on one side of the fault and semischist is exposed on the other side (Plate 3, cross sections A–D; see Fig. 11).

Prominent original grain-size variations from metasiltstone-metashale (phyllite) to metasandstone-metaconglomerate (semischist) occur on a scale of millimeters to a meter(s). Semischist contains very thin to medium-bedded phyllitic interlayers; massive metasandstone and pebble conglomerate zones locally display distinct grain-size variations reflecting crude to distinct primary graded bedding. Graded beds are locally observed in sand-rich rocks (for example, unit $Jph_{dj}$) and are defined by variations of the relative proportions of relict clast and protolith matrix material. Finer grained protoliths are darker, mostly as a result of primary matrix organic material that reacted to form graphite during metamorphism. Intercalations of phyllite (metasiltstone to metapelite) in semischistose sandstone occur on a scale of millimeters to meters, typically centimeters, defining very thin to thick beds; rip-up clasts of phyllite (meta-argillite) occur sporadically in metasandstones and metaconglomerates and are typically larger than other clast types.

$Jph_d$, $Jph_{dj}$ **Darrington Phyllite (Jurassic)**—Graphitic quartzose phyllite with lesser calcareous graphitic quartzose phyllite (metamarl?) to micaceous quartzite with 0 to 50 percent interlayered metasandstone and rare metaconglomerate; light green-gray, green-gray, greenish gray, light olive-gray, medium light gray, medium-gray, and light bluish gray. Dominant metamorphic minerals include polygonal granoblastic to slightly sutured quartz (3–69%, avg. 51%), lepidioblastic phengitic to sericitic white mica (0–40%, avg. 22%), chlorite (0–30%, avg. 5%), graphite (0–22%, avg. 6%), and epidote (0–5%, avg. 1%); other minerals include albite (0–15%), calcite (0–14%), actinolite (0–18%), and rare pumpellyite and probable spessartine garnet. Accessory minerals include opaques, titanite (sphene), iron oxide, and rare tourmaline. Mostly subangular, very fine sand- to silt-size (0.05–0.3 mm) relict clasts of monocrystalline and polycrystalline quartz and plagioclase occur in meta-argillaceous varieties. Gallagher (1986) reports rare lawsonite from the unit.

$Jph_j$, $Jph_{jd}$ **Semischist and phyllite of Mount Josephine (Jurassic)**—Semischistose lithic-subquartzose sandstone and rare pebble metaconglomerate and interlayered greenschist (metabasaltic tuff, described below); 0 to 50 percent interlayered phyllite; light green-gray, green-gray, light olive-gray, greenish gray, medium light gray, medium-gray, and light bluish gray. Dominant metamorphic minerals include polygonal granoblastic to slightly sutured quartz (3–39%, avg. 23%), albite (0–14%, avg. 4%), lepidioblastic phengitic to sericitic white mica (0–37%, avg. 9%), actinolite (0–38%, avg. 6%), chlorite (0–25%, avg. 9%), stilpnomelane (0–7%, avg. 1%), and epidote (0–10%, avg. 4%). Schmidt (1972) indicates that relict plagioclase grains are mostly decalcified to $An_{4-6}$ in the phyllite and are locally sericitized and that semischist contains some larger, non-albitized relict labradorite or andesine ($An_{24-35}$). Other minerals are calcite (0–10%), graphite (0–2%, avg. 1%), and pumpellyite (0–1%); accessory minerals include opaques (including pyrite), titanite, and iron oxide. Minor potassium feldspar is present in mylonitized rocks adjacent to Tertiary faults as a result of metamorphic retrogression during low temperature shear deformation.

Stretched subrounded to subangular relict sand- (typically 0.1–2 mm in diameter) to pebble-size clasts include polycrystalline quartz (approximately 40–60%), monocrystalline quartz (5–30%), and albitized plagioclase (5–30%). Other relict clasts include anhe-

dral pleochroic brown hornblende[1] (0–10%), graphitic to micaceous metamorphosed pelitic to semipelitic rip-up clasts (0–15%), and various metavolcanic clasts (mostly dacitic?)(0–15%) displaying acicular actinolite and (or) microlitic plagioclase lathwork grains in an aphanitic matrix. Pelitic to semipelitic rip-up clasts contain fine lawsonite needles[2].

Meter-thick interlayers of probably tuffaceous metabasaltic to basaltic andesite greenschist on Chuckanut Mountain (volcanic symbol, Plate 1) are light olive-gray to greenish gray with a strong metamorphic foliation that parallels the foliation in the adjacent semischists and phyllites. Similar greenschists occur on Anderson Mountain directly north of the Alger quadrangle (Fig. 3, loc. 41H). They are composed of albite, actinolite, chlorite, white mica, and epidote with minor quartz, calcite, pumpellyite, and titanite. The greenschists are continuous along strike and, where well exposed, are clearly interlayered with semischists. Schmidt (1972) described these rocks as green phyllites, recognized some relict pyroxene in these rocks, and separated, as we do, these lepidioblastic rocks from the tectonically overlying greenstones that we correlate with the overlying HH nappe.

## MESOZOIC METAMORPHIC ROCKS OF THE HAYSTACK THRUST NAPPE OF WHETTEN AND OTHERS (1980a, 1988) OR THE HELENA–HAYSTACK MÉLANGE OF TABOR (1994)

We correlate blocks of greenstone and metasedimentary rock in a serpentinite-matrix mélange overlying the Shuksan Metamorphic Suite in the study area with the Helena–Haystack mélange (HH) of Tabor (1994) and the Haystack thrust nappe of Whetten and others (1988). Tabor (1994) emphasizes that the HH contains exotic elements from the upper and lower plates (see Fig. 9) and forms an imbricate zone between the Shuksan nappe and eastern and western mélange belts (Fig. 2). Tabor states,

> "the HH mélange is analogous to the Haystack thrust plate of Whetten and others (1980a) but differs in extent and mode of formation. It represents the bounding fault between the last Mesozoic terranes (the western and eastern mélange belts) to be accreted to North America in the Pacific Northwest."

The HH nappe overlies the Shuksan nappe south of the Skagit River (Whetten and others, 1988; Tabor, 1994; see Fig. 13) and consists of a mostly chaotic assemblage of ocean-floor or island-arc greenstone–metabasalt–metasedimentary rocks and associated ultramafite. In the study area, the HH overlies the Shuksan nappe along a thrust fault zone that displays top-to-the-north kinematics. Also, alpine ultramafic bodies (tectonically emplaced ultramafic bodies or slivers common to orogenic zones) delineate the thrust fault and are absent in the underlying Easton suite. We informally name this structure the *Whitehall Creek thrust fault*; it is well exposed and exhibits macro- to microstructures associated with thrusting mostly in the Whitehall Creek–Blanchard mountain area of the Bow quadrangle.

In the study area, the HH is divided into metabasaltic greenstone (unit $Jmv_h$), metagabbroic greenstone (unit $Jigb_h$), and ultramafite (unit $Ju_h$) of mostly ophiolitic origin. The heterogeneous metamorphic rocks of Butler Hill (unit $Jhmc_h$) apparently lack metagabbro and contain phyllitic to slaty meta-argillite, metasandstone, and rare metachert blocks. All these units are commonly bounded by a scattered ultramafite matrix of probable similar age and of basal ophiolitic origin. The dominant lithologies of the HH are metabasite (unit $Jmv_h$) and ultramafite (unit $Ju_h$). On Chuckanut, Colony, and Blanchard mountains in the Bow quadrangle, greenstone (metabasalt and metagabbro) is associated with ultramafite. Well-recrystallized greenschists associated with ultramafite along a thrust contact on Anderson Mountain may represent thrust-imbricated Shuksan Greenschist along the structural contact between the Shuksan and HH nappes (Fig. 5, Plate 1). We include this unit in the HH because we tentatively interpret it to be a klippe of greenschist along the base of the HH.

HH contacts are mostly structural and originate from a combination of mélange and probably younger thrust mechanisms; a few contacts appear to be primary (see below). More commonly, contacts are faulted and contain alpine ultramafic bodies of tectonic origin. Alpine ultramafic bodies (tectonic slices) are very common along the thrust contact of the Easton Metamorphic Suite and the overlying unit (Schmidt, 1972, this study); we correlate ultramafite with the HH. Probable primary contacts at which ocean-floor basalt grades to gabbro occur on northwestern Chuckanut Mountain (Fig. 5, locs. 39, 40). There, metabasalt that was about a hundred to hundreds of meters thick grades(?) to dominantly metagabbro and probably preserves primary contacts that survived structural disruption of the Helena–Haystack unit. The trace element metabasalt geochemistry of the rocks on Chuckanut Mountain is interpreted to be mostly MORB. (See Discussion for the geochemical signature of the HH.) This evidence, combined with the association of primary pyroxenite preserved in large serpentinite bodies with metagabbro and metabasalt, provide evidence that an ophiolite is locally preserved. Our mapping and structural interpretation suggest that the underlying Easton suite in the study area lacks *primary* ultramafic rocks and contains only ultramafite derived from the HH during Tertiary high-angle faulting that further disrupted the structural and lithologic sequences in the nappes and infaulted serpentinite into the Easton suite. We interpret moderately serpentinized clinopyroxenite pods and layers mostly surrounded by thick serpentinite to be primary, partially retrogressed mantle material that mostly escaped deformation. This is suggested by the central position of the two preserved pyroxenite bodies in the most extensive and thick serpentinite body in the study area east of Oyster Creek (Plate 1; Fig. 5, locs. 37, 38). Also, the major magnetic anomaly in the Oyster Creek–Pigeon Point area (R. Blakely, USGS, written commun., 1998) reflects the thick serpentinite body underlying HH greenstones in this area (Plate 3, cross section B) and is coincident with the exposed serpentinite around Oyster Creek that we map as HH (Plate 1).

Significant disruption of an ophiolite terrane during formation of the mélange occurred, for the most part, prior to structural emplacement of the unit over the Easton suite. Many "intraformational" structural contacts date from the mélange formation; individual mélange blocks are typically hundreds of meters to locally more than a kilometer in map extent. For exam-

[1] We did not observe any detrital pyroxene in the semischist of Mount Josephine, particularly augite, suggesting that the provenance for the sandstones is not the meta-igneous rocks (units $Jmv_h$ and $Jigb_h$) as has been suggested by Gallagher and others (1988).

[2] Lawsonite (orthorhombic) was distinguished from pumpellyite (monoclinic) by the straight extinction of lawsonite versus the +22° extinction of pumpellyite on (100) cleavage. Lawsonite occurs as nonpleochroic, euhedral, fine rectangular tabular crystals that have rhombic cross sections with good (010) and (001) cleavage; pumpellyite generally occurs as pleochroic crystals of varied form or habit (generally fibrous) with moderate (001) and (100) cleavage (Kerr, 1977).

ple, the heterogeneous unit on Butler Hill (unit $Jhmc_h$) contains small to very large (tens to hundreds of meters or more) serpentinite-encased blocks of metabasite and metasedimentary rock. A block-in-serpentinite mélange arrangement is substantiated by a few water-well logs (for example, Fig. 5, loc. 2). These wells show serpentinite below greenstones and, along with our surface mapping, indicate that matrix serpentinite surrounds mélange blocks in three dimensions. On Butler Hill, however, a probable unsheared depositional contact between metasedimentary rocks and metabasites suggests that protoliths of the metasedimentary rock of the mélange were deposited with metavolcanic rock of the mélange in an oceanic environment.

Three nearly concordant U-Pb zircon age estimates on plagiogranite from the HH directly south-southeast of the study area indicate an intrusive age of about 160 to 170 Ma for the unit (Whetten and others, 1980a, 1988). These ages are similar to U-Pb ages and radiolarian fossil ages from the Fidalgo ophiolite obtained by Brown and others (1979); Tabor (1994) includes the Fidalgo ophiolite in the broadly defined HH. A sample of chert (Fig. 5, loc. 4) contained coarsely recrystallized radiolarians that could not be identified to genus but indicate a Mesozoic, questionable Jurassic age (C. D. Blome, USGS, oral commun., 1998)

$Jhmc_h$ **Heterogeneous metamorphic rocks of Butler Hill (Jurassic)**—Metabasalt, phyllitic to slaty graphite-bearing meta-argillite, metasandstone, and rare metachert (Fig. 5, loc. 4); locally contains serpentinite matrix pods and layers (see unit $Ju_h$). Meta-argillite is medium gray, dark gray, and medium dark gray; metasandstone is medium light gray. Dominant metamorphic minerals in meta-argillite include fine-grained quartz (17–50%, avg. 30%), albite (3–5%), white mica (0–20%, avg. 13%), and Fe-chlorite (0–20%, avg. 8%); accessory minerals include graphite (0–12%, avg. 8%) with unknown dark matrix material (0–15%), iron oxide (0–2%), and rare possible pumpellyite. Angular to subangular, <0.05–0.1-mm relict clasts consist mostly of monocrystalline quartz, with lesser plagioclase and white mica (rip-up) grains. Dominant metamorphic minerals in metasandstone include quartz (~6%), plagioclase (~5%), white mica (~10%), chlorite (4%), and minor graphite and iron oxide. Relict clast types (0.1–0.4 mm) in metasandstone constitute about 75 percent of the rock and include polycrystalline quartz (~40%), plagioclase (~30%), and monocrystalline quartz (~25%), as well as meta-argillite (typically white-mica-rich) rip-up clasts to 2 mm; the metasandstone locally includes lithic grains (<1 mm in diameter).

The unit is characterized by a strong slaty cleavage that is phyllitic in micaceous variants. Rootless, disharmonically folded, disassociated, thin quartz veins (<1 mm wide) cut across the cleavage. The quartz veins appear to be shear folded during cleavage formation. Unlike structural features in the Easton suite, metasedimentary rock cleavage and bedding are locally distinctly nonparallel, quartzose metamorphic segregations are lacking, and the metasedimentary rocks are less recrystallized.

Meta-argillite is semipelitic to locally pelitic and occurs as beds typically a few centimeters to decimeters thick in metasandstone or as massive beds between sandstone outcroppings. Bedding is microscopically defined by decreased graphite and matrix content and increased clast size from silt or very fine sand to medium sand. Sedimentary structures in the meta-argillite include local graded bedding from meta-argillite to metasandstone. Metasandstone contains rare ripple cross-lamination. Rip-up clasts of meta-argillite are common in the sandstone, and they are commonly coarser grained than the crystal-lithic sand-size clasts of the unit.

$Jmv_h$ **Metabasite of the Helena–Haystack mélange (Jurassic)**—Mostly augite-bearing greenstone (metabasalt) and greenstone pillow breccia; light or medium green-gray, greenish gray, light olive-gray, grayish green. Dominant metamorphic minerals include albite (8–50%, avg. 31%; includes relict plagioclase laths), acicular actinolite (0–45%, avg. 15%), poikiloblastic and matrix epidote (0–20%, avg. 7%; mostly pistacite), and Fe- and Mg-chlorite (0–28%, avg. 9%); lesser metamorphic minerals include quartz (0–8%, avg. 2%), white mica (0–15%, avg. 1%), stellate or acicular pumpellyite (0–25%, avg. 5%), prehnite (0–2%, avg. 0.1%), calcite (0–10%, avg. 2%), aragonite (0–6%, avg. 0.4%), and stilpnomelane (0–15%, avg. 1%). Relict igneous minerals include locally sausseritized and albitized, euhedral to subhedral plagioclase laths (0.1–2 mm long), subhedral augite (0–25%, avg. 6%; 0.5–4 mm in diameter), corroded and replaced hornblende (typically ~1 mm long; 0–10%, avg. 1%), and locally unknown aphanitic semi-opaque matrix (0–25%, avg. 6%). Accessory minerals include titanite (0–4%, avg. 2%), opaques (0–2%, avg. 0.2%), and iron oxides (0–2%; avg. 1%). Gallagher (1986) reported rare blue Na-amphibole from metabasaltic rocks in the Bow quadrangle that we correlate with the HH.

A well-recrystallized greenschist body occurs as a klippe on Anderson Mountain (Fig. 5, loc. 18; Plate 1). The greenschist with localized preserved medium-grained igneous textures consists of granoblastic to slightly sutured quartz (12–15%), interstitial and relict albite (25–28%), Fe-chlorite (8–30%), and epidote (0–17%) with lesser metamorphic minerals that include acicular actinolite (6–15%) and stilpnomelane (3–4%). Accessory minerals include minor possible pumpellyite (0–1%). Relict hornblende (up to 35%) occurs in the minor, medium-grained portions of this well-foliated unit. This greenschist differs from the greenstones of the HH in the degree of recrystallization; we tentatively correlate it with the Shuksan Greenschist. We obtained a nearly concordant $^{206}Pb/^{238}U$ zircon age of 163.8 ±0.2 Ma and a $^{207}Pb/^{235}U$ zircon age of 164.0 ±0.2 Ma from this body (Appendix 6). Similarly, we obtained a nearly concordant $^{206}Pb/^{238}U$ zircon age of 163.2 ±0.4 Ma and a $^{207}Pb/^{235}U$ zircon age of 162.5 ±3.5 Ma from the HH metagabbroic body on Colony mountain (Appendix 6).

Metabasalts are commonly heterogeneously mylonitized to locally massive, typically with subhedral relict plagioclase laths that are mildly to strongly saussuritized, blocky augite, and lesser anhedral, commonly chloritized hornblende. Actinolite occurs interstitially as a static or semi-aligned matrix phase. Random to foliation-aligned actinolite needles occur in pressure shadows or have formed during microboudinage and

stretching associated with thrusting as replacement products of hornblende. Calcite, chlorite, and pumpellyite commonly occur with accessory minerals; quartz occurs in extensional veins perpendicular to the stretching direction. (See Discussion for microstructures.) Less common but notable petrologic relations include pumpellyite replacing augite and normally zoned relict plagioclase laths.

Pillow structures are common and locally well formed (for example, Fig. 5, loc. 28; Fig. 3, site 2F). Pillow breccia contains angular to subangular clasts. Clast textures are extremely varied, but most clasts are aphanitic or microlitic with felty feldspar textures. Some concentric microstructures are similar to primary spherulitic or hyalopilitic pillow or pillow breccia textures. Other relict igneous textures include chlorite- or pumpellyite-filled vesicles.

$Jigb_h$ **Augite-bearing metagabbro of the Helena–Haystack mélange (Jurassic)**—Medium-grained, mylonitic, or protomylonitic metagabbro or microgabbro; dominantly light green-gray, light greenish gray, greenish gray, light olive-gray, olive-gray, and dark greenish gray. Metamorphic minerals include albitized plagioclase (20–40%, avg. 35%; includes relict plagioclase laths and matrix), acicular actinolite (5–35%, avg. 17%), epidote (0–16%, avg. 6%), Fe-chlorite (0–30%, avg. 5%), Mg-chlorite (0–15%, avg. 3%), and pumpellyite (0–15%, avg. 6%). Dominant relict igneous minerals include mildly to strongly saussuritized plagioclase laths (0.4–3 mm long; see percentage above), augite (0.2–3 mm in diameter; 0–45%, avg. 12%), and pleochroic light-green or brown hornblende (0.5–1 mm long; 0–34%, avg. 8%). Augite is rarely uralitized (rims of amphibole around augite) and rarely exhibits primary blastophitic textures (Schmidt, 1972). Minor metamorphic minerals include quartz (0–8%, avg. 3%), potassium feldspar (0–2%, avg. 0.3%), white mica (0–4%, avg. 0.6%), calcite (0–11%, avg. 1%), and aragonite (0–5%, avg. 0.4%). Accessory minerals include opaques (0–1%), titanite (0–6%, avg. 1%), iron oxide (0–2%, avg. 1%), and rare clinozoisite or zoisite. Rare prehnite was tentatively identified from the unit.

Plagioclase is mostly albitized ($An_{4-5}$). Saussuritization of much of the plagioclase indicates that prior to metamorphism the plagioclase was more calcic (>$An_{50}$?) and thus these rocks are categorized as gabbros. Increased saussuritization in the cores of a few samples suggests normal igneous plagioclase zonation for these intrusive rocks. In the Chuckanut Mountain area, Gallagher (1986) categorized the more silica-rich intrusives as metadiorites ($SiO_2$ 53–60%) and less silica rich rocks as metagabbros.

Our microscopic studies show that (1) hornblende is ragged and replaced by actinolite or actinolite with chlorite and (2) subhedral augite grains are locally replaced by actinolite or actinolite plus chlorite. Actinolite occurs in pressure shadow tails or microboudinage zones, and chlorite, quartz , or quartz and pumpellyite occur in pressure shadows or veins; pumpellyite rarely replaces relict plagioclase laths.

$Ju_h$ **Ultramafite of the Helena–Haystack mélange (Jurassic)**—Serpentinite with lesser talc schist, talc-tremolite schist, and tremolite schist with rare allotriomorphic-granular textured, diopside-bearing clinopyroxenites; greenish black, green-gray to light olive-gray; typically weathers to a distinctive yellow or orangish yellow-gray. Serpentinites contain serpentine-group minerals with localized veins of chrysotile asbestos (serpentinite minerals 80–90%, avg. 87%) with accessory talc, magnesite, chromite, magnetite, and rare epidote or pyroxene ghosts. Talc and (or) tremolite schists consist of talc (5–95%), acicular semi-random to well-aligned tremolite (5–95%), serpentine minerals (0–5%), with minor Fe- or Mg-chlorite (0–10%). Olivine(?) pyroxenite and pyroxenite consist of augite (about 35%) or diopside (about 80%) with serpentine minerals (15–40%), magnesite (5–17%), and accessory actinolite (after augite), chromite, and magnetite. (Olivine is readily replaced by serpentine and may be the primary serpentinized mineral in the pyroxenites.)

Ultramafic bodies occur as small to mappable (Plate 1; see Fig. 11) tectonic pods and layers in three fairly distinct field settings:

(1) As generally small bodies forming intraformational mélange matrix (for example, in unit $Jhmc_h$ on Butler Hill).

(2) As mappable to small bodies concentrated along the Whitehall Creek thrust or thrust zone (Plate 1, see Fig. 14). The ultramafic bodies are spatially and genetically related to metavolcanic rocks including greenstones (metabasalts and metagabbro). Serpentinite surrounds rare pyroxenite; metagabbroic blocks occur sporadically in some of the thick ultramafic bodies.

(3) As tectonically remobilized ultramafic lenses along high-angle Tertiary faults throughout the study area, Tertiary faulting having displaced the weak serpentinite from the HH (1 and 2, above) into the lower Shuksan nappe. For example, serpentinite along the Anderson Mountain fault zone (Plate 1) is spatially associated with a HH klippe and could demark a high-angle, Tertiary fault-modified mid-Cretaceous thrust zone. High-angle faults on Chuckanut Mountain contain serpentinite layers and pods, particularly near the HH (Plate 3, cross sections A–D).

# DISCUSSION

## Pleistocene Glacial Deposits, Depositional Environments, and Paleogeography

Sparse previous Quaternary geologic mapping in the quadrangles (Fig. 3) has provided only a glimpse of the complexities of the deposits, depositional facies, and environments implied by the glacial deposits of the uplands (Plate 1; Plate 3, cross sections E–G). Dragovich and Grisamer (in press) further describe the Holocene Samish and Skagit valley fills and some aspects of the glacial paleogeography and stratigraphy. Here, we compare and contrast our findings and observations with those of other glacial studies in and around the study area.

### SUMAS STADE

The nature, extent, and significance of the latest-glacial Sumas Stade ice resurgence in Whatcom County north of the study area are controversial topics and currently under revision. Mapping by Easterbrook (for example, 1979) suggested that the Sumas

deposits in the study area were simply valley-train outwash deposits originating from the Sumas ice re-advance just south of the U.S.–Canadian border. In his model, the major meltwater pathway through the westernmost northern Cascades would have been the Columbia valley–South Fork Nooksack River valley–Samish River valley via the open Skagit River valley (for example, Easterbrook, 1992, 1979; Fig. 1, arrows).

Recently, Easterbrook and Kovanen (1996a), Kovanen (1996), and Kovanen and Easterbrook (1996a,b) interpreted the Sumas re-advance from the Coast Mountains of British Columbia as concurrent with major alpine ice advance down the three major forks of the Nooksack River. These alpine deposits are mapped by Kovanen (1996) in the middle, north, and (most importantly) the south forks of the Nooksack River directly north and northeast of the Alger quadrangle. This scenario complicates the idea of a simple continuous outwash valley train originating near the U.S.–Canadian border and terminating in the study area. The composition of Sumas deposits in the study area may support a model of latest-glacial alpine ice contribution from upper reaches of the Nooksack River north-northeast of the study area. Cobbly gravel Sumas outwash deposits in the study area contain significant percentages of distinctive rock units northeast of the study area, including Twin Sisters dunite and probable Mount Baker andesite, consistent with a derivation of the ice from the western North Cascades. However, the presence of these clasts in the deposits does not preclude simple mixing of far-traveled outwash from a Sumas ice front near the U.S.–Canadian border with detritus from local sources such as the Nooksack River (R. A. Haugerud, USGS, oral commun., 1997). Qualitatively, Sumas outwash in the study area appears to be coarser than much of the Sumas outwash in the Deming quadrangle (Fig. 1), opposite to the expected overall clast-size trend. A qualitative estimate of average grain size in the Kendall and Deming quadrangles by Dragovich and others (1997d) *suggests* that outwash clast size diminishes to the south from cobbly gravel in the Kendall quadrangle to sandy gravel in the Deming quadrangle with a higher percentage of sand in the Deming quadrangle. In the present study area, terraced cobbly gravel deposits reflect either (1) a coarse sediment load of the Sumas braided streams emanating from near the border, contrary to our previous qualitative suggestion of a north-to-south reduction of grain size (Dragovich and others, 1997d) or (2) an abundant sediment load from alpine glaciation down the Nooksack valleys directly north of the study area.

The presence of Sumas outwash valley-train deposits in the study area (Easterbrook, 1979) is confirmed by our surface and subsurface mapping along the Samish River valley, which appears to overfit the present Samish River erosive power. The Samish River valley owes most of its present geomorphology to Vashon, Everson, and Sumas Stade or Interstade glacial sculpting and deposition. The Sumas deposits contain rip-up clasts of, and overlie, Everson deposits. Glaciomarine drift is typically observed under Sumas deposits (Easterbrook and Kovanen, 1996b; Dragovich and others, 1997b,c) in the major valleys of the Kendall and Deming quadrangles north of the study area (Fig. 1). Terraces 8 to 30 ft above the modern Samish River flood plain and perched terraces 80 to 120 ft above the flood plain are composed of Sumas outwash. During late Sumas Stade recession and early Holocene time sea level dropped to within a few tens of feet of its present position. As a result, fluvial incision excavated the Samish River valley and incised the Sumas valley train outwash deposits, producing these isolated outwash terraces.

We equate the Samish River excavation and incision with re-equilibration of the river to a relatively lowered marine base level during the latest Pleistocene to Holocene. The presence of Sumas deltas at the junction of the Sumas outwash valley trains and the estuarine lower Skagit valley (Easterbrook, 1979) is confirmed by (1) the occurrence of fine bottomset beds along the southernmost portion of one of the deltaic deposits (Fig. 5, loc. 5, 6, 7) and (2) observation that major valleys, such as the Skagit River valley, fed by active Cascade volcanoes, such as Glacier Peak, carried enormous volumes of sediment. This sediment contributed to rapidly prograding deltaic systems during the Holocene (for example, the Puyallup embayment; Dragovich and others, 1994). By analogy, rapid deltaic progradation rates for major valley deltaic systems such as the Skagit River suggest massive infilling of the lower Skagit valley during the Holocene and imply a marine embayment along the lower Skagit valley during the Sumas Stade. Topset bed altitudes suggest that relative sea level was about 100 ft higher than present sea level during the Sumas Stade (Easterbrook, 1979; this study).

The valley now contains only a veneer of Holocene Samish River fluvial deposits and has been downcut to or into the Everson glaciomarine section along its upper part. (See Appendix 3, water well 558). The Samish River has also cut into and removed most of its Sumas outwash fill and stranded outwash in erosional terraces, pockets, and perched valley trains above the present Samish River flood plain. Perched Sumas erosional terraces along the Samish River valley (for example, Fig. 5, locs. 8, 12, 13; see also Plate 3, cross sections F, G) are 10 to 120 ft above the present river. The depth of this incision is about the same as the total latest Sumas or Holocene sea-level drop—about 100 ft—implied by the altitude difference between Sumas deltaic topset beds (see unit $Qgod_s$) and present sea level.

We tentatively suggest that the presence of boulders in locally cobbly sands and gravels indicates that Sumas outwash in some places in the study area contains glacier outburst flood deposit(s). These catastrophic floods are capable of transporting such relatively poorly sorted, locally bouldery sandy gravel deposits.

## EVERSON INTERSTADE

The Everson Interstade of the Fraser glaciation began with marine incursion during retreat of the Puget glacial lobe and ended in the Fraser lowland during the advance of Sumas ice (Armstrong and others, 1965, p. 327). The maximum altitude of the resultant blanket of generally gravelly clay to clay glaciomarine drift in the northern Puget Lowland (Easterbrook, 1962; Armstrong and others, 1965) increases to the north and locally to the east as a result of greater postglacial isostatic rebound in those directions (for example, Dethier and others, 1995).

Pioneering work by Easterbrook (for example, 1962), Armstrong and Brown (1954), and Armstrong and others (1965) led to the recognition of the importance of glaciomarine sedimentation in the northern part of the Puget Lowland. Glaciomarine diamicton is formed by mixing of ice-rafted sediment such as gravel and boulder dropstones with fine marine deposits such as silt and clay. The resultant deposit is typically a low-density, commonly clayey diamicton locally containing shells. However, the widely held view that late-glacial sediments are dominated by glaciomarine diamicton of intermixed iceberg melt-out and marine origin is oversimplified. Several recent detailed glaciomarine stratigraphic studies have emphasized the diverse nature of the Everson deposits (Dethier and others, 1995, 1996; Pessl and others, 1989; Croll, 1980; Carlstad, 1992; Domack,

1982, 1983, 1984). The varied depositional facies and stratigraphies are the result of a complex interplay of ice-marginal and distal sedimentary environments within the context of *both* marine ice shelf and stranded-ice conditions over time. Sedimentary facies reflect ice-marginal fluvial-alluvial fan, beach, deltaic, turbidite depositional settings and a more open-water marine setting in which ice-rafted and suspended sediment constantly dropped to the basin floor.

We divide the Everson deposits into three general map units: outwash (unit $Qgom_e$), fine sediments and diamicton (unit $Qgdm_e$), and beach or emergence deposits (unit $Qgom_{ee}$) (Fig. 5). Unit $Qgdm_e$ includes both ice-rafted proximal and distal marine diamicton deposits and corresponds to the mass-flow, ice-rafted, and dispersed meltwater facies of Domack (1982, 1983) or the marine diamicton and marine subtidal deposits of Dethier and others (1996). Unit $Qgom_e$ includes both terrestrial fluvial and alluvial fan deposits and proximal marine deltaic and turbidite facies, corresponding to the turbidite channel and proximal meltwater fan facies of Domack or the marine outwash deposits of Dethier and others (1996)(Figs. 6, 7).

Two principal findings result from our mapping and subsurface analysis of the Everson deposits in the study area:

(1) The Chuckanut Mountain–Anderson Mountain bedrock promontory was the most significant topographic obstacle to Everson Interstade ice recession via simple open-water ice calving in the northern Puget Sound region. The promontory led to ice stranding, stagnation, and significantly increased deposition of terrestrial to marine sand and (or) gravel adjacent to this promontory.

(2) The Everson glaciomarine sequence in the study area is an overall fining-upward sequence (OFUS) from proximal, moderately to well-sorted fluvial-deltaic-turbiditic gravels and sands to moderately distal clayey (dropstone) diamictons to distal clays containing few or no dropstones.

The upward-fining sequences reflect progressively more northern ice limits producing more distal, lower energy sedimentary environments (Fig. 7) (for example, Plate 3, cross sections E–G; Appendix 3, wells 116, 311, 315, 480, 588, 669, 671, 679, 683). An OFUS is the direct result of ice-front retreat whereby localized proximal terrestrial to marine facies are overlain by generally more distal marine facies during ice retreat. Departures from the OFUS are the result of the complexities of the ice-marginal environment or poor documentation of some strata in water wells. For example, we envision sand or gravel outwash interlayers in diamicton or clay as shifting submarine outwash conditions (for example, Figs. 6–8) in which delta-front or turbidite grain underflow outwash is interlayered with more distal marine deposits (for example, Fig. 5, loc. 24). Similarly, some diamictons deposited adjacent to the ice front and interlayered with outwash may be flow till or the sediment flow facies of Domack (1983) where till has flowed onto proximal outwash.

### Deglaciation and Ice Stranding on the Promontory

Paleogeography controlled the distribution, thickness, and types of glaciomarine and terrestrial deposits associated with Everson deglaciation. Stranding of ice on bedrock topographic promontories led to ice stagnation and a significant departure from the coeval open-marine deposition of fine sediments and diamicton. The Chuckanut Mountain–Blanchard mountain–Colony mountain–Anderson Mountain bedrock promontory along the northern part of the study area (Figs. 5–7 and Plate 1) forms a semi-continuous mountain chain that connects the bedrock of the San Juan Islands with the northwestern Cascades. This promontory is the most significant barrier between the southern Puget Sound and the glacial ice source in the Coast Mountains of British Columbia and must have supported a temporary cover of stranded glacial ice. Stranding and stagnation slowed Puget lobe ice-front retreat on the promontory relative to floating ice off the promontory, where floating ice was subject to effective backwasting mechanisms such as ice-front calving. (For example, see Powell, 1984). "Glaciers that calve into tidewater can retreat rapidly, owing to the relatively high temperature of marine water and to tidal effects" (Thorson, 1980). The probable development of calving bays in the tidewater portions of the Puget lobe (for example, Strait of Juan de Fuca) resulted in the deep marine basins of the Puget Lowland becoming deglaciated before the adjacent uplands covered by land-based ice (for example, Thorson, 1980; this study).

Stranding and stagnation resulted in high sedimentation rates and thus a thick accumulation of recessional deposits adjacent to the promontory. This is indicated by the overall thickening and coarsening of the Everson marine section toward the promontory. Fossil marine shells or even shell fragments were not found in *any* Everson sediments near the promontory. We observed some possible marine fossil fragments in distal marine clays on western Bay View Ridge of the Bow quadrangle, an area significantly south of the promontory. We also obtained a shell age of 13,270 ±50 yr B.P. from marine diamicton near the glaciomarine limit (see below) on Burlington Hill south of the study area. This shell-bearing diamicton is typical of the more open marine, fossiliferous Everson dropstone diamictons south of the promontory as well as in the Whatcom basin (Fig. 1) north of the study area and the promontory. Marine clay sedimentation implies a more distal setting but not necessarily low sedimentation rates. Given the relatively short time span (~2,500 yr) of the Everson Interstade, high sedimentation rates are inferred from field observations and several wells that contain thick (locally more than 300 ft) accumulations of diamicton and clays (Plate 3, cross sections E–G). Turbidity, high sedimentation rates, and other factors such as low salinity south of the promontory would have discouraged establishment of marine organisms near the stagnating ice front. Powell (1984, p. 40) states,

> "fossils may be absent from ice-proximal sediments because of poor lighting under an ice shelf, high environmental energy at the glacier front, and very high sedimentation rates and brackish water in melting/freezing base glacier regimes."

Combining the map pattern of reported (Appendix 2) shell locations and the lack of shells or shell fragments virtually throughout the study area indicates that a connection exists between the promontory, high sedimentation rates, lack of fossils, sedimentary record near the promontory, and lack of strandlines on the promontory.

Distinct lobes of terrestrial to marine outwash grade south from nonmarine gravelly glacial outwash above the glaciomarine limit (see below) and on the promontory to sandy gravels to sands and sandy silts (see Plate 1 and 2, fining) south of the promontory. These sands and silts are locally rhythmically bedded and may record turbidite-style deposition as described by Domack (1984). Elevated outwash on Anderson and Chuckanut Mountains (Fig. 5, for example, locs. 20, 33) contain a high proportion of angular to subrounded phyllite and vein quartz detritus, indicating their local basal-ice source. Local clast derivation provides evidence for a mostly unfrozen, meltwater-rich, ice base capable of eroding local bedrock. (See Powell, 1984,

## A Vashon Stade ice advance (Alger quadrangle)

Deposition of advance outwash over the previous intraglacial topography.

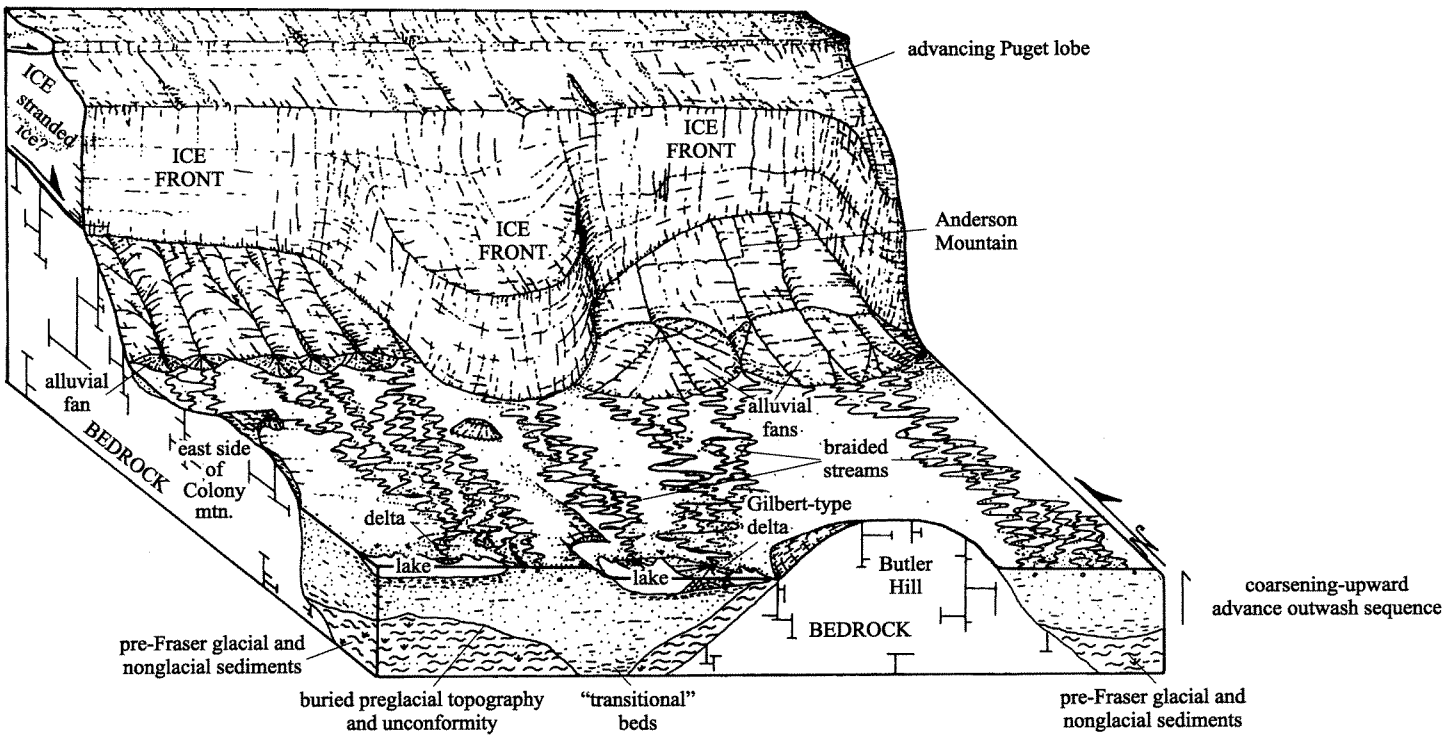


## B Everson Interstade ice recession (Alger quadrangle)

Stagnating and thinning ice, till deposition, and subglacial creation of the Samish River valley.

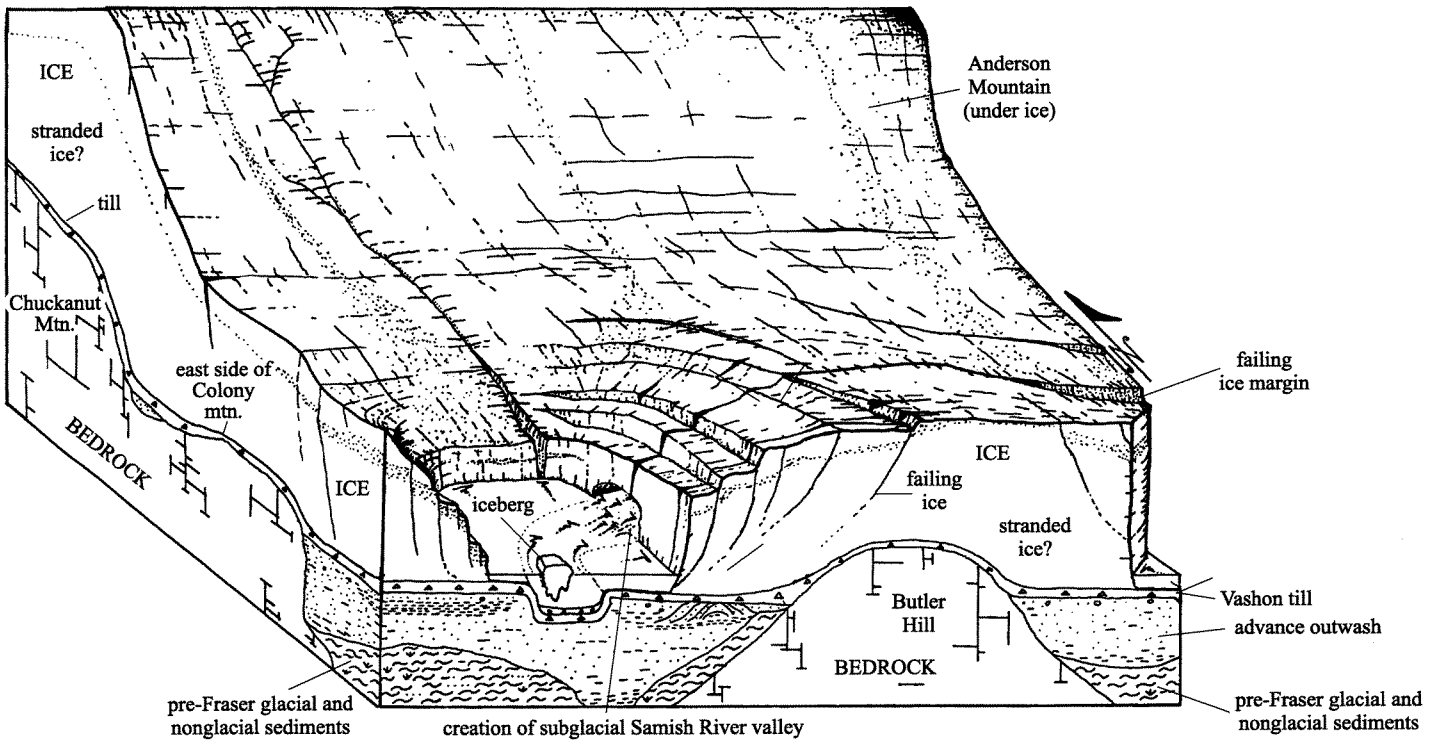

## C Everson Interstade ice recession (Alger quadrangle)

Ice stagnation on Chuckanut–Anderson Mountain promontory and further glaciomarine sediment deposition.

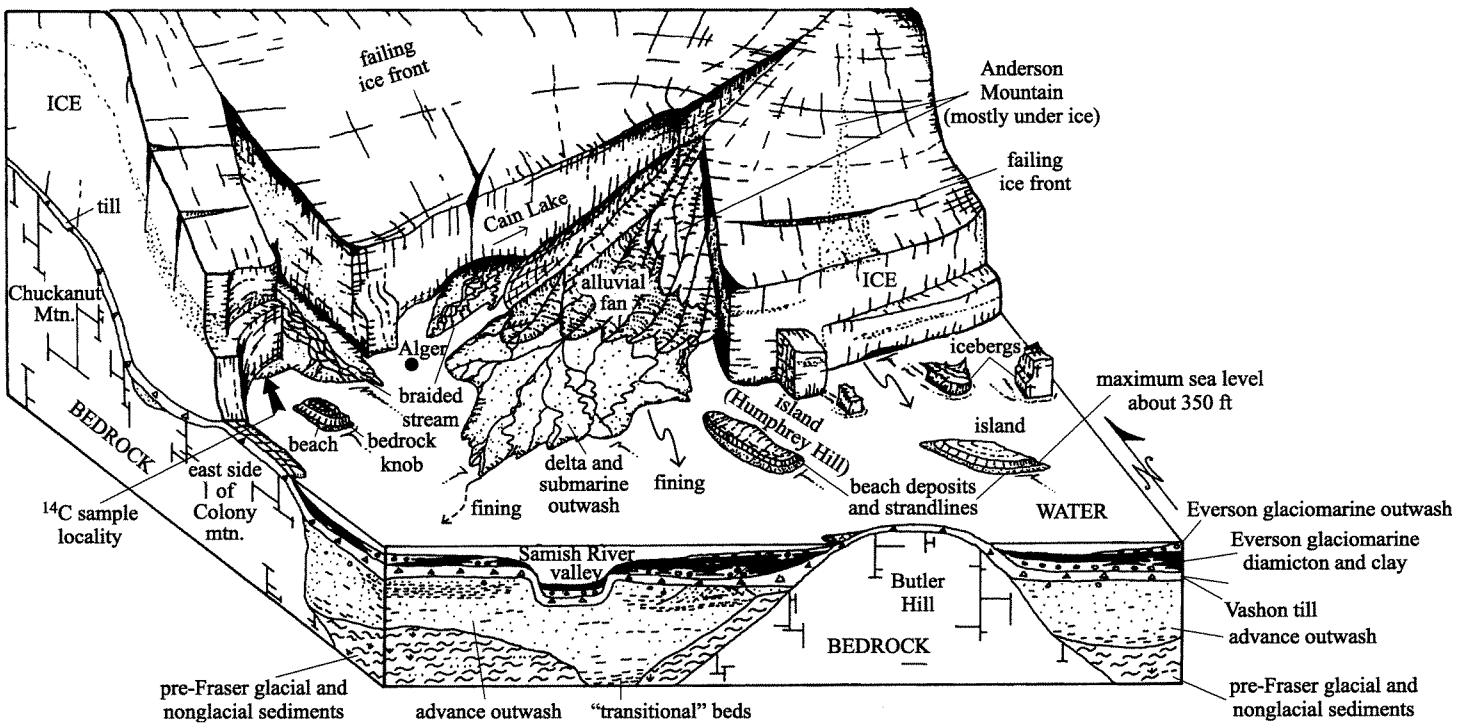


**Figure 6.** Schematic block diagrams showing the interpreted Vashon Stade advance (**A**) and Everson Interstade recessional paleogeography and depositional setting for the Alger quadrangle. The degree of glacial ice thinning is a critical factor in controlling the depositional setting of the Everson Interstade stratigraphy (**B, C**). Thin ice results in a mostly floating ice front, less stranding, and increased ice-marginal outwash sedimentation. The overall distribution and thickness of Everson outwash sediments indicates ice stranding on the promontory north of the Skagit River valley. See Figure 7 for a more detailed schematic of the inferred Everson Interstade stratigraphy and depositional setting. View to the north-northeast.

for glaciomarine processes and inductive lithofacies modeling of ice shelf and tidewater glacier sediments based on Quaternary examples.) These phyllite-rich, fluvial-deltaic-alluvial fan bodies can be continuously traced southward below the glaciomarine limit to sand and locally silt outwash of similar phyllitic composition. Similarly, water-well and geotechnical boring logs also typically describe dark, shaley (phyllitic) clasts in the Everson outwash gravels. We have traced gravelly Everson outwash on the promontory to sand outwash deposits directly south of the promontory off both Chuckanut (Fig. 5, loc. 32) and Anderson (Fig. 5, locs. 14, 17) Mountains. Gravelly outwash above the glaciomarine limit near Colony mountain (Fig. 5, near loc. 26) is higher but at the same stratigraphic level as outwash sands that contain lenses of glaciomarine diamicton and clays to the south of the promontory (Fig. 5, loc. 24). These uppermost outwash deposits also locally interfinger with fine glaciomarine drift along southernmost Anderson Mountain (Fig. 5, locs. 15, 16). Powell (1984, p. 39) concludes that,

> "subglacial and lateral meltwater streams are extremely important influences on the lithofacies produced under melting/freezing base glacier regimes. They supply the majority of mud to dropstone diamictons and dropstone muds and contribute facies that are indicative of grounding line proximity. Ice proximal glaciomarine sediment is probably more stratified and reworked under tidewater than [continental] ice shelf regimes because it has a higher energy environment from waves, iceberg calving, and higher subglacial stream discharges."

The reversal of the fining-upward sequence near the promontory, with outwash generally on top of the glaciomarine diamict (Figs. 5, 7, 8), suggests that stagnation-sedimentation and (or) sea-level fall (as result of early glacial rebound) induced a progradation of the stratigraphic sequence.

Very latest Pleistocene and Holocene erosion and dissection of the extensive outwash bodies on the promontory are important in latest glacial paleogeographic reconstructions. For example, erosively truncated outwash bedding surfaces on the steep slopes of southern Chuckanut Mountain imply (1) a much more extensive fluvial-alluvial fan-deltaic outwash complex than presently observed and (2) that this complex has been dramatically truncated or undercut by Holocene erosion (such as by lateral incision along the southwest part of Blanchard and Chuckanut Mountains by the ancient Skagit River and (or) by marine bluff backwasting).

Two factors may play a key role in the outline or geometry of the ice front during Everson deglaciation:

(1) Ice stagnation on the promontory probably locally slowed the disintegrating Puget lobe; and

(2) Deep-water reaches of the Puget Sound must have existed in late glacial times. These deep marine basins (including the present deep Puget Sound troughs) must have supported, at least locally, floating glacial ice shelves. Ice shelves are subject to breakup and fairly rapid backwasting via mechanisms such as ice calving. "Ice retreat, the marine incursion, and locally deep troughs created highly embayed, calving margins

on the ice lobes (Thorson, 1980) in the northern Puget Lowland" (Dethier and others, 1995). We offer that rapid backwasting of the Everson ice through the deep channels of the San Juan Islands and into the Bellingham Bay area produced a deeply embayed ice margin with ice occupying the promontory while ice-free conditions existed in the marine embayments (for example, Bellingham Bay and other Puget Sound troughs west to northwest of the study area). Relatively thick Everson sedimentary sequences occur north and south of the promontory (for example, Whatcom basin, Fig. 1). These basins also contain relatively more glaciomarine diamicton, underscoring the role of more open glaciomarine sedimentation away from topographic barriers and terrestrial sediment sources during deglaciation. This point is further exemplified by Pessl and others (1989), who mapped extensive Everson Interstade continental recessional sequences at the interface of the Cascade Range and the Puget Lowland and directly south of the study area. In general, they mapped more glaciomarine diamictons, silts, and clays away (basinward) from the Cascade Range. Near upland areas such as the Cascade foothills and other topographic highs, stranded ice and meltwater constructed ice-contact, outwash, and alluvial fan deposits that are higher energy, lateral, temporal equivalents of the glaciomarine diamictons, silts, and clays deposited in more quiescent marine basins. Pessl and others (1989) ascribe their general recessional-continental deposits unit to tidal flat and estuarine, ice-margin marine, shallow marine, and distal glaciomarine depositional settings similar to our inferred Everson depositional settings.

### Sea Level Information and Ice-Contact Deposits

The latest Pleistocene (pre-Sumas) lower Skagit valley appears to have been a marine embayment whose outline shifted as the isostatically depressed crust rebounded from the Vashon ice load (Easterbrook, 1979; Siegfried, 1978; this study; Dragovich and Grisamer, in press). The Everson glaciomarine limit (EGL) in the study area (340–360 ft; 104–110 m) is well defined by the

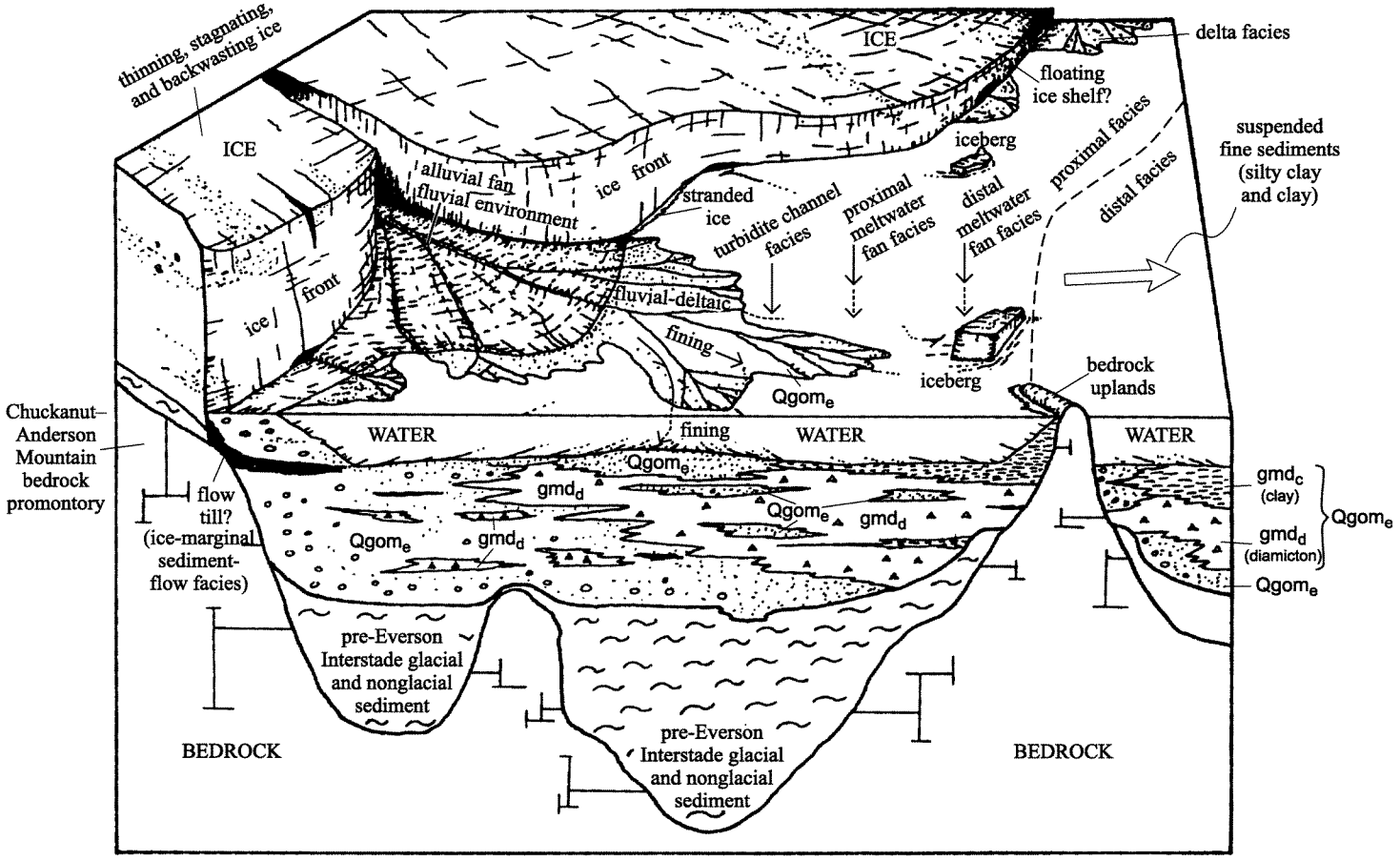


**Figure 7.** Schematic block diagram showing the interpreted Everson Interstade recessional paleogeography and depositional setting. Everson Interstade unit Qgdm$_e$ is subdivided into units gmd$_d$ (diamicton) and gmd$_c$ (clay). (See Plate 3, cross sections E–G, and table accompanying Appendix 3.) fining →, schematically shows the inferred depositional environment of the Everson glaciomarine outwash (unit Qgom$_e$) wherein mostly gravelly terrestrial alluvial fan-fluvial sediments fine to the south (below the glaciomarine limit) to deltaic-turbidite sands and silty sands that are locally rhythmically bedded. (Also see Plate 1.) Everson stratigraphic fining, thinning, and fossil distribution information indicate ice stagnation on the Chuckanut–Anderson Mountain promontory in the study area. Water-well logs and field observations indicate an *overall* upward-fining sequence from lower ice-proximal outwash deposits (unit Qgom$_e$) to more distal diamicton representing ice-rafting of sediment (unit Qgdm$_e$) away from the ice front. This sequence is commonly capped by silty clays and clays (also included in unit Qgdm$_e$) that contain little or no dropstone gravel and represent environments away from significant iceberg influence and (or) mostly distal meltwater fan sedimentation (Appendix 3, for example, water wells 116, 311, 315, 480, 588, 669, 671, 679, 683; Plate 3, cross sections E–G). View to the north-northeast.

highest glaciomarine diamictons and clays and is consistent over the study area (Plate 1; Plate 3, cross sections E–G). South of the bedrock promontory, we repeatedly mapped low-density, typically clayey marine deposits up to the EGL and observed there a contact with older glacial deposits, commonly Vashon till (for example, Fig. 5, loc. 11). Subsurface data (Dragovich and Grisamer, in press) suggest that the EGL rises slightly to the north-northeast. For example, the EGL near Cain Lake just north of the Alger quadrangle is nearly 360 ft. This limit is consistent with the EGL projected into the study area by Dethier and others (1995) and Mathews and others (1970); the EGL increases to the north toward the Coast Mountains of British Columbia, the ultimate source of the continental ice, because of thicker ice load and thus greater rebound.

We commonly observed thin (meter or less) emergence sands and gravels as the uppermost stratum in many Everson outcrops in the study area. These coarse deposits probably record brief reworking of the underlying strata, such as Vashon till or Everson diamicton, during emergence. Strandlines and associated beach deposits are common in the southern half of the study area (Plate 1; also see Easterbrook, 1979, and Siegfried, 1978). The linear features demark significant but probably relatively short-lived sea level positions during crustal rebound. Although we observed no shells associated with emergence deposits, shells are common in these deposits regionally (Appendix 2). We relate the lack of beach or emergence deposits below the EGL on the southern slopes of Anderson and Chuckanut Mountains to high-energy sedimentation and the progradation of Everson outwash deposits across the upland areas. In this scenario, progradation of alluvial fan and deltaic systems emanating from the uplands prevails over beach reworking processes, thus effectively burying beach terraces, reworked surfaces, and other vestiges of sea-level stillstands.

Everson outwash deposits occur hundreds of feet above the EGL on the promontory as well as interlayered with marine deposits at and below the EGL, as discussed above, indicating that marine facies interfinger with terrestrial facies near this glaciomarine limit. Possible ice-contact and stranded ice features are evident locally near the EGL—for example, convolute and oversteepened bedding (Fig. 5, locs. 21, 24; Fig. 8) and possible kettled topography in Everson outwash in the north-central part of the Alger quadrangle (Fig. 5, loc. 22). We evoke burial of stranded ice blocks by recessional fluvial outwash deposits near or just above the EGL to explain the local association of undulate terrain, low-density tills, and outwash. This is similar to observations of Dethier and others (1995) elsewhere,

> "where large ice blocks apparently were buried in [gravel-rich proximal facies] that subsequently collapsed, producing a kettled landscape. In some places, planar-bedded, pebble poor marine silt overlies deformed sand and gravel, indicating that marine sediment was deposited after melting of the ice blocks."

Poorly studied, low-density silty sandy diamicton mapped north of Alger as Vashon till may be morainal or ice-marginal

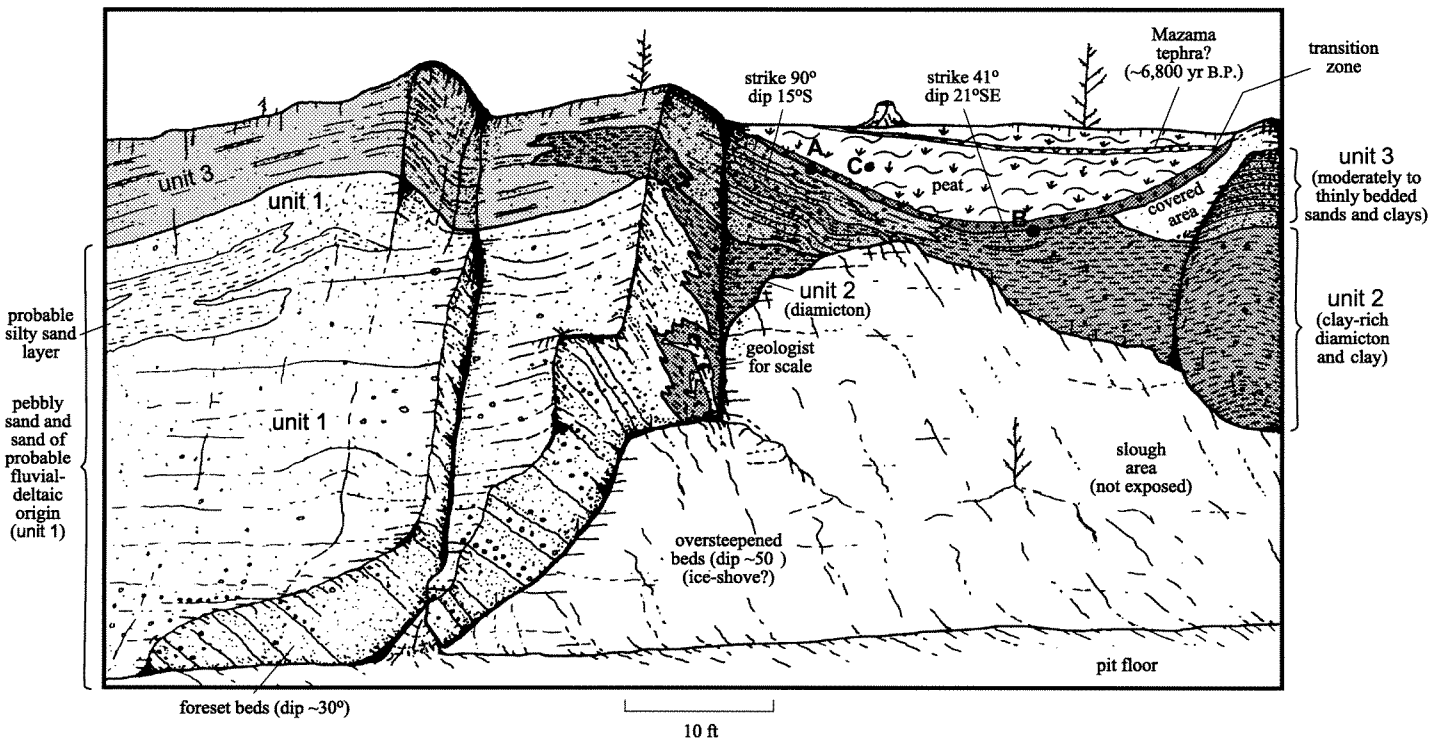


**Figure 8.** Schematic diagram showing the stratigraphic relations of the Everson outwash radiocarbon sample site (Appendix 1) in the Bow quadrangle (Fig. 3, location 37L; Fig. 5, loc. 21). Contacts locally inferred. The thin transition zone between the peat and underlying units contains a mixture of organics, sand, and gravel. **A**, sample 97-37L(A); stick from the bottom of the transition zone dated at 11,500 ±60 yr B.P. **B**, sample 97-37L(B); stick from the bottom of the transition zone dated at 11,990 ±110 yr B.P. **C**, sample 97-19T; large bark fragment in peat dated at 11,550 ±80 yr B.P. The radiometric age estimates from the peat and transition zone provide minimum age estimates for the underlying units and suggest an age of more than 12,000 yr B.P. for the uppermost Everson outwash, consistent with other Everson Interstade age estimates for sites in and near the study area (Appendices 1 and 2). Unit 2 diamicton may be flow till, which would be consistent with a stranded ice-marginal environment as suggested at the site by oversteepened foreset bedding in the fluvial-deltaic deposits of Unit 2 and the possible kettle topography north of this site. We interpret the deposits as interlayered glaciomarine drift of dropstone origin and fluvial-deltaic deposits. We interpret Unit 3 deposits as deltaic bottomset or turbidite beds in a more distal sedimentary setting than the coarser Unit 1. This stratigraphy is similar to the proximal outwash and morainal facies reported by Dethier and others (1995) suggesting ice stranding near this site.

flow-till associated with Everson proximal outwash (Plate 3, cross section F).

The EGL is at about the same altitude as marine clays under basal peat directly east of the study area that provides a limiting $^{14}C$ age of 12,900 yr B.P. (Rigg, 1958; Rubin and Alexander, 1958) for the maximum marine inundation (data and further references in Appendix 2). This age combined with the altitude and stratigraphic relations of our $^{14}C$ ages (Appendix 1; Figs. 7, 8) and limiting $^{14}C$ ages of Siegfried (1978) indicate maximum glaciomarine inundation in the study area and south of the stagnating ice front between 11,000 and 12,000 yr B.P.

The overall regularity of the Everson stratigraphic section, including the EGL and OFUS, suggests an uncomplicated sea-level history. We envisage maximum marine inundation during ice retreat through the study area. This is consistent with the concept that maximum crustal depression would immediately precede deglaciation. Very rapid rebound from the EGL would commence upon ice removal (for example, Mathews and others, 1970), or possibly somewhat earlier if the thinning ice during Everson retreat reduced the crustal load prior to deglaciation. The simplest explanation derived from the data of this and other studies is rapid early rebound followed by a decreasing uplift rate, producing successively lower relative sea levels and strandlines during the Everson. The OFUS does not suggest a significant resubmergence during the Everson, as suggested by Easterbrook (1963a,b) and Armstrong (1960a,b) for the Whatcom basin north of the promontory and near Bellingham and the U.S.–Canadian border (Fig. 1). These studies cite the occurrence of sandy or gravelly *terrestrial* beds between glaciomarine drifts as indicating hundreds of feet of submergence-uplift-resubmergence. Other studies (for example, Dragovich and others, 1997a, and Croll, 1980) suggest that these granular deposits interlayered with definitive glaciomarine drifts are submarine outwash deposits like those mapped south of the Whatcom basin. Dragovich and others (1997a) relate the terrestrial (fluvial) evidence, composition, and geographic position of the Deming Sand *at the type section* (Fig. 1; directly west of the Deming quadrangle and east of the Whatcom basin) to Quaternary uplift along the Macaulay Creek thrust and suggest that coarse deposits in glaciomarine drift to the west are submarine in origin.

During the Sumas re-advance, sea level was approximated by the altitude of the Sumas deltaic topset-foreset beds, now about 100 ft apsl, bordering the northern part of the Skagit valley (Easterbrook, 1979). (See unit $Qgod_s$.) Easterbrook (1979) suggests that the deltaic deposits were incised by meltwater before the end of the Sumas, implying that sea level dropped to less than 20 ft apsl by the end of the Sumas (~10,000 yr B.P.). Regionally, complete isostatic rebound by 9,000 yr ago is suggested by Mathews and others (1970), with oldest and least uplift to the west (that is, Vancouver Island) probably as a result of a tapered glacial load to the west.

Some of the Everson Interstade beach deposit altitudes and $^{14}C$ "beach" shell ages of Pessl and others (1989) and Dethier and others (1996)(Appendix 2) south and west of the study area, respectively, suggest almost complete isostatic rebound (sea level near present level) at the close of the Everson Interstade. These findings may contradict the evidence for a 100-ft-apsl sea level during deposition of the Sumas deltaic deposits (~11–10 ka). Could the spatial distribution of the regional beach deposits and nearshore ages reflect not only differing ice loads or thicknesses across the northern part of the Puget Sound basin but also an irregular waning ice-sheet margin controlled by topographic barriers? The dated shells may have been deposited in deeper water glaciomarine facies (not beach facies). More likely, earlier uplift to the south and west of the study area due to earlier deglaciation and a somewhat thinner Vashon ice load may explain the reduced isostatic compensation (for example, Dethier and others, 1995) and resultant different rebound history. Furthermore, stranded ice along the Chuckanut Mountain–Anderson Mountain promontory, in particular, and in the Northwest Cascades, in general, may have delayed and complicated the glacial rebound history in the mountainous westernmost Cascades as compared to the open and embayed Puget Sound basin to the west where ice-shelf processes were dominant. We contend that some of the Everson stratigraphic complexities (both vertical and lateral) may be the result of the interplay of late glacial topography (for example, our promontory), crustal rebound, ice thickness variations, and an irregular or embayed waning ice-margin that was *both* stranded on prominences and floating in deep basins during Everson deglaciation. (Also see, for example, Dethier and others, 1995, for a discussion of the complexities of late glacial emergence.)

## VASHON STADE

Vashon Stade advance outwash and overlying till deposits occur widely in the quadrangles. The advance outwash significantly modified the pre-Fraser glacial landscape. The outwash *blanket*, the "great Lowland fill", was deposited by coalescing braided stream systems (for example, Booth, 1994) discharging large volumes of mostly sand and gravel onto a dissected topography created during the previous interglacial time (Fig. 6A). The outwash locally filled lakes and depressions with deltaic-lacustrine sediments, as is shown by high-amplitude, south-dipping foreset beds (Fig. 5, loc. 9) and the occurrence of fine "transitional beds", which consist mostly of probable lake deposits. (See "trans", Plate 3, cross sections; Fig. 6A; Appendix 3, for example, wells 2, 116, 120, 683).

Booth (1994) and Booth and Hallet (1993) show that many Puget Lowland troughs were formed almost entirely during ice occupation by subglacial meltwater scour. The Samish River valley, which incises the glacial uplands of the Alger quadrangle, is the result of subglacial scour. Scour is evidenced by the till mantling of the valley sides and, locally, the valley bottom over much of the river's length, as well as by the truncation of the advance outwash blanket at many locations underneath the valleywall till (Plate 1; Plate 3, cross sections E–G). Water-well logs and surface observations hint that both buried and exposed bedrock topography directed the subglacial channel in a west-southwesterly direction.

Till locally contains pods and interlayers of compacted or dense sand and gravel that we informally term dynamic till (Plates 1, 2). These pockets appear to mark locations of ephemeral subglacial meltwater channels. The dynamic till interlayers along the south sides of major bedrock highs such as Anderson and Chuckanut Mountains probably represent periodic opening of subglacial meltwater channels that later closed as a result of basal ice adjustments on the lee side of the bedrock promontory. Some dynamic till is spatially associated with the subglacial Samish River channel (Fig. 5, loc. 10)

## PRE-FRASER GLACIAL AND NONGLACIAL SEDIMENTS

Water-well and geotechnical boring logs (Fig. 4) (Dragovich and Grisamer, in press) provide evidence for several pre-Fraser glacial units beneath the study area (Plate 3, cross sections E–G;

Appendix 3 and associated table of general characteristics). The units include:

- "transitional beds" similar to those described by Pessl and others (1989). The beds probably represent both early advance outwash lake deposits and underlying interglacial sediments of the Olympia nonglacial interval (informal unit trans);
- commonly organic-rich, probable Olympia nonglacial interval sediments (informal unit pf); and
- older outwash (informal unit oo) as well as older diamictons (informal units ot and very rare oot) that are apparently buried under extensive dissected blankets of older till(s) and (or) glaciomarine diamicton that we tentatively correlate with the Possession glaciation of Easterbrook and others (1967) or Easterbrook (1994).

The geometry (as now inferred) of the pre-Fraser sediments suggests that many of these deposits occur below a veneer of Fraser and (or) Everson sediments (Figs. 6, 7) and that some current topography is a modified relic of earlier glaciations. For example, Humphrey Hill appears to be an older till hillock or drumlin that is cored by older till and outwash (Plate 3, cross section F). Our observations are consistent with $^{14}C$ dates of *exposed* pre-Fraser sediments in the Port Townsend quadrangle (Pessl and others, 1989) directly south of the study area; there, pre-Fraser sediments correlated with the Olympia nonglacial interval of Armstrong and others (1965) and the Possession glaciation of Easterbrook and others (1967) or Easterbrook (1994) crop out in bluffs. (See Appendix 2).

## Bedrock Structural Development of the Quadrangles

### CORRELATIONS AND EMPHASES OF PREVIOUS STUDIES

We correlate the assemblage containing metamorphosed basalts, gabbros, ultramafites, and localized metasedimentary rocks with the Helena–Haystack mélange (HH) of Tabor (1994)(Fig. 9) or the Haystack terrane of Whetten and others (1980a, 1988). (See Fig. 13.) Central to this correlation is our interpretation of the structural development of the study area, including the contrasting structural styles of the HH and the Shuksan nappe, as well as the subtle yet locally distinct differences in metamorphic grade, depositional environment, and metabasalt geochemistry. We provide evidence that the HH was thrust from south to north over the Shuksan nappe along a fairly discrete thrust plane in the mid-Cretaceous. Mylonites and fractures associated with thrusting conform to a Riedel thrust shear model (for example, Rutter and others, 1986; Logan and others, 1979, 1981). Later Tertiary synthetic and antithetic strike-slip and block faulting dissected the thrust stratigraphy, juxtaposing various structural levels. (See Fig. 11, p. 34.)

Geologists attempting tectonic and structural syntheses in the lower Skagit River area of the Northwest Cascades system are faced with a bewildering profusion of nappe and rock assemblage correlations and resulting structural interpretations (listed below). Many of these correlations predated detailed mapping that has used geochemistry, structure, and other characteristics to progressively clarify the characteristic attributes of the nappe rock units (for example, Brown and others, 1987, and Tabor and others, 1994). Particularly important in this regard is the recognition of the imbricate zone below the Easton suite and associated with the Shuksan thrust. This imbricate zone is termed the Bell Pass mélange, which itself includes diverse rock units such as the Yellow Aster Complex, Elbow Lake Formation, ultramafite (for example, Twin Sisters Dunite), and the Vedder Complex (Fig. 10). The *dominantly mafic volcanic-intrusive-ultramafic rock assemblage* (hereafter, the *ophiolite*) recently named the Helena–Haystack mélange by Tabor (1994) and that includes parts of the Haystack terrane of Whetten and others (1988; see Fig. 13) is a continuous lithologic assemblage that is mapped to the east-southeast of the study area (Fig. 2). The HH, as defined by Tabor (1994), lies north of the Darrington–Devils Mountain fault and south of the Skagit River. In this area, the HH was thrust over the Shuksan nappe at Table Mountain (see Fig. 13) and to the east near Deer Peak (Fig. 10), more than 10 mi east-southeast of the study area, during mid-Cretaceous orogeny (Reller, 1986; Tabor, 1994). Other contacts between the HH and the Easton suite are Tertiary high-angle faults (for example, Tabor, 1994). We can now extend the HH into the study area and north of the Skagit River. (See Figs. 9, 10, and 13 for illustration of the current Northwest Cascades system nappe nomenclature.)

Studies of the Northwest Cascades system, some of which covered the study area in a reconnaissance manner, are listed below. Note the contradictory interpretations.

- Bechtel, Inc. (1979) and Miller (1979), following reconnaissance mapping by Misch (1966), correlated the ophiolite, including meta-igneous rocks in the study area, with the Chilliwack Group. The approximate extent of Miller's (1979) study area is shown by our Haystack terrane distribution (see Fig. 13). Their correlation places Easton suite rocks structurally above the Chilliwack Group, suggesting to Miller and Bechtel, Inc., that meta-igneous rocks in the study area are erosional windows into the lower Chilliwack Group (Fig. 10). Correlation of the ophiolite with the volcanic-arc Chilliwack Group has been rejected by several studies citing compelling age, geochemical, and structural dissimilarities of the ophiolite and the Chilliwack Group (for example, Sevigny and Brown, 1989; Brown and others, 1981; Whetten and others, 1988).
- Carroll (1980) mapped on Lummi Island (northwest of the study area; see Fig. 13) and described pumpellyite- and stilpnomelane-bearing metabasalts and metahypabyssal intrusive gabbros similar in age and lithology to the ophiolite. Carroll correlated these rocks with the Fidalgo ophiolite of Brown and others (1979).
- Whetten and others (1980a) mapped previously disparate local rock units (including several subunits of the ophiolite) as the Haystack terrane. They correlated the ophiolite with the Twin Sisters Dunite (now part of the Bell Pass mélange of Brown and others, 1987) and the lower metamorphic grade Fidalgo ophiolite. They also included isolated rock units south of the Darrington–Devils Mountain fault that Tabor (1994) has more recently correlated with the eastern or western mélange belts (Figs. 2, 9). They correlated magnetically prominent serpentinites in the Bow quadrangle around Oyster Creek with the ophiolite. Mapping of the Port Townsend 1:100,000-scale quadrangle by Whetten and others (1988) documents important structural features such as the Haystack Mountain thrust fault (see Fig. 13, p. 28), which places the ophiolite over the Easton suite. Our usage is mostly compatible with Whetten and others (1980a) regional Haystack nappe concept, wherein ophiolitic rocks of Jurassic age (~160 Ma) overlie the Shuksan nappe as best documented southeast of the study area (Whetten and others, 1988). The

Haystack terrane is similar to type III "scaly serpentinite" mélange of Cowan (1985), which contains strongly foliated scaly serpentinite matrix and "blocks of partly to wholly serpentinized ultramafic rocks, mafic igneous rocks, and, in some cases, a wide variety of sedimentary-rock types". Unlike most mudstone-matrix mélange types, many type III serpentinite-matrix mélanges contain tectonic inclusions measured in kilometers (Cowan, 1985).

- Vance and others (1980), in a conclusion somewhat similar to that of Miller (1979), interpreted the ophiolite south of the Skagit River and north of the Darrington–Devils Mountain fault (Fig. 2) as "a tectonically mixed zone or mélange at the base of the Shuksan thrust" and thus tectonically over the Chilliwack Group. Using now-current structural and geologic map syntheses, it can be inferred that they correlated the ophiolite with the island-arc basaltic Elbow Lake Formation (Fig. 10; Brown and others, 1987) of the Bell Pass mélange that occurs in the imbricate zone below the Shuksan nappe north of the Skagit River. Therefore, by inference, they agreed with Whetten and others (1980a, 1988) on the general oceanic origin of the meta-igneous rocks of the suite but differed in their interpretation of the structural position of the ophiolite within the northwest Cascades framework.
- Frasse (1981) mapped about 10 mi east-northeast of the study area and tentatively concluded that results of his study were consistent with those of both Vance and others (1980) and Whetten and others (1980a). He questioned the validity of the concept of the Bell Pass mélange as proposed conceptually by Christenson (1981). The Twin Sisters Dunite of Frasse's study area is currently widely considered to be part of the Bell Pass mélange (for example, Brown and others, 1987), and the metagabbroic-dioritic rocks of his study area have been correlated with the Easton suite by Gallagher and others (1988; below).
- Schmidt (1972) mapped part of the Chuckanut Mountain–Blanchard mountain area of the Bow quadrangle and correlated the ultramafic and mafic meta-igneous rocks there with

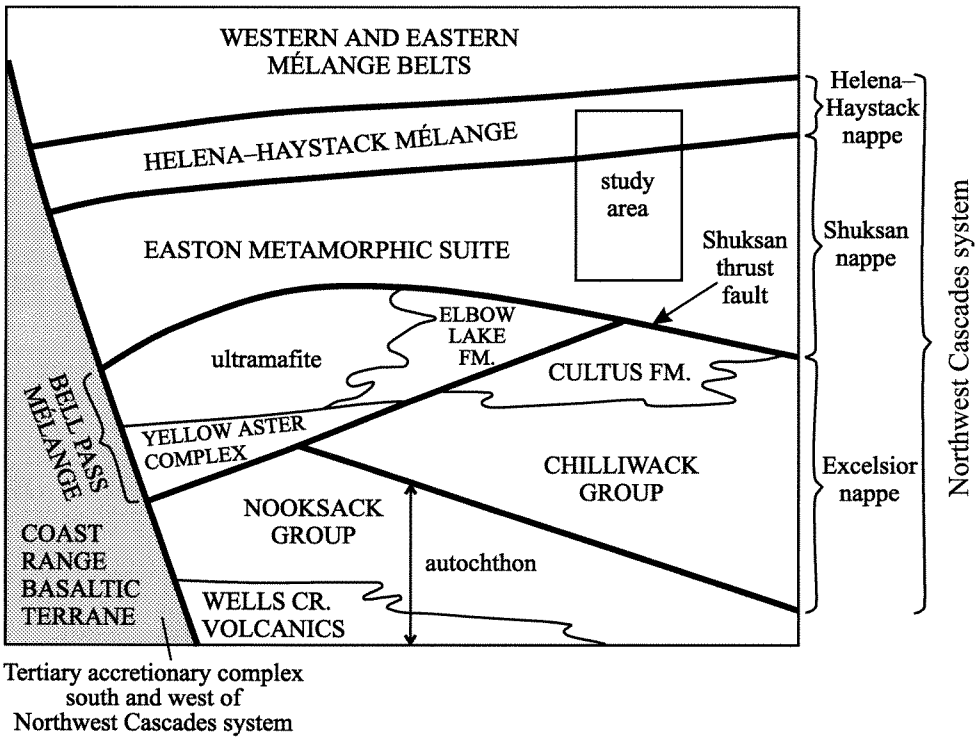


**Figure 9.** Structural stacking of terranes in the North Cascades (modified from Tabor, 1994). Box shows the structural position of the study area. The Helena–Haystack mélange (HH) of Tabor (1994) is similar to the Bell Pass mélange of Brown and others (1987) in that it contains imbricate bodies from the adjacent nappes, exotic rock units of unknown affinity to the adjacent nappes, ultramafite, and a distinctive oceanic sequence. (See Tabor, 1994, for the regional setting of the HH.)

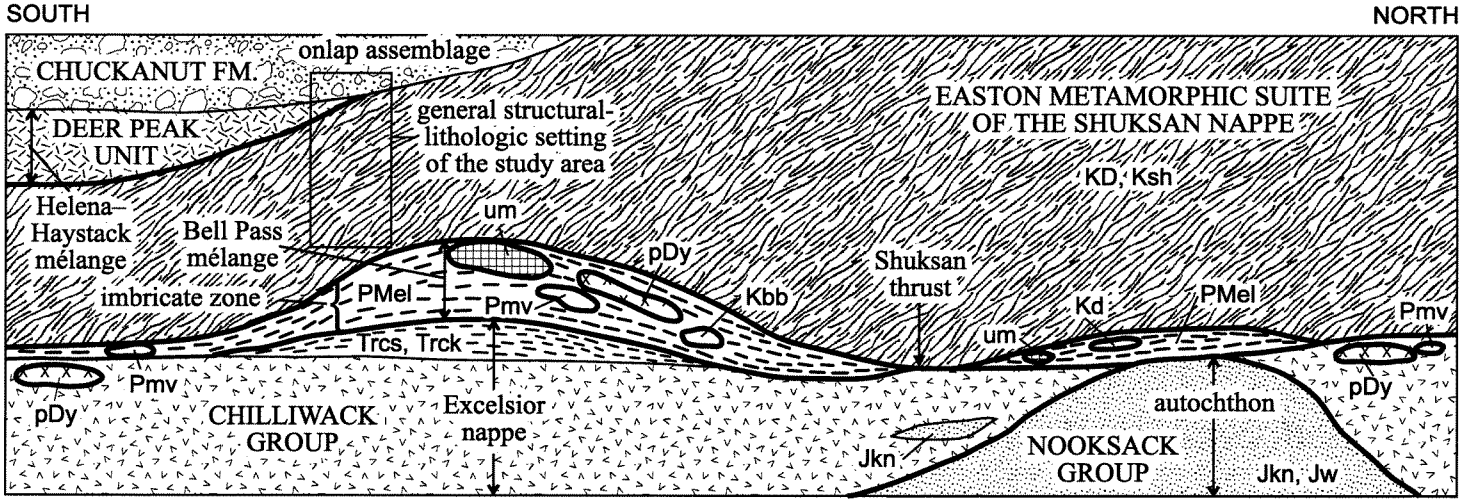


**Figure 10.** Schematic representation of thrust-faulted stratigraphy in the northwest Cascades (modified from Brown and others, 1987). Box shows the structural position of the study area. Thick lines, thrust faults; thin lines, unconformities. The Deer Peak unit is included in the Helena–Haystack mélange by Tabor (1994). Kd, Darrington Phyllite; Ksh, Shuksan Greenschist; Jkn, Nooksack Group; Jw, Wells Creek volcanics; um, ultramafic rocks; pDy, Yellow Aster Complex; Pmv, Vedder Complex; Pmel, uPcs, Elbow Lake Formation; uPcv, uPcs, Chilliwack Group metavolcanic and metasedimentary rocks; Trcs, Trk, Cultus Formation sedimentary rocks and keratophyre.

the basic intrusive-textured rocks of the Yellow Aster Complex. The Yellow Aster Complex is now included in the Bell Pass mélange *below* the Shuksan nappe (Fig. 10). Several geologic attributes indicate that the meta-igneous rocks in the study area are not Yellow Aster rocks (for example, our U-Pb ages). However, Schmidt interpreted the mylonites and associated structures along the contact between the meta-igneous rocks and the Easton suite as *indicating a thrust*; he mapped the mafite intrusives as a thrust klippe *on* the Shuksan nappe, a structural concept that we forward here. (See Gallagher, below.)

- In the Deer Peak area, Reller (1986) mapped the ophiolite and more siliceous metavolcanic rocks of his Deer Peak unit and showed this unit thrust over the Easton suite. This mapping was incorporated into Brown and others' (1987) 1:100,000-scale regional map, which shows the Deer Peak unit as the highest nappe in the Northwest Cascades system (Fig. 10). Tabor (1994) includes the Deer Peak unit in the HH. The occurrence of siliceous metavolcanic rocks in the HH broadens the original HH environment to include more-evolved island-arc rocks.
- Gallagher (1986) and Gallagher and others (1988) studied the Chuckanut Mountain–Blanchard mountain area of the Bow quadrangle as well as the Bowman Mountain area northeast of the Alger quadrangle. These studies rejected Schmidt's (1972) structural arguments and included the meta-igneous (as well as ultramafic) rocks *in* the Easton suite of the Shuksan nappe; Gallagher and others (1988) expanded the definition of the Easton suite to include near-arc metavolcanic rocks and transform-fault-related ultramafic detritus and bodies, thus broadening the depositional and tectonic environment envisioned for the Easton suite.
- Cruver (1983) studied the Table Mountain area directly southeast of the study area as well as the Skagit valley bedrock knobs (including Butler Hill) in and directly south of the Alger quadrangle. Cruver, as had Vance and others (1980), correlated the ophiolitic rocks with the imbricate zone overlying the Shuksan nappe; this imbricate zone is now termed the Bell Pass mélange.
- Tabor mapped extensively in the Mount Baker, Sauk River, and Skykomish River 1:100,000-scale quadrangles (Fig. 1; Tabor and others, 1988, 1993, 1994). He included some of the local rock units previously correlated with the different structural levels or units—for example, some of the Haystack terrane of Whetten and others (1980a) and the Bell Pass mélange of Cruver (1983)—in the HH (Fig. 9). (See Tabor, 1994, for a discussion of the correlations.) We extend the HH structural and rock assemblage concept of Tabor (1994) into the study area. The concept of the HH of Tabor (1994) is structurally and lithologically similar to the concept of the Bell Pass mélange of Brown and others (1987) or Sevigny and Brown (1983). The Bell Pass contains an oceanic sequence called the Elbow Lake Formation as well as several exotic lithologic elements and defines an imbricate zone between the Shuksan and Excelsior (Chilliwack Group) nappes of Tabor and others (1994)(Fig. 10).
- Brown and others (1981) summarized the metamorphic grade of the Northwest Cascades system nappes and terranes of poorly known nappe affinity (for example, the Fidalgo ophiolite of the Decatur terrane). They suggested that the greenstone-slate-phyllite unit in the lower Skagit valley and on Cultus Mountain (see southernmost Alger quadrangle and southeastern portion of Fig. 13), rocks we include in the HH, was metamorphosed at similar peak metamorphic pressures but probably at lower temperatures than the Shuksan nappe, as discussed below.

## DEPOSITIONAL ENVIRONMENT, GEOCHEMISTRY, AND AGE OF THE EASTON METAMORPHIC SUITE AND THE HELENA–HAYSTACK MÉLANGE

Depositional (stratigraphic, provenance, and geochemical) and geochronologic information is crucial to elucidating the geologic and tectonic history of the Helena–Haystack mélange (HH) and Shuksan nappe and to comparing these rocks regionally. This information indicates that, although the HH and Shuksan nappe in the study area are interpreted by us as separate structural entities, they may have originated in the same or nearby Jurassic, locally arc-proximal, oceanic basins.

### Geochemistry

Our meta-igneous rock geochemical data including rare earth elements (REE) are presented in Appendix 4. Appendix 5 is divided into table and figure sections and presents the results of our effort to discern the original tectonic environment using discrimination and spidergram plots. Metavolcanic rocks in the study area are tholeiitic to calc-alkaline basalts and trachybasalts and minor basaltic andesites and trachybasaltic andesites and their intrusive equivalent gabbro-diorite (Figs. A1, B1, A2, B2 in Appendix 5). Metabasaltic rocks of both the HH and the Easton suite are predominantly tholeiitic, whereas intrusive rocks are both calc-alkaline and tholeiitic. In our analysis, we have divided the geochemical samples into (1) metabasaltic greenstones of the HH and (2) miscellaneous meta-igneous rocks including HH metagabbro, HH ultramafite, and Easton suite greenschists. Metamorphism, weathering, and alteration can change the abundances of the more mobile (low field strength) major and trace element abundances. In contrast, several studies document the relative resistance of REE to metamorphism and alteration (for example, Michard, 1989). We present evidence below that the geochemistry of the meta-igneous rocks in the study area has been affected by metamorphism and alteration events that partially masked the geochemical signature(s) of the original tectonic environment. We therefore favor the data for REE and other relatively immobile trace elements (for example, Ti) and resultant spidergram and tectonic discrimination plots discussed below. We note here that the overall clustering of the data on the tectonic discrimination plots and the similar spidergram patterns support our separation of rocks we mapped as HH greenstones from Easton suite greenschists.

We have applied a variety of tectonic discrimination diagram plots using relatively immobile trace elements to constrain the depositional environment of metabasaltic greenstones. We obtained a scatter of tectonic environments from discrimination diagrams that use the relatively mobile major elements. In comparison, trace elements produced a clustering of data and results mostly in the mid-ocean ridge basalt (MORB) or island-arc tholeiite fields. (For example, compare discrimination diagram results in table columns J and K in Appendix 5 with table columns L to Y).

We base the following comments concerning the geochemistry of the metabasalts and metagabbros of the HH on our preliminary evaluation of several petrographic, geochemical discrimination and REE plots with the aid of the geochemical plotting program IGPET (Appendix 5 table and figures). HH

metabasalts and metagabbros are characterized by slightly depleted to flat light rare earth element (LREE) patterns on rock/chondrite normalization plots (Figs. A5 and B5 in Appendix 5). These primitive LREE patterns are characteristic of either MORB or island-arc tholeiite tectonic environments (for example, Garcia, 1978; Jakes and Gill, 1970; Gust and Perfit, 1987). Further discrimination between these two environments using major elements (Figs. A3, B3 in Appendix 5) and other trace elements (Figs. A4, B4, A9, A10 in Appendix 5) indicates that (1) the HH metabasaltic greenstones are dominantly MORB to locally island-arc tholeiites (see interpretation in Appendix 5 table) and (2) the HH metagabbros show both island-arc tholeiite and MORB attributes. However, the tectonic discrimination diagrams we used are designed for basalt and basaltic andesite flows and are not directly applicable to mafic intrusive rocks, which can be affected by differentiation and other chemical isolating mechanisms. We thus emphasize the geochemistry of the metabasalts of the HH (Appendix 5, column A figure series), which are predominantly tholeiitic.

The Ta-Tb and Rb-Hf-Ta and granite discrimination diagrams of Pearce and others (1984) and Harris and others (1986), respectively, suggest that the metagabbros on Colony and Chuckanut Mountains are volcanic-arc or oceanic-ridge granites. These diagrams are more applicable than the tectonic environment results presented in Appendix 5 (B series figures and associated tables) using the basalt discrimination diagrams.

Although the diagrams are intended for intrusive rocks with $SiO_2$ greater than about 5 percent and thus are not directly applicable to the mostly quartz-free intrusive rocks of the study area, they are more applicable for intrusive rocks than the diagrams presented in Appendix 5 (B series diagrams). We obtained contradictory volcanic-arc and oceanic tectonic environments from the Pigeon Point metagabbro samples using the discrimination diagram of Harris and others (1986). We obtained an oceanic-ridge tectonic environment for the Colony mountain metagabbro rocks (samples 2G and 2G1), which supports our contention that most of the HH greenstones in the study area are dismembered oceanic crust. Although Harris and others (1986) used the relatively mobile major elements such as $SiO_2$, $Na_20$, MgO, and $FeO_t$, the metagabbroic greenstone geochemical samples in the study area (samples 2G, 2G1, 28C, 28E, 24I) have a geochemical signature very similar to that of the Fidalgo ophiolite layered and foliated gabbros of Brown and others (1979). The greenstone data also compare favorably with the geochemical ranges of oceanic gabbro and California ophiolite gabbro compiled by Brown and others (1979 and references therein). Analytical results for all the metagabbroic greenstones in the study area compare very favorably with the $TiO_2$ versus $FeO_t$/MgO oceanic gabbro–Fidalgo ophiolite gabbro geochemical signature presented by Brown and others (1979). Most notable is the 163 Ma Colony mountain intrusive that has a geochemical signature similar to that of both the oceanic gabbro (Brown and others, 1979) and the arc diorite of the Fidalgo ophiolite (Brown and others, 1979; Brandon and others, 1988).

A MORB origin for the rocks of the HH is supported by the rock/MORB spidergram patterns that parallel unity or one on the Y-axes (Figs. A6, A7, B6, B7 in Appendix 5). Relatively mobile elements (for example, Ba, K, Rb, Cs) along the left side of the Rock/MORB spidergrams in Appendix 5 display a more chaotic pattern indicative of element dispersal during metamorphism or alteration. Element mobility is also suggested by the conflicting results obtained from the major element discrimination diagrams and relatively immobile trace element plots and spidergrams that show more systematic results. Trace element data for two samples of tuffaceous greenschist (8D1 and 41H3) that forms interlayers in the metasedimentary rocks of the Easton suite at Windy Point and Anderson Mountain show a distinct LREE enrichment rock/chondrite pattern, similar to one HH metabasalt (sample 23P). This pattern, along with the mostly calc-alkaline volcanic arc discrimination plot attributes of these samples, support the volcanic-arc setting for the western Easton suite proposed by Gallagher and others (1988). The greenschist klippe on Anderson Mountain that we correlate with the Shuksan Greenschist appears to be MORB, as documented elsewhere for the Easton suite (see below). Tuffaceous greenschist occurs directly north of the Alger quadrangle (Fig. 3, loc. 41H).

A MORB to tholeiitic island-arc setting for the HH is mostly consistent with Easton suite, HH, and Fidalgo ophiolite geochemical studies elsewhere in the region (Vance and others, 1980; Brown and others, 1979; Tabor, 1994; Brandon and others, 1988; Gallagher, 1986; Sevigny and Brown, 1989; Dragovich and others, 1997a; Cruver, 1983; Reller, 1986; and Blackwell, 1983). Our observations are similar to those of Tabor (1994), who indicates that the HH is dominated by basalts with an ocean-floor to oceanic island-arc geochemical signature. Our findings are also similar to those of Gallagher (1986), who noted that some of the Chuckanut Mountain intrusive rocks (unit $Jigb_h$) are mostly alkalic to slightly calc-alkaline, suggestive of an island-arc component. However, we present geochemical evidence, which is supported by our spidergram REE patterns, that the greenstones of the HH, particularly the metabasalts, are predominantly MORB in origin.

The metabasaltic greenstone patterns compare most favorably to the average Atlantic ocean-floor basalt (mid-Atlantic ridge) or MORB geochemical signature of Garcia (1978)(Appendix 5, Fig. A5). Samples 14D, 61N, and 17F have a lower REE/chondrite ratio that compares most favorably with the average oceanic island-arc tholeiite (IAT) pattern from Japan presented by Garcia (1978). These three samples graph in the IAT (volcanic arc) fields on some tectonic discrimination diagrams (for example Appendix 5, Figs. A9 and A10) or in the MORB/island-arc tholeiite field on other plots or less commonly in the MORB field relative to the other plots (Appendix 5, metabasaltic greenstone summary tables). For example, the V versus Ti plot of Shervais (1982) indicates that the greenstone metabasaltic rocks are MORB or back-arc basin basalts (BAB)—except samples 61N and 14D, which plot in the island-arc tholeiite field, and sample 17F, which plots in the calc-alkaline arc basalt/MORB/BAB field. This pattern correlates with the lower REE/chondrite ratio suggestive of island-arc tholeiites alluded to above.

We interpret the HH greenstones in the study area as a tectonic mixture of mostly MORB and less island-arc tholeiite. The MORB geochemistry is "transitional" on some plots. The samples commonly plot in the overlapping MORB/IAT field or plot in the MORB field but close to the IAT field in plots that have no overlapping field between the tectonic environments. On the basis of this "transitional" geochemistry and the only slight REE depletion of the samples, we suggest a more complex oceanic environment, possibly a modified back-arc basin or rifted arc setting.

### Depositional Setting

An ocean-floor depositional setting is evidenced for most of the Easton suite east of the study area by the MORB geochemistry of the Shuksan Greenschist (Dungan and others, 1983), Fe-Mn-rich sediments (Street-Martin, 1981), and a primary stratigraphy—metabasalt, Fe-Mn pelagic metasedimentary rocks, and

pelitic schists at the top (Haugerud and others, 1981). However, geochemistry of six phyllites and four semischists from Chuckanut Mountain indicates that "compared to samples of metasedimentary rock of the eastern part of the [Easton suite] analyzed by Street-Martin (1981), the samples of the present study are less enriched in Ba, Ni, and Mn and are chemically more immature, bearing a similarity to near source deposits such as Franciscan graywackes" (Gallagher, 1986, p. 9). Thus, a near-arc setting is probable for much of western Easton suite as indicated by Gallagher and others (1988). Our petrographic observations confirm the presence of minor metatuffs and volcanic clasts in semischistose metasandstone of Mount Josephine interlayered with the phyllite (for example, unit $Jph_j$). The locally near-arc, oceanic character of the metasandstones and phyllites, combined with stratigraphic characteristics of the sequence, are consistent with a mid-fan to distal depositional environment for much of the Easton suite metasedimentary rocks in the study area.

We stress, however, the pelagic composition of the protoliths and (or) eroded source area of some of the semischists and phyllites of the suite. Minor lithologic variants associated with phyllite include probable metachert (quartzite) (for example, Fig. 5, loc. 23) and metamarl (calcareous phyllites). These lithologies indicate pelagic quiescent-water deposition. (Also see Brown and O'Neil, 1982, for a discussion of quartzites.) *Phyllites* of the study area, particularly around Chuckanut Mountain, are generally only semipelitic quartz muscovite phyllites that generally lack aluminous index minerals such as lawsonite (Brown and others, 1981) and contain abundant recrystallized quartz. *Semischists* contain relict plagioclase, lathwork volcanic relicts, and detrital monocrystalline quartz with minor hornblende that reflect a volcanic (mixed with a granitic?) source area. However, "metasandstones" also contain abundant recrystallized detrital polycrystalline quartz in a quartz-rich (albite poor) matrix. Granoblastic to very fine grained polycrystalline quartz or quartzite clasts typically equal or exceed in abundance all other detrital components combined. This suggests a chert-rich source area. Furthermore, rip-up clasts of phyllite in the metasandstones and metaconglomerates suggest incision and reworking of the basin. Important in this regard are (1) the observation by Gallagher and others (1988) that western Easton suite metasedimentary rocks lack metalliferous enrichment compared to the eastern pelitic and metalliferous phyllites and (2) the discovery of Precambrian zircons derived from the North American craton in Easton metasedimentary rocks of the central Washington Cascades (Tabor and others, 1988). We tentatively conclude that the sequence evolved in a distal to proximal forearc setting and that the quartz-rich polycrystalline clastic component was derived from recycling of basin sediments during deformation or erosion of older chert-rich basement rocks near the craton.

On the basis of petrologic and structural arguments and field relations, we contend that the greenstone meta-igneous rocks in the study area are not Easton suite rocks and that several of the conclusions presented by Gallagher and others (1988) are thus fortuitous. Our correlation of the greenstones, including mostly primitive *MORB-like* metabasites and associated metagabbros, with the HH ophiolitic nappe suggests that the Easton suite *in the study area* is not a volcanic arc intrusive/extrusive complex. The HH greenstones (units $Jmv_h$ and $Jigb_h$) contain ubiquitous augite as a relict igneous phase. The semischists do not contain augite as a detrital mineral, but do contain equally unstable minor but ubiquitous relict hornblende, suggesting that the source lacked augite. (Both mafic phases should disintegrate at about equal rates during transport.) This furthers our contention that the greenstone protoliths in the Bow quadrangle were not an eroded volcanic/intrusive basement sediment source to the Easton metasandstones as suggested by Gallagher and others (1988). Furthermore, Gallagher (1986) spatially correlates semischist with the metavolcanic rocks. However, semischist is mapped regionally (for example, Tabor and others, 1994; Dragovich and others, 1997d) in the Shuksan nappe, and in most localities it shows no convincing spatial relationship to Easton meta-igneous rocks.

Gallagher and others (1988) indicate that the semischistose metasandstone on Chuckanut Mountain (for example our unit $Jph_j$) contains minor clasts of chromite within porphyroblasts of fuchsite (a Cr-mica) and chlorite, indicating that the semischistose metasandstone was also sourced by ultramafite or that the lithologic association of ultramafite and ultramafite-metasedimentary rocks indicates a near-ultramafic-lined transform fault scarp setting for the western Easton suite. However, our correlation of the ultramafites with the HH suggests that the source of the inferred ultramafic detritus is probably not the ultramafites on Chuckanut Mountain. Gallagher (1986) and Gallagher and others (1988) contend that the tremolite-mica schists on Chuckanut Mountain containing clastic mafic and ultramafic *relict* minerals are metamorphosed *sediments* of the Easton suite. However, a comparison of our mapping with sample site descriptions of Gallagher (1986) places most of these bodies along the periphery of the HH metavolcanic rocks. Our observations suggest that the talc-tremolite schists are metasomatized primary ultramafic material in the HH and thus most of these bodies are ultramafic, not sedimentary, in origin. We did not microscopically observe any mafic detritus in the rocks but have noted that ultramafic bodies along Tertiary faults were locally cataclasized, a process that could possibly have tectonically intermixed ultramafite with nearby mafic HH metavolcanic rocks during shearing. We observed high-angle tectonic interleaving of various ultramafic rock types with rocks of both the upper HH nappe and the lower Shuksan nappe at a few important localities (for example, Fig. 5, loc. 27). For example, in the Bow quadrangle, we included most of the ultramafic or ultramafic-rich metasedimentary rocks discussed by Gallagher (1986) in the HH because of their distinct spatial association with the greenstone-ultramafite unit.

At Windy Point, Gallagher (1986) describes a 2-m-thick layer of tremolite-chromite-mica schist that occurs in metatuffs that are interlayered with metabasalt and metabasaltic breccia.

> "The contacts appear to be gradational. Mineralogically this unit contains detrital chromite, albite, and hornblende. Metamorphic tremolite, muscovite, and chlorite have developed extensively and define an extremely friable foliation. Similar to chromite in the semischist, the chromites of this unit are surrounded by fuchsite."

The association of these rocks with serpentinite, some or all of which occurs along an east-west Tertiary fault, suggests tectonic intermixing of HH metabasalt and serpentinite with tremolite-mica schists. We interpret tremolite-rich rocks away from Windy Point as metasomatized HH ultramafic protolith materials, not ultramafic-rich metasedimentary rocks of the Easton suite. We have mapped the Windy Point rocks as semischist with greenschist interlayers (unit $Jph_j$) and included the ultramafite as tectonic slices of HH along a Tertiary fault. Therefore, we reject a direct source-sediment link between the Chuckanut Mountain diorite of Gallagher and others (1988) and the semischistose metasandstones and metaconglomerates. We

accept, however, that the fuchsite-chromite clasts in rocks along Windy Point and in metaclastic rocks elsewhere in the Shuksan nappe may indicate a minor ultramafite source for the metasedimentary rocks of the Easton suite in the study area. Furthermore, we confirm the important observation that the semischists have a minor but distinct volcanic-arc signature but, as discussed above, do not believe that the *greenstones* in the Bow quadrangle are Easton metavolcanic arc rocks.

### Age of the Easton Metamorphic Suite and Helena–Haystack Mélange

The HH is relatively well dated by the U-Pb zircon method. HH ages from the region, including its possible correlatives, suggest an intrusive age for the metagabbro, metadiorite, trondhjemite, and plagiogranite of the broadly defined HH of about 160 Ma, or early Late Jurassic. Whetten and others (1980a, 1988) obtained three concordant U-Th-Pb ages of 160 to 170 Ma from three tectonic blocks of plagiogranite (one of which is associated with greenstone and argillaceous metasedimentary rocks) at three separate localities in the HH directly south to southeast of the study area. (See Fig. 13.) The ages are similar to other U-Pb zircon ages from the lower grade, but lithologically similar, Decatur terrane of Brandon and others (1988), which includes mostly ophiolitic rocks on Lummi and Fidalgo Islands. Ages include a 160 ±3 Ma date from hypabyssal gabbro and trondhjemite collected from the northern half of Lummi Island (Carroll, 1980) and a 167 ±5 Ma age from plagiogranite (Whetten and others, 1978, p. 122) from the Fidalgo (ophiolite) Complex part of the Decatur terrane of Brown and others (1979). See Brown and others (1979) and Brandon and others (1988) for lithologic details of the Decatur ophiolite-arc environment. These ages are validated by Late Jurassic radiolarians from the ophiolite (D. L. Jones, written commun. cited in Whetten and others, 1988). The consistency of the ages of the HH and its potential correlatives is strong evidence that these rocks are temporally, and possibly spatially, related. (See Bowman Mountain below.)

We obtained a $^{206}Pb/^{238}U$ age of 163.8 ±0.2 Ma and a $^{207}Pb/^{235}U$ age of 164.0 ±0.2 Ma from the greenschist on Anderson Mountain (Fig. 5, loc. 18; Appendix 5). We tentatively interpret this rock as a tectonic slice of the Shuksan Greenschist at the base of the HH (Fig. 9). Unlike greenstones in the study area, the rock is well recrystallized and homogeneously foliated and contains a metamorphic assemblage consistent with Shuksan metamorphism (~350–400°C; E. H. Brown, Western Wash. Univ., oral commun., 1998). We cannot exclude the possibilities that this body is (1) a recrystallized HH greenstone or (2) Shuksan Greenschist stratigraphically *in* the Easton suite metasedimentary sequence on Anderson Mountain. However, we were unable to trace the body along strike, and it appears to be a thin klippe of greenschist on phyllite with intervening alpine ultramafite. A tectonic origin for this body is suggested by (1) the occurrence of serpentinite along the base of the slab; (2) the correspondence of this body with a distinct positive, circular magnetic anomaly (R. J. Blakely, USGS, written commun., 1998) suggestive of a shallow, disk-shaped serpentinite body between the greenschist and underlying phyllite; and (3) the occurrence of "tectonic clasts" of Shuksan Greenschist elsewhere in the HH (Tabor, 1994). The geochemistry of the body (Appendix 5) suggests that this rock is tholeiitic MORB (with lesser evidence for an island-arc origin), which is compatible with an ocean-floor Easton suite or HH parentage but not consistent with a calc-alkaline island arc as indicated for meta-igneous rocks elsewhere in the Easton suite by Gallagher and others (1988).

We obtained a nearly concordant $^{206}Pb/^{238}U$ age of 163.2 ±0.4 Ma and a $^{207}Pb/^{235}U$ age of 162.5 ±3.5 Ma from the HH metagabbro on Colony mountain (Fig. 3; Fig. 5, loc. 25; Appendix 6). This age is very similar to the 160 to 170 Ma U-Th-Pb zircon ages reported by Whetten and others (1980a) for the HH southwest of the study area. The geochemistry of this sample (Appendix 5) indicates an island-arc environment or MORB tectonic environment for this intrusive body.

Gallagher and others (1988) report a U-Pb zircon age of 163 ±2 Ma from the Bowman Mountain metaquartz diorite about 10 mi northeast of the study area; they interpret this intrusive body as "a shallow intrusive vent that fed tuffaceous detritus to nearby sediments" and thus its age dates the Easton suite metasedimentary rocks. This is supported by our $^{206}Pb/^{238}U$ age of 163.8 ±0.2 Ma and $^{207}Pb/^{235}U$ age of 164.0 ±0.2 Ma from the Shuksan Greenschist on Anderson Mountain. Similarly, on the basis of K-Ar and Rb-Sr isotope analysis, Armstrong (1980), Brown and others (1982), Brown (1986), and Armstrong and others (1983) considered the Easton suite to have a Middle to Late Jurassic depositional age (~150–160 Ma) and an Early Cretaceous metamorphic age (~110–130 Ma; perhaps locally as old as 160 Ma).

### Synopsis of Depositional Environment, Geochemistry and Age

The current geochronology, therefore, suggests the Easton suite protolith is Jurassic and about 163 million years old. The current geochronology of the Easton suite and the HH indicate that the protoliths of the separable nappe units are very similar in age. The structural and metamorphic differences combined with the temporal similarities of the HH and the Easton suggest mid-Cretaceous structural coupling via thrusting of a similarly aged oceanic crust over an island-arc sequence.

More broadly, the Easton suite, HH, and Fidalgo ophiolite are all latest Middle Jurassic and appear to be oceanic crust with locally superimposed island-arc rocks. Structural and metamorphic differences between these terranes appear to be the result of later Jurassic and early Cretaceous tectonic environs, such as differing subduction regimes and (or) structural positions during obduction. In other words, even though the HH, Easton suite, and Fidalgo ophiolite may have formed in the same or nearby oceanic basin(s), they have different Late Jurassic to Early Cretaceous metamorphic assemblages or recrystallization fabrics that we relate to different temperature-pressure or burial conditions during subduction.

## JURASSIC–CRETACEOUS DEFORMATIONS AND METAMORPHISMS PRIOR TO NORTHWEST CASCADES SYSTEM THRUSTING

Haugerud and others (1981) and Dungan and others (1983) hypothesized that an early static metamorphism (or hydrothermal alteration?) occurred before the main regional blueschist facies metamorphism, probably in a low-pressure ocean-floor environment. Some of the oldest known metamorphic ages of the Easton suite are 164 Ma K-Ar hornblende and muscovite age estimates (Brown, 1986; Armstrong, 1980) from anomalous amphibolites and related rocks in the Gee Point–Iron Mountain area east-southeast of the study area. Brown and others (1982) interpret these rocks as having been metamorphosed adjacent to hot mantle material in the upper mantle during subduction. However, the bulk of the Easton suite is lower grade rocks that bear evidence of a later regional, syntectonic blueschist-facies metamorphism.

Apparently, only the regional, Early Cretaceous blueschist facies metamorphism affects metamorphic rocks in the study area (for example, this study, Gallagher, 1986, and Cruver, 1983). This metamorphism and associated deformation (1) postdates the subduction-related(?) Late Jurassic high-grade amphibolite facies aureole associated with the juxtaposition of mantle with ocean-floor rocks of the Easton suite (Brown and others, 1982; Armstrong and Misch, 1987) and (2) caused nearly complete recrystallization of the Easton suite primary mineralogy and is manifested in a regionally observed S1 foliation and an L1 stretching lineation. (See Fig. 12, p. 36, first deformation or D1.) Brown (1986) indicates that the only vestiges of primary mineralogy and texture in Easton metabasalts are rare augite phenocrysts, albitized plagioclase phenocrysts, chlorite-epidote amygdules, and rare flattened pillows, as well as relict deformed bedding in some metasedimentary rocks. This main Early Cretaceous metamorphism produced a strong deformational fabric that, in rocks of appropriate bulk composition, has produced syntectonic key index minerals such as blue amphiboles, lawsonite, and pumpellyite. Regional and local data demonstrate that the D1 fabric is a granoblastic or lepidioblastic blueschist-facies fabric that is regionally strongly developed, synmetamorphic, and easily recognized in the field (for example, Brown, 1986; Misch, 1966, 1969; Haugerud and others, 1981). Brown and others (1981) and Brown (1986) estimate peak metamorphic conditions for the regional blueschist facies metamorphism of the Easton suite as 330° to 400° C at 7 to 9 kb. (See comparison of metamorphic fabrics below.)

A strongly developed S1 foliation is present in phyllites, semischists, and greenschists of the Easton suite throughout the study area. (See Fig. 12A.) The foliation is defined by a strong alignment of metamorphic minerals such as muscovite and stilpnomelane and is accompanied by a pronounced, millimeter-scale quartzose metamorphic segregation layering. Thick (as much as a few centimeters) quartz veins commonly parallel the S1 foliation. A distinct L1 stretching lineation is observed on the S1 foliation, particularly in metasandstones, and is defined by stretched clasts and the preferred alignment of metamorphic minerals. The quartzofeldspathic matrix in D1 tectonites is polygonal and unstrained to mildly undulose and shows little evidence of mylonitization or grain reduction. As recognized regionally (Haugerud and others, 1981; Tabor and others, 1994), the first foliation (S1) is folded into open to tight to rarely isoclinal folds (F2) that range in amplitude from approximately a millimeter (crenulations forming the L2 lineation) to hundreds of meters. (See Fig. 12B.) In the field, we divided D2 folds into F2 folds that contain a distinct axial planar S2 foliations and "F3" folds that lack this new cleavage in the cores of the folds. F2 folds are generally tighter than "F3" folds and are probably higher strain flexural slip folds that have undergone some recrystallization late in the regional metamorphic cycle as defined locally by some aligned muscovite-chlorite along their axial planes. Thus, we assign "F3" folds to the second deformation as lower strain variants of F2 folds. Probable polygonal arcs of actinolite defining an F2 microfold in one semischist may be more indicative of the metamorphic grade during the second deformation than the local white mica-chlorite S2 fabric. Polygonal arcs in this case are recrystallized actinolite defining an F2 microfold that reversed evidence for D2 strain by post-deformation recrystallization. However, the sweeping extinction of micaceous F2 microfolds indicates that recrystallization of the S1 foliation during D2 was not total and that the rare polygonal arcs of actinolite defining the micro-F2 fold may be indicative of the heterogeneity of F2 folding via flexural slip mechanisms (that is, strain was partitioned during D2 deformation).

Recrystallization and metamorphism of the HH greenstones in the study area prior to thrusting appear to be nontectonic. Nontectonic or static metamorphic textures are best represented by random, fine-grained, acicular actinolite in low-strain zones in HH mafic igneous rocks such as greenstones. (See textural-metamorphic contrasts between the HH and Shuksan nappe, below.)

## THRUSTING OF THE HELENA–HAYSTACK MÉLANGE OF TABOR (1994) OR THE HAYSTACK TERRANE OF WHETTEN AND OTHERS (1980a, 1988) OVER THE EASTON METAMORPHIC SUITE

We present further field, structural, textural-metamorphic, and geochemical-lithologic evidence for a thrust contact between the HH and the underlying Shuksan nappe, which in the study area includes Darrington Phyllite and semischist of Mount Josephine. The structural evidence below should be considered in concert with the map and cross sections (Plates 1, 2, 3; Figs. 11, 12, and see Fig. 14) and is mostly derived from the Whitehall Creek–Blanchard–Colony–Chuckanut Mountain area of the Bow quadrangle where the contacts are locally well exposed. We informally name this structure the Whitehall Creek thrust.

### Textural-Metamorphic Contrasts between the Helena–Haystack Mélange and the Easton Metamorphic Suite

The synmetamorphic S1 fabrics in the Shuksan nappe are probably Early Cretaceous in age (110–130 Ma) and correlate with the regional S1 foliation described by several workers (for example, Brown, 1986). (See above.) A fission-track age on zircon from HH plagiogranite directly southeast of the study area is 113 ±11 Ma (C. W. Naseser, written commun. cited in Whetten and others, 1988). It represents the age of recrystallization and suggests that the HH had cooled to less than 200° C in the Early Cretaceous. Comparison of the penetrative homogeneous S1 fabric in Easton greenschists with the lack of a pervasive penetrative fabric in HH greenstones that predates thrusting (see below) suggests that these units have different D1 blueschist-facies metamorphic histories (Fig. 12A). We suggest that this contrast in fabric development, as well as other textural differences, is most likely the result of higher maximum metamorphic temperatures for the Easton suite. Increased temperatures (as well as other factors; see Spry, 1986) promote ionic mobility and generally lead to penetrative ductile deformation, as well as increased metamorphic differentiation and grain size. Genetically, a temperature difference between the nappes may reflect different thermal positions during subduction and high-pressure blueschist metamorphism.

Our observations of the textures are similar to those of Blake and others (1967) for blueschists and metasedimentary rocks in California and Oregon. The HH corresponds to their textural zones 1 and 2, and the Shuksan nappe corresponds to their textural zone 3. Away from the Whitehall Creek thrust, the S1 foliation in metasedimentary rocks of the Easton suite is remarkably texturally granoblastic—a polygonal quartzose matrix with minor recrystallized albite and well-aligned, lepidioblastic metamorphic minerals such as actinolite, chlorite and muscovite. This foliation regionally displays a pronounced millimeter-scale quartzose segregation banding that parallels the foliation. The foliation also *parallels* rare bedding features, except in the hinges of rare F1 folds (Fig. 12A). This fabric corresponds to the

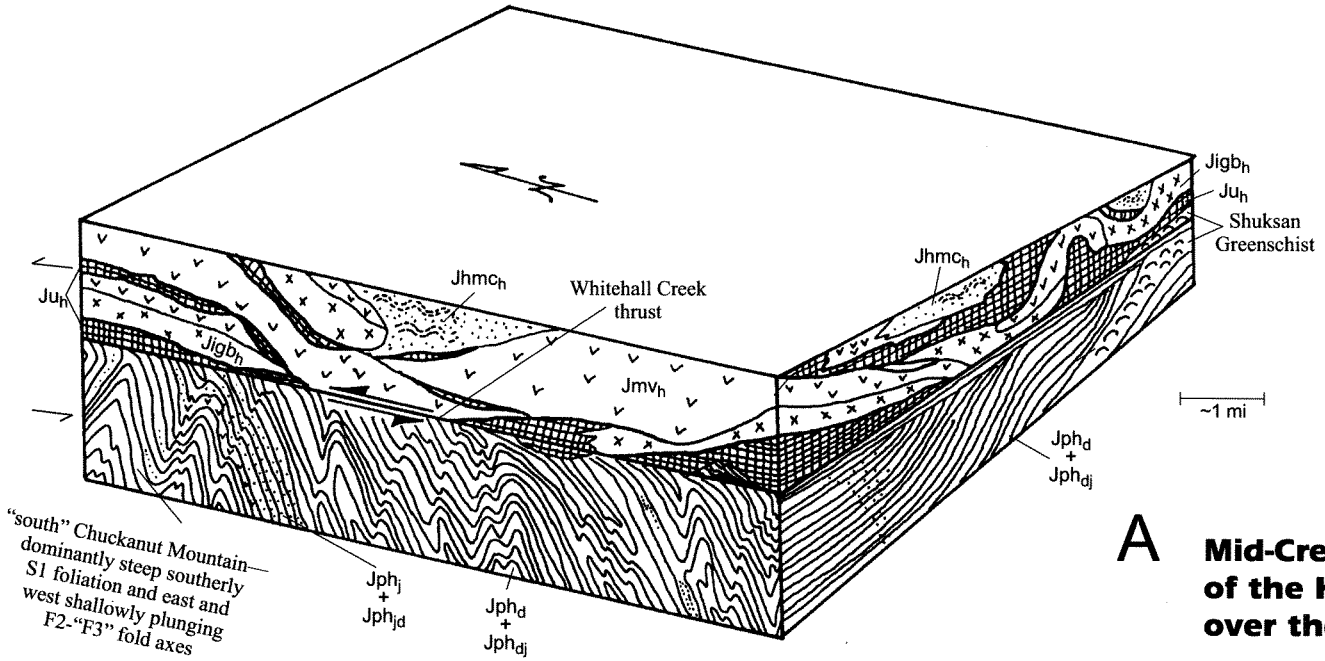


**A** **Mid-Cretaceous (~100–90 Ma) thrusting of the Helena–Haystack mélange over the Shuksan nappe**

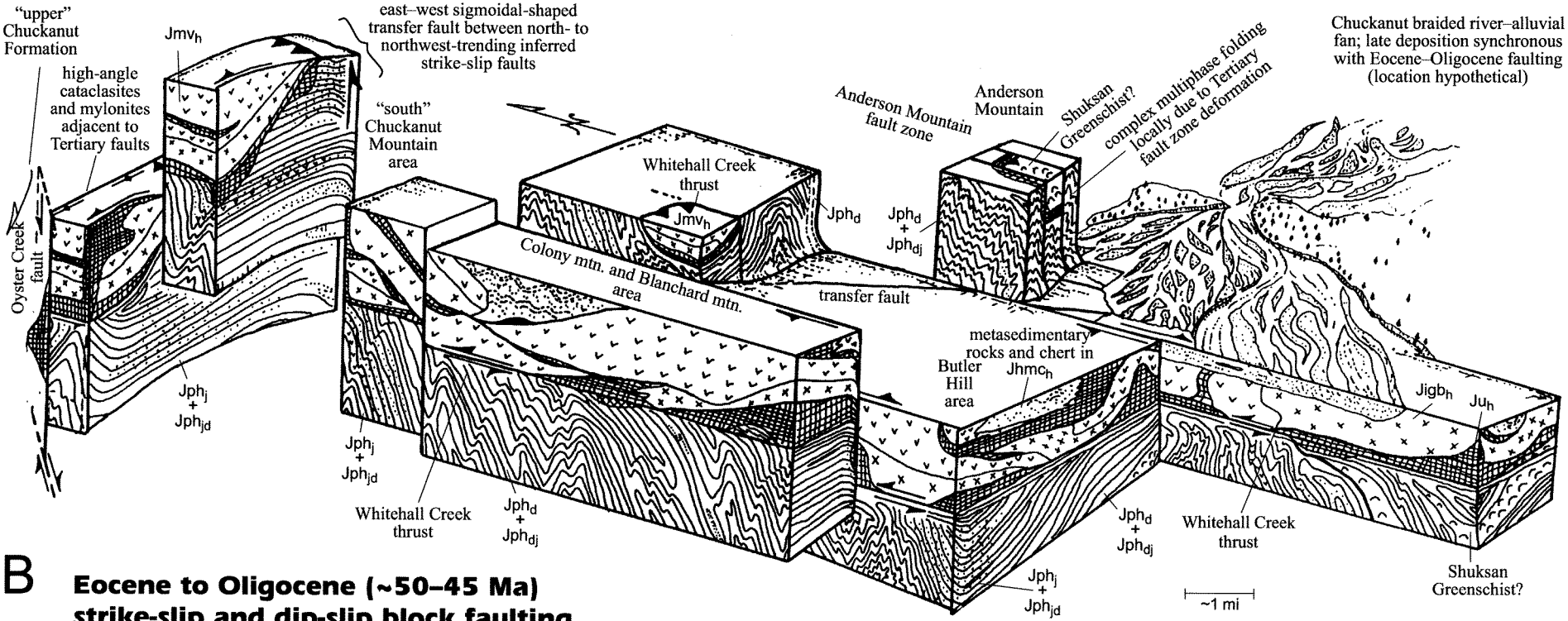


**B** **Eocene to Oligocene (~50–45 Ma) strike-slip and dip-slip block faulting**

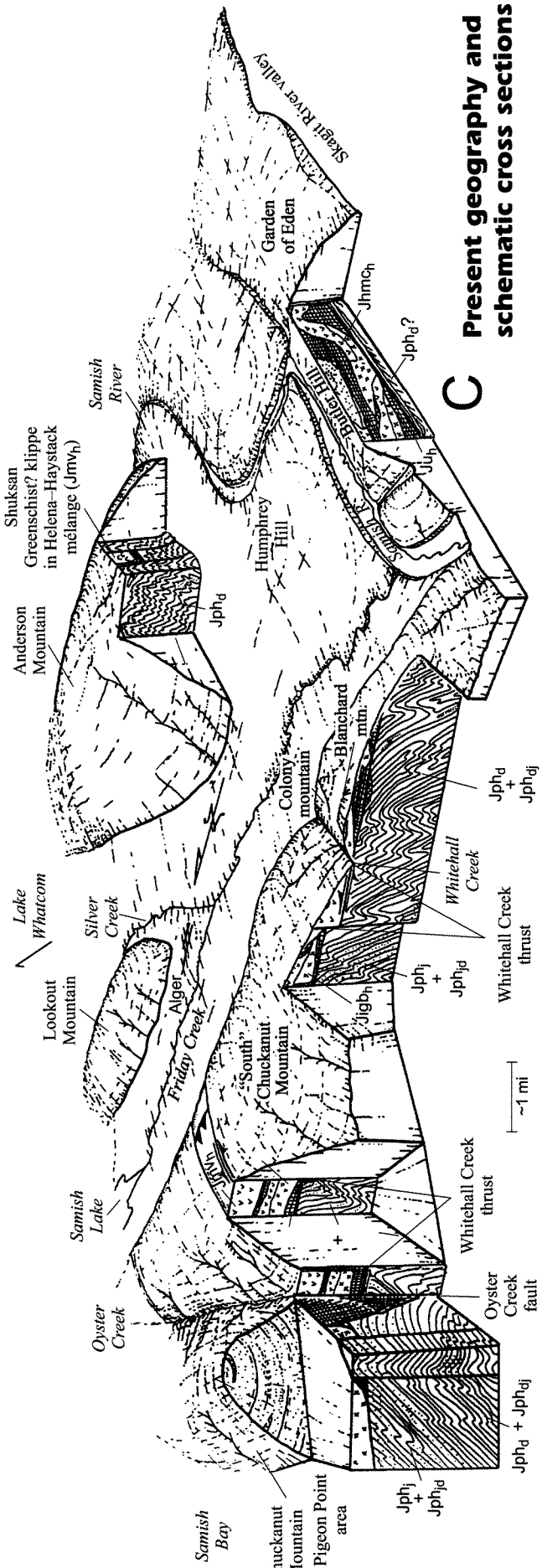


**Figure 11.** Schematic block diagrams showing (**A**) mid-Cretaceous thrusting of the Helena–Haystack mélange over the Shuksan nappe, (**B**) Tertiary disjointing of the thrust stratigraphy via high-angle faulting across the study area and juxtaposition of different mid-Cretaceous structural levels, and (**C**) present geography. Regional, through-going master faults (for example, Y in Fig. 14, block diagram viewed from a map perspective) and subsidiary transverse faults (R1 and R2, Fig. 14, block diagram viewed as a map perspective) structurally controlled deposition of syntectonic sediments such as the Chuckanut Formation. Localized en echelon folding of these Tertiary sediments reflects continued shear and compression of the basin. Thin-skinned thrusting of the Tertiary sediments may be important in basin evolution (R. A. Haugerud, USGS, oral commun., 1997; Dragovich and others, 1997a; England and Calon, 1991).

metagraywacke textural zone 3 of Blake and others (1967). Conversely, the slaty to phyllitic metasandstones, metasiltstones, and lesser metapelites of the HH (unit Jhmc$_h$) on Butler Hill have compositions comparable to the Shuksan nappe phyllites and semischistose metasandstones but differ texturally in several respects. Poor recrystallization of the HH metasedimentary rocks on Butler Hill is reflected in the predominantly fine grain size of the metamorphic minerals, good preservation of original clastic grain outlines, including angularity, and the preservation of the original cryptocrystalline matrix. Additionally, these rocks *lack* segregation layering; commonly they have only a slaty appearance, and foliation is locally transverse to bedding. Truncated grains and other features suggest a pressure solution cleavage locally. This fabric corresponds to the metagraywacke textural zone 2 of Blake and others (1967).

Other distinct textural differences exist between the regionally recognized foliated appearance of the well-recrystallized Shuksan Greenschist and the HH metabasaltic and metagabbroic greenstones of the study area. Regionally, Shuksan Greenschist (metabasalt) rarely displays primary structures such as pillows, is characteristically strongly granoblastic and foliated or schistose, and is thus classified as a *greenschist* (for example, Tabor and others, 1994). In contrast, the *greenstones* of the HH commonly show primary igneous outcrop structures such as pillows and pillow breccia and display a strong penetrative P-foliation only near the thrust with the underlying Easton suite. (See Fig. 14 for P-foliation and Riedel shear structures.)

Microscopically, the HH greenstones are broken by heterogeneous, few-millimeters-thick, fine-grained mylonitic Riedel R1, R2, and Y shear zones (see, for example, Fig. 14 and Plate 3, cross sections A–D explanations) or by weakly to moderately foliated S surfaces adjacent to C surfaces. Primary igneous textures and mostly static metamorphic minerals are preserved in the massive to weakly foliated lensoidal zones between the crossing mylonitic zones. These structures differ dramatically from those in *greenschists* mapped in the Shuksan nappe. The strongly foliated greenschist bodies have been convincingly shown to reside within a primary Easton suite stratigraphy (for example, Haugerud and others, 1981). For example, the S1 in the greenschists parallels the S1-bedding surface in nearby metasedimentary rocks and the interlayered greenschists can be traced semicontinuously to continuously along strike (Street-Martin, 1981). Similarly, tuffaceous *greenschists* interlayered with semischist on Chuckanut Mountain (this study and Gallagher, 1986) and Anderson Mountain (Fig. 3, loc. 41H) are a few to tens of meters thick and contain a strong, well-recrystallized, granoblastic synmetamorphic S1 foliation with metamorphic segregations and crenulations. The greenschist body on Chuckanut Mountain (Fig. 5, locs. 29, 28, 31, 33, 34, 35) has (1) a distinct S1 fabric and can be traced along the S1 strike, suggesting a localized semicontinuous primary stratigraphy on Chuckanut Mountain, and (2) S1 and L2 crenulations that parallel the fabric in the adjacent Shuksan nappe metasediments such as the semischist of Mount Josephine (also unlike HH metavolcanic bodies).

Textural and metamorphic-assemblage differences provide evidence for a metamorphic discontinuity be-

| Event | Location and Extent | Notes | Figure |
|---|---|---|---|
| **D1 deformation**<br>Late Jurassic to Early Cretaceous<br>Deformation syn-blueschist facies metamorphism observed regionally; S1 defined by strong mineral alignment, quartzose segregation layering, and moderate to strong recrystallization of primary minerals. | S1 foliation observed in all rocks of the suite; S1 overprinted locally where mylonitized adjacent to high- and low-angle faults (see below); L1 stretching (clast) lineation prominent in metasandstones and metaconglomerates of the Easton suite. | The S1 foliation typically dips steeply to the south in the Bow quadrangle (particularly in units $Jph_j$ and $Jph_{jd}$) (Fig. 11A) and does not show the multiple crenulations and variable S1 orientation of low-competence, phyllite-rich areas such as Anderson Mountain where post-D2 faulting and related(?) folding has complicated structural analyses. | 12A |
| **D2 deformation**<br>Early to mid-Cretaceous(?)<br>Isoclinal to open folding of the D1 fabric; "F3" folds lack axial planar cleavage and tend to be more open structures We envision most "F3" folds as lower strain variants of F2 folds. Note that "F3" in this nomenclature is best categorized as an F2 open fold without axial planar cleavage. | F2 and "F3" folding pervasive in the study area; locally overprinted by later structures (see below). Folds developed mostly in phyllite and are the only crenulations in the thick, poorly bedded to massive meta-sandstone–metaconglomerate lithologies (for example, unit $Jph_j$ displays homoclinal S1 with L2-L3 crenulations). | Bow quadrangle (for example, Chuckanut Mountain) F2 and "F3" folds have sub-horizontal east- to west-trending axes that parallel crenulation lineations; Anderson Mountain F2 and "F3" folds are more variable as a result of later pervasive superimposed deformation (see below). | 12B |
| **D3 deformation**<br>Mid-Cretaceous<br>Thrust-fault fabrics and related overturned folding. | Thrust-fault fabrics and folds developed in the Easton suite within tens of meters of the thrust fault contact with the overlying Helena–Haystack mélange; F2-"F3" folds distant from the thrust fault contact are pre-thrusting of the mélange over the suite and thus probably of D2, not D3 origin. F2 folds are overturned or overprinted near the thrust contact. | Mylonitic thrust-fault fabrics mostly flat to gently dipping; thrust-fault stretching lineations and striations largely shallowly north to south plunging. Some of the variation in the fabric orientations is interpreted to be the result of Tertiary deformation, such as tilting or warping of crustal blocks between high-angle faults. (See Plate 3, cross sections A–D, and Fig. 11.) | 12C |
| **D4 deformation**<br>Eocene to Oligocene<br>Faulting and associated cataclastic to mylonitic fabrics that modify pre-existing structures. Folding locally developed. | Observed adjacent to high-angle faults; faults are subparallel high-angle to vertical mylonites on Chuckanut and Anderson Mountains; refolding of F2 and "F3" folds (locally kinked) tentatively correlated with Tertiary faulting on Anderson Mountain. | Two generations of crenulations (L2 and later) observed on Anderson Mountain of the Alger quadrangle and very locally in the Bow quadrangle near Tertiary faults indicate post-D2 refolding of earlier structures. For example, see L4 lineations on Plates 1 and 2. | 12D |

**Figure 12.** *(above)* Fabric characteristics, extent, and location of the Easton Metamorphic Suite in the study area (Darrington Phyllite, semischist of Mount Josephine, and rare interlayered metavolcanic rocks). Somewhat similar, but probably lower temperature, metamorphic fabrics are observed in the metasedimentary rocks of the Helena–Haystack mélange (unit $Jhmc_h$) on Butler Hill. Metavolcanic and meta-intrusive rocks of the mélange (for example, $Jmv_h$) record a simpler structural history dominated by thrust-related structures (C type structures).

*(facing page)* The various metasedimentary rocks of the Easton suite have reacted differently to D1 and D2 deformations. The different deformational styles are related to the competency contrast between the phyllites and semischistose metasandstones as well as the thinner layering of the phyllites. The competent and generally massive to thickly bedded semischistose metasandstone displays a very consistent steeply south-dipping S1 foliation (**A**) (Plate 3, cross sections A–C). F2 folding in the semischist is only manifested as L2 microfolds or crenulations. In contrast, the less competent and well-layered Darrington phyllite is pervasively F2 folded on a microscopic to macroscopic scale. On Chuckanut Mountain, semischist composes a majority of the exposed Easton suite (Plate 1). The differing lithologically controlled structural styles of semischist and phyllite are best demonstrated at outcrops where distinctly F2-folded phyllitic interlayers occur between homoclinally S1 foliated semischist. Semischist in these outcrops contains only L2 crenulations that parallel the shallowly east- or west-plunging F2 fold axes in the phyllite (**B**). L1 stretching lineations are best developed in the semischist and commonly show a downdip south plunge, but varied orientations are a result of D2 folding and localized Tertiary mylonitization. Tertiary deformation in the competent semischist on Chuckanut Mountain is focused into discrete Tertiary high-angle faults and zones. This structural style contrasts with that of the Darrington Phyllite-rich rocks on Anderson Mountain, which have a more complex polyfold history and more pervasive record of younger deformations (**D**).

tween the HH and Shuksan nappes in the study area. The units contain similar key metamorphic minerals[1]. However, aragonite is conspicuously absent in the Shuksan nappe of the study area and is only rarely observed (Evans and Misch, 1976) in the Easton suite elsewhere. Brown and others (1981) tentatively ascribed the general lack of aragonite in the Shuksan nappe and the common occurrence of aragonite in rocks we assign to the HH (their Skagit valley greenstone-slate-phyllite-serpentinite unit) to an inversion of aragonite to calcite in the Shuksan nappe due to higher peak metamorphic conditions. (Aragonite and calcite occurrences in the study area are shown on Figure 3.) An inversion of aragonite to calcite with increasing metamorphic temperature is consistent with peak metamorphic temperatures and pressures (Brown and others, 1981) of about 400°C at about 8 kb for the Shuksan nappe and, perhaps, less than 300°C at similar pressures for the HH. Aragonite is commonly preserved in directionless to weakly foliated rocks between mylonitic zones in the HH. Calcite is observed in D3 protomylonites and mylonites and in extensional veins of mylonites of the HH, providing some evidence of a lowered pressure and (or) increased temperature and resultant conversion of aragonite to calcite during mid-Cretaceous thrusting.

Mylonitic fabric development along the thrust contact is late metamorphic as indicated by probable metamorphic discontinuity across the thrust and microboudinage of metamorphic minerals (such as actinolite) in greenstones near the thrust. However, mylonitization did not outlast metamorphism, as is indicated by

[1] In the Shuksan nappe and HH, the lack of blue Na-amphiboles characteristic of the blueschist facies is compositionally controlled by the Fe(+3) protolith composition (Brown, 1986), although Gallagher (1986) reports rare blue amphibole from the HH (our correlation) in the study area.

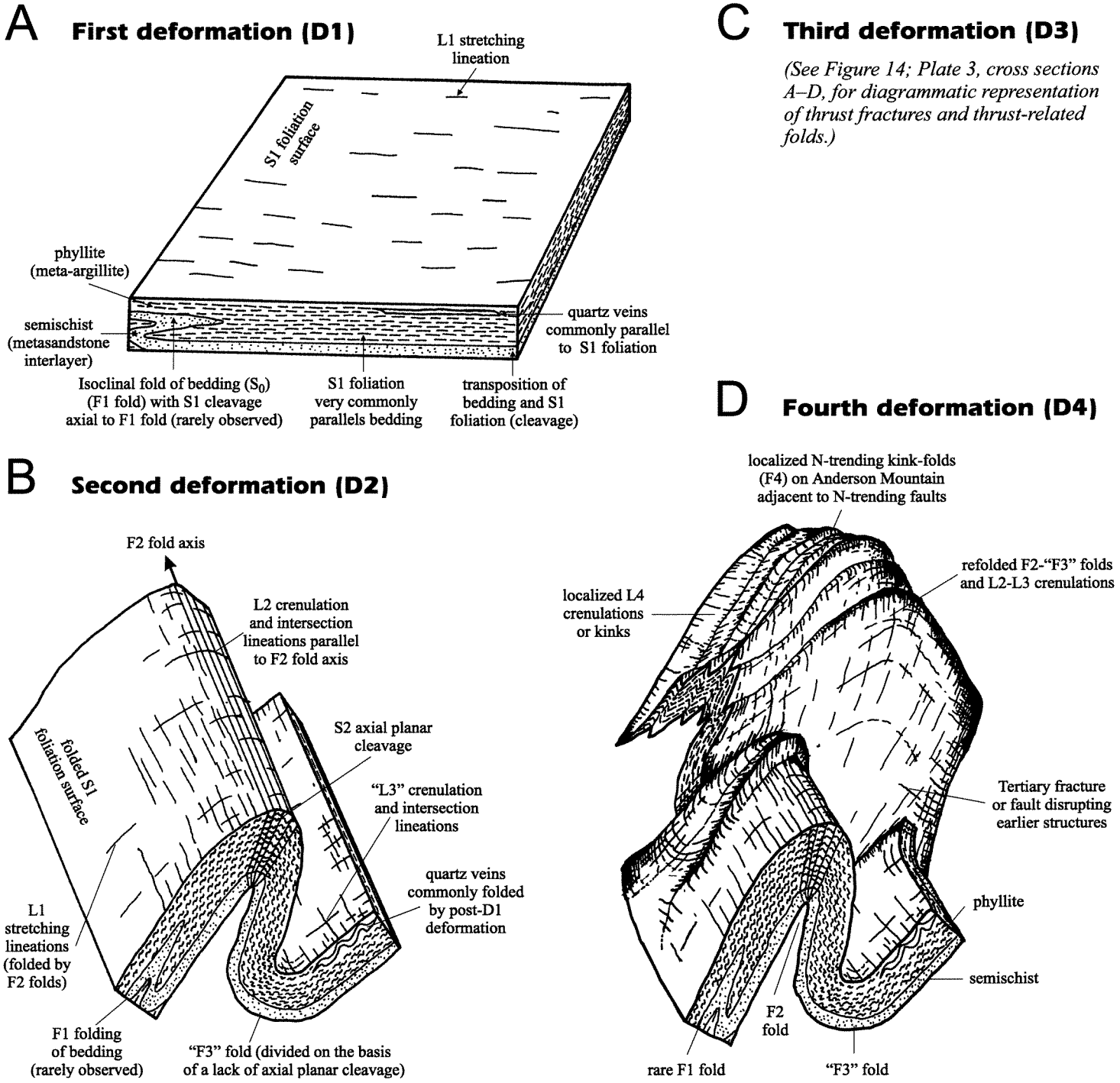


the growth of actinolite in pressure shadows associated with microboudinage and the stretching of primary igneous grains (such as augite) subparallel to the stretching or tectonic transport direction. Pumpellyite- and chlorite-filled extensional veins that we relate to thrusting also attest to the metamorphic conditions during mylonitization.

An episode of metasomatism and production of talc- and tremolite-rich ultramafite lithologies in the HH during thrusting is evidenced by (1) the strong mineralogic alignment of the thrust-related schistosity and extensional veins, (2) the general paucity of static mineralization features, (3) the common occurrence of talc- and tremolite-rich ultramafite varieties near or on the thrust contact, (4) the mostly flat to shallow-dipping thrust fabrics in serpentinites, talc schists, and tremolite schists that are subparallel to nearby thrust-generated fabrics, and (5) the observation by Schmidt (1972) that the pyroxenite is evidently a primary igneous body that has been mylonitized, hydrated or serpentinized, and finely granulated near the mylonitic contact with the underlying Shuksan nappe. Possibly, thrust strain-enhanced chemical gradients between the serpentinites and underlying rocks of the Shuksan nappe led to metasomatism of the near-thrust ultramafic bodies.

### Field and Structural Evidence for Thrusting of the Helena–Haystack Mélange over the Easton Metamorphic Suite

The various outcrop-scale fabrics and structures associated with the HH reflect protolith type, competence and ductility

contrasts, degree of layering, and proximity to the underlying thrust contact with the Easton Metamorphic Suite. The mesoscale mylonitic shear zones and fabrics are consistent with a through-going Riedel thrust shear zone model (see Fig. 14)(for example, Rutter and others, 1986; Logan and others, 1979, 1981). Fabrics in meta-igneous rocks near the thrust are mostly inhomogeneous mylonitic and strongly discordant to concordant with the horizontal to gently dipping thrust contact. Heterogeneous thin to very thin mylonitic zones locally parallel a prominent fracture cleavage and discrete fault surfaces near the thrust. Mylonitization clearly decreases away from the thrust contact with the Easton suite. Horizontal mylonitic or fracture surfaces typically cut weakly to moderately developed foliations that typically dip moderately southward. HH greenstones away from the thrust contact are typically nonfoliated to weakly or moderately foliated or fracture cleaved. Greenstones typically display heterogeneous protomylonitic to mylonitic zones. These millimeter-thick mylonitic shear zones are spaced millimeters to a few centimeters apart and are defined by a sutured or strained matrix, aligned chlorite, pumpellyite, and actinolite needles, and microboudinage of the pre-existing porphyroclasts (for example, igneous hornblende, augite, or plagioclase). Moderately to weakly foliated zones are commonly defined by moderate to weakly aligned actinolite, chlorite, and pumpellyite and semi-aligned to aligned relict igneous phases. Between mylonitic zones, equigranular metagabbro contains static or unaligned to weakly aligned actinolite in hypidiomorphic granular-textured lenses and preserves pre-mylonitic textures. Crosscutting Riedel shear zones and mineral foliation locally define S-C type mylonites, particularly near thrust contacts with the underlying Shuksan nappe.

Results of the heterogeneity of mylonitization and subsidiary shear zone development adjacent to the thrust are:

(1) Originally medium-grained, now mylonitized metagabbroic rocks are not easily distinguished in the field from fine-grained metabasaltic rocks of similar chemistry and petrology. Thus, some of the contacts between these units are approximate and reflect our combined field and office petrographic efforts to distinguish these units. Conversely, metavolcanic rocks are locally easily distinguished from metagabbroic rocks by basalt pillows, pillow breccias, or vesicles that locally survived thrust shear because of the heterogeneity of mylonitization; and

(2) Even the most strongly mylonitized metagabbroic rocks near the thrust contact contain lensoidal areas among the mylonitic shear zones. These areas preserve medium-grained, salt-and-pepper or microgabbroic textures characteristic of the intrusive phase of the unit.

Metasedimentary rocks of the HH on Butler Hill record a more complex structural history than the greenstones and generally contain an early, well-developed cleavage (possible pressure solution features) and two later fold-crenulation sets.

Generally, the greenstones and ultramafite of the HH reside topographically high (Plate 1) as isolated mountain-top bodies—a geometry most simply interpreted as klippen. Furthermore, the lack of chill zones, apophyses, xenoliths, or unconformable sedimentary relations suggests that there was not a premetamorphic intrusive or depositional contact between the greenstones and the Easton metasedimentary rocks (this study; Schmidt, 1972). Schmidt (1972) was the first to interpret the contact between greenstones and the Shuksan nappe metasedimentary rocks in the study area as a thrust fault. He also spatially associated the thrust with the occurrence of ultramafic bodies, mylonitization, and disruption of the underlying S1 fabric in the Easton suite. Gallagher and others (1988) also acknowledged that "the occurrence of sheared serpentinite at some contacts indicates that some were tectonically emplaced." Except for scattered mélange matrix ultramafic bodies, particularly in Butler Hill of the Alger quadrangle, most ultramafic bodies occur along the mapped thrust fault that separates the HH and Shuksan nappe. No ultramafic bodies were observed in the Shuksan nappe as primary lithologies. The few occurrences of ultramafite in the Shuksan nappe appear to represent mobilized pods or layers displaced into the lower plate by Tertiary faulting (for example, Fig. 5, locs. 34, 19).

As also observed by Schmidt (1972), the approach to the contact between the HH and Shuksan nappe is characterized by an increase in mylonitization. Phyllites and semischists of the Shuksan nappe directly under the thrust contact (Plate 1; Plate 3, cross sections A–D; Fig. 5, for example, locs. 27–30; see Fig. 14) are phyllonitized and show abundant microscopic evidence of grain reduction and stretching. Mafic intrusive and volcanic rocks of the HH are typically more massive away from the contact and distinctly mylonitized adjacent to the contact and exhibit horizontal or generally shallowly dipping foliation planes. The inhomogeneous mylonitic shear zones and P-foliation in the HH conform to a Riedel model for thrust shear (Plate 3, cross section C; see Fig. 14). The synmetamorphic S1 foliation in the phyllites and semischists of the Shuksan nappe dramatically differs from the mylonitic fabric of the HH. Gallagher and others (1988) base their correlation of their meta-igneous bodies in the Bow quadrangle (their Chuckanut Mountain metadiorite; our units $Jmv_h$ and $Jigb_h$) largely on the structural argument that the foliation of these rocks is an essentially vertical, east-striking fabric that parallels the foliation in the phyllites and semischists of the Shuksan nappe. However, several lines of evidence indicate that the fabrics in these disparate units are of different ages, probably of different metamorphic grades, and (as discussed above) of overall different orientation (especially near the thrust).

In the Bow quadrangle, the S1 foliation in the Shuksan nappe below the influence of the thrust dips steeply to the south, parallel to abundant bedding structures (Plate 1; Plate 3, cross sections A–D; Fig. 11). Local deviations from this orientation are attributed to (1) folding of the S1 along horizontal to shallowly plunging F2 or "F3" fold hinges or (2) Tertiary deformation of the earlier metamorphic fabrics near faults. Shallowly to moderately north- or south-dipping P-foliations or R1 mylonitic shear zones in the HH (Plate 1; Plate 3, cross section C; Fig. 5, locs. 18, 25, 27, 28, 29, 30, 35, 36, 39; see Fig. 14) are strongly discordant to the steeply south-dipping S1 foliation in underlying Shuksan nappe, contrary to observations of Gallagher (1986) and Gallagher and others (1988). E. H. Brown (Western Wash. Univ., oral commun., 1998) maintains that the concordancy or subparallelism of the HH and Easton suite fabrics across the contact at Colony mountain suggests that the S1 in the underlying phyllites and semischists is the same age as the fabric in the HH greenstones that we relate to later thrusting. However, we contend that foliation concordancy along a mylonitic zone should be expected due to transposition of earlier fabrics subparallel to the Y-shear plane and the new development of mylonitic fabrics in a high-strain thrust fault zone. Additionally, the fabrics in Easton *phyllonites* (mylonitic phyllites) and HH greenstones and serpentinites adjacent to the thrust are flat to gently dipping, whereas the Easton phyllites and semischists away from the thrust preserve a steeply dipping S1 foliation that

is older than the thrust tectonites (for example, Plate 3, cross sections A–D; see Fig. 14).

F2 and "F3" fold limbs in the Shuksan nappe away from the thrust contact typically dip at a high angle subparallel to the regionally steeply south-dipping S1 foliation (Plate 1; Bow quadrangle). Meters to tens of meters directly below the thrust, S2 axial planes are folded or transposed subparallel to the flat thrust plane. (See Fig. 14.) We observed overturned thrust-related flexural slip folds of phyllonites directly below the thrust at many places along the well-exposed bluffs in the Whitehall Creek–Blanchard mountain–Chuckanut Mountain area (for example, Fig. 5, locs. 27–30). Refolding of the F2 axial planes indicates that thrusting is post-D2 folding. In or directly below the thrust, a crosscutting shear foliation is developed in the phyllonites, and, as also noted by Schmidt (1972), lens-shaped fragments containing the original S1 lepidioblastic fabric are surrounded by a flat mylonitic D3 thrust fabric.

## MID-CRETACEOUS THRUSTING OF THE HELENA–HAYSTACK MÉLANGE OVER THE SHUKSAN NAPPE—STRUCTURAL OBSERVATIONS AND KINEMATICS

Thrusting appears to have occurred in the mid-Cretaceous (for example Misch, 1966; Brown, 1987; Tabor and others, 1994; Brown and others, 1987; Brandon and others, 1988). Our structural findings in the quadrangles (Plates 1, 2, 3; Dragovich, unpub. data) complement those of some previous studies and extend the thrust nappe architecture of the Northwest Cascades system from south of Skagit River (Whetten and others, 1980a; Tabor and others, 1994) to Chuckanut Mountain and surrounding areas. Where not altered by later Tertiary faults and fault zone structures, several inhomogeneously developed structural elements indicate that HH thrusting over the Shuksan nappe was generally north directed in the quadrangle:

- the north-south orientation of thrust-related stretching lineations (including stretched porphyroclasts and aligned metamorphic minerals) and striations (tectonic transport criteria of Shackleton and Ries, 1984), on mostly flat *thrust-related shear foliations* (including Riedel shear mylonites and fracture patterns),
- the orientation of extensional veins roughly perpendicular to the tectonic transport direction lineations, and
- the overturned geometry of folds in the Shuksan nappe directly under the thrust.

Thrust-related P-foliations are commonly gently south dipping in the HH, consistent with the Riedel top-to-the-north thrust shear model. (See Fig. 14.) These fabrics are locally subparallel to the axial planes of small- and moderate-scale, tight to isoclinal, overturned folds in the underlying phyllite or semischist. These folds deform earlier F2 fold axial planes, and, although requiring more systematic study, the sense of drag on the axial planes appears to be consistent with a top-to-the-north shear. Kinematic analysis of the mylonites related to thrusting in the study area indicates a north-south displacement direction, with a probable top-to-the-north thrust sense, thus placing the HH over the Shuksan nappe (Plate 3, cross sections B, C).

We observed top-to-the-north shear sense indicators in several horizontal or shallowly dipping mylonitic zones that display mostly north-south stretching lineations and striations on or near the thrust fault; a few sites are in subsidiary mylonitic zones away from the thrust but are included here with thrusting because of their orientation. Kinematic analysis involved Riedel fracture patterns, S-C mylonites, and rare asymmetric pressure shadows adjacent to porphyroclasts (Lister and Snoke, 1984; Groshong, 1988; Simpson and Schmidt, 1983, Rutter and others, 1986). These kinematic indicators are derived from a similar kinematic model. For example, the C and S surfaces of S-C mylonites correspond to the Y shear plane and P-foliation, respectively, in a Riedel shear model, and thus we essentially applied a Riedel shear model to the fractures and foliations observed near the thrust (for example, Rutter and others, 1986; Logan and others, 1979, 1981). The main thrust is well exposed along Whitehall Creek (Plate 1). We found 14 sites that contain phyllonites or mylonites suitable for more detailed petrographic kinematic analysis. Of the fourteen, seven displayed good to excellent kinematic evidence for top-to-the-north displacement; five displayed moderately good to poor evidence for top-to-the-north displacement; and two displayed moderately good to poor evidence for top-to-the-south displacement. Noteworthy is the site along the westernmost portion of Blanchard mountain (see Fig. 14) where several well-exposed outcroppings above, on, and below the thrust provide a top-to-the-north shear sense and therefore are excellent kinematic analysis sites. S-C mylonites providing a top-to-the-north displacement direction were petrographically verified for three of the outcroppings at this site. Our north-northwest displacement direction is consistent with that of previous structural analyses in the Northwest Cascades system (for example, Brown, 1986, 1987; Brown and others, 1987; Smith, 1986; Monger, 1966; Ziegler, 1985; Dragovich and others, 1997a). The data support Brown's continental margin-parallel thrust displacement model, in which oblique subduction of outboard oceanic plates drove the nappes northward onto the rigid buttress of the southern Coast Mountains of British Columbia. In this model the HH was driven over the Shuksan plate during widespread mid-Cretaceous thrusting.

Several studies have noted the gross similarities of the rock assemblages constituting the nappes of the San Juan Islands to the mainland portions of the thrust belt; thus most workers consider them as parts of a continuous Northwest Cascades system orogen. However, two apparently unexplained fundamental differences exist between the mainland and San Juan Islands parts of the orogen:

(1) Thrust mylonites in the San Juan Islands contain syn-high pressure metamorphic minerals (lawsonite and aragonite), and thrusting and metamorphism occurred in a fold-and-thrust orogen from about 88 to 100 Ma (Brandon and others, 1988). Conversely, thrusting on the mainland appears to be mostly late- to post-metamorphic, as shown by the metamorphic disparity between the thrust nappes (for example, Brown and others, 1981), minor recrystallization of quartz, chlorite, muscovite, stilpnomelane, and calcite in thrust-related mylonites, and the lack of metamorphic minerals overprinting thrust mylonites (Brown, 1986). Thrust mylonites appear to be of lower prehnite-pumpellyite grade on the mainland portion of the orogen (Armstrong and Misch, 1987).

(2) Brandon and others (1988) consider the San Juan portion of the orogen to have east-west nappe transport directions. Conversely, Vance (1975, 1977) and Maekawa and Brown (1991, 1993) consider the San Juan kinematics to indicate north-south vergence, similar to the findings of Brown (1986) for the mainland part of the orogen.

## TERTIARY DEFORMATION AND DISMEMBERMENT OF THE THRUST STRATIGRAPHY

High-angle faults in the study area displace Cretaceous structures and are best ascribed to the Tertiary; this faulting is likely dominantly Eocene to Oligocene on the basis of the age of syn-faulting fluvial sediments, including the Chuckanut Formation, rocks of Bulson Creek, and the Huntingdon Formation (Miller and Misch, 1963; Johnson, 1984b; Evans and Ristow, 1994) as well as regional geologic considerations, including the ages of sedimentary and volcanic rocks involved in faulting (for example, Tabor and others, 1994; Whetten and others, 1988; Brown and others, 1987). The syntectonic, gently folded Oligocene Huntingdon Formation unconformably overlies the Chuckanut and postdates the tight folding of the upper Chuckanut north of the study area (Miller and Misch, 1963; Dragovich and others, 1997d). (Also see Marcus, 1980, syntectonic deposition of the rocks of Bulson Creek.) Vance (1985) proposed that major north-trending faulting ended before intrusion of the Chilliwack batholith and Cascade magmatic arc in the earliest Oligocene. Furthermore, rapid middle Eocene to Oligocene upper Chuckanut sedimentation due to local tectonic events, including exhumation of pre-Tertiary basement along basin-bounding faults, is indicated by several studies (Dragovich and others, 1997d; Evans and Ristow, 1994; Mustoe and Gannaway, 1997).

Eocene to Oligocene faulting was probably part of a regional dextral strike-slip regime (Johnson, 1984a; Vance, 1985; Dragovich and others, 1997d) and involved long, through-going strike-slip faults (for example, Straight Creek fault; Fig. 2), localized, conjugate transfer faults, and development of Eocene pull-apart basins (Johnson 1984a, 1985a) with vertical or extensional motions on some faults. The Eocene to Oligocene Puget Sound basin contains several pull-apart subbasins in an overall dextral strike-slip regime (Johnson, 1985a). Fault trends may have been modified by Tertiary accretion of the Olympic terrane (Tabor, 1994). It should be noted that some of these high-angle faults may be rejuvenated older structures, such as the syn-thrust, mid-Cretaceous, high-angle faults envisioned by Brown (1987).

High-angle faults have disrupted the thrust stratigraphy in the study area, locally resulting in a significant rearrangement of the Cretaceous structures (Fig. 11B,C). Recognition of Tertiary faults in the area is important in reconstructing the previous thrust stratigraphy that, we contend, places the HH over the Easton suite in the study area (Plates 1, 3, cross sections A–D).

High-angle Tertiary faults in the study area are mapped mostly on the basis of aerial photograph lineaments and field observation. Faults are associated with striated cataclastic zones, subparallel fractures (many of which are semipenetrative), protomylonitization, and mylonitization. Also, many of the mapped Tertiary fault zones, mostly inferred from other evidence, contain fragments of HH ultramafite (mostly serpentinite). Indirect evidence for faults includes changes in rock types or interpreted structural levels across lineaments. For example, an east-west fault near Whitehall Creek (Fig. 5) is implied by both a change in the general altitude of the thrust that separates the Shuksan nappe and HH nappe as well as by the distinct break from dominantly semischistose metasandstone to phyllite in the Easton suite across the fault. Other deformational effects on Cretaceous structures include:

- localized folding of the normally east-striking S1 foliations of the Shuksan nappe along the west side of Chuckanut Mountain, resulting in steep to vertical, northwest-striking foliations near Oyster Creek; we ascribe folding to drag along the north-northeast striking, high-angle Oyster Creek fault;
- localized tilting of the HH klippen along a northerly axis; the blocks occur within small structural domains, particularly where they are bounded by intersecting sets of Tertiary faults (for example, the Blanchard–Colony mountain area); and
- some S-C mylonites associated with fault zones appear to contain Tertiary C-surfaces intersecting older Cretaceous foliations (S-surfaces). Most of the faults show evidence for strike-slip motion; however, dip-slip motion is locally suggested by striation measurements and the apparent offset of similar rock bodies.

### The Anderson Mountain Fault Zone

The Anderson Mountain fault zone and nearby subparallel faults (Plate 1, Fig. 5) strike to the north and are associated with cataclasite and apparently in-sheared serpentinite of HH origin. Faulting on Anderson Mountain is pervasive; many outcrops display a fracture cleavage or jointing subparallel to the north-trending faults. An S-C mylonite on Anderson Mountain contains spaced C surfaces and displays kinematics consistent with dextral strike-slip fault motion. Inhomogeneous Tertiary faulting has kink folded or warped the previous S1 or S2 cleavages of the phyllite on the mountain, locally leading to two fold sets and crenulations (Fig. 12D) and complex refolding of the phyllites.

### The Chuckanut Mountain Fault Zone—Transfer Faults?

We suggest that the east-trending, S-shaped (Plate 1, Fig. 13), high-angle faults on Chuckanut Mountain are antithetic transfer faults accommodating strain between a concealed north- to northwest-trending strike-slip fault(s) east of the mountain and the Oyster Creek fault to the west (Figs. 5, 13). The S shape of the transfer faults suggests an R2 fault zone (Fig. 14, block diagram) in an overall north-northwest strike-slip fault system (Wilcox and others, 1973). Mandl (1988) states that

> "in both experiments and the field example, the R2 shears show clear evidence of *rotation* [our emphasis], which accommodates basement wrenching. From experimental evidence it may be inferred that the R2 shears outside the *overlap region* [our emphasis] of neighboring R1-shears started rotating and acquiring *a sigmoidal [S-]shape* [our emphasis] after their formation as conjugates of the first-generation R1 shears, while the R2 shears inside the overlap region form as rotating cross-faults when unfavorably oriented R1 shears can no longer accommodate further basement wrenching."

The correlation of protomylonitized semischists that have horizontal stretching lineations and striations on vertical planar foliations and fractures with Tertiary cross-faults on Chuckanut Mountain clarifies the geometry of older structures, such as the L1 lineation and S1 foliation in the Easton suite. For example, correlation of many of the shallowly east- or west-plunging stretching lineations with Tertiary proto-mylonitization (Plates 1, 2) produces a more distinct L1 downdip stereonet distribution. This semi-girdle distribution of southerly trending L1 lineations is more easily interpreted as F2 folding of L1 lineations on Chuckanut Mountain (Dragovich, unpub. data) (Fig. 12B). A 1-m-thick S-C vertical mylonite zone with a dextral strike-slip sense of shear and very shallowly east-trending stretching lineation clearly intersects a shallowly south-dipping,

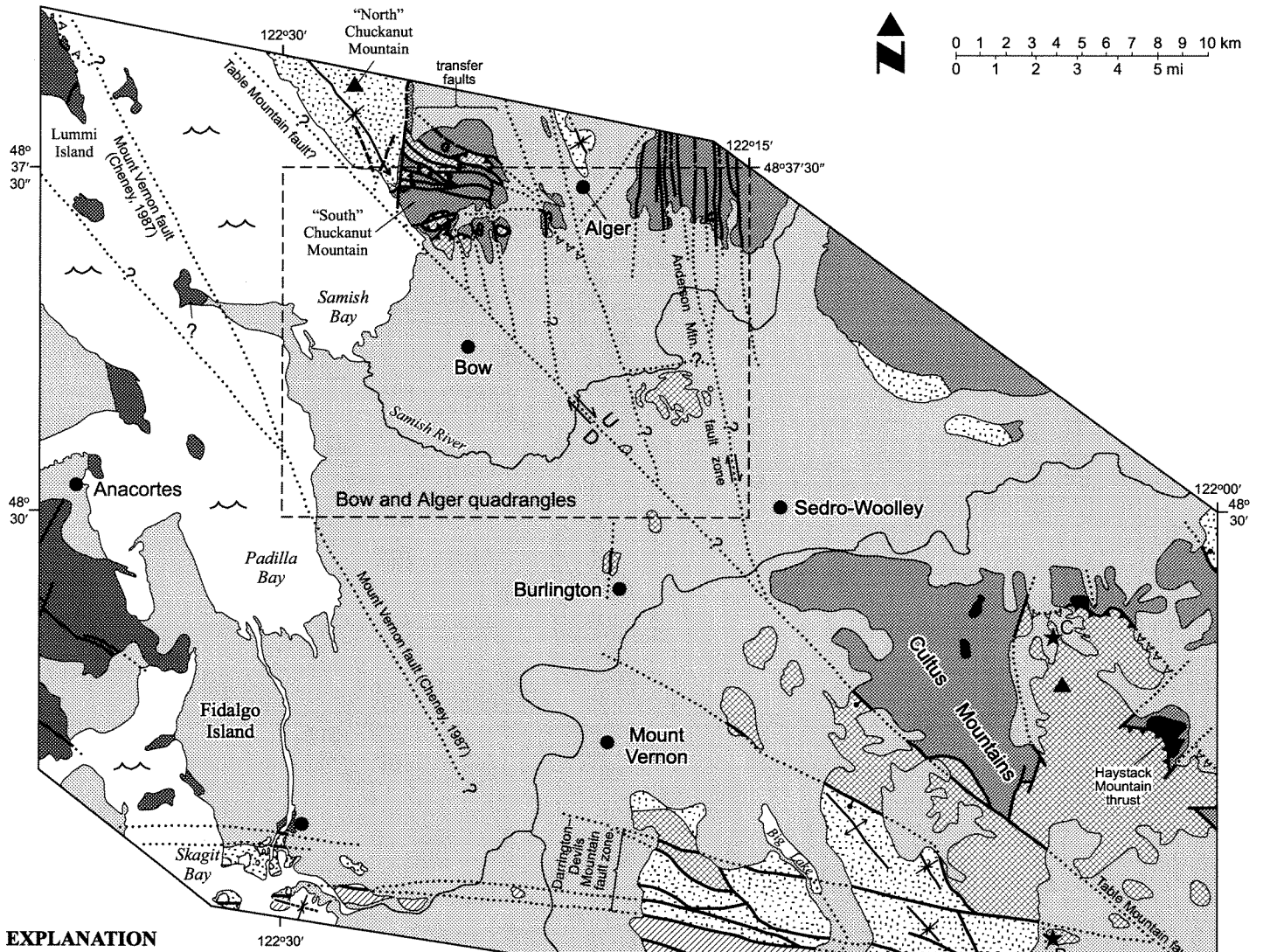


**EXPLANATION**

**Geologic Units**

Sedimentary deposits

Surficial glacial and nonglacial deposits (Holocene and Pleistocene)

Continental and volcanic rocks

Bulson Creek unit (Lovseth, 1975) (Oligocene and Eocene) and rhyolite (Eocene), undivided

Chuckanut Formation and rhyolite (Eocene), undivided

Low-grade metamorphic rocks of the Northwest Cascades system

Eastern mélange belt of Tabor (1994) (Jurassic–Mississippian); includes the Goat Island and Tafton terranes (Whetten and others, 1988)

Helena–Haystack mélange of Tabor (1994) (this study) and Haystack terrane of Whetten and others (1988), undivided (Jurassic)

Decatur terrane, including the Lummi Formation (Cretaceous and Jurassic) and Fidalgo ophiolite (Jurassic) of Brown and others (1979)

Darrington Phyllite and semischist of Mount Josephine of the Shuksan Metamorphic Suite (Jurassic); includes rare metavolcanic rocks

Shuksan Greenschist in the Darrington Phyllite around Haystack Mountain (Whetten and others, 1988)

**Geologic Symbols**

High-angle fault; dashed where inferred, dotted where concealed; ball on the downthrown side

Thrust fault; dotted where concealed; sawteeth on upper plate

Fold axis; arrow indicates direction of plunge

160–170 Ma U-Th-Pb zircon ages (quartz diorite tectonic blocks in the Helena–Haystack mélange; Whetten and others, 1988)

**Figure 13.** Simplified geologic map of the study area and surrounding region. Map compiled from Cheney (1987), Tabor (1994), Brown and others (1979), Garver (1988), Bechtel, Inc. (1979), Whetten and others (1980a, 1988), Carroll (1980), and Johnson (1982). Analysis and restoration of Tertiary faulting in the area is complicated by the concealing Quaternary deposits. However, the orientation and kinematics of exposed probable Eocene to Oligocene structures and continental sediments are consistent with a pull-apart basin into which the Chuckanut Formation was deposited in an overall northwest-trending strike-slip regime (Johnson, 1984a).

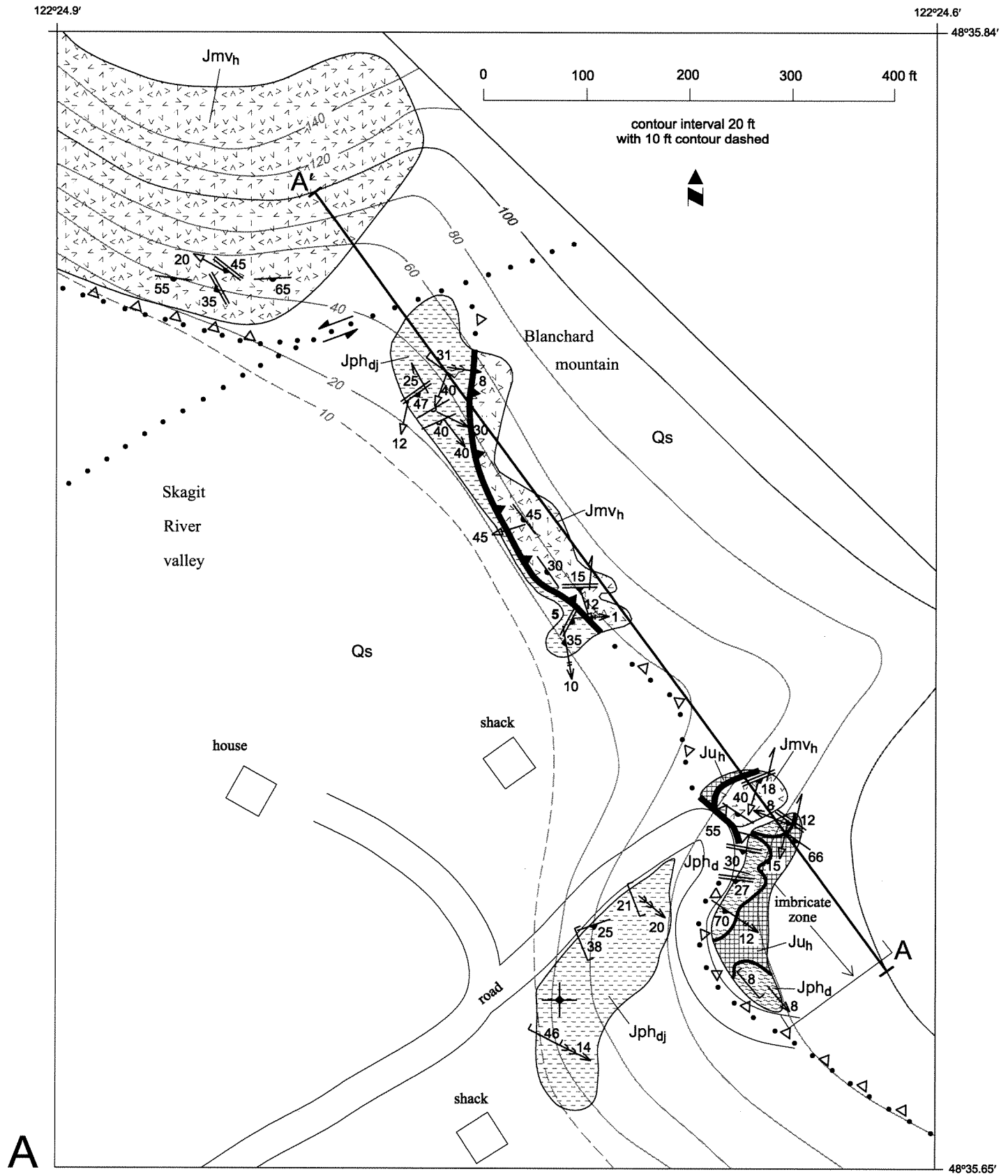


**Figure 14.** Blanchard mountain critical site map (**A**), cross section (**B**), and schematic block diagram of typical structures (**C**). See Figures 3 (site 101B) and 5 (site 27 map outline in the Bow quadrangle). This critical site is near the southernmost part of cross section B on Plate 3. This site and several excellent exposures of the Whitehall Creek thrust in Whitehall Creek north of this site demonstrate the horizontal nature of the structural contact between the Helena–Haystack mélange nappe and Shuksan nappe in the study area. Three sites shown with the tectonic transport direction symbol provide convincing macroscopic and microscopic evidence for top-to-the-north thrust displacement. These sites have flat C-surfaces and a new mylonitic to protomylonitic thrust foliation (S-foliations) that mostly obliterates or overprints the previous S1 foliation, including the segregation layering. The S1 foliation with overturned folds is observed microscopically directly under the thrust as less-sheared islands or zones in the phyllonites. Greenstone mylonite foliations and fracture patterns are consistent with the Riedel shear model.

## EXPLANATION

Qs — Undivided surficial deposits

Metabasite (unit $Jmv_h$); see this map for fabric orientations

Serpentinite (unit $Ju_h$) and phyllonitized Darrington Phyllite of the imbricate zone with rare enclaves of phyllite that preserve S1 cleavage

Schematic representation of thrust-shear fold S1 cleavage of the Darrington Phyllite (unit $Jph_d$); S1 rare or absent near the thrust and in the imbricate zone where mylonites containing Y, R1, and P foliations are the predominant fabric elements; S1 folation is inferred to steepen below sea level and thus to become conformable with the S1 foliation observed away from the South Chuckanut Mountain thrust

### Contacts

Contact

### Faults

Low-angle fault contacts between phyllite, serpentinite, and metabasite in the imbricate zone

Thrust fault; dotted where concealed

Thrust and parallel to sub-parallel Y and R1 shear zones

### Foliations

Tectonic transport direction of the top plate using macroscopic and microscopic kinematic indicators (combined with foliation symbols) (7 on the block diagram)

S1 cleavage (8 on block diagram)

Flat S1 cleavage (5 on block diagram)

Weak S2 spaced axial planar cleavage to overturned thrust-related folded S1 cleavage; observed in phyllites of the imbricate zone and below the thrust fault zone; note progressive increase of axial planar dip below the thrust (3 on block diagram)

Inhomogeneous mylonitic P-foliation; locally includes preserved S1 foliations in the imbricate zone (1 on block diagram), locally includes slickensided R-1 fracture planes

Y or C foliation or fracture plane (2 on block diagram)

### Lineations

L2 crenulation lineations (F2 microfolds) (4 on block diagram)

Stretching lineations; locally includes parallel striations and elongate asbestos fibers in the serpentinites (6 on block diagram)

Striations (6 on the block diagram)

### Folds

Asymmetric, overturned, mostly S-shaped F2 folds in the Darrington Phyllite; parallel to L2 crenulation lineations (4 on the block diagram)

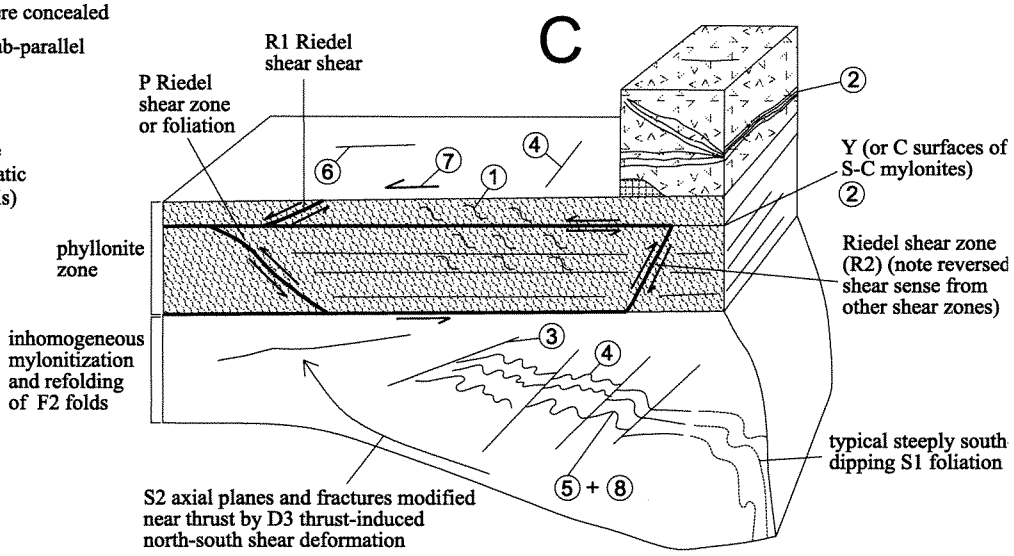


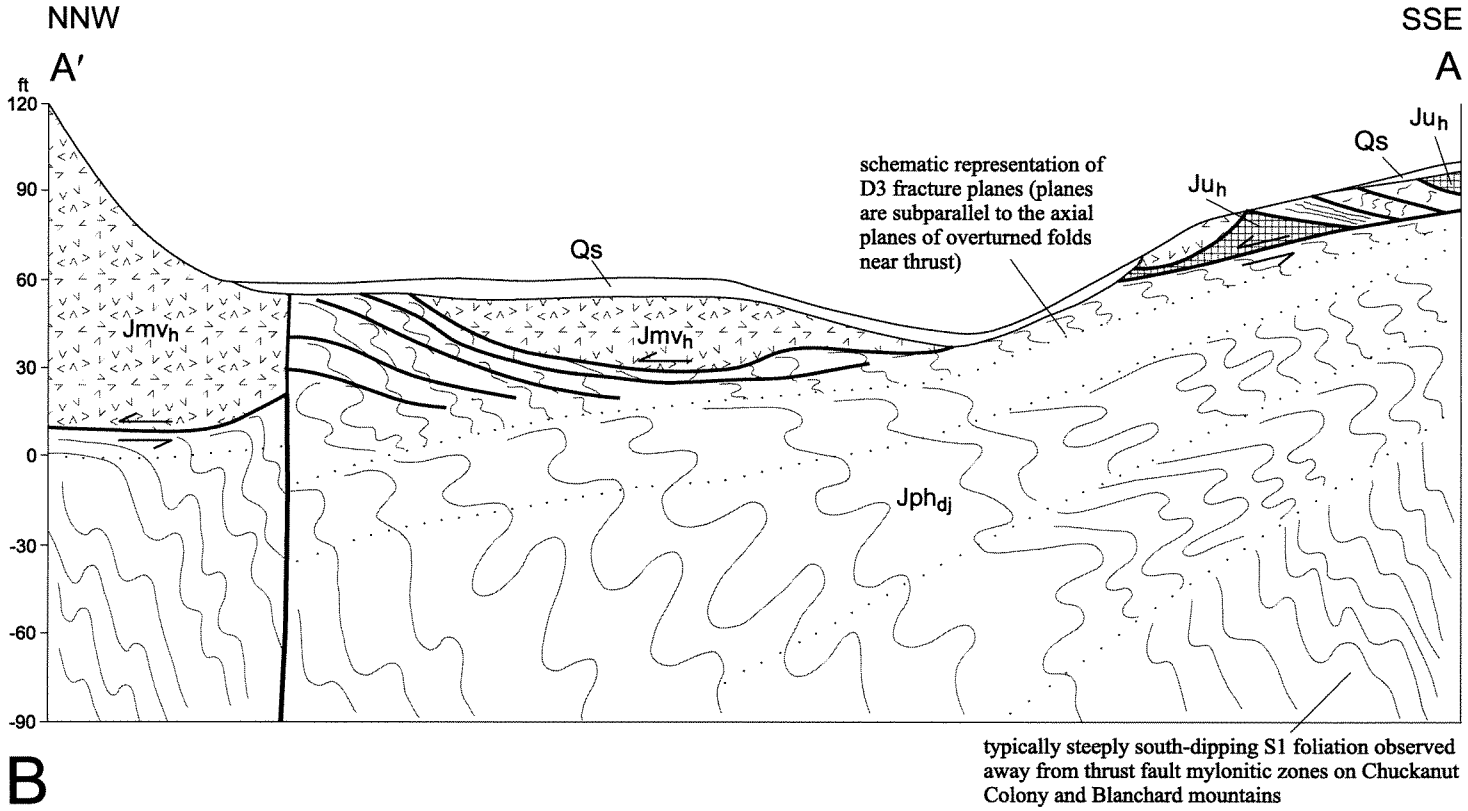

granoblastic S1 foliation with a downdip L1 stretching lineation on Chuckanut Mountain (Fig. 3, site 9H). Gallagher and others (1988) mapped several vertical to near-vertical foliations as S1 on Chuckanut Mountain, suggesting that the greenstones, ultramafite, phyllites, and semischists have essentially vertical subparallel S1 fabrics. We suspect that many of the vertical foliations are Tertiary in age on the basis of their proximity to our mapped east-west-striking faults, and thus we ascribe most of these vertical cataclastic fractures or mylonitic foliations to Tertiary D4 deformation (Fig. 12D). These fabrics are distinctly younger than the predominantly moderately south-dipping S1 foliation (Plate 3, cross sections A–D).

Petrographic microkinematics of the four mylonites associated with the Tertiary faults provide evidence for both sinistral (2 samples) and dextral offset (1 sample), and almost pure dip-slip displacement with north side down (1 sample). The apparent sinistral offset of most of the HH klippen on Chuckanut Mountain (Plate 1; Figs. 5, 13) is most consistent with an R2 Riedel model for these faults, and we interpret them as transfer structures accommodating strain between the more northerly striking, master dextral faults east and west of Chuckanut Mountain. Synchronous(?) and possibly later vertical motions on these faults exhumed and cut the nappes and led to the diced appearance of the HH klippen on the Shuksan nappe in the study area. Evidence for *both* horizontal and vertical components leading to pull-apart basin formation in an overall transpressional strike-slip regime is consistent with the strike-slip fault modeling of Dauteuil and Mart (1998).

### Tertiary Fault Offset of the Helena–Haystack Mélange and Regional Fault Restoration

Both Whetten and others (1980a) and Tabor (1994) tentatively correlate the HH with the Fidalgo ophiolite of Brown (1977). They proposed that the Fidalgo ophiolite of the Decatur terrane and Helena–Haystack mélange (parts of the Haystack terrane of Whetten and others, 1980a) may have been formed in the same or nearby oceanic basins. This conjecture was made on the basis of their similar Jurassic ages, stratigraphic similarities, and ophiolite to island-arc depositional environment. The MORB–island-arc Easton Metamorphic Suite may have been part of this basin.

Several mapped or inferred high-angle faults may have played a role in the Tertiary dispersal of the HH and probable correlatives such as ophiolitic rocks on northern Lummi Island and the lower grade Decatur terrane. The Jurassic metagabbros and MORB augite-bearing metabasalts on Lummi Island (Carroll, 1980) contain aragonite, pumpellyite, and lawsonite. These greenstones both lithologically and metamorphically resemble the HH rocks. The HH in the study area and ophiolitic rocks on Lummi Island are of significantly higher grade (higher pressure) than the Fidalgo ophiolite portion of the Decatur terrane (Brown and others, 1981; this study), implying post-Cretaceous faulting between the HH–Lummi Island belt and the Fidalgo ophiolite of the Decatur terrane to the southwest. Regionally important candidate faults (Fig. 13) include the Table Mountain fault of Whetten and others (1988) and the Mount Vernon fault of Cheney (1987). The Table Mountain fault soles or curves into the regionally important Darrington–Devils Mountain fault zone (Tabor, 1994; Figs. 2, 13). Offset along the Table Mountain fault and our northwestward projection of this structure (Fig. 13) may be responsible for the northwestward movement of the probable correlatives of the HH on Lummi Island (Carroll, 1980) relative to HH klippen in the study area. Significant apparent dip-slip faulting on the Table Mountain fault vertically juxtaposes the HH and Shuksan nappe southeast of the study area. This apparent dip-slip faulting may partially explain the lack of exposure of the Easton suite west of both the Table Mountain fault and our inferred northwestern continuation of this fault west of Chuckanut Mountain (Fig. 13). Down-to-the-west dip-slip faulting along the Table Mountain and (or) similarly oriented Tertiary faults concealed under the Skagit valley Quaternary fill may have played a significant role in the juxtaposition and dispersal of ophiolitic terranes and the Easton suite in and around the study area.

According to Cheney (1987), the Mount Vernon fault (Fig. 13) has offset the once-continuous Darrington–Devils Mountain fault (south of the study area) from the Haro fault (west of the study area). This structural correlation does not seem probable in light of the similarity of Tertiary rock types across this Darrington–Devils Mountain fault zone as mapped by Whetten and others (1988). However, evidence for the Mount Vernon fault of Cheney (1987) northwest of the study area appears more probable, and we suggest that this structure may be a part of the northwestward extension of the Table Mountain fault presently projected directly to the west of this structure (Fig. 13).

## ACKNOWLEDGMENTS

This report was produced in cooperation with the U.S. Geological Survey National Cooperative Geologic Mapping Program Agreement Number 1434-HQ-97-AG-01809. Field mapping was performed by all the authors. Dragovich and Norman have an ongoing project compiling geochemical analyses of the region; Grisamer aided Dragovich with subsurface investigations (in press) and some map compilation; Logan helped with the petrographic analyses for the study area. We greatly thank Keith Ikerd and Carl Harris for their cartographic support on the map, figures, correlation diagram, and explanations. We are indebted to Ralph Haugerud (USGS) and E. H. "Ned" Brown of Western Washington University (WWU) for joining us in the field and providing enlightening discussions concerning structures and petrology in the study area. We also thank Scott Babcock for a review of our geochemical data and interpretations. Rex Davis and Jason Shutt were our capable field assistants. Paul Pittman (WWU) aided us in the field for one day. We thank Rowland Tabor (USGS emeritus), Ned Brown, and Mike Gallagher (Sehome High School) for helpful discussions and Dave Engebretson (WWU) and Clark Blake (USGS retired) for sharing some results of their in-progress study of the pre-Tertiary rocks in the western San Juan Islands. Richard Blakely (USGS) kindly shared the results of his in-progress magnetic survey maps. Chuck Blome (USGS) and Kitty Reed (Division of Geology and Earth Resources [DGER]) examined two chert samples. We appreciate the assistance of Phil Ambrosino (Washington Dept. of Transportation Materials Lab.) with our geotechnical boring compilation. Thanks also to DGER staff members Eric Schuster, Tim Walsh, and Ray Lasmanis for reviews of the manuscript; Kitty Reed for her editing expertise; Jari Roloff for computer drafting, text editing, and layout; Connie Manson and Lee Walkling for assistance with references; and Cathrine Kenner, Phillip Dobson, and Jan Allen for clerical support.

## REFERENCES CITED


Armstrong, J. E., 1960a, Surficial geology of Sumas map-area, British Columbia: Geological Survey of Canada Paper 55-9.

Armstrong, J. E., 1960b, Surficial geology, Chilliwack, New Westminster, British Columbia: Geological Survey of Canada Map 53-1959.

Armstrong, J. E., 1980, Post-Vashon Wisconsin glaciation, Fraser Lowland, British Columbia: Geological Survey of Canada Bulletin 322, p. 33.

Armstrong, J. E.; Brown, W. L., 1954, Late Wisconsin marine drift and associated sediments of the lower Fraser Valley, British Columbia, Canada: Geological Society of America Bulletin, v. 65, no. 4, p. 349-364.

Armstrong, J. E.; Crandell, D. R.; Easterbrook, D. J.; Noble, J. B., 1965, Late Pleistocene stratigraphic chronology in southwestern British Columbia and northwestern Washington [abstract]: Geological Society of America Special Paper 82, p. 237.

Armstrong, R. L., 1980, Geochronometry of the Shuksan Metamorphic Suite, North Cascades, Washington [abstract]: Geological Society of America Abstracts with Programs, v. 12, no. 3, p. 94.

Armstrong, R. L.; Harakal, J. E.; Brown, E. H.; Bernardi, M. L.; Rady, P. M., 1983, Late Paleozoic high-pressure metamorphic rocks in northwestern Washington and southwestern British Columbia—The Vedder Complex: Geological Society of America Bulletin, v. 94, no. 4, p. 451-458.

Armstrong, R. L.; Misch, Peter, 1987, Rb-Sr and K-Ar dating of mid-Mesozoic blueschist and late Paleozoic albite-epidote-amphibolite and blueschist metamorphism in the North Cascades, Washington and British Columbia, and Sr-isotope fingerprinting of eugeosynclinal rock assemblages. *In* Schuster, J. E., editor, Selected papers on the geology of Washington: Washington Division of Geology and Earth Resources Bulletin 77, p. 85-105.

Artim, E. R.; Wunder, J. M., 1976, Preliminary geologic map of the La Conner quadrangle in Skagit County, Washington: Washington Division of Geology and Earth Resources Open File Report 76-1, 1 sheet, scale 1:24,000.

Balzarini, M. A., 1981, Paleoecology of Everson-age glacialmarine drifts in northwestern Washington and southwestern British Columbia: University of Washington Master of Science thesis, 109 p.

Balzarini, M. A., 1983, Paleoecology of late Pleistocene glacialmarine sediments in northwestern Washington and southwestern British Columbia. *In* Molnia, B. F., editor, Glacial-marine sedimentation: Plenum Press, p. 571-592.

Beale, Harriet, 1990, Relative rise in sea-level during the late Holocene at six salt marshes in the Puget Basin, Washington: Western Washington University Master of Science thesis, 157 p.

Bechtel, Inc., 1979, Report of geologic investigations in 1978–1979; Skagit Nuclear Power Project: Puget Sound Power and Light Company, 3 v.

Beget, J. E., 1981, Postglacial eruption history and volcanic hazards at Glacier Peak, Washington: University of Washington Doctor of Philosophy thesis, 192 p.

Beget, J. E., 1982, Postglacial volcanic deposits at Glacier Peak, Washington, and potential hazards from future eruptions: U.S. Geological Survey Open-File Report 82-830, 77 p.

Blackwell, D. L., 1983, Geology of the Park Butte–Loomis Mountain area, Washington (eastern margin of the Twin Sisters dunite): Western Washington University Master of Science thesis, 253 p., 4 plates.

Blake, M. C., Jr.; Irwin, W. P.; Coleman, R. G., 1967, Upside-down metamorphic zonation, blueschist facies, along a regional thrust in California and Oregon: U.S. Geological Survey Professional Paper 575-C, p. C1-C9.

Booth, D. B., 1987, Timing and processes of deglaciation along the southern margin of the Cordilleran ice sheet. *In* Ruddiman, W. F.; Wright, H. E., Jr., editors, North America and adjacent oceans during the last glaciation: Geological Society of America DNAG Geology of North America, v. K-3, p. 71-90.

Booth, D. B., 1994, Glaciofluvial infilling and scour of the Puget Lowland, Washington, during ice-sheet glaciation: Geology, v. 22, no. 8, p. 695-698.

Booth, D. B.; Hallet, B., 1993, Channel networks carved by subglacial water—Observations and reconstruction in the eastern Puget Lowland of Washington: Geological Society of America Bulletin, v. 105, no. 5, p. 671-683.

Brandon, M. T.; Cowan, D. S.; Vance, J. A., 1988, The Late Cretaceous San Juan thrust system, San Juan Islands, Washington: Geological Society of America Special Paper 221, 81 p., 1 plate.

Brown, E. H., 1977, Ophiolite on Fidalgo Island, Washington. *In* Coleman, R. G.; Irwin, W. P., editors, North American ophiolites: Oregon Department of Geology and Mineral Industries Bulletin 95, p. 67-73.

Brown, E. H., 1986, Geology of the Shuksan Suite, North Cascades, Washington, U.S.A. *In* Evans, B. W.; Brown, E. H., editors, Blueschists and eclogites: Geological Society of America Memoir 164, p. 143-154.

Brown, E. H., 1987, Structural geology and accretionary history of the Northwest Cascades system, Washington and British Columbia: Geological Society of America Bulletin, v. 99, no. 2, p. 201-214.

Brown, E. H.; Bernardi, M. L.; Christenson, B. W.; Cruver, J. R.; Haugerud, R. A.; Rady, P. M.; Sondergaard, J. N., 1981, Metamorphic facies and tectonics in part of the Cascade Range and Puget Lowland of northwestern Washington: Geological Society of America Bulletin, v. 92, no. 4, Part I, p. 170-178.

Brown, E. H.; Blackwell, D. L.; Christenson, B. W.; Frasse, F. I.; Haugerud, R. A.; Jones, J. T.; Leiggi, P. A.; Morrison, M. L.; Rady, P. M.; and others, 1987, Geologic map of the northwest Cascades, Washington: Geological Society of America Map and Chart Series MC-61, 1 sheet, scale 1:100,000, with 10 p. text.

Brown, E. H.; Bradshaw, J. Y.; Mustoe, G. E., 1979, Plagiogranite and keratophyre in ophiolite on Fidalgo Island, Washington: Geological Society of America Bulletin, v. 90, no. 5, p. I 493-I 507.

Brown, E. H.; O'Neil, J. R., 1982, Oxygen-isotope geothermometry and stability of lawsonite and pumpellyite in the Shuksan Metamorphic Suite, North Cascades, Washington: Contributions to Mineralogy and Petrology, v. 80, no. 3, p. 240-244.

Brown, E. H.; Wilson, D. L.; Armstrong, R. L.; Harakal, J. E., 1982, Petrologic, structural, and age relations of serpentinite, amphibolite, and blueschist in the Shuksan suite of the Iron Mountain–Gee Point area, North Cascades, Washington: Geological Society of America Bulletin, v. 93, no. 11, p. 1087-1098.

Cabanis, B.; Lecolle, M., 1989, Le diagramme La/10-Y/15-Nb/8 un outil pour la discrimination des series volcaniques et la mise en evidence des processus de melange et/ou de contamination crustale: Comptes Rendus des Seances de l'Academie des Sciences, Paris, Série II, v. 309, p. 2023-2029.

Carlstad, C. A., 1992, Late Pleistocene deglaciation history at Point Partridge, central Whidbey Island, Washington: Western Washington University Master of Science thesis, 1 v.

Carroll, P. R., 1980, Petrology and structure of the pre-Tertiary rocks of Lummi and Eliza Islands, Washington: University of Washington Master of Science thesis, 78 p., 1 plate.

Cheney, E. S., 1987, Major Cenozoic faults in the northern Puget Lowland of Washington. *In* Schuster, J. E., editor, Selected papers on the geology of Washington: Washington Division of Geology and Earth Resources Bulletin 77, p. 149-168.

Christenson, B. W., 1981, Structure, petrology and geochemistry of the Chilliwack group near Sauk Mountain, Washington: Western Washington University Master of Science thesis, 181 p.

Clague, J. J., 1976, Quadra sand and its relation to the late Wisconsin glaciation of southwest British Columbia: Canadian Journal of Earth Sciences, v. 13, no. 6, p. 803-815.

Clague, J. J., 1980, Late Quaternary geology and geochronology of British Columbia; Part 1, Radiocarbon dates: Geological Survey of Canada Paper 80-13, 28 p.

Clague, J. J., 1981, Late Quaternary geology and geochronology of British Columbia; Part 2, Summary and discussion of radiocarbon-dated Quaternary history: Geological Survey of Canada Paper 80-13, 28 p.

Cowan, D. S., 1985, Structural styles in Mesozoic and Cenozoic mélanges in the western Cordillera of North America: Geological Society of America Bulletin, v. 96, no. 4, p. 451-462.

Croll, T. C., 1980, Stratigraphy and depositional history of the Deming Sand in northwestern Washington: University of Washington Master of Science thesis, 57 p.

Cruver, J. R., 1983, Petrology and geochemistry of the Haystack Mountain unit, lower Skagit valley, Washington: Western Washington University Master of Science thesis, 149 p., 1 plate.

Dauteuil, O.; Mart, Y., 1998, Analogue modeling of faulting pattern, ductile deformation, and vertical motion in strike-slip fault zones: Tectonics, v. 17, no. 2, p. 303-310.

Dethier, D. P.; Pessl, Fred, Jr.; Keuler, R. F.; Balzarini, M. A.; Pevear, D. R., 1995, Late Wisconsinan glaciomarine deposition and isostatic rebound, northern Puget Lowland, Washington: Geological Society of America Bulletin, v. 107, no. 11, p. 1288-1303.

Dethier, D. P.; Whetten, J. T., 1980, Preliminary geologic map of the Clear Lake SW quadrangle, Skagit and Snohomish Counties, Washington: U.S. Geological Survey Open-File Report 80-825, 11 p., 2 plates, scale 1:24,000.

Dethier, D. P.; Whetten, J. T., 1981, Preliminary geologic map of the Mount Vernon 7½ minute quadrangle, Skagit County, Washington: U.S. Geological Survey Open-File Report 81-105, 9 p., 1 plate, scale 1:24,000.

Dethier, D. P.; Whetten, J. T.; Carroll, P. R., 1980, Preliminary geologic map of the Clear Lake SE quadrangle, Skagit County, Washington: U.S. Geological Survey Open-File Report 80-303, 11 p., 2 plates, scale 1:24,000.

Dethier, D. P.; White, D. P.; Brookfield, C. M., 1996, Maps of the surficial geology and depth to bedrock of False Bay, Friday Harbor, Richardson, and Shaw Island 7.5-minute quadrangles, San Juan County, Washington: Washington Division of Geology and Earth Resources Open File Report 96-7, 7 p., 2 plates.

Dickinson, W. R., 1970, Interpreting detrital modes of graywacke and arkose: Journal of Sedimentary Petrology, v. 40, n. 2, p. 695-707.

Domack, E. W., 1982, Facies of late Pleistocene glacial marine sediments on Whidbey Island, Washington: Rice University Doctor of Philosophy thesis, 312 p., 11 plates.

Domack, E. W., 1983, Facies of late Pleistocene glacial-marine sediments on Whidbey Island, Washington—An isostatic glacial-marine sequence. *In* Molnia, B. F., editor, Glacial-marine sedimentation: Plenum Press, p. 535-570.

Domack, E. W., 1984, Rhythmically bedded glaciomarine sediments on Whidbey Island, Washington: Journal of Sedimentary Petrology, v. 54, no. 2, p. 589-602.

Dragovich, J. D.; Dunn, Andrew; Parkinson, K. T.; Kahle, S. C.; Pringle, P. T., 1997c, Quaternary stratigraphy and cross sections, Nooksack, Columbia, and Saar Creek Valleys, Kendall and Deming 7.5-minute quadrangles, western Whatcom County, Washington: Washington Division of Geology and Earth Resources Open File Report 97-4, 13 p., 8 plates.

Dragovich, J. D.; Grisamer, C. L., in press, Quaternary stratigraphy and cross-sections of the Bow and Alger 7.5 minute quadrangles, western Skagit County, Washington: Washington Division of Geology and Earth Resources Open File Report 98-8.

Dragovich, J. D.; Norman, D. K.; Haugerud, R. A.; Pringle, P. T., 1997d, Geologic map and interpreted geologic history of the Kendall and Deming 7.5-minute quadrangles, western Whatcom County, Washington: Washington Division of Geology and Earth Resources Open File Report 97-2, 39 p., 3 plates.

Dragovich, J. D.; Pringle, P. T.; Dunne, Andrew; Parkinson, K. T.; Kahle, S. C., 1997b, Quaternary geologic mapping and stratigraphy in the Deming and Kendall 7.5-minute quadrangles, Whatcom County, Washington—Implications for valley hydrostratigraphy in the foothills of the North Cascades [abstract]. *In* Washington Department of Ecology; Washington Hydrologic Society, Abstracts from the 2nd symposium on the hydrogeology of Washington State: Washington Department of Ecology, p. 18.

Dragovich, J. D.; Pringle, P. T.; Walsh, T. J., 1994, Extent and geometry of the mid-Holocene Osceola mudflow in the Puget Lowland—Implications for Holocene sedimentation and paleogeography: Washington Geology, v. 22, no. 3, p. 3-26.

Dragovich, J. D.; Zollweg, J. E.; Qamar, A. I.; Norman, D. K., 1997a, The Macaulay Creek thrust, the 1990 5.2-magnitude Deming earthquake, and Quaternary geologic anomalies in the Deming area, western Whatcom County, Washington—Cause and effects?: Washington Geology, v. 25, no. 2, p. 15-27.

Dungan, M. A.; Vance, J. A.; Blanchard, D. P., 1983, Geochemistry of the Shuksan greenschists and blueschists, North Cascades, Washington—Variably fractionated and altered metabasalts of oceanic affinity: Contributions to Mineralogy and Petrology, v. 82, no. 2-3, p. 131-146.

Easterbrook, D. J., 1962, Pleistocene geology of the northern part of the Puget Lowland, Washington: University of Washington Doctor of Philosophy thesis, 160 p.

Easterbrook, D. J., 1963a, Late Pleistocene glacial events and relative sea-level changes in the northern Puget Lowland, Washington: Geological Society of America Bulletin, v. 74, no. 12, p. 1465-1483.

Easterbrook, D. J., 1963b, Vashon glaciation and late Wisconsin relative sea-level changes in the northern part of the Puget Lowland, Washington [abstract]: Geological Society of America Special Paper 73, p. 37.

Easterbrook, D. J., 1966a, Glaciomarine environments and the Fraser glaciation in northwest Washington—Guidebook for first Annual Field Conference, Pacific Coast Section, Friends of the Pleistocene, September 24–25, 1966: [Privately published by the author], 52 p.

Easterbrook, D. J., 1966b, Radiocarbon chronology of late Pleistocene deposits in northwest Washington: Science, v. 152, no. 3723, p. 764-767.

Easterbrook, D. J., 1969, Pleistocene chronology of the Puget Lowland and San Juan Islands, Washington: Geological Society of America Bulletin, v. 80, no. 11, p. 2273-2286.

Easterbrook, D. J., 1971, Geology and geomorphology of western Whatcom County: Western Washington State College Department of Geology, 68 p.

Easterbrook, D. J., 1976a, Geologic map of western Whatcom County, Washington: U.S. Geological Survey Miscellaneous Investigations Series Map I-854-B, 1 sheet, scale 1:62,500.

Easterbrook, D. J., 1976b, Quaternary geology of the Pacific Northwest. *In* Mahaney, W. C., editor, Quaternary stratigraphy of North America: Dowden, Hutchinson and Ross, p. 441-462.

Easterbrook, D. J., 1979, The last glaciation of northwest Washington. *In* Armentrout, J. M.; Cole, M. R.; Ter Best, Harry, Jr., editors, Cenozoic paleogeography of the western United States: Society of Economic Paleontologists and Mineralogists Pacific Section, Pacific Coast Paleogeography Symposium 3, p. 177-189.

Easterbrook, D. J., 1992, Advance and retreat of Cordilleran ice sheets in Washington, U.S.A.: Geographie physique et quaternaire, v. 46, no. 1, p. 51-68.

Easterbrook, D. J., 1994, Chronology of pre-late Wisconsin Pleistocene sediments in the Puget Lowland, Washington. *In* Lasmanis, Raymond; Cheney, E. S., convenors, Regional geology of Washington State: Washington Division of Geology and Earth Resources Bulletin 80, p. 191-206.

Easterbrook, D. J.; Crandell, D. R.; Leopold, E. B., 1967, Pre-Olympia Pleistocene stratigraphy and chronology in the central Puget Lowland, Washington: Geological Society of America Bulletin, v. 78, no. 1, p. 13-20.

Easterbrook, D. J.; Kovanen, D. J., 1996b, Everson glaciomarine deposits in fiords of the Nooksack River drainage, North Cascades, WA [abstract]: Geological Society of America Abstracts with Programs, v. 28, no. 5, p. 64.

Easterbrook, D. J.; Kovanen, D. J., 1996a, Evidence for 45-km-long, post-Cordilleran-ice-sheet, alpine glaciers in the Nooksack north fork, North Cascades, WA, between 11,500 and 10,000 $^{14}$C-yrs. B.P. [abstract]: Geological Society of America Abstracts with Programs, v. 28, no. 7, p. a-434.

England, T. D. J.; Calon, T. J., 1991, The Cowichan fold and thrust system, Vancouver Island, southwestern British Columbia: Geological Society of America Bulletin, v. 103, no. 3, p. 336-362.

Evans, B. W.; Misch, Peter, 1976, a quartz-aragonite-talc schist from the lower Skagit valley, Washington: American Mineralogist, v. 61, no. 9-10, p. 1005-1008.

Evans, J. E.; Ristow, R. J., Jr., 1994, Depositional history of the southeastern outcrop belt of the Chuckanut Formation—Implications for the Darrington–Devil's Mountain and Straight Creek fault zones, Washington (U.S.A.): Canadian Journal of Earth Sciences, v. 31, no. 12, p. 1727-1743.

Floyd, P. A.; Winchester, J. A., 1975, Magma-type and tectonic setting discrimination using immobile elements: Earth and Planetary Science Letters, v. 27, p. 211-218.

Folk, R. L., 1980, Petrology of sedimentary rocks: Hemphill Publishing Company, 182 p.

Frasse, F. I., 1981, Geology and structure of the western and southern margins of Twin Sisters Mountain, North Cascades, Washington: Western Washington University Master of Science thesis, 87 p., 2 plates.

Garver, J. I., 1988, Stratigraphy, depositional setting, and tectonic significance of the clastic cover to the Fidalgo Ophiolite, San Juan Islands, Washington: Canadian Journal of Earth Sciences, v. 25, no. 3, p. 417-432.

Gallagher, M. P., 1986, Structure and petrology of meta-igneous rocks in the western part of the Shuksan Metamorphic Suite, northwestern Washington, U.S.A.: Western Washington University Master of Science thesis, 59 p., 3 plates.

Gallagher, M. P.; Brown, E. H.; Walker, N. W., 1988, a new structural and tectonic interpretation of the western part of the Shuksan blueschist terrane, northwestern Washington: Geological Society of America Bulletin, v. 100, no. 9, p. 1415-1422.

Garcia, M. O., 1978, Criteria for the identification of ancient volcanic arcs: Earth-Science Reviews, v. 14, p. 147-165.

Groshong, R. H., Jr., 1988, Low-temperature deformation mechanisms and their interpretation: Geological Society of America Bulletin, v. 100, no. 9, p. 1329-1360.

Gust, D. A., Perfit, M. R., 1987, Phase relations of a high-Mg basalt from the Aleutian Island Arc: Implications for primary island arc basalts and high-Al basalts: Contributions to Mineralogy and Petrology, v. 97, p. 7-18.

Harris, N. B. W.; Pearce, J. A.; Tindle, A. G., 1986, Geochemical characteristics of collision-zone magmatism. *In* Coward, M. P.; Reis, A. C., editors, Collision tectonics: Geological Society Special Publication 19 [Geological Society of London], p. 67-81.

Haugerud, R. A., 1980, The Shuksan Metamorphic Suite and Shuksan thrust, Mt. Watson area, North Cascades, Washington: Western Washington University Master of Science thesis, 125 p., 2 plates.

Haugerud, R. A.; Morrison, M. L.; Brown, E. H., 1981, Structural and metamorphic history of the Shuksan Metamorphic Suite in the Mount Watson and Gee Point areas, North Cascades, Washington: Geological Society of America Bulletin, v. 92, no. 6, Part I, p. 374-383.

Heller, P. L., 1979, Pebble-count diagrams and late Wisconsin ice-flow directions in the lower Skagit drainage, North Cascades, Washington [abstract]: Geological Society of America Abstracts with Programs, v. 11, no. 3, p. 83.

Heller, P. L., 1981, Small landslide types and controls in glacial deposits—Lower Skagit River drainage, northern Cascade Range, Washington: Environmental Geology, v. 3, no. 4, p. 221-228.

Hooper, P. R.; Johnson, D. M.; Conrey, R. M., 1993, Major and trace element analyses of rocks and minerals by automated x-ray spectrometry: Washington State University Geology Department Open File Report, 36 p.

Jakes, P.; Gill, J., 1970, Rare earth elements and the island arc tholeiitic series: Earth and Planetary Science Letters, v. 9, no. 1, p. 17-28.

Johnson, S. Y., 1982, Stratigraphy, sedimentology, and tectonic setting of the Eocene Chuckanut Formation, northwest Washington: University of Washington Doctor of Philosophy thesis, 221 p., 4 plates.

Johnson, S. Y., 1984c, Cyclic fluvial sedimentation in a rapidly subsiding basin, northwest Washington: Sedimentary Geology, v. 38, no. 1-4, p. 361-391.

Johnson, S. Y., 1984a, Evidence for a margin-truncating transcurrent fault (pre-late Eocene) in western Washington: Geology, v. 12, no. 9, p. 538-541.

Johnson, S. Y., 1984b, Stratigraphy, age, and paleogeography of the Eocene Chuckanut Formation, northwest Washington: Canadian Journal of Earth Sciences, v. 21, no. 1, p. 92-106.

Johnson, S. Y., 1985a, Eocene strike-slip faulting and nonmarine basin formation in Washington. *In* Biddle, K. T.; Christie-Blick, Nicholas, editors, Strike-slip deformation, basin formation, and sedimentation: Society of Economic Paleontologists and Mineralogists Special Publication 37, p. 283-302.

Johnson, S. Y.; Whetten, J. T.; Naeser, C. W.; Zimmermann, R. A., 1983, Fission track ages from the Chuckanut Formation, northwest Washington [abstract]: Geological Society of America Abstracts with Programs, v. 15, no. 5, p. 393.

Kerr, P. F., 1977, Optical mineralogy; 4th ed.: McGraw-Hill, 492 p.

Klungland, M. W.; McArthur, Michael, 1989, Soil survey of Skagit County area, Washington: U.S. Soil Conservation Service, 372 p., 67 plates.

Kovanen, D. J., 1996, Extensive late-Pleistocene alpine glaciation in the Nooksack River Valley, North Cascades, Washington: Western Washington University Master of Science thesis, 186 p.

Kovanen, D. J.; Easterbrook, D. J., 1996a, Extensive readvance of late Pleistocene (YD?) alpine glaciers in the Nooksack River Valley, 10,000 to 12,000 years ago, following retreat of the Cordilleran ice sheet, North Cascades, Washington: Western Washington University Geology Department; Friends of the Pleistocene Pacific Coast Cell Field Trip Guidebook, 74 p.

Kovanen, D. J.; Easterbrook, D. J., 1996b, New evidence for late-glacial, post-Cordilleran-ice-sheet, readvance of alpine glaciers in the North Cascades, Washington [abstract]: Geological Society of America Abstracts with Programs, v. 28, no. 5, p. 83.

Le Bas, M. J.; Le Maitre, R. W.; Streckeisen, A. L.; Zanettin, Bruno, 1986, a chemical classification of volcanic rocks based on the total alkali-silica diagram: Journal of Petrology, v. 27, no. 3, p. 745-750.

Lister, G. S.; Snoke, A. W., 1984, S-C mylonites: Journal of Structural Geology, v. 6, no. 6, p. 617-638.

Logan, J. M., Friedman, M., Higgs, N., Dengo, C., Shimamoto, T., 1979, Experimental studies of simulated gouge and their application to studies of natural fault zones. *In* Speed, R. C.; Sharp, R. V., editors, Proceedings of Conference VIII—Analysis of actual fault zones in bedrock: U.S. Geological Survey Open-File Report 79-1239, p. 305-343.

Logan, J. M.; Higgs, N. G.; Friedman, M., 1981, Laboratory studies on natural gouge from the U.S. Geological Survey Dry Lake valley no. 1 well, San Andreas fault zone. *In* Carter, N. L.; Friedman, M.; Logan, J. M., editors, Mechanical behavior of crustal rocks—The Handin volume: American Geophysical Union Geophysical Monograph 24, p. 121-134.

Lovseth, T. P., 1975, The Devils Mountain fault, northwestern Washington: University of Washington Master of Science thesis, 29 p.

Maekawa, Hirokazu; Brown, E. H., 1991, Kinematic analysis of the San Juan thrust system, Washington: Geological Society of America Bulletin, v. 103, no. 8, p. 1007-1016.

Maekawa, Hirokazu; Brown, E. H., 1993, Kinematic analysis of the San Juan thrust system, Washington—Discussion and reply; Reply: Geological Society of America Bulletin, v. 105, no. 6, p. 841-844.

Mandl, G., 1988, Mechanics of tectonic faulting—Models and basin concepts: Elsevier Developments in Structural Geology 1, 407 p.

Marcus, K. L., 1980, An Eocene–Oligocene age basin in the northern Puget Sound of Washington [abstract]: Geological Society of America Abstracts with Programs, v. 12, no. 3, p. 117.

Mathews, W. H.; Fyles, J. G.; Nasmith, H. W., 1970, Postglacial crustal movements in southwestern British Columbia and adjacent Washington State: Canadian Journal of Earth Sciences, v. 7, no. 2, part 2, p. 690-702.

Meschede, M., 1986, A method of discriminating between different types of mid-ocean ridge basalts and continental tholeiites with the Nb-Zr-Y diagram: Chemical Geology., v. 56, p. 207-218.

Michard, A., 1989, Rare earth element systematics in hydrothermal fluids: Geochimica et Cosmochimica Acta, v. 49, p. 601-610.

Miller, G. M., 1979, Western extent of the Shuksan and Church Mountain thrust plates in Whatcom, Skagit, and Snohomish Counties, Washington: Northwest Science, v. 53, no. 4, p. 229-241.

Miller, G. M.; Misch, Peter, 1963, Early Eocene angular unconformity at western front of northern Cascades, Whatcom County, Washington: American Association of Petroleum Geologists Bulletin, v. 47, no. 1, p. 163-174.

Minard, J. P., 1985, Geologic map of the Tulalip quadrangle, Snohomish County, Washington: U.S. Geological Survey Miscellaneous Field Studies Map MF-1744, 1 sheet, scale 1:24,000.

Misch, Peter, 1966, Tectonic evolution of the northern Cascades of Washington—a west-cordilleran case history. *In* Canadian Institute of Mining and Metallurgy; and others, a symposium on the tectonic history and mineral deposits of the western Cordillera in British Columbia and neighboring parts of the United States, Vancouver, 1964: Canadian Institute of Mining and Metallurgy Special Volume 8, p. 101-148.

Misch, Peter, 1969, Paracrystalline microboudinage of zoned grains and other criteria for synkinematic growth of metamorphic minerals: American Journal of Science, v. 267, no. 1, p. 43-63.

Miyashiro, Akiho, 1974, Volcanic rock series in island arcs and active continental margins: American Journal of Science, v. 274, no. 4, p. 321-355.

Monger, J. W. H., 1966, The stratigraphy and structure of the type-area of the Chilliwack Group, southwestern British Columbia: University of British Columbia Doctor of Philosophy thesis, 173 p., 3 plates.

Mullen, E. D., 1983, $MnO/TiO_2/P_2O_5$—A minor element discriminant for basaltic rocks of oceanic environments and its implications for petrogenesis: Earth and Planetary Science Letters, v. 62, p. 53-62.

Mullineaux, D. R.; Waldron, H. H.; Rubin, Meyer, 1965, Stratigraphy and chronology of late interglacial and early Vashon glacial time in the Seattle area, Washington: U.S. Geological Survey Bulletin 1194-O, 10 p.

Mustard, P. S.; Rouse, G. E., 1994, Stratigraphy and evolution of Tertiary Georgia Basin and subjacent Upper Cretaceous sedimentary rocks, southwestern British Columbia and northwestern Washington. *In* Monger, J. W. H., editor, Geology and geological hazards of the Vancouver region, southwestern British Columbia: Geological Survey of Canada Bulletin 481, p. 97-169.

Mustoe, G. E.; Gannaway, W. L., 1997, Paleogeography and paleontology of the early Tertiary Chuckanut Formation, northwest Washington: Washington Geology, v. 25, no. 3, p. 3-18.

Nakamura, Noboru, 1974, Determination of REE, Ba, Fe, Mg, Na, and K in carbonaceous and ordinary chondrites: Geochimica et Cosmochimica Acta, v. 38, no. 5, p. 757-775.

Nystrom, J. O.; Levi, Beatriz; Skiold, Torbjorn; Fallick, A. E.; Darce, Mauricio, 1993, Cenozoic volcanism within the Nicaraguan geotraverse: Revista Geologica de America Central, v. 16, p. 107-111.

Obradovich, D. J., 1994, An updated time scale for the Cretaceous of North America [abstract]: American Association of Petroleum Geologists and Society of Economic Paleontologists and Mineralogists Annual Meeting Abstracts, p. 227.

Pearce, J. A., 1975, Basalt geochemistry used to investigate past tectonic environment on Cyprus: Tectonophysics, v. 25, no. 1-2, p. 41-47.

Pearce, J. A., 1982, Trace element characteristics of lavas from destructive plate boundaries. *In* Thorpe, R. S., editor, Andesites-Orogenic andesites and related rocks: John Wiley and Sons, p. 525-548.

Pearce, J. A., 1983, Role of the sub-continental lithosphere in magma genesis at active continental margins. *In* Hawkesworth, C. J.; Norry, M. J., editors, Continental basalts and mantle xenoliths: Shiva, Nantwich, p. 230-249.

Pearce, J. A.; Cann, J. R., 1973, Tectonic setting of basic volcanic rocks determined using trace elements analyses: Earth and Planetary Science Letters, v. 19, no. 2, p. 290-300.

Pearce, J. A.; Harris, N. B. W.; Tindle, A. G., 1984, Trace element discrimination diagrams for the tectonic interpretation of granitic rocks: Journal of Petrology, v. 25, p. 956-983.

Pearce, J. A.; Norry, M. J., 1979, Petrogenetic implications of Ti, Zr, Y and Nb variations in volcanic rocks: Contributions to Mineralogy and Petrology, v. 69, p. 33-47.

Pearce, T. H.; Gorman, B. E.; Birkett, T. C., 1977, The relationship between major element chemistry and tectonic environment of basic and intermediate volcanic rocks: Earth and Planetary Science Letters, v. 36, no. 1, p. 121-132.

Pessl, Fred, Jr.; Dethier, D. P.; Booth, D. B.; Minard, J. P., 1989, Surficial geologic map of the Port Townsend 30- by 60-minute quadrangle, Puget Sound region, Washington: U.S. Geological Survey Miscellaneous Investigations Series Map I-1198-F, 1 sheet, scale 1:100,000, with 13 p. text.

Powell, R. D., 1984, Glacimarine processes and inductive lithofacies modeling of ice shelf and tidewater glacier sediments based on Quaternary examples: Marine Geology, v. 57, p. 1-52.

Reiswig, K. N., 1982, Palynological differences between the Chuckanut and Huntingdon Formations, northwestern Washington: Western Washington University Master of Science thesis, 61 p.

Reller, G. J., 1986, Structure and petrology of the Deer Peaks area, western North Cascades, Washington: Western Washington University Master of Science thesis, 106 p., 2 plates.

Rigg, G. B., 1958, Peat resources of Washington: Washington Division of Mines and Geology Bulletin 44, 272 p.

Rubin, Meyer; Alexander, Corrinne, 1958, U.S. Geological Survey radiocarbon dates IV: Science, v. 127, no. 3313, p. 1476-1487.

Rutter, E. H.; Maddock, R. H.; Hall, S. H.; White, S. H., 1986, Comparative microstructures of natural and experimentally produced clay-bearing fault gouges: Pure and Applied Geophysics, v. 124, no. 1-2, p. 3-30.

Salvador, Amos, 1985, Chronostratigraphic and geochronometric scales in COSUNA stratigraphic correlation charts of the United States: American Association of Petroleum Geologists Bulletin, v. 69, no. 2, p. 181-189.

Sceva, J. E., 1950, Preliminary report on the ground-water resources of southwestern Skagit County, Washington: U.S. Geological Survey Ground-Water Report 1, 40 p., 2 plates.

Schmidt, S. L., 1972, Geology of the south part of Chuckanut Mountain, a structural and petrological study: Western Washington State College Master of Science thesis, 51 p., 1 plate.

Scott, K. M.; Pringle, P. T.; Vallance, J. W., 1992, Sedimentology, behavior, and hazards of debris flows at Mount Rainier, Washington: U.S. Geological Survey Open-File Report 90-385, 106 p., 1 plate.

Sevigny, J. H.; Brown, E. H., 1983, Large-scale imbricate structures in the Yellow Aster Meadows region, North Cascades, Washington [abstract]: Geological Society of America Abstracts with Programs, v. 15, no. 5, p. 316.

Sevigny, J. H.; Brown, E. H., 1989, Geochemistry and tectonic interpretation of some metavolcanic rock units of the western North Cascades, Washington: Geological Society of America Bulletin, v. 101, no. 3, p. 391-400.

Shackleton, R. M.; Ries, A. C., 1984, The relation between regionally consistent stretching lineations and plate motions: Journal of Structural Geology, v. 6, no. 1/2, p. 111-117.

Shaw, J. D., 1972, Late Pleistocene paleontology of Orcas, Shaw, Lopez, and San Juan Islands of the San Juan archipelago: University of Washington Master of Science thesis, 60 p.

Shervais, J. W., 1982, Ti-V plots and the petrogenesis of modern and ophiolitic lavas: Earth and Planetary Science Letters, v. 59, p. 101-118.

Siegfried, R. T., 1978, Stratigraphy and chronology of raised marine terraces, Bay View Ridge, Skagit County, Washington: Western Washington University Master of Science thesis, 52 p., 1 plate.

Simpson, Carol; Schmidt, S. M., 1983, An evaluation of criteria to deduce the sense of movement in sheared rocks: Geological Society of America Bulletin, v. 94, no. 11, p. 1281-1288.

Smith, M. T., 1986, Structure and petrology of the Grady Ridge–Lake Shannon area, North Cascades, Washington: Western Washington University Master of Science thesis, 156 p., 2 plates.

Spry, A., 1969, Metamorphic textures: Pergamon Press, 352 p.

Stoffel, K. L., 1986, Stratigraphy of pre-Vashon Quaternary sediments applied to the evaluation of a proposed major tectonic structure in Island County, Washington: U.S. Geological Survey Open-File Report 81-292; Washington Division of Geology and Earth Resources Open File Report, 161 p.

Streckeisen, A. L., 1973, Plutonic rocks—Classification and nomenclature recommended by the IUGS Subcommission on the Systematics of Igneous Rocks: Geotimes, v. 18, no. 10, p. 26-30.

Street-Martin, L. V., 1981, The chemical composition of the Shuksan Metamorphic Suite in the Gee Point–Finney Creek area, North Cascades, Washington: Western Washington University Master of Science thesis, 76 p., 1 plate.

Sun, S.-S.; McDonough, W. F., 1989, Chemical and isotopic systematics of oceanic basalts, implications for mantle composition and processes. *In* Saunders, A. D.; Norry, M. J., editors, Magmatism in the ocean basins: Geological Society Special Publication 42, p. 313-345.

Tabor, R. W., 1994, Late Mesozoic and possible early Tertiary accretion in western Washington State—The Helena–Haystack mélange and the Darrington–Devils Mountain fault zone: Geological Society of America Bulletin, v. 106, no. 2, p. 217-232, 1 plate.

Tabor, R. W.; Booth, D. B.; Vance, J. A.; Ford, A. B.; Ort, M. H., 1988, Preliminary geologic map of the Sauk River 30 by 60 minute quadrangle, Washington: U.S. Geological Survey Open-File Report 88-692, 50 p., 2 plates.

Tabor, R. W.; Frizzell, V. A., Jr.; Booth, D. B.; Waitt, R. B.; Whetten, J. T.; Zartman, R. E., 1993, Geologic map of the Skykomish River 30- by 60-minute quadrangle, Washington: U.S. Geological Survey Miscellaneous Investigations Series Map I-1963, 1 sheet, scale 1:100,000, with 42 p. text.

Tabor, R. W.; Haugerud, R. A.; Booth, D. B.; Brown, E. H., 1994, Preliminary geologic map of the Mount Baker 30- by 60-minute quadrangle, Washington: U.S. Geological Survey Open-File Report 94-403, 55 p., 2 plates.

Thorson, R. M., 1980, Ice-sheet glaciation of the Puget Lowland, Washington, during the Vashon Stade (late Pleistocene): Quaternary Research, v. 13, no. 3, p. 303-321.

Vance, J. A., 1975, Bedrock geology of San Juan County. *In* Russell, R. H., editor, Geology and water resources of the San Juan Islands, San Juan County, Washington: Washington Department of Ecology Water-Supply Bulletin 46, p. 3-19.

Vance, J. A., 1977, The stratigraphy and structure of Orcas Island, San Juan Islands. *In* Brown, E. H.; Ellis, R. C., editors, Geological excursions in the Pacific Northwest; Geological Society of America annual meeting, 1977: Western Washington University, p. 170-203.

Vance, J. A., 1985, Early Tertiary faulting in the North Cascades [abstract]: Geological Society of America Abstracts with Programs, v. 17, no. 6, p. 415.

Vance, J. A.; Dungan, M. A.; Blanchard, D. P.; Rhodes, J. M., 1980, Tectonic setting and trace element geochemistry of Mesozoic ophiolitic rocks in western Washington. *In* Irving, A. J.; Dungan, M. A., editors, The Jackson volume: American Journal of Science, v. 280-a, part 1, p. 359-388.

Varnes, D. J., 1958, Landslide types and processes. *In* Eckel, E. B., editor, Landslides and engineering practice: Highway Research Board Special Report 29, p. 20-47.

Varnes, D. J., 1978, Slope movement types and processes. *In* Schuster, R. L.; Krizek, R. J., editors, Landslides—Analysis and control: National Research Council Transportation Research Board Special Report 176, p. 11-33.

Washington Department of Ecology, 1978, Coastal zone atlas of Washington; volume 2, Skagit County: Washington Department of Ecology, 1 v., maps, scale 1:24,000.

Whetten, J. T.; Carroll, P. I.; Gower, H. D.; Brown, E. H.; Pessl, Fred, Jr., 1988, Bedrock geologic map of the Port Townsend 30- by 60-minute quadrangle, Puget Sound region, Washington: U.S. Geological Survey Miscellaneous Investigations Series Map I-1198-G, 1 sheet, scale 1:100,000.

Whetten, J. T.; Dethier, D. P.; Carroll, P. R., 1979, Preliminary geologic map of the Clear Lake NE quadrangle, Skagit County, Washington: U.S. Geological Survey Open-File Report 79-1468, 10 p., 2 plates, scale 1:24,000.

Whetten, J. T.; Zartman, R. E.; Blakely, R. J.; Jones, D. L., 1980a, Allochthonous Jurassic ophiolite in northwest Washington: Geological Society of America Bulletin, v. 91, no. 6, p. I 359-I 368.

Whetten, J. T.; Dethier, D. P.; Carroll, P. R., 1980b, Preliminary geologic map of the Clear Lake NW quadrangle, Skagit County, Washington: U.S. Geological Survey Open-File Report 80-247, 13 p., 2 plates, scale 1:24,000.

Wilcox, R. E.; Harding, T. P.; Seely, D. R., 1973, Basic wrench tectonics: American Association of Petroleum Geologists Bulletin 57, no. 1, p. 74-96.

Wood, D. A., 1980, The application of a Th-Hf-Ta diagram to problems of tectonomagmatic classification and to establishing the nature of crustal contamination of basaltic lavas of the British Tertiary volcanic province: Earth and Planetary Science Letters, v. 50, p. 11-30.

Zanettin, Bruno, 1984, Proposed new chemical classification of volcanic rocks: Episodes, v. 7, no. 4, p. 19-20.

Ziegler, C. B., 1985, The structure and petrology of the Swift Creek area, western North Cascades, Washington: Western Washington University Master of Science thesis, 191 p., 5 plates. ■

# Appendix 1. Radiocarbon ages, this study

Samples 97-37L(A), 97-37L(B), and 97-19T: stratigraphic relations shown schematically in Figure 8. Samples collected by Joe Dragovich and Dave Norman. $^{14}C$ analyses performed by Beta Analytic, Inc. (Miami, Fla.). Dates are reported as radiocarbon years before present (yr B.P.)(present = A.D. 1950) and are not calibrated. By international convention, the modern reference standard was 95 percent of the $^{14}C$ content of the National Bureau of Standards' Oxalic Acid and calculated using the Libby $^{14}C$ half-life (5,568 years). Quoted errors represent 1 standard deviation (68 percent probability) and are based on combined measurements of the sample, background, and modern reference standards. Measured $^{13}C/^{12}C$ ratios were calculated relative to the PDB-1 international standard, and the radiocarbon years before present ages were normalized to -25 per mil. If the ratio and age are accompanied by a (*), then the $^{13}C/^{12}C$ value was estimated, based on values typical of the material type. The quoted results are *not* calibrated to calendar years. Calibration to calendar years should be calculated using the conventional $^{14}C$ age.

### Sample 97-2C: Unit $Qgdm_e$, fossiliferous diamicton

Shell fragments in glaciomarine diamicton (gravelly silty clay) from Burlington Hill, directly south of the Alger quadrangle. Shells occur in a ≈1-m-thick diamicton overlying pre-Tertiary bedrock. Diamicton is overlain by about 10 cm of sand and gravel of emergence (beach) origin. Sample site is about 320 ft (97 m) above present sea level. **, subtraction of 800 yr from the conventional $^{14}C$ age to approximately correct for marine water reservoir effects.

| Measured $^{14}C$ age (yr B.P.) | $^{13}C/^{12}C$ ratio | Conventional $^{14}C$ age (yr B.P.) |
|---|---|---|
| 12,890 ±50 | -1.6‰ | 13,270 ±50; **12,470 ±50 |

Beta-108961
Analysis: standard-AMS
Material (pretreatment): shell (acid etch)
Location: Fig. 3, loc. 97-2C

### Sample 97-37L(A): Unit $Qgom_e$, gravelly sand

Stick (about 1 cm in diameter and about 4 cm long) at the top of unit. Occurrence of organic debris and position at the top of the unit and directly below the peat indicates waning outwash sedimentation; analytical result provides a "stratigraphic top" age for the unit. (See Fig. 8.)

| Measured $^{14}C$ age (yr B.P.) | $^{13}C/^{12}C$ ratio | Conventional $^{14}C$ age (yr B.P.) |
|---|---|---|
| 11,500 ±60 | -25.0*‰ | 11,500 ±60 |

Beta-108958
Analysis: radiometric standard
Material (pretreatment): wood (acid/alkali/acid)
Comment: The small sample was given extended counting time.
Location: Fig. 3, loc. 37LA

### Sample 97-37L(B): Unit $Qgom_e$, diamicton layer

Stick (about 1 cm in diameter and about 3 cm long) from the top of gray, fine pebbly diamicton about 10 cm below the peat deposit. The diamicton is glaciomarine drift with dropstone or, alternatively, possibly flow till. Occurrence of organic debris and position at the top of the unit or directly below the peat indicates waning glaciomarine-submarine outwash sedimentation. Analytical result provides a "stratigraphic top" age for the unit. (See Fig. 8.)

| Measured $^{14}C$ age (yr B.P.) | $^{13}C/^{12}C$ ratio | Conventional $^{14}C$ age (yr BP) |
|---|---|---|
| 11,990 ±110 | -27.2‰ | 11,960 ±110 |

Beta-108959
Analysis: radiometric standard
Material (pretreatment): wood (acid/alkali/acid)
Comment: The small sample was given extended counting time.
Location: Fig. 3, loc. 37LB

### Sample 97-19T: Peat overlying unit $Qgom_e$

Tree bark (complete layer about 40 cm long, 15 cm wide, and 2 cm thick; about 1 kg). (See above and Fig. 8.) Bark was collected about 1 m above the $Qgom_e$/peat contact. Ash of probable Mount Mazama origin (2 cm thick) is present a few centimeters below the top of the ~4-m thick peat. Bark is from mature tree, thus tree age suggests that this age is at least 100 yrs too young as compared to fine organic materials deposited at the same stratigraphic level in the peat deposit.

| Measured $^{14}C$ age (yr B.P.) | $^{13}C/^{12}C$ ratio | Conventional $^{14}C$ age (yr B.P.) |
|---|---|---|
| 11,550 ±80 | -25.0*‰ | 11,550 ±80 |

Beta-108960
Analysis: radiometric standard
Material (pretreatment): wood (acid/alkali/acid)
Location: Fig. 3, loc. 19T

# Appendix 2. Selected radiocarbon ages from previous studies

Easterbrook's (1966) data have the laboratory indicated by the prefix before the sample number: I, Isotopes, Inc.; W, U.S. Geological Survey; UW, University of Washington. Pessl and others (1989) $^{14}C$ age data: *, indicates dates on sample splits from different laboratories; USGS, U.S. Geological Survey laboratory; B, Beta Analytical Laboratory; NA, not applicable. **Uncalib. $^{14}C$ age**, in yr B.P.; **$^{14}C$ age**, 800 yr was subtracted to compensate for marine reservoir effect in shells. Our Quarternary subunits are further defined in Appendix 3 (for example, $gmd_c$, Everson glaciomarine drift clay unit; trans, transitional beds). Sample altitudes are given in the original reported unit.

| Sample (lab ID no.) | Location relative to study area | General geologic setting and altitude | Remarks (other studies) | Uncal. $^{14}C$ age; dated material | $^{14}C$ age | Reference | Notes |
|---|---|---|---|---|---|---|---|
| **Older Alluvium (lahar deposits; unit Qoa)** | | | | | | | |
| Sk-D (USGS-866) | Skagit Valley (1 mi SE of Sterling Hill; Fig. 3, site 3) | Charcoal in green-blue clayey silt overlain by sandy lahar forming low (12 m high) terrace along lower Skagit River; altitude 13 m. | Charcoal closely predates influx of Glacier Peak dacitic debris probably associated with volcanic activity at Glacier Peak (Beget, 1981, 1982). | 1,790±75; charcoal; minimum age | NA | Pessl and others (1989) | Maximum age of Qoa in the study area, although close correspondence of age with major Glacier Peak lahar inundation upvalley suggested to Beget (1981) that age closely approximates Qoa lahar-runout age in lower Skagit Valley. |
| **Everson Interstade beach deposits, undivided (unit $Qgom_{ee}$)** | | | | | | | |
| SJ-A (Beta-1717) (USGS-1234) | Lopez Island (19 mi SW of Bow quadrangle) | *In situ* marine shells in oxidized coarse sand and small-pebble gravel with associated shell hash; overlies fossiliferous marine stony silt and clay. | See SJ-A below | 12,740±150*; shells<br>12,480±70*; shells | 11,940±150*<br>11,680±70*; intraformational age | Pessl and others (1989) | Suggests uplift by mostly isostatic emergence, essentially complete by about 12,000 yr B.P. in San Juan Islands. (See unit $Qgom_e$ in text.) |
| UW-9779 (B-73065) | Shaw Island 7.5-minute quadrangle (about 20 mi west of the Bow quadrangle) | Altitude 107 ft | Emergence deposit(?). Unit generally composed of sand or gravel overlying Everson marine deposits or till and locally overlain by eolian deposits; 1 to 27 ft thick (Dethier and others, 1996). | 12,620±130; shells | 11,820±130; intraformational age | Dethier and others (1996) | Possible beach deposit |
| UW-9790 (B-73066) | Shaw Island 7.5-minute quadrangle (about 20 mi west of the Bow quadrangle) | Altitude 40 ft | Emergence deposit generally composed of sand or gravel overlying Everson marine deposits or till and locally overlain by eolian deposits; 1 to 27 ft thick (Dethier and others, 1996). | 12,320±90; shells | 11,520±90; intraformational age | Dethier and others (1996) | Probable beach deposit |
| DW-127b (B-1717) | Davis Bay on Shaw Island (19 mi WSW of the SW corner of Bow quadrangle) | Altitude 1 ft | Emergence deposit generally composed of sand or gravel overlying Everson marine deposits or till and locally overlain by eolian deposits; 1 to 27 ft thick; sample from fine gravel or coarse sand (Dethier and others, 1996). | 12,740±150; shells | 11,940±150; intraformational age | Dethier and others (1996) | Probable beach deposit |
| SK-E (USGS-1235) (Beta-1322) | Big Lake (7 mi directly S of SE corner of Bow quadrangle) | Marine shells in sand and gravel lenses (beach deposit?); overlying shell-bearing marine silt and fine sand; overlain by laminated sand and silt with peat lenses and gastropod shells; altitude 23 m. | Beach deposit(?). Records isostatic emergence of land sometime after marine sedimentation. | 13,515±140*; shells<br>13,180±70*; shells | 12,715±140*<br>12,380±70*; intraformational age | Pessl and others (1989) | |

| Sample (lab ID no.) | Location relative to study area | General geologic setting and altitude | Remarks (other studies) | Uncal. $^{14}C$ age; dated material | $^{14}C$ age | Reference | Notes |
|---|---|---|---|---|---|---|---|
| SK-C (USGS-1236) (Beta 1321) | Mount Vernon (4 mi south of Sterling Hill and the Alger quadrangle) | Marine shells in oxidized sand and gravel overlying compact blocky-weathering silty clay diamicton; altitude 23 m. | Shells date beach to intertidal deposit associated with isostatic emergence. | 12,350±70*; shells 12,500±130*; shells | 11,550±70* 11,700±130*; intraformational age | Pessl and others (1989) | See unit Qgod$_S$; isostatic emergence through 100 ft contour later to the north?; possible submarine outwash unit, and thus date may be pre-emergence. |
| **Everson Interstade glacial marine drift, undivided (unit Qgdm$_e$)(units gmd$_d$ and gmd$_c$, Plate 2, cross sections E–G, and Fig. 7)** | | | | | | | |
| I-1035 | Bellingham (9.2 mi north of Bow quadrangle) | | Glaciomarine drift | 10,370±300; wood; intraformational age | NA | Easterbrook (1966b) | |
| W-940 | Nooksack R. (12.1 mi north of Alger quadrangle) | Fluvial Deming Sand of Easterbrook (for example, 1962) | Within glaciomarine sequence | 11,640±275; peat; intraformational age | NA | Easterbrook (1966b) | |
| W-996 | Bellingham (7.2 mi north of Bow quadrangle) | | Glaciomarine drift | 11,660±350; shells | 10,860±350; intraformational age | Easterbrook (1966b) | |
| I-1037 | Nooksack R. (12.1 mi north of Alger quadrangle) | | Glaciomarine drift | 11,800±400; wood; intraformational age | NA | Easterbrook (1966b) | |
| I-1448 | Penn Cove, Whidbey Island (20.3 mi SSW of SW corner of Bow quadrangle | | Glaciomarine drift | 11,850±240; shells | 11,050±240; intraformational age | Easterbrook (1966b) | |
| I-1471 | Sucia Island (19.8 mi WNW of NW corner of Bow quadrangle) | | Glaciomarine drift | 12,000±450; shells | 11,200±450; intraformational age | Easterbrook (1966b) | |
| W-984 | Bellingham (10.2 mi north of NW corner of Bow quadrangle) | | Within glaciomarine sequence | 12,090±350; peat; intraformational age | NA | Easterbrook (1966b) | Deming Sand near Bellingham and west of the fluvial (terrestrial) type section may be correlative with submarine outwash mapped elsewhere (for example unit Qgom$_e$ of this study). |
| I-1470 | N tip of San Juan Island (29.2 mi west of Bow quadrangle) | | Glaciomarine drift | 12,160±290; shells | 11,360±290; intraformational age | Easterbrook (1966b) | |
| I-1469 | S tip of San Juan Island (22.5 mi WSW of SW corner of Bow quadrangle) | | Glaciomarine drift | 12,350±330; shells | 11,550±330; intraformational age | Easterbrook (1966b) | |

| Sample (lab ID no.) | Location relative to study area | General geologic setting and altitude | Remarks (other studies) | Uncal. $^{14}C$ age; dated material | $^{14}C$ age | Reference | Notes |
|---|---|---|---|---|---|---|---|
| I-969 | Orcas Island (19.4 mi west of NW corner of Bow quadrangle) | | Glaciomarine drift | 12,350±400; shells | 11,550±400; intraformational age | Easterbrook (1966b) | |
| I-1079 | Point Partridge, Whidbey Island (22.8 mi SW of SW corner of Bow quadrangle) | | Glaciomarine drift | 12,535±300; shells | 11,735±300; intraformational age | Easterbrook (1966b) | |
| I-1881 | SW Orcas Island (21.9 mi W of Bow quadrangle) | | Glaciomarine drift | 12,600±190; shells | 11,800±190; intraformational age | Easterbrook (1966b) | |
| I-1447 | Nooksack River E of Deming (11 mi N of NE top of Alger quadrangle) | | Glaciomarine drift | 12,970±280; shells | 12,170±280; intraformational age | Easterbrook (1966b) | |
| UW-32 | Penn Cove, Whidbey Island (20.9 mi SSW of SW corner of Bow quadrangle) | | Glaciomarine drift | 13,010±170; shells | 12,210±170; intraformational age | Easterbrook (1966b) | |
| **Everson Interstade glaciomarine clays (unit $Qgdm_e$; unit $gmd_c$, Plate 3, cross sections E–G, and Fig. 7)** | | | | | | | |
| I-A (Beta-1716) | Whidbey Island (11 mi S and 9 mi E of SW corner of Bow quadrangle) | In-situ marine shells in sandy silt which overlies compact massive stony silt-clay; underlies oxidized pebble- cobble gravel; altitude 1–2 m. | Shells date shallow-water subtidal sedimentation associated with early stage of isostatic emergence. | 13,595±145; shells | 12,795±145; intraformational age | Pessl and others (1989) | Distal marine sedimentation (this study) (also see Domack, 1982, 1983, 1984). |
| SK-B (Beta-1715) | Kiket Island (2.2 mi E and 5.2 mi S of SW corner of Bow quadrangle) | Marine shells in sandy silt overlying stony diamicton. | Shells date shallow (<10 m) marine sedimentation during Vashon recession (Pessl and others, 1989). | 12,865±110; shells | 12,065±110; intraformational age | Pessl and others (1989) | Distal marine sedimentation (this study) |
| SN-A (USGS-808) | Marysville (31 mi directly S of SE corner of Bow quadrangle) | Marine shells at base of laminated silt and clay that unconformably overlies Vashon till; altitude 12 m. | Shells occur in tidal-flat or estuarine sediments and record shallow marine sedimentation during Vashon recession. | 13,300±55; shells | 12,500±55; intraformational age | Pessl and others (1989) | Distal marine sedimentation (this study) |
| DW-83c (Beta-73072 | False Bay, southern San Juan Island (25.7 mi WSW of SW corner of Bow quadrangle) | Fine to medium sand or silty sand overlying gravel; altitude 43 ft . | Marine subtidal deposit characterized by sand, silty sand, and silt containing local pods and lenses of gravel; beds massive to locally cross-stratified; 1 to 27 ft thick; unconformably overlies other marine diamicton, till, and undifferentiated deposits and can be differentiated from these units by lack of clasts (Dethier and others, 1996). | 12,650±100; shells | 11,850±100; intraformational age | Dethier and others (1996) | Probable deposition distal to the ice front; overlies more ice-proximal deposits such as marine diamicton (dropstones). Uppermost stratigraphic position probably analogous to unit $gmd_c$ of this study, which is composed mostly of fine sediment (Fig. 7; Plate 3, cross sections E–G). |

| Sample (lab ID no.) | Location relative to study area | General geologic setting and altitude | Remarks (other studies) | Uncal. $^{14}C$ age; dated material | $^{14}C$ age | Reference | Notes |
|---|---|---|---|---|---|---|---|
| DW-58 (B-73071) | Friday Harbor 7.5-minute quadrangle (W of SW corner of Bow quadrangle) | Altitude 150 ft | Marine subtidal deposit characterized by sand, silty sand, and silt containing local pods and lenses of gravel; beds massive to locally cross-stratified; 1 to 27 ft thick; unconformably overlies other marine diamicton, till, and undifferentiated deposits and can be differentiated from these units by lack of clasts (Dethier and others, 1996). | 12,640±210; shell | 11,840±210; intraformational age | Dethier and others (1996) | Probable deposition distal to the ice front; overlies more ice-proximal deposits such as marine diamicton (dropstones). Uppermost stratigraphic position probably analogous to unit gmdc of this study, which is composed mostly of fine sediment (Fig. 7; Plate 3, cross sections E–G). |
| DW-21 (B-73069) | NW of Mt. Finlayson on the southernmost portion of San Juan Island (22.7 mi W of SW corner of Bow quadrangle) | Altitude 11 ft; near UW-9795, -9798, -9799 of Shaw (1972) and W-1214 of Easterbrook (1969). Easterbrook reported an age of 12.35 ±12.35 yr B.P. (I-1469) for shell. | Marine subtidal deposit characterized by sand, silty sand, and silt containing local pods and lenses of gravel; beds massive to locally cross-stratified; 1 to 27 ft thick; unconformably overlies other marine diamicton, till, and undifferentiated deposits and can be differentiated from these units by lack of clasts (Dethier and others, 1996). | 12,600±80; shells; intraformational age | 11,800±80; | Dethier and others (1996) | Probable deposition distal to the ice front; overlies more ice-proximal deposits such as marine diamicton (dropstones). Uppermost stratigraphic position probably analogous to unit gmdc of this study, which is composed mostly of fine sediment (Fig. 7; Plate 3, cross section E–G). |
| UW-9778 (B-73064) | Shaw Island quadrangle; San Juan Island (~20 mi W of Bow quadrangle) | Altitude 150 ft | Marine subtidal deposit(?). General marine subtidal deposits characterized by sand, silty sand, and silt containing local pods and lenses of gravel; beds massive to locally cross-stratified; 1 to 27 ft thick; unconformably overlies other marine diamicton, till, and undifferentiated deposits and can be differentiated from these units by lack of clasts (Dethier and others, 1996). | 12,600±380; shells | 11,800±380; intraformational age | Dethier and others (1996) | Probable deposition distal to the ice front; overlies more ice proximal deposits such as marine diamicton (dropstones). Uppermost stratigraphic position probably analogous to unit gmdc of this study, which is composed mostly of fine sediment (Fig. 7; Plate 3, cross sections E–G). |
| USGS-342 | Bay View Ridge (Fig. 3, site 2) | Basal peat altitude 148 ft | Peat deposit overlying silty clay (unit gmdc; Fig. 7, Plate 3, cross sections E–G). | 11,700 ±100; peat; minimum age | NA | Siegfried (1979) | Basal peat probably closely dates onset of terrestrial conditions and isostatic emergence on the basis of other wood and shell ages in the study area and regionally. |
| W-398 | Thomas Lake; SW1/4 sec. 31, T36N, R5E (3 mi N of Sedro-Woolley and 1.25 mi E of Alger quadrangle) | Basal peat at 27.2 ft depth; bog altitude about 320 ft (about 27 ft to basal peat sample), thus sample altitude about 290 ft or about 50 ft below our probable glaciomarine limit altitude in the study area directly to the west. | Sphagnum, wood, muck, and hypnum with local pumicite (Rigg, 1958); peat body is 21 to 32 ft deep. | 12,900 ±330; peat; minimum age | NA | Rigg (1958); age reported by Rubin and Alexander (1958); Matthews and others (1970) and Siegfried (1978) discuss the age significance | Underlying clay is unit Qgome (unit gmdc on Fig. 7 and Plate 3, cross sections E–G) (this study; Dragovich and Grisamer, in press); age and altitude suggest that the date approximates the onset of terrestrial conditions after isostatic rebound. |
| 44A-2 (B-099698) | Nooksack River W of Deming (12.7 mi directly N of NE corner of Alger quadrangle) | Altitude 280 ft | Glaciomarine sandy silt and clay overlying probable Vashon till. | 11,610 ±80; wood; intraformational age | NA | Dragovich and others (1997d) | |

| Sample (lab ID no.) | Location relative to study area | General geologic setting and altitude | Remarks (other studies) | Uncal. $^{14}C$ age; dated material | $^{14}C$ age | Reference | Notes |
|---|---|---|---|---|---|---|---|
| 44A-1 (B-099697) | Nooksack River W of Deming (12.7 mi directly N of NE corner of Alger quadrangle) | Altitude 280 ft | Glaciomarine sandy silt and clay overlying probable Vashon till. | 11,920 ±60; wood; intraformational age | NA | Dragovich and others (1997d) | |
| **Everson Interstade Marine Outwash (unit $Qgom_e$)** | | | | | | | |
| DW-15 (B-70971) | 1 mi S of Friday Harbor on San Juan Island (22.5 mi directly W of Bow quadrangle) | Altitude 50 ft; fine gravel and coarse sand | Marine outwash consisting of gravel and sand, matrix-supported gravel and sand-rich diamicton, and lenses and beds of pebbly silt; generally well stratified with mostly south-dipping cross-beds extending 33–165 ft downdip; local collapse features; 16 to 200+ ft thick | 13,240±70; shells | 12,440±70; intraformational age | Dethier and others (1996) | Unit generally overlain by marine diamicton and underlain by till or undifferentiated diamicton consistent with our findings (Fig. 7; Plate 3, cross sections E–G) |
| **Everson Interstade glaciomarine diamicton (unit $Qgdm_e$; unit $gmd_d$, Plate 3, cross sections E–G, and Fig. 7)** | | | | | | | |
| D+W-30 (B-73071) | San Juan Island 1 mi SW of Friday Harbor (24.1 mi directly W of SW corner of Bow quadrangle) | Marine diamicton; altitude 92 ft | Marine diamicton and well-sorted pebbly silt with sparse boulders; lenses and layers of silt, sand and gravel; overlies marine outwash or till and overlain by gravelly emergence deposits or marine subtidal deposits; 1 to 27 ft thick to locally 50 ft thick; below 200 altitude (glaciomarine limit) in the area (Dethier and others, 1996) | 13,050±370; shells | 12,250±370; intraformational age | Dethier and others (1996) | Diamicts same sedimentary facies as $gmd_d$ on Fig 7 and Plate 3, cross sections E–G. Note similar stratigraphic sequence in the San Juan Islands as documented by Dethier and others (1996)(see Remarks)—$gmd_c$ over $gmd_d$ over $Qgom_e$. This sequence probably reflects proximal to distal sedimentary facies for an area during recession of the Puget lobe. |
| DW-14 (B-73068) | San Juan Island 1 mi W of Cattle Point on southernmost San Juan Island (21.9 mi WSW of SW corner of Bow quadrangle) | Altitude 21 ft; marine diamicton underlain by submarine outwash and overlain by estuarine deposits and emergence deposits; probably near W-1214 of Easterbrook (1969) who reported an age of 12.35 ±0.33 yr B.P. (I-1469) for shells. | Marine diamicton and well-sorted pebbly silt with sparse boulders; lenses and layers of silt, sand and gravel; overlies marine outwash or till and overlain by gravelly emergence deposits or marine subtidal deposits; 1 to 27 ft thick to locally 50 ft thick; below 200 altitude (glaciomarine limit) in the are (Dethier and others, 1996). | 13,000±150; shells | 12,200±150; intraformational age | Dethier and others (1996) | Diamicts same sedimentary facies as $gmd_d$ on Fig 7 and Plate 3, cross sections E–G. Note similar stratigraphic sequence in the San Juan Islands as documented by Dethier and others (1996)(see Remarks)—$gmd_c$ over $gmd_d$ over $Qgom_e$. This sequence probably reflects proximal to distal sedimentary facies for an area during recession of the Puget lobe. |
| UW-9778 (B-73067) | San Juan Island 1 mi W of Cattle Point on southernmost San Juan Island (21.9 mi WSW of SW corner of Bow quadrangle) | Altitude 150 ft; marine diamicton underlain by submarine outwash and overlain by estuarine deposits and emergence deposits. | Marine diamicton and well-sorted pebbly silt with sparse boulders; lenses and layers of silt, sand and gravel; overlies marine outwash or till and overlain by gravelly emergence deposits or marine subtidal deposits; 1 to 27 ft thick to locally 50 ft thick; below 200 altitude (glaciomarine limit) in the area (Dethier and others, 1996). | 12,800±100; shells | 12,000±100; intraformational age | Dethier and others (1996); Shaw (1972) | Diamicts same sedimentary facies as $gmd_d$ on Fig 7 and Plate 3, cross sections E–G. Note similar stratigraphic sequence in the San Juan Islands as documented by Dethier and others (1996)(see Remarks)—$gmd_c$ over $gmd_d$ over $Qgom_e$. This sequence probably reflects proximal to distal sedimentary facies for an area during recession of the Puget lobe. |
| SJ-A (Beta-1723) | Lopez Island (19 mi SW of Bow quadrangle) | Fresh- to brackish-water gastropods in silty sand with sparse, scattered pebbles; overlies fossiliferous, marine sand and gravel noted below; altitude 1 m. | Marine and nonmarine shells have overlapping ages that together date isostatic emergence of land. | 12,885±225; shells | 12,005±225; intraformational age | Pessl and others (1989) | Age, altitude, and stratigraphic relations data imply isostatic emergence of the San Juans prior to the study area. (See text.) |

| Sample (lab ID no.) | Location relative to study area | General geologic setting and altitude | Remarks (other studies) | Uncal. $^{14}C$ age; dated material | $^{14}C$ age | Reference | Notes |
|---|---|---|---|---|---|---|---|
| **Olympia nonglacial interval ages (units pf and trans, Plate 3, cross sections E–G, and Fig. 7) and Older Glaciations (units ot, oot, and oo, Plate 3, cross sections E–G)** | | | | | | | |
| SK-A (Beta-1320) | Anacortes (2 mi E and 2.5 mi S of W corner of Bow quadrangle) | Logs with associated peat in silt and fine sand; unconformably overlain by gray friable till; underlain by a (25–30 m) thick sequence of cross-bedded medium- to well-sorted medium to coarse sand, which is underlain in turn by subhorizontally bedded iron-stained pebble-cobble gravel. | Wood and associated peat dates a pre-Vashon nonglacial(?) interval, perhaps correlative with the Olympia nonglacial sediments (Armstrong and others, 1965; Easterbrook, 1969) | 28,595±1,035; logs; intraformational age | NA | Pessl and others (1989) | |
| SK-F (USGS-117) | 3 mi E and 1 mi S of SE corner of Alger quadrangle | Peat and wood in gray-blue, organic-rich silt and fine sand overlain by oxidized sand with minor silt; underlain by oxidized sand and gravel with prominent west-dipping cross-beds. | Wood and associated peat date a nonglacial interval, perhaps correlative with the Olympia nonglacial interval (Armstrong and others, 1965; Easterbrook, 1969). | 25,500±350; wood | NA | Pessl and others (1989) | |
| SN-C (USGS-770) | 4 mi S of Sterling Hill and Alger quadrangle (Fig. 3, site 3) | Wood at top of massive sandy pebble gravel with local lenses and interbeds of coarse sand and gravel with local silt, clay, and fine sand beds (Minard, 1985); altitude 15 m. | Wood probably dated coarse grained fluvial facies of Olympia nonglacial sediments. | 39,700±1,100; wood; intraformational age | NA | Pessl and others (1989) | |
| SN-B (USGS-771) | Norman (20 mi directly S of Sterling Hill and Alger quadrangle) | Altitude 14 m; peat interbedded with silt and sand overlying marine shell-bearing pebbly mud (Minard, 1985). Dated beds overlain by Vashon till and recessional outwash. | Marine diamicton beneath dated peat-bearing bed probably is deposit of the Possession Drift (Easterbrook and others, 1967). | 1,000; peat; minimum formational age | NA | Pessl and others (1989) | Outcroppings of pre-Vashon glacial deposits south of the study area. |

# Appendix 3. Table of characteristics for geologic units, determined using water wells and geotechnical borings, and selected water-well strip logs

The table below provides some of the field and water-well descriptions of characteristics used to distinguish the Quaternary subsurface geologic units. (Also see Dragovich and Grisamer, in press.) Lithology: g, gravel; s, sand; si, silt; c, clay; or combinations (for example, sisc, silty sandy clay). Relative gross stratigraphic position of the upland glacial units is implied by the unit order in the table. For example, Sumas Stade deposits (such as $Qgo_s$) commonly overlie Everson Interstade deposits (such as $gmd_d$), which commonly overlie Vashon Stade deposits (such as $Qgt_v$). Relative stratigraphic position and other unit characteristics (for example, density and sorting) are important in differentiating subsurface units. Holocene Skagit valley fill units, such as alluvium, overlie Sumas, Everson, or Vashon glacial deposits at depth. (See "glacial" in valley strip logs.) Plate 3, cross sections E–G, incorporate some of the strip logs shown here. Well locations are shown on Figure 4. Units $gmd_c$, $gmd_d$, and older glacial units (such as "trans") are also defined in the text or Plate 3, explanation of cross sections E–G.

**PLEISTOCENE GLACIAL UPLAND UNITS**

| Unit | Dominant lithology | Secondary lithology | Minor lithology | Unit density; diagnostic clast compositions (*unit sorting*) | Notes (*well-driller descriptions*); correlations |
|---|---|---|---|---|---|
| **Sumas Stade deposits** | | | | | |
| $Qgo_s$ | sg, s, g | sis, cs | "pea gravel" | Low density; dunite and Mount Baker andesite (*moderately to well-sorted*) | Mostly occurs as isolated terraces in the Samish River valley |
| $Qgod_s$ | g, s, sg | | | Low density; dunite and Mount Baker andesite (*moderately to well-sorted*) | Deltaic deposits extend below the Skagit River Holocene valley fill |
| **Everson Interstade deposits** | | | | | |
| $Qgom_{ee}$ | gs, sg, g | | | Low density; reworked older units (*typically well-sorted*) | Reworked deposits from older glacial units |
| $gmd_c$ | c, sisc, s, sic | si | s, ssi, cs | Low density; (*moderately to well-sorted*) | *Described as soft; rare reports of oil and methane*; fining-upward sequence |
| $gmd_d$ | cg, cgs, gsc, sis, gssi (diamictons) | | si, sis | Low density; commonly phyllite-rich (*poorly sorted*) | *Commonly described as soft silt or clay with scattered gravel; described as shaley (phyllite-rich)*; local fining-upward sequences; *commonly described as clay strips in hardpan* |
| $Qgom_e$ | sg, gs, g | sigs, sis, cs, gsis, gsi | interlayers | Low density; commonly phyllite-rich (*typically well-sorted*) | *Often noted as black (Darrington Phyllite?) sands; described as shaley (phyllite-rich)*; locally layered on a scale of centimeters; contains wood; typically define fining-upward sequences; rarely *described as fine sand with layers of hard clay* |
| **Vashon Stade deposits** | | | | | |
| $Qgt_v$ | cssig, scg, cg, ssig, gsc, (diamictons) | sg, si interlayers | locally bouldery | Moderate to high density; polymictic clast composition or locally described as shaley (phyllitic?) (*poorly sorted*) | *Commonly described as dense or hardpan*; locally phyllite-rich with sandy gravel "dynamic till" interlayers (see text) |
| "dynamic till" | csg, gs, g, cssi | c, ssi, s | locally bouldery | Moderate to high density; polymictic clast compositions (*moderate to well sorted*) | *Described as dense or hardpan* |
| $Qga_v$ | sg, gsis, cgs, sc, s, g | fs, si, ssig, sis, csi | c, csg, wood | Moderate to high density, polymictic clast compositions (*typically well-sorted*) | *Near upland rock areas described as containing shale (phyllite)*; locally may contain mass-wasting deposits (4–10 ft thick); locally coarsening-upward sequence |
| **Pre-Vashon glacial deposits** | | | | | |
| "transitional beds" (unit trans) | c, sc, sisc, sis, s, csi | sg | cg | Moderate to high density; polymictic clast compositions? (*typically well-sorted*) | Thinly interbedded diamictons probably are mass-wasting deposits; sand and gravels commonly interlayered with clays; correlated with the "transitional beds" of Pessl and others (1989) |
| pre-Fraser deposits (unit pf) | c, sc, s | si, sgc | gs, gc | Moderate to high density; local clast compositions? (*moderately to well-sorted*) | *Commonly contains wood and peat*; correlated with the "Olympia inter-glacial unit" of Armstrong and others (1965) |
| older till (unit ot) | gsc, cg, sgc (diamictons) | sicgs | sg, g locally bouldery | Moderate to high density; polymictic clast compositions? (*poorly sorted*) | *sg rare, often only 5 ft thick; gravel commonly described as scattered*; tentatively correlated with the Possession drift of Easterbrook (for example, 1994) |
| older outwash (unit oo) | sg, c, g, s | si | | Moderate to high density; polymictic clast compositions? (*typically well-sorted*) | Tentatively correlated with the Possession drift of Easterbrook (for example, 1994) |
| older till (unit oot) | g and hardpan | | | Moderate to high density | Locally described as hardpan below unit oo only in well 618; tentatively correlated with the Possession drift of Easterbrook (for example, 1994) |

## HOLOCENE VALLEY UNITS

| Unit | Dominant lithology | Secondary lithology | Unit density; diagnostic clast compositions (*unit sorting*) | Notes (*well-driller descriptions*) |
|---|---|---|---|---|
| Qa | gs, sg, s, cs, ssi, csi, sis, sc, c, sic, g | cs, shells | Low-density; polymictic clast compositions (*typically well-sorted*) | *Contains shells, wood and peat*; common fining-upward sequence (point bar model) |
| Qaf | g, gsis, ssig | cg | Low-density; polymictic clast compositions (*typically moderately to well-sorted*) | Commonly described as black loose shale (phyllite?) |
| Diamict (mostly Qoa) | cg, scg, gc, gsc, gs | | Low density; commonly volcanic clast-rich (*poorly sorted*) | Commonly pumice and dacite clast-rich unit Qoa; may include glacial diamicts |
| Volcanics/ Qoa | s, sg | | Low density; volcanic clast-rich compositions (*typically moderately to well-sorted*) | Described as black sand |

## SELECTED WATER-WELL STRIP LOGS

**2** Alger quadrangle
sec. 1, T35N, R3E
uplands – Bow Hill Road

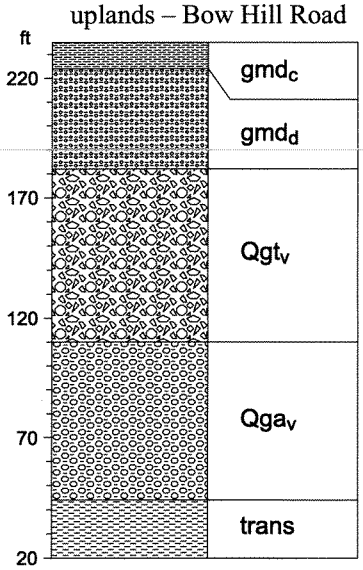


**24** Alger quadrangle
sec. 2, T35N, R3E
uplands – Bow Hill Road

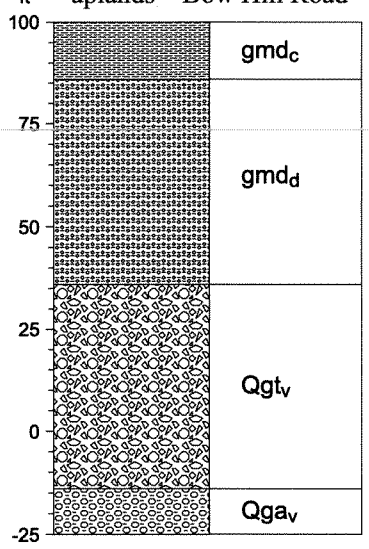


**29** Bow quadrangle
sec. 3, T35N, R3E
Skagit Valley – directly W. of Chuckanut Dr.

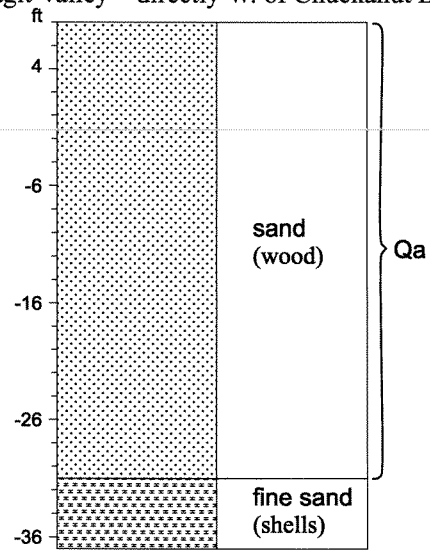


**41** Bow quadrangle
sec. 10, T35N, R3E
Skagit Valley – Thomas Rd.

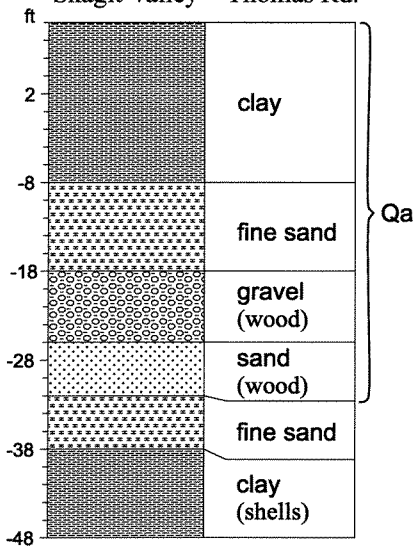


**45** Bow quadrangle
sec. 11, T35N, R3E
Skagit Valley – Chuckanut Drive

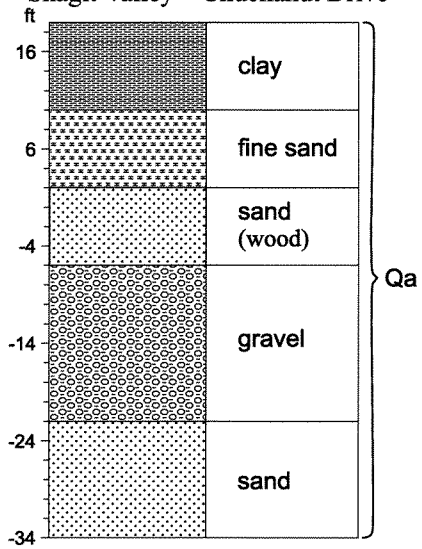


**54** Alger quadrangle
sec. 12, T35N, R3E
uplands – Allen Road

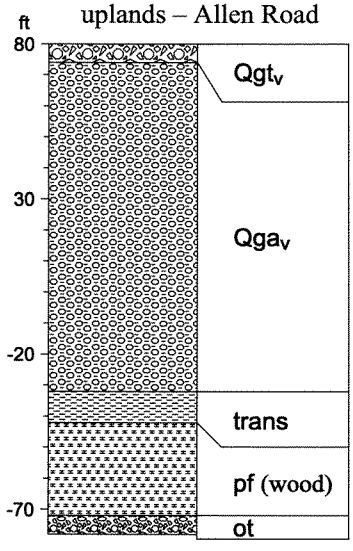

**84** Alger quadrangle
sec. 13, T35N, R3E
uplands – Allen Road

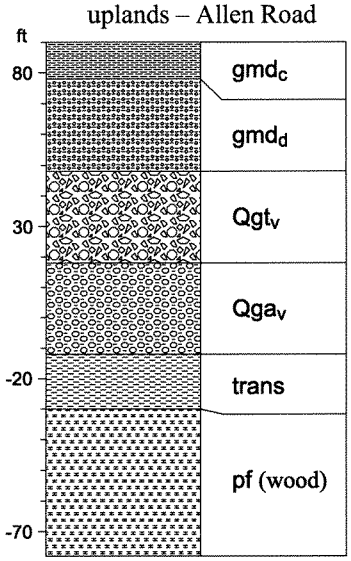


**98** Alger quadrangle
sec. 13, T35N, R3E
Skagit Valley – N. of Sam Bell Rd.

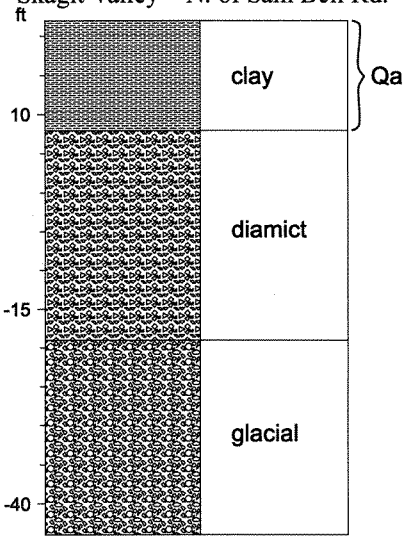


**100** Bow quadrangle
sec. 15, T35N, R3E
Skagit Valley – Field Rd.

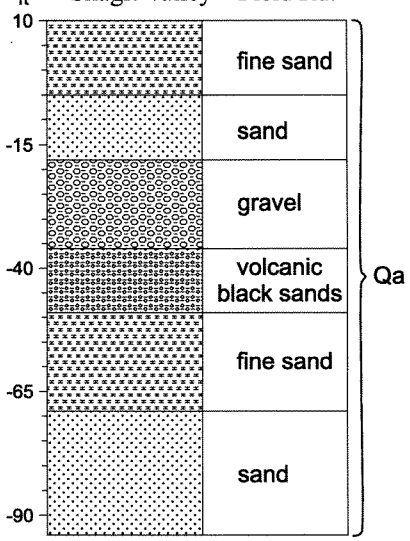


**103** Bow quadrangle
sec. 16, T35N, R3E
Skagit Valley – Field Road

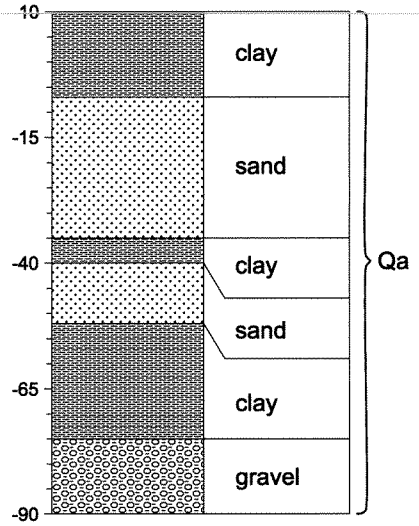


**106** Bow quadrangle
sec. 17, T35N, R3E
Skagit Valley – Darcy Road

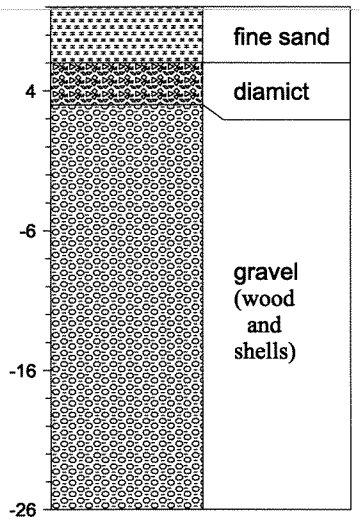


**107** Bow quadrangle
sec. 17, T35N, R3E
Skagit Valley – Darcy Road

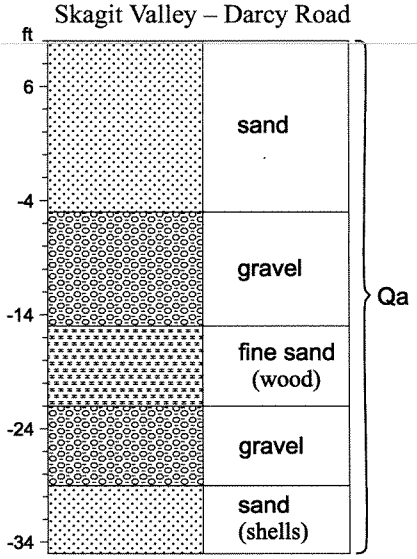


**110** Bow quadrangle
sec. 19, T35N, R3E
uplands – Bay View Ridge

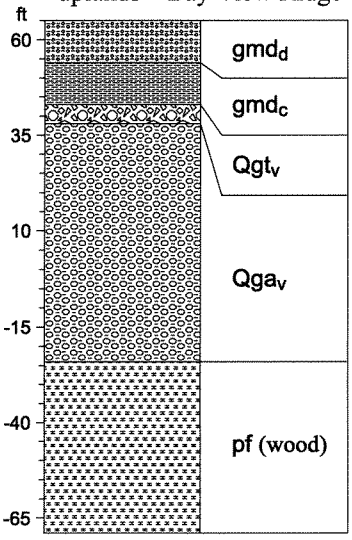


**116** Bow quadrangle
sec. 20, T35N, R3E
uplands – Bay View Ridge

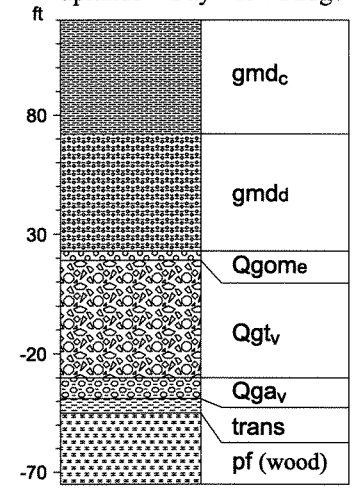


**120** Bow quadrangle
sec. 21, T35N, R3E
uplands – Bay View Ridge

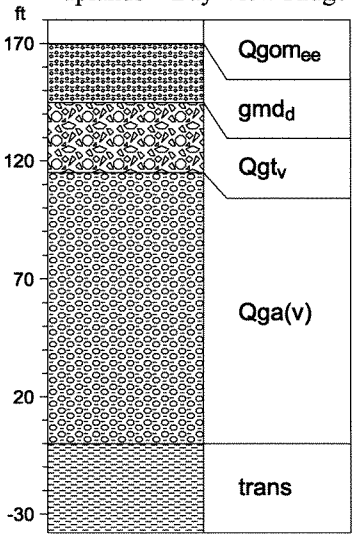

**133** Bow quadrangle
sec. 22, T35N, R3E
Skagit Valley – Thomas Rd.

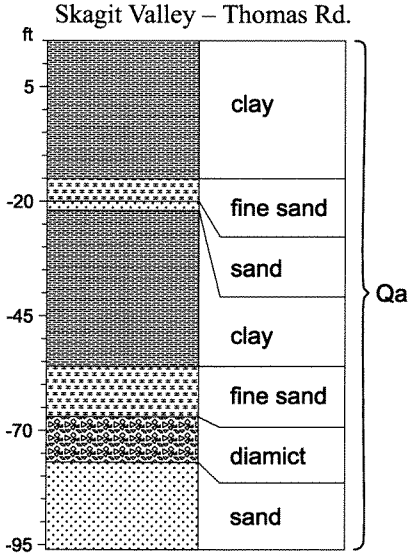


**142** Alger quadrangle
sec. 24, T35N, R3E
Skagit Valley – Sam Bell Rd.

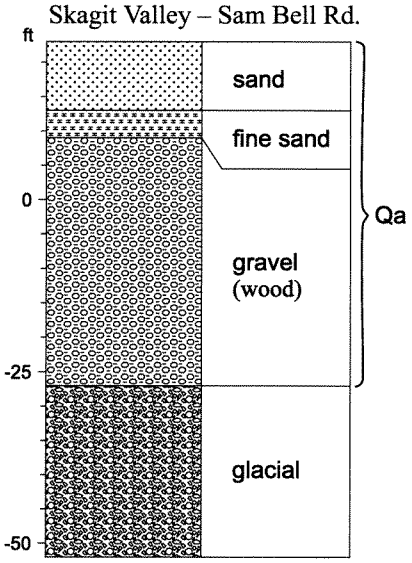


**161** Bow quadrangle
sec. 29, T35N, R3E
uplands – Bay View Ridge

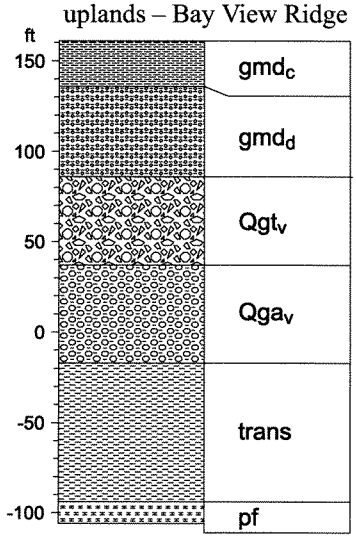


**263** Alger quadrangle
sec. 3, T35N, R4E
uplands – N.E. of Butler Hill

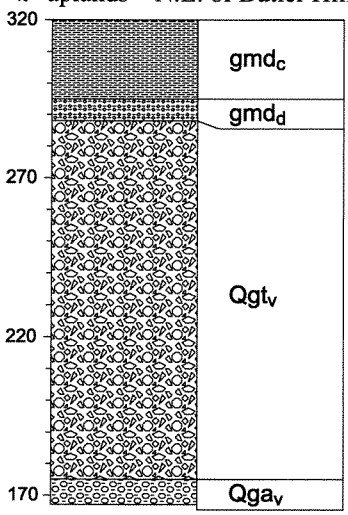


**269** Alger quadrangle
sec. 4, T35N, R4E
uplands – F & S Grade Rd.

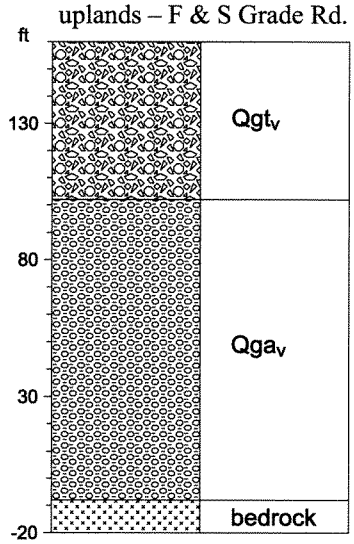


**272** Alger quadrangle
sec. 5, T35N, R4E
uplands S. of Jarman Prairie

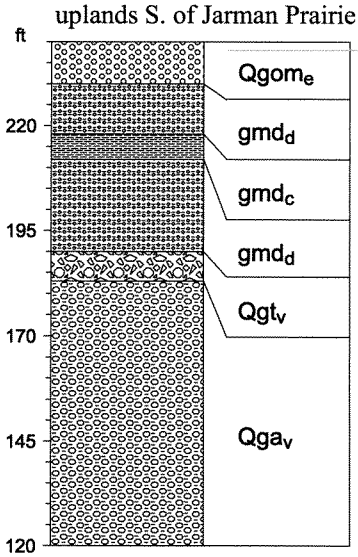


**284** Alger quadrangle
sec. 7, T35N, R4E
uplands – directly W. of I-5

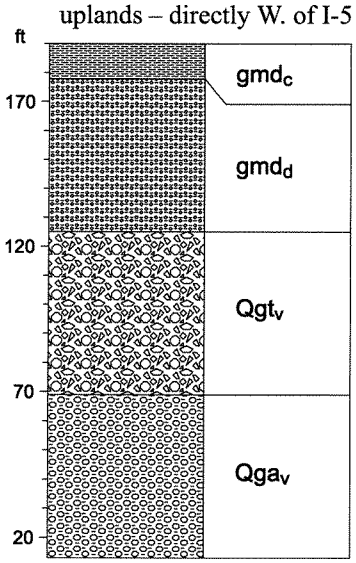


**287** Alger quadrangle
sec. 8, T35N, R4E
uplands – N. of Thomas Rd.

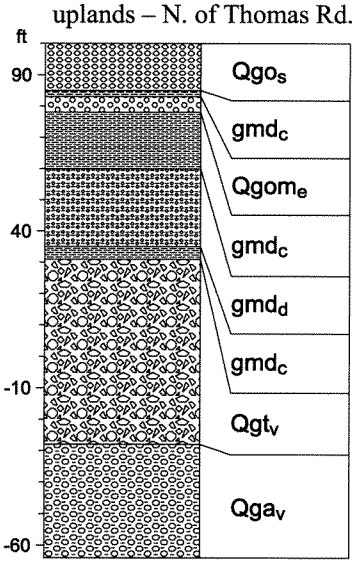


**293** Alger quadrangle
sec. 9, T35N, R4E
uplands – F & S Grade Rd.

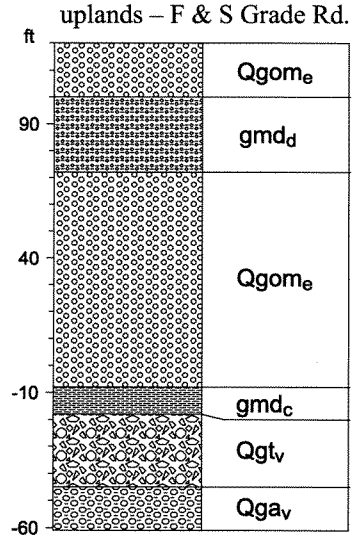

**311** Alger quadrangle
sec. 10, T35N, R4E
uplands – directly E. of Thomas Cr.

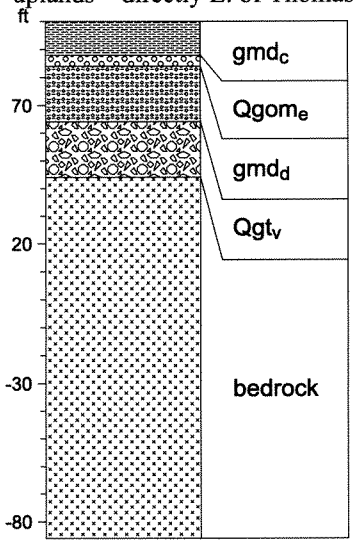


**315** Alger quadrangle
sec. 11, T35N, R4E
uplands – Garden of Eden

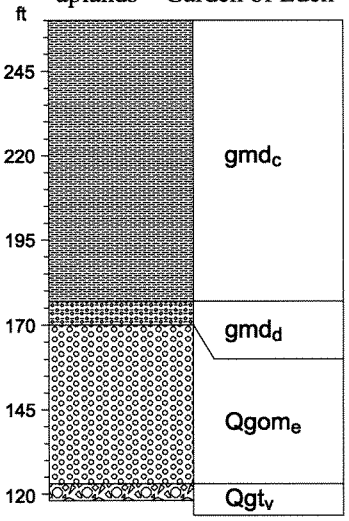


**347** Alger quadrangle
sec. 14, T35N, R4E
Skagit Valley – F & S Grade Rd.

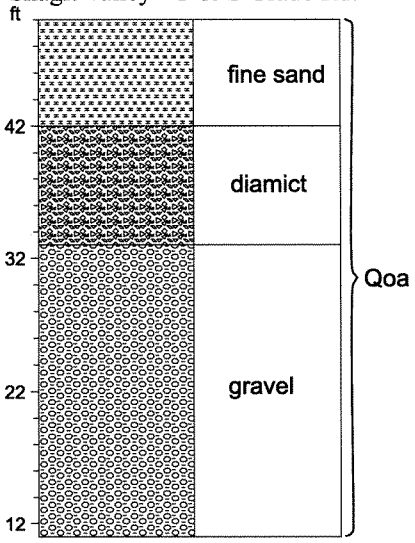


**348** Alger quadrangle
sec. 15, T35N, R4E
Skagit Valley – District Line Rd.

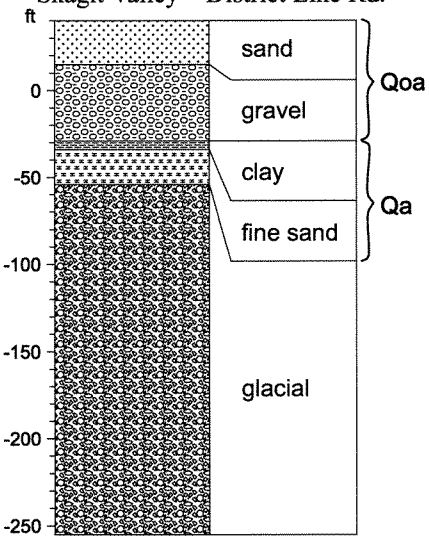


**354** Alger quadrangle
sec. 15, T35N, R4E
Skagit Valley – Collins Rd.

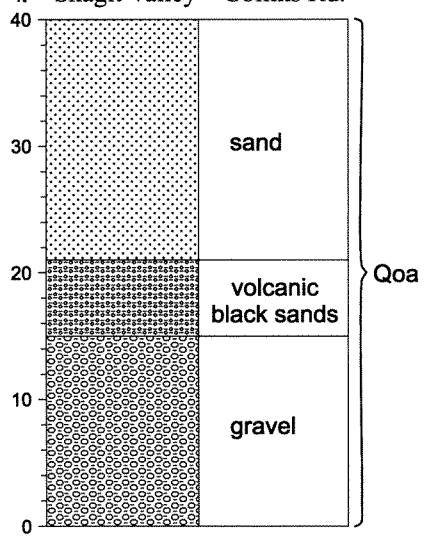


**358** Alger quadrangle
sec. 16, T35N, R4E
Skagit Valley – Dahlstedt Rd.

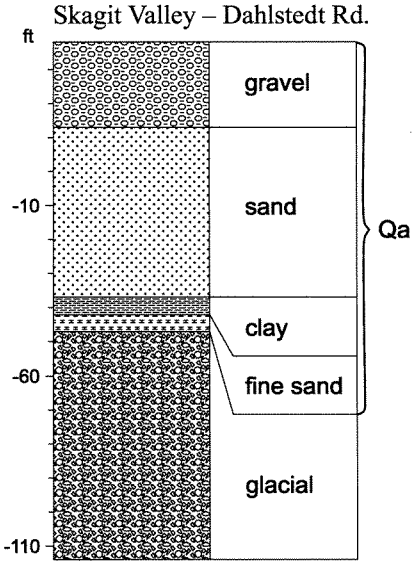


**362** Alger quadrangle
sec. 17, T35N, R4E
uplands – N. of Kelleher Rd.

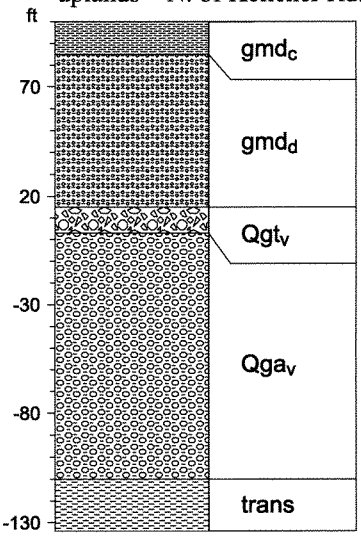


**368** Alger quadrangle
sec. 19, T35N, R4E
Skagit Valley – Pulver Rd.

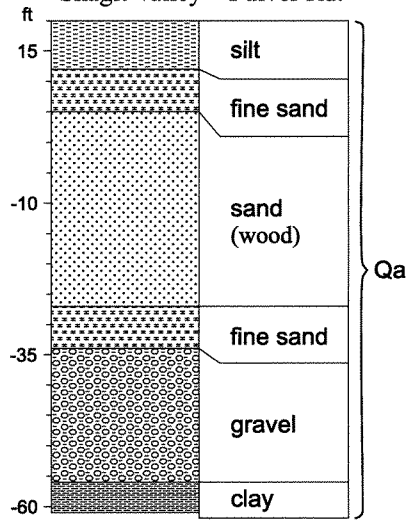


**381** Alger quadrangle
sec. 21, T35N, R4E
Skagit Valley – District Line Rd.

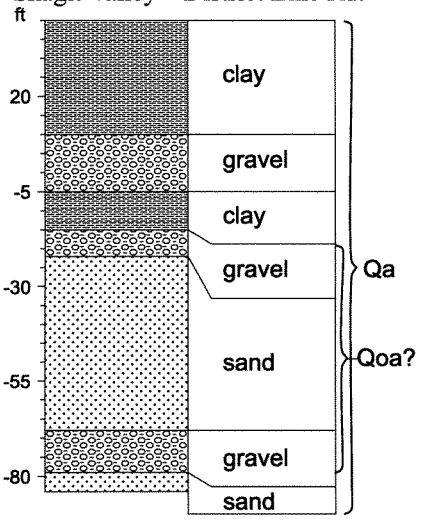

**385** Alger quadrangle
sec. 22, T35N, R4E
Skagit Valley – Cook Road

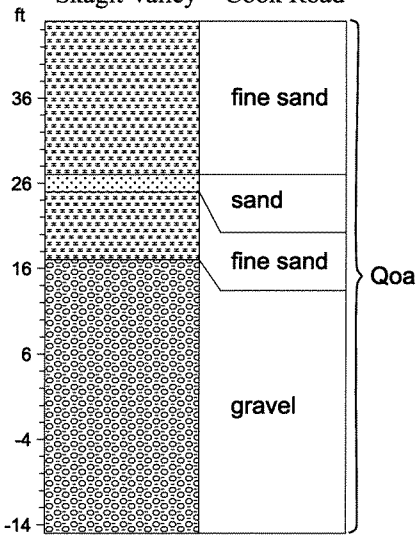


**391** Alger quadrangle
sec. 23, T35N, R4E
Skagit Valley – Cook Road

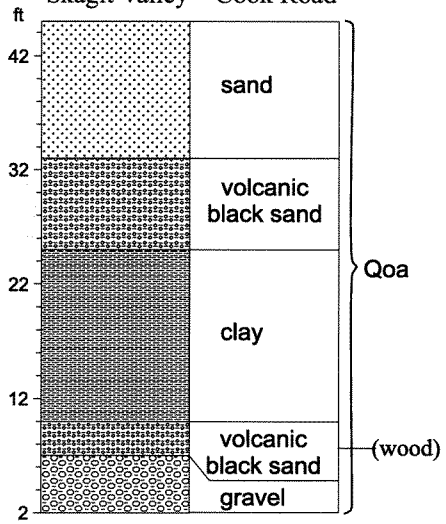


**427** Bow quadrangle
sec. 36, T36N, R3E
uplands – Bow Hill Road

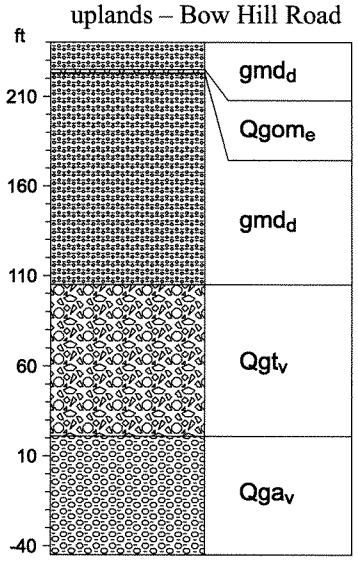


**430** Bow quadrangle
sec. 35, T36N, R3E
uplands – N. of Bow Hill Rd.

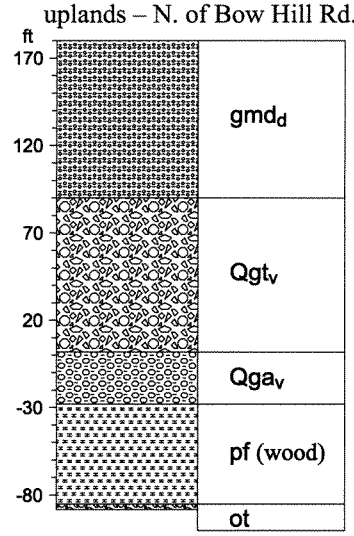


**470** Bow quadrangle
sec. 26, T36N, R3E
uplands – S. of Colony Crk.

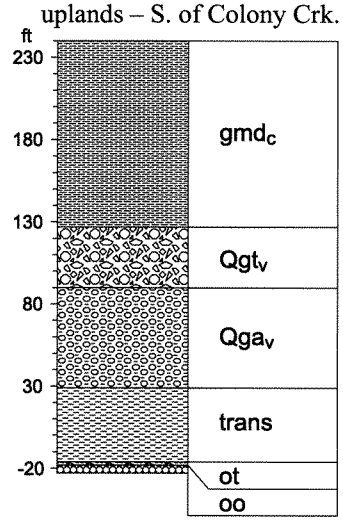


**476** Alger quadrangle
sec. 25, T36N, R3E
uplands – Colony Road

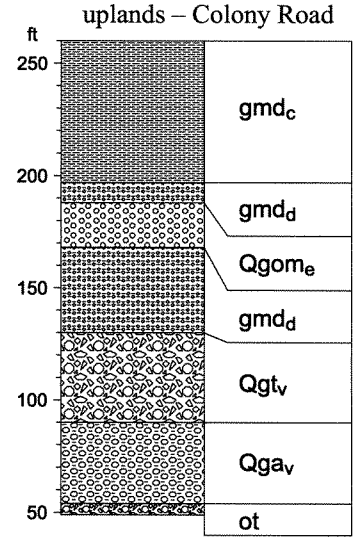


**480** Alger quadrangle
sec. 24, T36N, R3E
uplands – W. of Colony Rd.

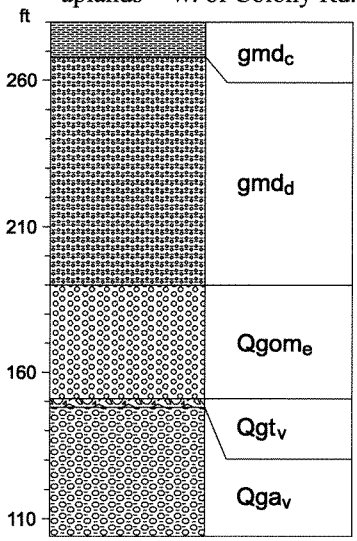


**486** Bow quadrangle
sec. 23, T36N, R3E
uplands – N. of Wood Rd.

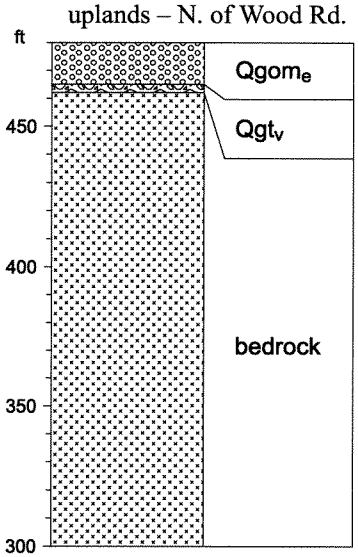


**492** Alger quadrangle
sec. 13, T36N, R3E
uplands – Barrel Springs Rd.

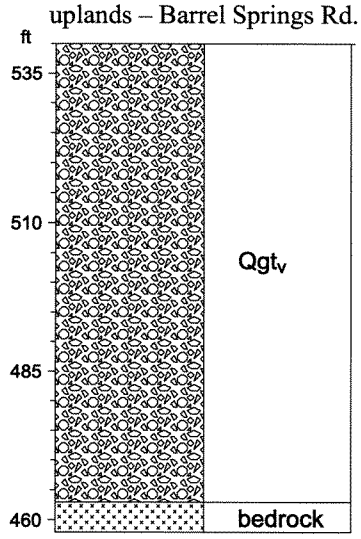

**493** Alger quadrangle
sec. 12, T36N, R3E
uplands – Barrel Springs Rd.

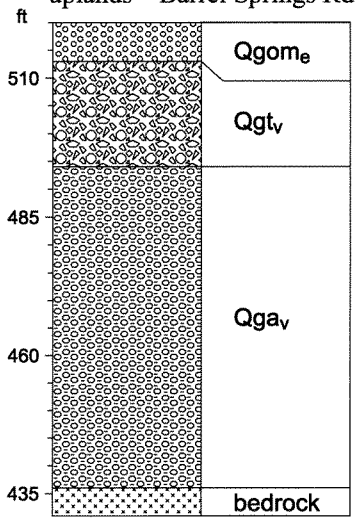


**546** Alger quadrangle
sec. 8, T36N, R4E
uplands – S. of Cain Lake Rd.

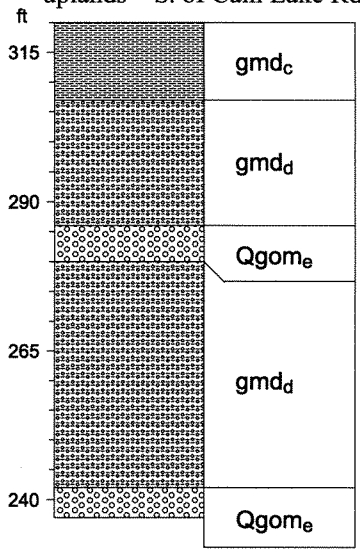


**563** Alger quadrangle
sec. 17, T36N, R4E
uplands – Butler Creek Rd.

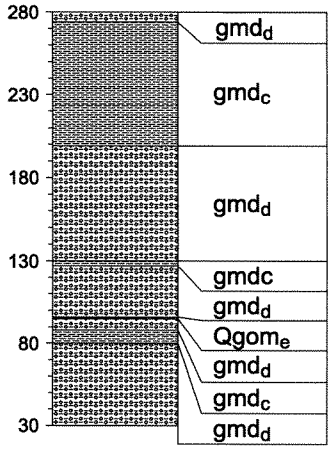


**582** Alger quadrangle
sec. 18, T36N, R4E
uplands – Friday Creek

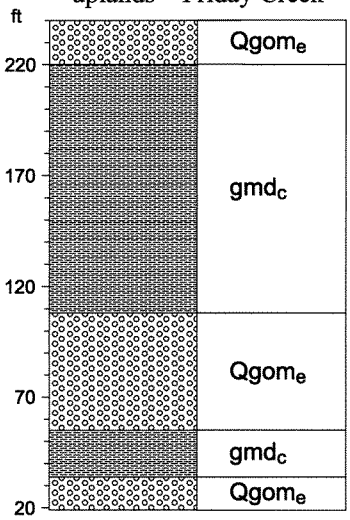


**584** Alger quadrangle
sec. 19, T36N, R4E
uplands – Colony Road

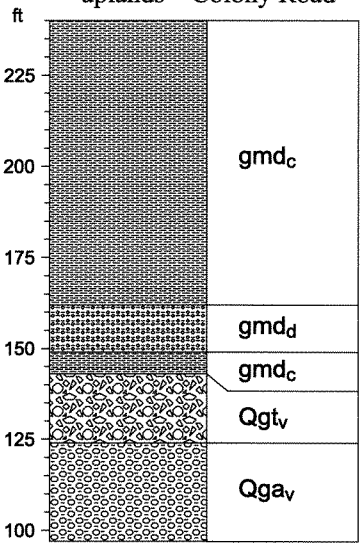


**588** Alger quadrangle
sec. 20, T36N, R4E
uplands – directly W. of Friday Crk.

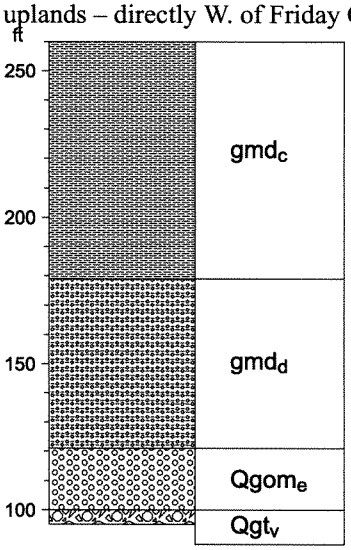


**605** Alger quadrangle
sec. 21, T36N, R4E
uplands – Echo Hill Rd.

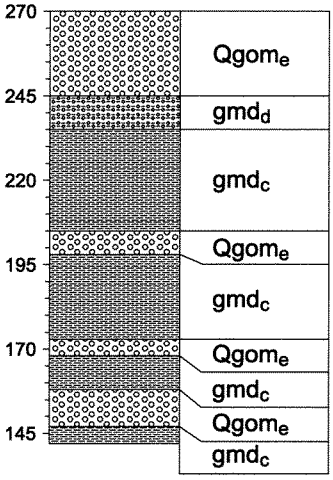


**619** Alger quadrangle
sec. 23, T36N, R4E
uplands – N. of Prairie Rd

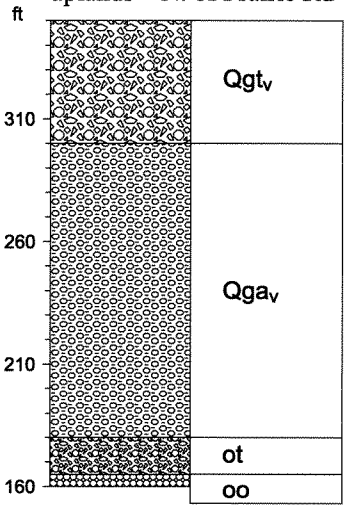


**644** Alger quadrangle
sec. 26, T36N, R4E
uplands – N. of Prairie Rd

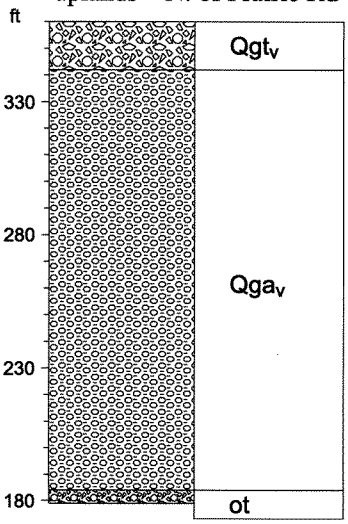

**658** Alger quadrangle
sec. 26, T36N, R4E
Samish R. valley – Warner Prairie

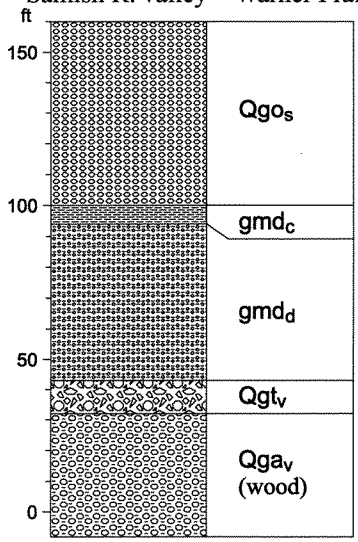


**663** Alger quadrangle
sec. 27, T36N, R4E
uplands – S. of Samish R. valley

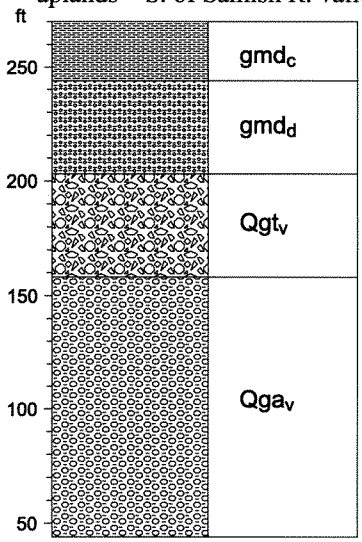


**669** Alger quadrangle
sec. 29, T36N, R4E
uplands – Skagit Speedway

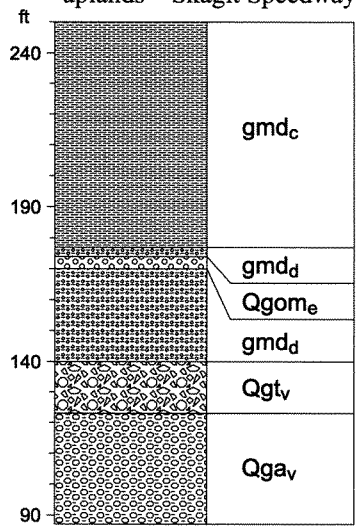


**671** Alger quadrangle
sec. 30, T36N, R4E
uplands – E. of Colony Rd.

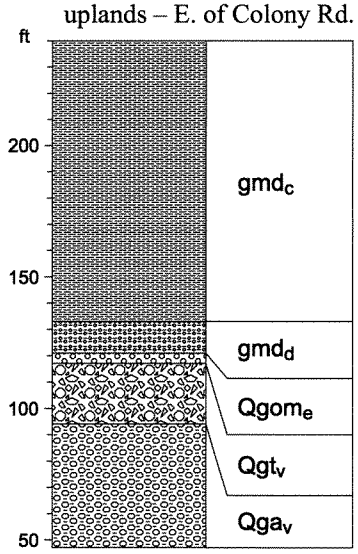


**679** Alger quadrangle
sec. 31, T36N, R4E
uplands – N. of Bow Hill Rd.

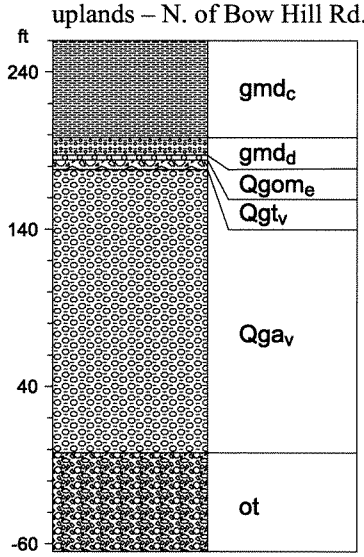


**683** Alger quadrangle
sec. 32, T36N, R4E
uplands – N. of Prairie Rd.

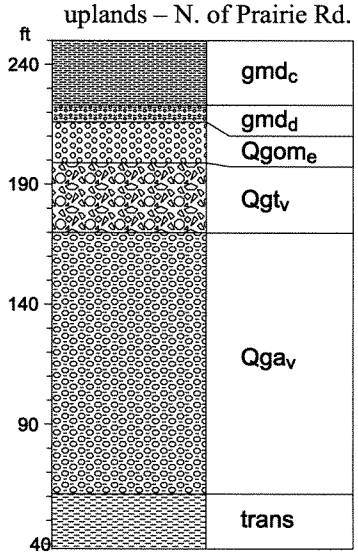


**698** Alger quadrangle
sec. 32, T36N, R4E
uplands – Humphrey Hill

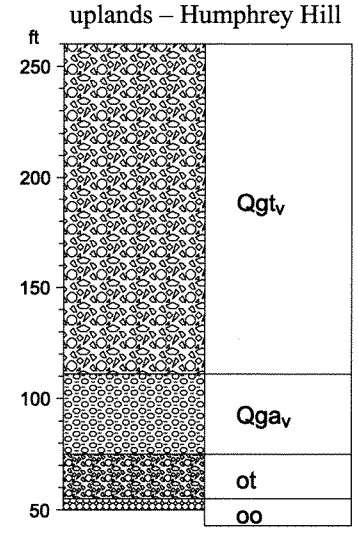


**709** Alger quadrangle
sec. 33, T36N, R4E
Samish R. valley – W. of Samish R.

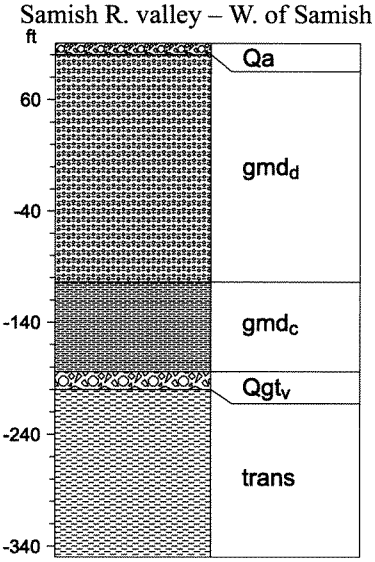


**722** Alger quadrangle
sec. 34, T36N, R4E
uplands – N. of Swede Crk.

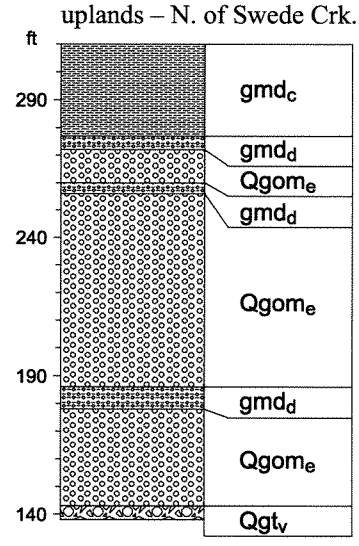

**724** Alger quadrangle
sec. 35, T36N, R4E
uplands – N. of Swede Crk.

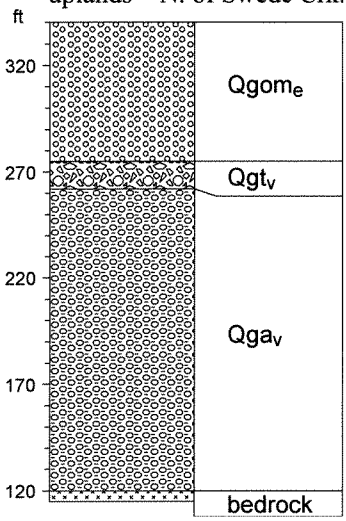

# Appendix 4. Major and minor element geochemical analyses, this study

Major, minor, and trace element geochemical analyses of rock units in the Bow and Alger quadrangles (this study). All analyses are Rigaku x-ray fluorescence analyses performed at the Geology Department, Washington State University (WSU), Pullman, WA 99164, under the direction of Diane Johnson. Major elements are normalized on a volatile-free basis, with total Fe expressed as FeO. **R** after a sample number indicates a rerun or duplicate bead made from the same rock powder; **A**, average of two runs; †, values >120% of WSU highest standard. A description of the method and estimates of the precision and accuracy are given in Hooper and others (1993). **LOI**, loss on ignition (roughly reflects the water content); **No.**, sample number; sample locations shown in Fig. 3. See Appendix 5 for rock unit designations and geochemical discrimination synopses.

**Unnormalized results (weight percent)**

| No. | LOI (%) | $SiO_2$ | $Al_2O_3$ | $TiO_2$ | FeO | MnO | CaO | MgO | $K_2O$ | $Na_2O$ | $P_2O_5$ | Total |
|---|---|---|---|---|---|---|---|---|---|---|---|---|
| 2G | 2.19 | 55.34 | 13.68 | 0.323 | 6.01 | 0.142 | 12.26 | 8.29 | 0.02 | 3.61 | 0.024 | 99.70 |
| 2G1 | 2.48 | 54.07 | 15.99 | 0.817 | 9.31 | 0.174 | 7.68 | 6.16 | 0.02 | 5.18 | 0.056 | 99.46 |
| 2F | 7.95 | 47.80 | 14.21 | 1.830 | 8.53 | 0.166 | 15.12 | 5.61 | 1.13 | 4.05 | 0.264 | 98.71 |
| 5B | 4.46 | 50.64 | 18.95 | 1.068 | 9.04 | 0.161 | 6.83 | 7.43 | 0.01 | 4.64 | 0.079 | 98.85 |
| 8A1 | 2.54 | 53.83 | 14.73 | 1.868 | 8.03 | 0.135 | 9.04 | 5.43 | 0.60 | 4.90 | 0.305 | 98.87 |
| 8C | 3.39 | 49.89 | 15.75 | 1.169 | 11.64 | 0.198 | 7.51 | 8.01 | 1.80 | 2.73 | 0.082 | 98.78 |
| 8D1 | 2.47 | 53.48 | 14.81 | 1.506 | 9.37 | 0.191 | 7.12 | 7.58 | 0.64 | 4.75 | 0.165 | 99.61 |
| 14D | 3.54 | 48.28 | 15.19 | 0.504 | 11.00 | 0.181 | 11.85 | 9.84 | 0.04 | 2.52 | 0.018 | 99.42 |
| 17F | 4.51 | 48.40 | 18.94 | 0.758 | 8.14 | 0.160 | 8.43 | 10.24 | 2.74 | 2.02 | 0.057 | 99.88 |
| 23P | 4.22 | 50.14 | 16.86 | 1.823 | 8.55 | 0.148 | 10.48 | 5.30 | 1.07 | 4.47 | 0.291 | 99.13 |
| 23O | 9.51 | 47.12 | 1.68 | 0.056 | 7.30 | 0.165 | 16.59 | 25.13 | 0.00 | 0.08 | 0.024 | 98.14 |
| 24I | 4.10 | 48.73 | 17.40 | 0.295 | 5.13 | 0.175 | 15.74 | 9.01 | 0.26 | 2.23 | 0.020 | 98.99 |
| 28C | 4.31 | 47.61 | 15.31 | 0.182 | 5.22 | 0.121 | 16.95 | 13.11 | 0.24 | 0.94 | 0.014 | 99.70 |
| 28E | 3.51 | 50.60 | 15.08 | 0.546 | 6.36 | 0.122 | 13.97 | 10.39 | 0.03 | 2.16 | 0.036 | 99.29 |
| 27J | 3.48 | 43.69 | 16.63 | 1.509 | 10.53 | 0.208 | 18.56 | 6.94 | 0.24 | 0.88 | 0.130 | 99.32 |
| 32L | 3.31 | 49.70 | 14.69 | 0.863 | 9.59 | 0.169 | 13.01 | 8.94 | 0.02 | 2.21 | 0.063 | 99.26 |
| 41H3 | 2.96 | 52.52 | 17.47 | 0.797 | 9.57 | 0.221 | 8.13 | 5.82 | 0.30 | 4.09 | 0.107 | 99.02 |
| 52A | 2.96 | 51.62 | 14.49 | 1.102 | 8.81 | 0.163 | 11.53 | 7.85 | 0.45 | 3.12 | 0.088 | 99.22 |
| 52EA | 3.66 | 49.01 | 14.93 | 1.354 | 10.29 | 0.552 | 9.31 | 9.59 | 0.16 | 2.97 | 0.108 | 98.27 |
| 52F | 3.11 | 49.57 | 14.15 | 2.011 | 11.22 | 0.182 | 9.56 | 7.80 | 0.98 | 3.06 | 0.221 | 98.75 |
| 57A | 3.45 | 51.87 | 20.91 | 1.172 | 7.13 | 0.110 | 9.52 | 3.48 | 0.22 | 5.20 | 0.226 | 99.84 |
| 57H | 2.53 | 49.25 | 13.52 | 2.483 | 12.16 | 0.257 | 11.61 | 6.38 | 0.07 | 3.04 | 0.246 | 99.02 |
| 61N | 4.75 | 47.56 | 18.35 | 0.262 | 4.33 | 0.107 | 19.25 | 7.89 | 0.04 | 1.35 | 0.025 | 99.16 |
| 68G | 2.92 | 45.61 | 14.33 | 1.534 | 11.06 | 0.204 | 18.56 | 7.16 | 0.19 | 1.03 | 0.122 | 99.80 |
| 24I | — | 48.73 | 17.40 | 0.295 | 5.13 | 0.175 | 15.74 | 9.01 | 0.26 | 2.23 | 0.020 | 98.99 |
| 24I **R** | — | 48.93 | 17.49 | 0.296 | 5.55 | 0.176 | 15.72 | 8.99 | 0.26 | 2.24 | 0.020 | 99.67 |
| 24I **A** | — | 48.83 | 17.44 | 0.30 | 5.34 | 0.18 | 15.73 | 9.00 | 0.26 | 2.24 | 0.02 | 99.33 |

**Normalized results (weight percent)**

| No. | $SiO_2$ | $Al_2O_3$ | $TiO_2$ | FeO | MnO | CaO | MgO | $K_2O$ | $Na_2O$ | $P_2O_5$ |
|---|---|---|---|---|---|---|---|---|---|---|
| 2G | 55.51 | 13.72 | 0.324 | 6.03 | 0.142 | 12.30 | 8.32 | 0.02 | 3.62 | 0.024 |
| 2G1 | 54.37 | 16.08 | 0.821 | 9.36 | 0.175 | 7.72 | 6.19 | 0.02 | 5.21 | 0.056 |
| 2F | 48.42 | 14.40 | 1.854 | 8.64 | 0.168 | 15.32 | 5.68 | 1.14 | 4.10 | 0.267 |
| 5B | 51.23 | 19.17 | 1.080 | 9.15 | 0.163 | 6.91 | 7.52 | 0.01 | 4.69 | 0.080 |
| 8A1 | 54.45 | 14.90 | 1.889 | 8.12 | 0.137 | 9.14 | 5.49 | 0.61 | 4.96 | 0.308 |
| 8C | 50.51 | 15.94 | 1.183 | 11.78 | 0.200 | 7.60 | 8.11 | 1.82 | 2.76 | 0.083 |
| 8D1 | 53.69 | 14.87 | 1.512 | 9.41 | 0.192 | 7.15 | 7.61 | 0.64 | 4.77 | 0.166 |
| 14D | 48.56 | 15.28 | 0.507 | 11.06 | 0.182 | 11.92 | 9.90 | 0.04 | 2.53 | 0.018 |
| 17F | 48.46 | 18.96 | 0.759 | 8.15 | 0.160 | 8.44 | 10.25 | 2.74 | 2.02 | 0.057 |
| 23P | 50.58 | 17.01 | 1.839 | 8.62 | 0.149 | 10.57 | 5.35 | 1.08 | 4.51 | 0.294 |
| 23O | 48.01 | 1.71 | 0.057 | 7.44 | 0.168 | †16.90 | 25.60 | 0.00 | 0.08 | 0.024 |
| 24I | 49.23 | 17.58 | 0.298 | 5.18 | 0.177 | 15.90 | 9.10 | 0.26 | 2.25 | 0.020 |
| 28C | 47.75 | 15.36 | 0.183 | 5.24 | 0.121 | †17.00 | 13.15 | 0.24 | 0.94 | 0.014 |
| 28E | 50.96 | 15.19 | 0.550 | 6.41 | 0.123 | 14.07 | 10.46 | 0.03 | 2.18 | 0.036 |
| 27J | 43.99 | 16.74 | 1.519 | 10.60 | 0.209 | †18.69 | 6.99 | 0.24 | 0.89 | 0.131 |
| 32L | 50.07 | 14.80 | 0.869 | 9.66 | 0.170 | 13.11 | 9.01 | 0.02 | 2.23 | 0.063 |
| 41H3 | 53.04 | 17.64 | 0.805 | 9.66 | 0.223 | 8.21 | 5.88 | 0.30 | 4.13 | 0.108 |
| 52A | 52.02 | 14.60 | 1.111 | 8.88 | 0.164 | 11.62 | 7.91 | 0.45 | 3.14 | 0.089 |
| 52EA | 49.87 | 15.19 | 1.378 | 10.47 | †0.56 | 9.47 | 9.76 | 0.16 | 3.02 | 0.110 |
| 52F | 50.20 | 14.33 | 2.036 | 11.36 | 0.184 | 9.68 | 7.90 | 0.99 | 3.10 | 0.224 |
| 57A | 51.95 | 20.94 | 1.174 | 7.14 | 0.110 | 9.54 | 3.49 | 0.22 | 5.21 | 0.226 |
| 57H | 49.74 | 13.65 | 2.508 | 12.28 | 0.260 | 11.73 | 6.44 | 0.07 | 3.07 | 0.248 |
| 61N | 47.96 | 18.50 | 0.264 | 4.37 | 0.108 | †19.41 | 7.96 | 0.04 | 1.36 | 0.025 |
| 68G | 45.70 | 14.36 | 1.537 | 11.08 | 0.204 | †18.60 | 7.17 | 0.19 | 1.03 | 0.122 |
| 24I | 49.23 | 17.58 | 0.298 | 5.18 | 0.177 | 15.90 | 9.10 | 0.26 | 2.25 | 0.020 |
| 24I **R** | 49.09 | 17.55 | 0.297 | 5.57 | 0.177 | 15.77 | 9.02 | 0.26 | 2.25 | 0.020 |
| 24I **A** | 49.16 | 17.56 | 0.30 | 5.38 | 0.18 | 15.84 | 9.06 | 0.26 | 2.25 | 0.02 |

**Trace Elements (ppm)**

| No. | Ni | Cr | Sc | V | Ba | Rb | Sr | Zr | Y | Nb | Ga | Cu | Zn | Pb | La | Ce | Th |
|---|---|---|---|---|---|---|---|---|---|---|---|---|---|---|---|---|---|
| 2G | 60 | 119 | 43 | 140 | 46 | 1 | 71 | 20 | 15 | 0.3 | 12 | 49 | 33 | 0 | 0 | 13 | 0 |
| 2G1 | 26 | 112 | 35 | 298 | 42 | 1 | 211 | 38 | 15 | 1.4 | 17 | 15 | 55 | 2 | 4 | 7 | 1 |
| 2F | 25 | 103 | 41 | 267 | 78 | 15 | 233 | 140 | 28 | 9.4 | 14 | 67 | 70 | 1 | 16 | 39 | 4 |
| 5B | 192 | 301 | 27 | 199 | 28 | 0 | 123 | 60 | 23 | 1.1 | 15 | 77 | 71 | 0 | 0 | 25 | 1 |
| 8A1 | 28 | 172 | 26 | 209 | 108 | 10 | 188 | 130 | 23 | 18.9 | 16 | 51 | 71 | 2 | 0 | 25 | 1 |
| 8C | 52 | 226 | 39 | 343 | 200 | 16 | 46 | 34 | 24 | 2.0 | 21 | 103 | 74 | 0 | 3 | 10 | 0 |
| 8D1 | 27 | 77 | 28 | 322 | 59 | 11 | 77 | 92 | 33 | 2.8 | 17 | 62 | 80 | 0 | 0 | 34 | 1 |
| 14D | 37 | 108 | 42 | 448 | 49 | 2 | 274 | 21 | 5 | 0.2 | 16 | 103 | 50 | 0 | 1 | 3 | 2 |
| 17F | 184 | 211 | 32 | 184 | 582 | 59 | 43 | 43 | 18 | 0.9 | 16 | 100 | 51 | 1 | 0 | 4 | 0 |
| 23P | 61 | 195 | 27 | 216 | 279 | 15 | 367 | 150 | 27 | 13.9 | 19 | 26 | 70 | 2 | 0 | 36 | 4 |
| 23O | 786 | 2628 | 31 | 61 | 29 | 1 | 67 | 11 | 4 | 0.9 | 1 | 10 | 42 | 0 | 0 | 0 | 1 |
| 24I | 115 | 615 | 47 | 140 | 131 | 6 | 61 | 13 | 8 | 0.0 | 16 | 69 | 30 | 0 | 0 | 0 | 0 |
| 28C | 195 | 728 | 49 | 126 | 48 | 5 | 61 | 12 | 5 | 1.0 | 10 | 5 | 21 | 0 | 13 | 19 | 0 |
| 28E | 93 | 164 | 46 | 189 | 14 | 0 | 83 | 28 | 14 | 0.2 | 13 | 4 | 29 | 0 | 0 | 20 | 0 |
| 27J | 31 | 121 | 53 | 343 | 39 | 3 | 509 | 97 | 32 | 2.5 | 21 | 14 | 68 | 3 | 10 | 9 | 1 |
| 32L | 50 | 259 | 45 | 334 | 21 | 0 | 30 | 29 | 16 | 0.8 | 18 | 48 | 42 | 10 | 0 | 10 | 0 |
| 41H3 | 19 | 84 | 31 | 306 | 131 | 4 | 114 | 55 | 16 | 1.6 | 16 | 56 | 79 | 0 | 0 | 23 | 1 |
| 52A | 71 | 338 | 39 | 261 | 53 | 10 | 94 | 60 | 24 | 1.5 | 16 | 68 | 64 | 1 | 0 | 20 | 1 |
| 52EA | 68 | 326 | 39 | 301 | 141 | 5 | 50 | 68 | 26 | 4.3 | 16 | 123 | 78 | 0 | 0 | 28 | 1 |
| 52F | 44 | 119 | 38 | 308 | 377 | 23 | 77 | 125 | 34 | 10.4 | 16 | 53 | 78 | 0 | 0 | 29 | 5 |
| 57A | 76 | 403 | 28 | 179 | 63 | 5 | 321 | 73 | 33 | 3.5 | 16 | 44 | 68 | 0 | 12 | 15 | 2 |
| 57H | 40 | 139 | 44 | 435 | 7 | 0 | 90 | 145 | 51 | 5.4 | 21 | 56 | 108 | 0 | 0 | 42 | 1 |
| 61N | 128 | 479 | 40 | 121 | 25 | 0 | 135 | 26 | 8 | 0.0 | 25 | 12 | 19 | 0 | 0 | 10 | 0 |
| 68G | 38 | 162 | 46 | 352 | 25 | 0 | 185 | 86 | 30 | 1.4 | 16 | 0 | 73 | 2 | 1 | 16 | 3 |
| 24I | 115 | 615 | 47 | 140 | 131 | 6 | 61 | 13 | 8 | 0.0 | 16 | 69 | 30 | 0 | 0 | 0 | 0 |
| 24I **R** | 113 | 599 | 42 | 147 | 134 | 6 | 65 | 13 | 8 | 0.0 | 16 | 72 | 32 | 1 | 0 | 21 | 0 |
| 24I **A** | 114 | 607 | 44 | 144 | 132 | 6 | 63 | 13 | 8 | 0 | 16 | 70 | 31 | 0 | 0 | 10 | 0 |

**Rare Earth Elements (ppm)**

| No. | La | Ce | Pr | Nd | Sm | Eu | Gd | Tb | Dy | Ho | Er | Tm | Yb | Lu | Ba | Th | Nb | Y | Hf | Ta | U | Pb | Rb | Cs | Sr | Sc |
|---|---|---|---|---|---|---|---|---|---|---|---|---|---|---|---|---|---|---|---|---|---|---|---|---|---|---|
| 2G | 0.92 | 2.52 | 0.47 | 2.81 | 1.34 | 0.57 | 1.95 | 0.39 | 2.76 | 0.58 | 1.58 | 0.23 | 1.38 | 0.21 | 28 | 0.06 | 0.19 | 14.32 | 0.49 | 0.02 | 0.01 | 0.27 | 0.4 | 0.03 | 69 | 54.3 |
| 2G1 | 1.54 | 3.78 | 0.61 | 3.54 | 1.50 | 0.62 | 2.16 | 0.41 | 2.77 | 0.62 | 1.75 | 0.25 | 1.64 | 0.26 | 38 | 0.15 | 0.72 | 15.70 | 0.85 | 0.05 | 0.06 | 2.08 | 0.3 | 0.04 | 222 | 47.2 |
| 2F | 8.66 | 19.94 | 2.70 | 13.10 | 4.07 | 1.48 | 4.73 | 0.84 | 5.12 | 1.05 | 2.76 | 0.39 | 2.42 | 0.36 | 91 | 0.54 | 8.85 | 27.84 | 3.24 | 0.65 | 0.96 | 0.56 | 12.9 | 0.25 | 218 | 44.0 |
| 5B | 1.58 | 4.81 | 0.90 | 5.32 | 2.29 | 0.86 | 3.13 | 0.61 | 4.10 | 0.85 | 2.34 | 0.34 | 2.10 | 0.34 | 38 | 0.08 | 1.21 | 21.89 | 1.64 | 0.09 | 0.11 | 0.22 | 0.2 | 0.04 | 124 | 39.0 |
| 8A1 | 4.03 | 11.23 | 1.82 | 10.12 | 3.90 | 1.35 | 5.39 | 0.98 | 6.68 | 1.41 | 3.92 | 0.58 | 3.58 | 0.55 | 74 | 0.22 | 2.24 | 37.63 | 2.80 | 0.17 | 0.16 | 0.30 | 10.5 | 0.16 | 78 | 42.7 |
| 8C | 1.65 | 4.68 | 0.82 | 4.97 | 2.27 | 0.91 | 3.34 | 0.65 | 4.43 | 0.94 | 2.72 | 0.39 | 2.49 | 0.38 | 189 | 0.14 | 0.72 | 24.98 | 1.18 | 0.06 | 0.06 | 0.17 | 16.1 | 0.30 | 46 | 54.4 |
| 8D1 | 13.59 | 27.49 | 3.55 | 16.27 | 4.78 | 1.63 | 5.15 | 0.85 | 5.05 | 0.98 | 2.46 | 0.34 | 2.08 | 0.31 | 101 | 1.26 | 19.01 | 24.53 | 3.34 | 1.24 | 0.42 | 6.76 | 8.5 | 0.19 | 182 | 31.2 |
| 14D | 0.85 | 1.66 | 0.27 | 1.50 | 0.61 | 0.39 | 0.80 | 0.14 | 0.99 | 0.21 | 0.58 | 0.09 | 0.51 | 0.08 | 55 | 0.04 | 0.10 | 5.23 | 0.15 | 0.01 | 0.02 | 0.35 | 0.8 | 0.04 | 262 | 53.3 |
| 17F | 1.09 | 3.69 | 0.71 | 4.24 | 1.74 | 0.78 | 2.53 | 0.47 | 3.15 | 0.68 | 1.95 | 0.28 | 1.84 | 0.28 | 537 | 0.04 | 0.39 | 18.53 | 1.16 | 0.03 | 0.03 | 1.62 | 60.1 | 1.40 | 44 | 40.6 |
| 23P | 12.24 | 26.44 | 3.52 | 16.34 | 4.95 | 1.73 | 5.43 | 0.93 | 5.70 | 1.14 | 2.97 | 0.41 | 2.52 | 0.38 | 285 | 0.88 | 14.03 | 29.37 | 3.52 | 0.92 | 0.52 | 1.04 | 15.0 | 0.30 | 349 | 29.9 |
| 23O | 0.63 | 1.11 | 0.19 | 0.86 | 0.33 | 0.16 | 0.40 | 0.07 | 0.47 | 0.11 | 0.27 | 0.04 | 0.24 | 0.04 | 12 | 0.06 | 0.17 | 2.89 | 0.09 | 0.01 | 0.19 | 0.23 | 0.4 | 0.09 | 55 | 25.2 |
| 24I | 0.46 | 1.07 | 0.22 | 1.28 | 0.69 | 0.38 | 1.12 | 0.22 | 1.46 | 0.32 | 0.86 | 0.12 | 0.75 | 0.11 | 98 | 0.03 | 0.08 | 8.36 | 0.25 | 0.01 | 0.01 | 0.44 | 4.8 | 0.16 | 60 | 46.4 |
| 28C | 0.36 | 0.77 | 0.18 | 1.04 | 0.53 | 0.27 | 0.81 | 0.16 | 1.06 | 0.22 | 0.58 | 0.08 | 0.51 | 0.07 | 33 | 0.08 | 0.06 | 5.30 | 0.16 | 0.01 | 0.01 | 0.13 | 3.4 | 0.13 | 64 | 52.3 |
| 28E | 1.87 | 4.53 | 0.78 | 4.30 | 1.78 | 0.69 | 2.33 | 0.42 | 2.77 | 0.58 | 1.61 | 0.23 | 1.47 | 0.22 | 7 | 0.22 | 0.67 | 14.12 | 0.82 | 0.05 | 0.06 | 0.37 | 0.6 | 0.02 | 79 | 53.1 |
| 27J | 3.55 | 9.63 | 1.57 | 8.88 | 3.48 | 1.27 | 4.84 | 0.90 | 5.98 | 1.28 | 3.63 | 0.51 | 3.26 | 0.51 | 40 | 0.20 | 2.34 | 33.11 | 2.42 | 0.18 | 0.08 | 2.20 | 4.7 | 0.50 | 518 | 42.9 |
| 32L | 1.71 | 4.39 | 0.71 | 3.89 | 1.57 | 0.79 | 2.17 | 0.41 | 2.84 | 0.62 | 1.70 | 0.24 | 1.54 | 0.23 | 7 | 0.09 | 0.53 | 15.26 | 0.69 | 0.04 | 0.03 | 26.74 | 0.3 | 0.04 | 25 | 51.9 |
| 41H3 | 6.14 | 13.50 | 1.90 | 9.22 | 2.70 | 0.86 | 3.01 | 0.52 | 3.28 | 0.69 | 1.96 | 0.29 | 1.86 | 0.29 | 130 | 0.69 | 0.76 | 17.84 | 1.54 | 0.06 | 0.32 | 0.87 | 5.6 | 0.33 | 115 | 41.5 |
| 52A | 1.94 | 5.89 | 1.06 | 6.07 | 2.52 | 0.98 | 3.67 | 0.68 | 4.61 | 0.98 | 2.76 | 0.40 | 2.45 | 0.38 | 42 | 0.13 | 0.88 | 25.52 | 1.67 | 0.10 | 0.29 | 0.30 | 8.5 | 0.35 | 84 | 44.5 |
| 52EA | 2.93 | 7.59 | 1.19 | 6.41 | 2.52 | 0.70 | 3.61 | 0.67 | 4.51 | 0.95 | 2.63 | 0.37 | 2.34 | 0.36 | 129 | 0.24 | 3.70 | 24.16 | 1.80 | 0.28 | 0.26 | 0.26 | 4.0 | 0.16 | 48 | 47.6 |
| 52F | 7.60 | 18.12 | 2.64 | 13.68 | 4.60 | 1.59 | 5.78 | 1.02 | 6.55 | 1.34 | 3.66 | 0.51 | 3.19 | 0.48 | 356 | 0.61 | 9.19 | 34.00 | 3.55 | 0.64 | 0.22 | 0.34 | 22.7 | 0.95 | 72 | 47.8 |
| 57A | 4.08 | 6.98 | 1.51 | 8.60 | 3.10 | 1.21 | 4.37 | 0.80 | 5.29 | 1.13 | 3.02 | 0.43 | 2.63 | 0.39 | 49 | 0.19 | 2.36 | 32.24 | 1.73 | 0.18 | 0.11 | 0.26 | 3.7 | 0.18 | 311 | 39.8 |
| 57H | 6.07 | 16.75 | 2.73 | 15.18 | 5.75 | 2.12 | 7.99 | 1.45 | 9.69 | 2.09 | 5.74 | 0.84 | 5.23 | 0.80 | 24 | 0.28 | 4.43 | 54.94 | 4.29 | 0.34 | 0.25 | 0.86 | 1.3 | 0.05 | 89 | 52.5 |
| 61N | 1.31 | 2.85 | 0.44 | 2.20 | 0.83 | 0.46 | 1.14 | 0.22 | 1.43 | 0.31 | 0.88 | 0.12 | 0.77 | 0.12 | 9 | 0.15 | 0.35 | 8.30 | 0.51 | 0.04 | 0.04 | 0.14 | 0.6 | 0.03 | 115 | 34.3 |
| 68G | 3.42 | 9.21 | 1.51 | 8.21 | 3.20 | 1.35 | 4.49 | 0.84 | 5.56 | 1.22 | 3.32 | 0.49 | 3.11 | 0.48 | 33 | 0.20 | 2.10 | 31.38 | 2.40 | 0.17 | 0.08 | 0.30 | 2.5 | 0.28 | 210 | 49.2 |
| 14D **R** | 0.86 | 1.64 | 0.27 | 1.50 | 0.61 | 0.37 | 0.83 | 0.15 | 0.99 | 0.21 | 0.58 | 0.09 | 0.53 | 0.08 | 54 | 0.05 | 0.09 | 5.35 | 0.18 | 0.01 | 0.02 | 0.39 | 0.7 | 0.04 | 263 | 55.9 |
| 14D **A** | 0.86 | 1.65 | 0.27 | 1.50 | 0.61 | 0.38 | 0.82 | 0.15 | 0.99 | 0.21 | 0.58 | 0.09 | 0.52 | 0.08 | 55 | 0.05 | 0.10 | 5.29 | 0.17 | 0.01 | 0.02 | 0.37 | 0.8 | 0.04 | 262 | 54.6 |
| 57A **R** | 4.15 | 7.07 | 1.54 | 8.65 | 3.22 | 1.23 | 4.53 | 0.80 | 5.32 | 1.16 | 3.10 | 0.43 | 2.66 | 0.40 | 49 | 0.18 | 2.42 | 32.96 | 1.79 | 0.18 | 0.11 | 0.22 | 4.0 | 0.19 | 327 | 41.2 |
| 57A **A** | 4.11 | 7.02 | 1.53 | 8.63 | 3.16 | 1.22 | 4.45 | 0.80 | 5.30 | 1.14 | 3.06 | 0.43 | 2.64 | 0.40 | 49 | 0.18 | 2.39 | 32.60 | 1.76 | 0.18 | 0.11 | 0.24 | 3.9 | 0.19 | 319 | 40.5 |

# Appendix 5. Tables and figures showing geochemical discrimination diagram results

Geochemical sample analyses provided in Appendix 4. Samples locations are shown on Figure 3. Data are divided into tables showing classification and discrimination diagram results and spidergram results (see captions below). **NA**, not applicable or not available; **MORB**, mid-oceanic ridge basalt. (See p. 75–78 for discrimination diagram and spidergram figures.)

### CLASSIFICATION AND DISCRIMINATION DIAGRAM RESULTS

**Columns A–P:** **A**, sample number; **B**, sample symbol shown on the following figures; **C**, volcanic-equivalent rock type using the rock classification of Le Bas and others (1986); **D** and **E**, rock unit and location (see Plates 1 and 2 and Fig. 3); **F**, relict phenocrysts; **G** and **H**, calc-alkaline (CA) versus tholeiitic (Th) rock classifications using Miyashiro (1974) (FeO/MgO vs. $SiO_2$) and the standard ternary AFM diagram (alkalies [$Na_2O + K_2O$ vs. total iron oxide vs. Mg], respectively); **I**, alkaline (alk) vs. subalkaline (subalk) discrimination plot; **J**, $Al_2O_3$ vs. MgO vs. FeO (total) tectonic environment discrimination diagram of Pearce and others (1977) with MORB, ocean island (OI), continental (CONT), spreading-center island (SCI)(for example, Iceland), and orogenic (island arc and active continental margin) fields (only applicable to basaltic andesites (~51–56% $SiO_2$); **K**, $TiO_2$ vs. MnO x 10 vs. $P_2O_5$ tectonic discrimination diagram of Mullen (1983) with MORB, ocean-island or seamount tholeiite (OIT); ocean-island alkali basalt or seamount alkali basalt (OIA), island-arc calc-alkaline basalt (CAB), and island-arc tholeiite (IAT) fields; **L**, Ti/100 vs. Zr vs. Y x 3 tectonic discrimination diagram of Pearce and Cann (1973) with island-arc tholeiites (IA), calc-alkaline basalts (CA), within-plate basalts (WP), and MORB (OF) fields. Rocks that plot in the B field (diagram not shown) include island-arc tholeiites, calc-alkaline basalts, and MORB (most of our samples) and thus are ambiguous but can be separated by plotting on Ti-Zr-Sr diagram (diagram N); **M**, Ti vs. Cr discrimination diagram of Pearce (1975) as elucidated by Garcia (1978) with volcanic arc affinity (VAB)(includes either CAB or IAT) or tholeiitic ocean-floor basalts (MORB); **N**, Zr vs. Ti/100 vs. Sr/2 tectonic discrimination diagram of Pearce and Cann (1973) with island-arc tholeiite (IAT), calc-alkaline basalt (CAB), and MORB; **O**, Ti vs. Zr tectonic discrimination diagram of Pearce and Cann (1973) with MORB, calc-alkaline basalt, and a combined island-arc tholeiite and MORB field. Note that the samples in the study area fall on the ocean floor basalt (MORB) trend; **P**, interpretation of the tectonic environment of the sample on the basis of the tectonic discrimination results. Columns in **bold** type emphasize the overall tight clustering of the data and agreement with other trace element data (particularly the rare earth elements), indicating a probable MORB to locally oceanic island-arc origin for the meta-igneous rocks of the study area. (See interpretation of the trace element data, including rare earth element data, in tables below.)

| → Figure | | Fig. A1 (this appendix) | Plate 1 | Fig. 3 (text) | | Fig. A2 | | | Fig. A3 | | | Fig. A9 | Fig. A4 | Fig. A10 | |
|---|---|---|---|---|---|---|---|---|---|---|---|---|---|---|---|
| A | B | C | D | E | F | G | H | I | J | K | L | M | N | O | P |
| Sample no. | Symbol | Volcanic-equivalent rock type | Rock unit | Location | Phenocrysts | CA vs. Th | CA vs. Th | Alkaline vs. subalkaline | $Al_2O_3$ vs. MgO vs. FeO* | $TiO_2$ vs. MnO vs. $P_2O_5$ | Zr vs. Ti vs. Y | Ti vs. Cr | Zr vs. Ti vs. Sr | Ti vs. Zr | Interpretation |
| **Greenstones of the Helena–Haystack mélange (unit $Jmv_h$)** | | | | | | | | | | | | | | | |
| 2F | ☆ | pillowed trachy metabasalt | $Jmv_h$ | Sterling Hill | plag, augite | Th | CA | alk | **NA** | OIA | WP | **MORB** | **MORB** | **MORB** | MORB |
| 5B | △ | metabasalt | $Jmv_h$ | Butler Hill | NA | Th/ CA | CA | subalk | **IA/ MORB** | IAT | IA/OF/ CA | **MORB** | **MORB** | **MORB/ IAT** | MORB to IA |
| 8A1 | ■ | metabasaltic trachyandesite | $Jmv_h$ | Blanchard mountain | augite | CA | CA | subalk | **IA/ MORB** | OIA | IA/OF/ CA | **MORB** | **MORB** | **MORB** | MORB to IA |
| 8C | □ | pillowed metabasalt | $Jmv_h$ | Blanchard mountain | hbl, plag | Th | CA/ Th | subalk | **OI/ MORB** | IAT | IA | **MORB** | **NA** | **MORB/ IAT** | MORB to IA |
| 14D | ✣ | metabasalt | $Jmv_h$ | Colony mountain | NA | Th | Th | subalk | **NA** | CAB | WP | **VAB** | **NA** | **MORB/ IAT** | MORB to IA |
| 17F | + | metabasalt | $Jmv_h$ | Butler Hill | NA | Th/ CA | Th/ Ca | alk | **NA** | IAT | IA/OF/ CA | **MORB/ VAB** | **MORB** | **MORB/ IAT** | MORB |
| 52A | ▲ | pillow breccia metabasalt | $Jmv_h$ | Butler Hill | none | CA | Th/ CA | subalk | **MORB** | IAT | IA/OF/ CA | **MORB** | **MORB** | **MORB/ IAT** | MORB |
| 52 EA | ◊ | metabasalt | $Jmv_h$ | Butler Hill | NA | Th/ CA | Th | subalk | **NA** | CAB | IA/OF/ CA | **MORB** | **NA** | **MORB** | MORB |
| 52F | ♦ | metabasalt | $Jmv_h$ | Butler Hill | NA | Th | Th | subalk | **NA** | MORB | IA/OF/ CA | **MORB** | **NA** | **MORB** | MORB |
| 57A | ○ | metabasaltic trachyandesite | $Jmv_h$ | Butler Hill | none | Th | CA | subalk | **IA/SC** | OIA | IA/OF/ CA | **MORB** | **IAT** | **MORB/ IAT** | MORB to IA |
| 57H | ● | metabasalt | $Jmv_h$ | Butler Hill | augite | Th | Th | subalk | **OI** | MORB | IA/OF/ CA | **MORB** | **NA** | **MORB** | MORB |
| 61N | ★ | metabasalt | $Jmv_h$ | Chuckanut Mountain | plag, augite | NA | NA | subalk | **NA** | CAB | IA/OF/ CA | **VAB** | **CAB** | **MORB/ IAT** | IA to MORB |
| 68G | * | metabasalt | $Jmv_h$ | Chuckanut Mountain | NA | NA | Th | subalk | **NA** | IAT | IA/OF/ CA | **MORB** | **MORB** | **MORB** | MORB to IA |

**CLASSIFICATION AND TECTONIC DISCRIMINATION DIAGRAM RESULTS** *(Continued)*

**Columns Q–AA**: **Q**, V vs. Ti/1000 of Shervais (1982) with calc-alkaline arc basalt (CAB) and back-arc basin basalt (BAB) fields; BAB and MORB have similar geochemistry and predominantly cover in the same diagram field and thus are not separable; plot suggests the greenstones are mostly MORB or BAB. **R**, $TiO_2$ vs. Y/Nb of Floyd and Winchester (1975); diagram only allows for the discrimination of alkali basalts, continental tholeiites, and MORB. **S**, Cr vs. Y of Pearce (1982) distinguishes MORB from volcanic-arc basalts (VAB), including island-arc basalts; most of our samples plot in the small overlapping field between MORB and VAB (see" transitional" below); within-plate basalt settings overlap with the basalt field but can be eliminated from consideration using several other tectonic discrimination plots. **T**, Cr vs. Ce/Sr of Pearce (1982) discriminates MORB and VAB; many of the samples plot as MORB with some in the small transitional field between VAB and MORB. **U**, Y/15 vs. La/10 vs. Nb/8 of Cabanis and Lecolle (1989) discriminates island-arc tholeiites (IAT) and calc-alkaline basalts from continental basalts, back-arc basin basalts, normal to enriched MORB (N-MORB and E-MORB, respectively), and intraplate alkali basalts; it is noteworthy that many of the samples plot on the triple point separating the N-MORB, BAB, and IAT fields, suggestive of intermediate geochemistry for many of the greenstones between these tectonic environments and not a simple end-member tectonic environment. **V**, Ti/Y vs. Nb/Y of Pearce (1982) separates volcanic-arc basalts, MORB, and tholeiitic, transitional, and alkaline within-plate basalts; all the greenstone samples plot within the large overlapping field of MORB and VAB, suggestive of the transitional geochemistry (see interpretation below). **W**, Hf/3 vs. Th vs. Ta of Wood (1980) discriminates between calc-alkaline arc basalts, island-arc tholeiites (IAT), N-MORB, E-MORB, and within-plate tholeiites (WPT); E-MORB and WPT overlap (WPT tectonic environment can be eliminated using other plots). **X**, 2 x Nb vs. Zr/4 vs. Y of Meschede (1986) tectonic discrimination diagram fields separate within-plate alkali and basalts, within-plate tholeiitic basalts/volcanic-arc basalts (WPT), E-type MORB, N-type MORB/volcanic-arc basalts (VAB); all but one of the greenstones cluster in the N-MORB/VAB field. **Y**, Zr/Y vs. Zr of Pearce and Norry (1979) diagram discriminates between basalts of ocean-island arc (VAB), continental volcanic arc, MORB, and within-plate (WPB) settings; many of the greenstones plot in the overlapping field between MORB and island-arc basalts, indicative of the "transitional" geochemistry of the metabasalts. **Z**, yes, indicates a negative Ta-Nb depletion anomaly (Fig. A6), a common attribute of volcanic-arc rocks (S. Babcock, WWU, written commun., 1998); little to no correlation is observed between the tectonic discrimination diagrams that utilize Nb or Ta (columns U, V, and W), the existence of the negative anomaly, and a diagram indication of an arc environment (VAB or IAT). **AA**, high $Al_2O_3$ content suggestive of a non-MORB tectonic environment (S. Babcock, written commun., 1998); **Interpretation**, our interpretation of the original tectonic environment on the basis of this and the previous table; "transition", tectonic discrimination diagrams plot in a transitional field between MORB and island-arc tholeiite settings (many of the samples plot in the overlap area, on the line between these environments, or as MORB on many diagrams but as volcanic arcs on others); this is indicative of a more complex oceanic crust origin such as a back-arc basin setting or a rifted arc. **Bold columns**, discrimination plots that allow discrimination of mid-oceanic ridge basalts (MORB) and island-arc tholeiites (IAT). (See geochemistry discussion.)

| A | C | Q | R | S | T | U | V | W | X | Y | Z | AA | |
|---|---|---|---|---|---|---|---|---|---|---|---|---|---|
| Sample no. | Volcanic-equivalent rock type | V vs. Ti/1000 | $TiO_2$ vs. Y/Nb | Cr vs. Y | Cr vs. Ce/Sr | Y/15 vs. La/10 vs. Nb/8 | Ti/Y vs. Nb/Y | Hf/3 vs. Th vs. Ta | 2 x Nb vs. Zr/4 vs. Y | Zr/Y vs. Zr | Ta/Nb depletion | $Al_2O_3$ high | Interpre-ation |
| **Greenstones of the Helena–Haystack mélange (unit $Jmv_h$)** | | | | | | | | | | | | | |
| 2F | pillowed trachy metabasalt | **MORB/ BAB** | MORB | **MORB/ VAB** | **MORB** | **E-MORB** | MORB/ VAB | **E-MORB/ WPT** | WPT/ VAB | **MORB/ WPB** | **no** | **no** | MORB |
| 5B | metabasalt | **MORB/ BAB** | MORB | **MORB/ VAB** | **MORB/ VAB** | **N-MORB** | MORB/ VAB | **N-MORB** | N-MORB/ VAB | **MORB/ VAB** | **no** | **yes** | MORB or BAB to IAT (transitional) |
| 8A1 | metabasaltic trachyandesite | **MORB/ BAB** | MORB | **MORB** | **MORB** | **N-MORB/ BAB/IAT** | MORB/ VAB | **N-MORB** | N-MORB/ VAB | **MORB** | **yes** | **no** | MORB or BAB |
| 8C | pillowed metabasalt | **MORB/ BAB** | MORB | **MORB** | **MORB** | **N-MORB/ IAT** | MORB/ VAB | **N-MORB/ IAT** | N-MORB/ VAB | **NA/VAB?** | **yes** | **no** | MORB to IAT (transitional) |
| 14D | metabasalt | **NA/ IAT?** | MORB | **NA/ VAB?** | **NA/ VAB?** | **IAT** | MORB/ VAB | **IAT** | N-MORB/ VAB | **NA/VAB?** | **yes** | **no** | MORB to IAT (transitional) |
| 17F | metabasalt | **MORB/ BAB** | MORB | **MORB/ VAB** | **MORB** | **IAT/ N-MORB** | MORB/ VAB | **N-MORB** | N-MORB/ VAB | **MORB/ VAB** | **yes** | **yes** | MORB to IAT (transitional) |
| 52A | pillow breccia metabasalt | **MORB/ BAB** | MORB | **MORB/ VAB** | **MORB** | **IAT/ N-MORB** | MORB/ VAB | **N-MORB** | N-MORB/ VAB | **MORB/ VAB** | **no** | **no** | MORB to IAT (transitional) |
| 52 Ea | metabasalt | **MORB/ BAB/ CAB** | MORB | **MORB/ VAB** | **MORB** | **N-MORB** | MORB/ VAB | **E-MORB/ WPT** | N-MORB/ VAB | **MORB/ VAB** | **no** | **no** | MORB to IAT (transitional) |
| 52F | metabasalt | **MORB/ BAB** | MORB | **MORB** | **MORB** | **E-MORB** | MORB/ VAB | **E-MORB/ WPT** | N-MORB/ VAB | **MORB** | **no** | **no** | MORB |
| 57A | metabasaltic trachyandesite | **MORB/ BAB** | MORB | **MORB** | **VAB** | **N-MORB/ BAB/IAT** | MORB/ VAB | **N-MORB** | N-MORB/ VAB | **MORB/ VAB** | **no** | **yes** | MORB or BAB to IAT (transitional) |
| 57H | metabasalt | **MORB/ BAB** | MORB | **MORB** | **MORB** | **E-MORB/ BAB** | MORB/ VAB | **N-MORB** | N-MORB/ VAB | **MORB** | **no** | **no** | MORB to BAB (some transitional) |
| 61N | metabasalt | **IAT** | MORB | **VAB** | **VAB** | **IAT** | MORB/ VAB | **IAT** | N-MORB/ VAB | **VAB** | **yes** | **yes** | IAT to MORB (some transitional) |
| 68G | metabasalt | **MORB/ BAB** | MORB | **MORB/ VAB** | **MORB/ VAB** | **E-MORB/ BAB** | MORB/ VAB | **N-MORB** | N-MORB/ VAB | **MORB/ VAB** | **no** | **no** | MORB or BAB to IAT (transitional) |

**CLASSIFICATION AND DISCRIMINATION DIAGRAM RESULTS** *(Continued)*

**Columns A–P:** **A**, sample number; **B**, sample symbol shown on the following figures; **C**, volcanic-equivalent rock type using the rock classification of Le Bas and others (1986); **D** and **E**, rock unit and location (see Plates 1 and 2 and Fig. 3); **F**, relict phenocrysts; **G** and **H**, calc-alkaline (CA) versus tholeiitic (Th) rock classifications using Miyashiro, 1974 (FeO/MgO vs. $SiO_2$) and the standard ternary AFM diagram (alkalies [$Na_2O + K_2O$ vs. total iron oxide vs. Mg], respectively); **I**, alkaline (alk) vs. subalkaline (subalk) discrimination plot; **J**, $Al_2O_3$ vs. MgO vs. FeO (total) tectonic environment discrimination diagram of Pearce and others (1977) with MORB, ocean island (OI), continental (CONT), spreading-center island (SCI)(for example, Iceland), and orogenic (OR; island arc and active continental margin) fields (only applicable to basaltic andesites (~51–56% $SiO_2$)); **K**, $TiO_2$ vs. MnO x 10 vs. $P_2O_5$ tectonic discrimination diagram of Mullen (1983) with MORB, ocean-island or seamount tholeiite (OIT); ocean-island alkali basalt or seamount alkali basalt (OIA), island-arc calc-alkaline basalt (CAB), and island-arc tholeiite (IAT) fields; **L**, Ti/100 vs. Zr vs. Y x 3 tectonic discrimination diagram of Pearce and Cann (1973) with island-arc tholeiites (IA), calc-alkaline basalts (CA), within-plate basalts (WP), and MORB (OF) fields. Rocks that plot in the B field (diagram not shown) include island-arc tholeiites, calc-alkaline basalts, and MORB (most of our samples) and thus are ambiguous but can be separated by plotting on Ti-Zr-Sr diagram (diagram N); **M**, Ti vs. Cr discrimination diagram of Pearce (1975) as elucidated by Garcia (1978) with volcanic arc affinity (VAB)(includes either CAB or IAT) or tholeiitic ocean-floor basalts (MORB); **N**, Zr vs. Ti/100 vs. Sr/2 tectonic discrimination diagram of Pearce and Cann (1973) with island-arc tholeiite (IAT), calc-alkaline basalt (CAB), and MORB; **O**, Ti vs. Zr tectonic discrimination diagram of Pearce and Cann (1973) with MORB, calc-alkaline basalt, and a combined island-arc tholeiite and MORB field. Note that the samples in the study area fall on the ocean floor basalt (MORB) trend; **P**, interpretation of the tectonic environment of the sample on the basis of the tectonic discrimination results. **Bold columns** emphasize the overall tight clustering of the data and agreement with other trace element data (particularly the rare earth elements) indicating a probable MORB to locally oceanic island-arc origin for the meta-igneous rocks of the study area. (See interpretation of the trace element data, including rare earth element data, in tables below.)

| → Figure | | Fig. B1 (this appendix) | Plate 1 | Fig. 3 (text) | | Fig. B2 | | | Fig. B3 | | | Fig. B9 | Fig. B4 | Fig. B10 | |
|---|---|---|---|---|---|---|---|---|---|---|---|---|---|---|---|
| **A** | **B** | **C** | **D** | **E** | **F** | **G** | **H** | **I** | **J** | **K** | **L** | **M** | **N** | **O** | **P** |
| **Sample no.** | **Symbol** | **Volcanic-equivalent rock type** | **Rock unit** | **Location** | **Phenocrysts** | **CA vs. Th** | **CA vs. Th** | **Alkaline vs. subalkaline** | **$Al_2O_3$ vs. MgO vs. FeO*** | **$TiO_2$ vs. MnO vs. $P_2O_5$** | **Zr vs. Ti vs. Y** | **Ti vs. Cr** | **Zr vs. Ti vs. Sr** | **Ti vs. Zr** | **Interpre-tation** |
| **Metagabbros and ultramafites (units $Jigb_h$ and $Ju_h$) of the Helena–Haystack mélange, metatuffaceous greenschists of the Easton suite (Jphj), and Shuksan Greenschist of the Easton suite included as imbricates in the Helena–Haystack mélange (unit $Jmv_h$)** | | | | | | | | | | | | | | | |
| 2G | ● | metabasaltic andesite | $Jigb_h$ meta-gabbro | Colony Mountain | hbl, plag | CA | CA | subalk | **OR/ MORB** | CAB | NA | **VAB** | **IAT** | **MORB/ IAT** | IA to MORB |
| 2G1 | ○ | metabasaltic andesite | $Jigb_h$ mylonitic meta-gabbro | Colony Mountain | hbl, plag | CA | CA | subalk | **MORB/ IA/ CONT** | IAT | IA/OF/ CA | **VAB** | **IAT** | **MORB/ IAT** | IA to MORB |
| 8D1 | ◊ | metabasaltic trachyandesite | Jph(s) green-schist | Windy Point | none | CA | CA | subalk | **MORB** | MORB | IA/OF/ CA | **VAB** | **MORB** | **MORB** | MORB to IA |
| 23O | ■ | metabasalt | **$Ju_h$ olivine pyrox-enite** | Oyster Creek | augite | NA | NA | subalk | **NA** | CAB | CA | **VAB** | **CAB** | **MORB/ IAT** | *ultra-mafite* |
| 23P | ♦ | metatrachy basalt | $Jigb_h$/ $Jmv_h$ | Oyster Creek | plag | Th | CA | alk | **NA** | OIA | IA/OF/ CA | **MORB** | **MORB** | **MORB** | MORB |
| 24I | ☆ | metabasalt | $Jigb_h$ meta-gabbro | Chuckanut Mountain | plag, augite | CA | CA | subalk | **NA** | CAB | IA | **NA** | **IAT** | **MORB/ IAT** | IA |
| 28C | + | metabasalt | $Jigb_h$ meta-gabbro | Pigeon Point | augite, plag | NA | NA | subalk | **NA** | CAB | IA/OF/ CA | **NA** | **IAT** | **MORB/ IAT** | IA to MORB |
| 28E | ✱ | metabasalt | $Jigb_h$ meta-gabbro | Pigeon Point | augite, plag | CA | Th/ CA | subalk | **MORB** | IAT | IA/OF/ CA | **VAB** | **MORB** | **MORB/ IAT** | MORB to IA |
| 32L | ▲ | metabasalt | $Jmv_h$ green-schist | Anderson Mountain | plag | CA/ Th | Th | subalk | **MORB** | IAT | IA | **MORB** | **NA** | **MORB/ IAT** | MORB to IA |
| 41 H3 | △ | metabasaltic andesite | $Jmv_h$ | Anderson Mountain | hbl, plag, qtz(?) | CA/ Th | CA | subalk | **IAT** | IAT | IA/OF/ CA | **VAB** | **MORB** | **MORB/ IAT** | MORB to IA |
| 27J | □ | metapicrobasalt | $Jmv_h$ tremolite schist | Chuckanut Mountain | none | NA | Th | subalk | **NA** | MORB/ IAT | IA/OF/ CA | **MORB** | **IAT** | **MORB** | MORB to IA |

**SPIDERGRAM RESULTS**

MORB, mid-oceanic ridge basalt; E-MORB, enriched MORB; N-MORB, normal MORB; x, multiple of Y-axis normalized value (for example, 2x equals twice the y-axis normalized value). **Columns A–F: A**, sample number; **B**, sample symbol shown on the following figures; **C**, volcanic-equivalent rock type using the rock classification of Le Bas and others (1986); **D** and **E**, rock unit and location (see Plates 1 and 2 and Fig. 3); **F**, relict phenocrysts. Columns **G–J** provide the maximum and minimum normalization values obtained from the spidergrams; flat, relatively flat spidergram pattern; >LREE, light rare earth element enriched; <LREE, light rare earth element depleted; MREE, middle rare earth elements; elements in parentheses indicate an anomaly. For example, (-Nb) indicates a negative niobium anomaly. We have divided some of the MORB normalized analyses into two columns to separate the effect of element mobility. **G**, rock/chondrite spidergram using chondrite values of Nakumara (1974); **H**, rock/chondrite spidergram using the chondrite rare earth element values of Sun and McDonough (1989); **I**, rock/N-MORB spidergram using the N-MORB trace element data of Sun and McDonough (1989); **J**, E-MORB trace element data of Sun and McDonough (1989); **K**, rock/MORB spidergram using trace element data of Nystrom and others (1993), **L**, rock/MORB spidergram using the MORB trace element data of Pearce (1983); **M**, final interpretation comparing the tectonic discrimination diagram results (above)(particularly columns J, M, N, O, Q, S, T, U, W, and Y) and spidergram results (below). Both island-arc tholeiites and MORB have primitive LREE-depleted rock/chondrite patterns, and thus columns M and O above aid in differentiating these basalts (Garcia, 1978). *Italicized row,* greenschists of the Easton Metamorphic Suite; note the relatively distinct patterns of the greenschist with LREE and other attributes not generally shared with the Helena–Haystack greenstones. (See Discussion.)

| → Figure | | Fig. A1 (this appendix) | Plate 1 | Fig. 3 (text) | None | Fig. A5 | None | None | | Fig. A7 (this appendix) | | None | Fig. A6 (this appendix) | | |
|---|---|---|---|---|---|---|---|---|---|---|---|---|---|---|---|
| A | B | C | D | E | F | G | H | I | | J | | K | L | | M |
| Sample no. | Symbol | Volcanic-equivalent rock type | Rock unit | Location | Phenocrysts | Rock/ chondrite | Rock/ chondrite | Rock/ N-MORB (Lu to La) | Rock/ N-MORB (K to Cs) | Rock/ E-MORB (Lu to La) | Rock/ E-MORB (K to Cs) | Rock/ MORB | Rock/MORB (Yb to Th and Sr) | Rock/MORB (Ba, Rb, K) | Interpre-tation |
| **Greenstones of the Helena–Haystack mélange (unit $Jmv_h$)** | | | | | | | | | | | | | | | |
| 2F | ☆ | pillowed trachy-metabasalt | $Jmv_h$ | Sterling Hill | plag, augite | 18-25x; flat | 15-28x; flat | 0.8-2x | 8-30x | 0.2-0.4x | 1-5x | 0.4-2x | 1-8x | 4-8x | MORB |
| 5B | △ | metabasalt | $Jmv_h$ | Butler Hill | NA | 11-7x; <LREE | 8-18x; <LREE | 0.6-1x | .05-8 | 0.2-1x | <0.1-0.8x | 0.7-9x | 0.3-1x | 0.01-2x | MORB |
| 8A1 | ■ | metabasaltic trachyandesite | $Jmv_h$ | Blanchard Mountain | augite | 12-18x; >MREE | 18-25; <LREE | 1-2x | 1-23x | 0.4-2x | 0.3-3x | 0.8-6x | 0.7-1x (-Nb) | 3-5x | MORB |
| 8C | □ | pillowed metabasalt | $Jmv_h$ | Blanchard Mountain | hbl, plag | 12-7x; <LREE | 17-19x; <LREE | 0.5-1x | 0.2-30x (-Nb) | 0.2-1x | 0.3-8x | 0.2-10x (+K) | 0.2-0.9x (-Nb) | 8-10x | MORB |
| 14D | ✠ | metabasalt | $Jmv_h$ | Colony Mountain | NA | 2-3x; flat (+Eu) | 2-6x; flat (+Eu) | 0.02-0.04x | 0-9x (-Nb) | 0.1-0.5x | <0.1-0.7x (-Nb) | 0.3-2x (-Nb) | 0.1-0.3x (-Nb) | 0.2-2x | MORB to IA |
| 17F | + | metabasalt | $Jmv_h$ | Butler Hill | NA | 4-9x; <LREE | 3-8x; <LREE | 0.4-0.6x | 0.5-100x (+K) (-Nb) | 0.2-2x (+Pb) | 0.1-20x (-Nb) | 0.1-30x (+K, Rb, Ba) (-Nb) | 0.1-0.7x (-Nb) | 18-30x | MORB to IA |
| 52A | ▲ | pillow breccia metabasalt | $Jmv_h$ | Butler Hill | none | 15-8x; <LREE | 8-18x; <LREE | 1-2x | 0.3-30x (-Nb) | 0.3-1x | 0.1-7x (-Nb) | 0.2-4x | 0.3-0.8x (-Nb) | 2-4x | MORB |
| 52 EA | ◊ | metabasalt | $Jmv_h$ | Butler Hill | NA | 15-8x; <LREE (-Eu) | 12-20x; <LREE | 0.9-1x | 1.5-20x | 0.2-1x | 0.2-0.6x | 0.4-8x | 0.8-1x | 1-8x | MORB |
| 52F | ♦ | metabasalt | $Jmv_h$ | Butler Hill | NA | 15-20x; <LREE | 20-30x; >LREE | 1-3x | 5-200x | 0.14-1x | 1-15x | 0.7-20x (+Ba) | 1-2x | 2-4x | MORB |
| 57A | ○ | metabasaltic trachyandesite | $Jmv_h$ | Butler Hill | none | 8-15x; <LREE | 11-18x; <LREE | 0.8-3x | 1-20x | 0.3-2x | 0.3-3x | 0.7-3x (-Nb) | 0.8-1x | ~2x | MORB |
| 57H | ● | metabasalt | $Jmv_h$ | Butler Hill | augite | 18-30x | 28-30x; <LREE | ~2x | 1-7x | 1-2x | 1.5-0.3x | 0.4-2x | 1-2x | 0.4-1x | MORB |
| 61N | ★ | metabasalt | $Jmv_h$ | Chuckanut Mountain | plag, augite | 3-4x (+Eu) | 4-8x (+Eu) | 0.2-1x | 0.15-4x (-Nb) | 0.15-6x | 0.1-0.5x (-Nb) | 0.1-2x | 0.1-0.8x (-Nb) | 0.3-0.4x | MORB to IA |
| 68G | ✱ | metabasalt | $Jmv_h$ | Chuckanut Mountain | NA | 10-18x; <LREE | 15-22; <LREE | ~1x | 2.5-13x | 0.5-1x | 0.2-5x | 0.7-2x | 0.8-1x (-Nb) | 1-2x | MORB |

**SPIDERGRAM RESULTS** *(Continued)*

| → Figure | | Fig. B1 (this appendix) | Plate 1 | Fig. 3 (text) | None | Fig. B5 | None | None | | Fig. B7 | | None | Fig. B6 | | |
|---|---|---|---|---|---|---|---|---|---|---|---|---|---|---|---|
| A | B | C | D | E | F | G | H | I | | J | | K | L | | M |
| Sample no. | Symbol | Volcanic-equivalent rock type | Rock unit | Location | Phenocrysts | Rock/ chondrite | Rock/ chondrite | Rock/ N-MORB (Lu to La) | Rock/ N-MORB (K to Cs) | Rock/ E-MORB (Lu to La) | Rock/ E-MORB (K to Cs) | Rock/ MORB | Rock/MORB (Yb to Th and Sr) | Rock/MORB (Ba, Rb, K) | Interpre-tation |
| **Metagabbros and ultramafites (units $Jigb_h$ and $Ju_h$) of the Helena–Haystack mélange, metatuffaceous greenschists of the Easton suite (Jphj), and Shuksan Greenschist of the Easton suite included as imbricates in the Helena–Haystack mélange (unit $Jmv_h$)** | | | | | | | | | | | | | | | |
| 2G | ● | metabasaltic andesite | $Jigb_h$ meta-gabbro | Colony Mountain | hbl, plag | 3-8x; <LREE | 4-10x; <LREE | 0.2-0.7x; flat | 0.1-4x (-Nb) | 0.2-0.7x; flat | <0.1-0.4x (-Nb) | 0.04-2x; flat (-Nb) | <0.11-0.5x (-Nb) | 0.15-1.5x | MORB to IA |
| 2G1 | ○ | metabasaltic andesite | $Jigb_h$ mylon-itic meta-gabbro | Colony Mountain | hbl, plag | 3-8x; <LREE | 7-10x; <LREE | 0.6-0.9x | 0.3-7x (-Nb) | 0.2-2x; flat | 0.3-2x (-Nb) | 2-4x (-Nb) | 0.2-0.8x (-Nb) | 0.15-2x | MORB to IA |
| *8D1* | ◇ | *metabasaltic trachyandesite (tuffaceous)* | *Jph(s) green-schist* | *Windy Point* | *none* | *18-40x; >LREE* | *12-60x; >LREE* | *0.6-20x; flat (+Pb)* | *8-28x* | *0.9-10x (+Pb)* | *2-3x* | *0.3-4x* | *0.6-8x* | *4-5x* | *Calc-alk-aline IA metatuff-aceous rocks* |
| 23O | ■ | metabasalt | $Ju_h$ olivine pyrox-enite | Oyster Creek | augite | 1-2x; flat | 2-3x; flat (+Eu) | 0.1-0.2x | 0.1-13 (-Nb) | <0.1-0.4x; flat | <0.1-1.5x (-Nb) | 0.04-10x (-Nb) | 0.1-0.3x (-Nb) | 0.2-0.5x | Ultra-mafite cumulate (?) |
| 23P | ♦ | metatrachy-basalt | $Jigb_h$/ $Jmv_h$ | Oyster Creek | plag | 10-4x; >LREE | 15-50x; >LREE | 0.8-7x | 6-43x | 1-2x; flat | 0.15-5x | 0.8-12x; flat | 0.7-6x | 3-15x | Calc-alk-aline to tholeiitic IA to MORB |
| 24I | ☆ | metabasalt | $Jigb_h$ meta-gabbro | Chuckanut Mountain | plag, augite | 1-5x; (+Eu) | 2-5x; <LREE (+Eu) | 0.1-0.4x | <0.1-24x (-Nb) | <0.1-0.7x | <0.1-3x (-Nb) | 0.02-4x (-Nb) | <0.1-0.3x (-Nb) | 0.4-5x | MORB to IA |
| 28C | + | metabasalt | $Jigb_h$ meta-gabbro | Pigeon Point | augite, plag | 1-3x; <LREE (+Eu) | 1-4x; <LREE | 0.1-0.6x | <0.1-18 (-Nb) | <0.1-0.4x | <0.1-2x (-Nb) | 0.02-3x (-Nb) | <0.1-0.2x (-Nb) | 0.5-2x | MORB to IA |
| 28E | ✱ | metabasalt | $Jigb_h$ meta-gabbro | Pigeon Point | augite, plag | 6-9x; <LREE (+Eu) | 8-10x; <LREE | 0.3-1; flat | 0.3-3x | 0.3-0.8x | <0.1-0.3x (-Nb) | 0.2-0.7x; flat | 0.2-0.5x (+Nb) | 0.2-0.7x | MORB to IA |
| *32L* | ▲ | *metabasalt* | *$Jmv_h$ green-schist* | *Anderson Mountain* | *plag* | *6-8x; <LREE (+Eu)* | *7-12x; <LREE (+Eu)* | *0.3-100x; flat* | *0.2-7x (-Nb)* | *0.2-50x (+Pb)* | *<0.1-0.7x (-Nb)* | *0.2-1x; flat* | *0.2-0.6x (-Nb)* | *0.15-3x* | *MORB to IA* |
| *41 H3* | △ | *metabasaltic andesite (tuffaceous)* | *$Jmv_h$ green-schist* | *Anderson Mountain* | *hbl, plag, qtz(?)* | *8-20x; <LREE* | *12-28x; <LREE* | *0.5-3x* | *0.3-40x (-Nb)* | *0.8-1x (-Nb) (+Pb)* | *1-6x* | *0.2-6x (-Nb)* | *0.2-1.5x (-Nb)* | *1-8x* | *Calc-alk-aline to tholeiitic IA to MORB* |
| 27J | □ | metapicrobasalt | $Jmv_h$ tremo-lite schist | Chuckanut Mountain | none | 10-20x; <LREE | 16-28x; flat to <LREE | 0.9-7x | 1-70x | 0.8-3x (+Pb) | 0.3-8x (-Nb) | 0.6-2x; flat | 0.8-1x (-Nb) | 2-5x | MORB |

**Metabasalts**

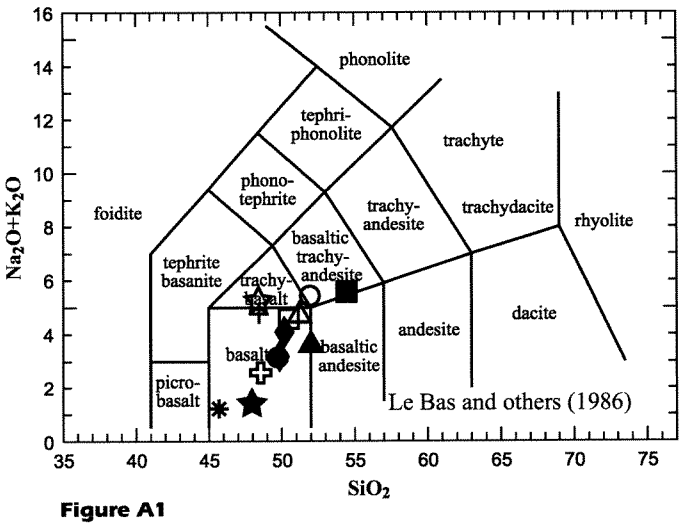


**Figure A1**

**Metagabbros, greenschists, ultramafites**

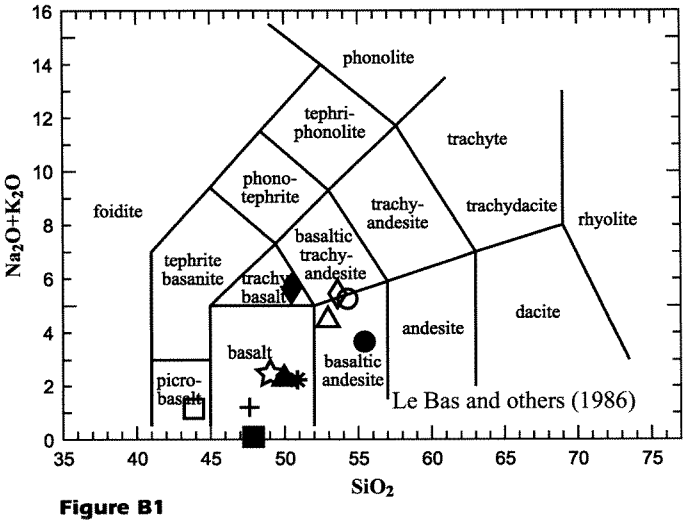


**Figure B1**

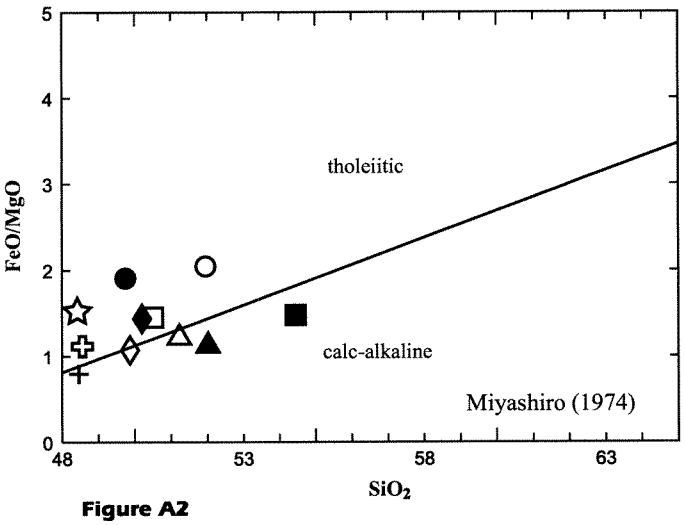


**Figure A2**

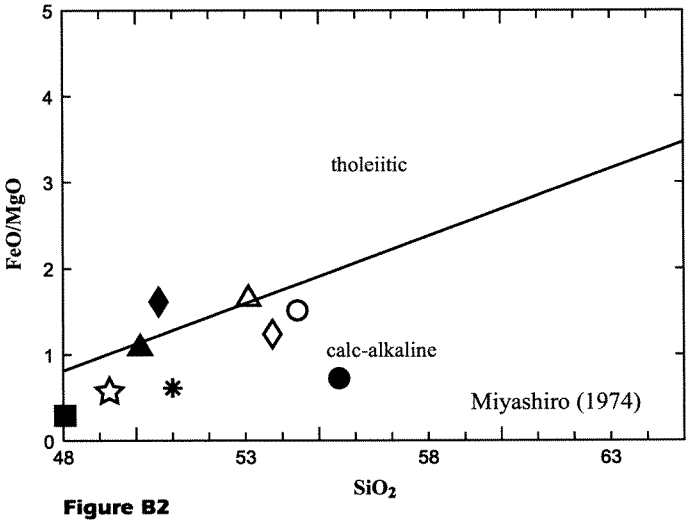


**Figure B2**

EXPLANATION

| "A" figures Sample no. | Symbol | "B" figures Sample no. | Symbol |
|---|---|---|---|
| 5B | △ | 41H3 | △ |
| 52A | ▲ | 32L | ▲ |
| 8C | □ | 27J | □ |
| 8A1 | ■ | 23O | ■ |
| 52EA | ◇ | 8D1 | ◇ |
| 52F | ◆ | 23P | ◆ |
| 57A | ○ | 2G1 | ○ |
| 57H | ● | 2G | ● |
| 17F | + | 28C | + |
| 68G | ✱ | 28E | ✱ |
| 2F | ☆ | 24I | ☆ |
| 61N | ★ | | |
| 14D | ✙ | | |

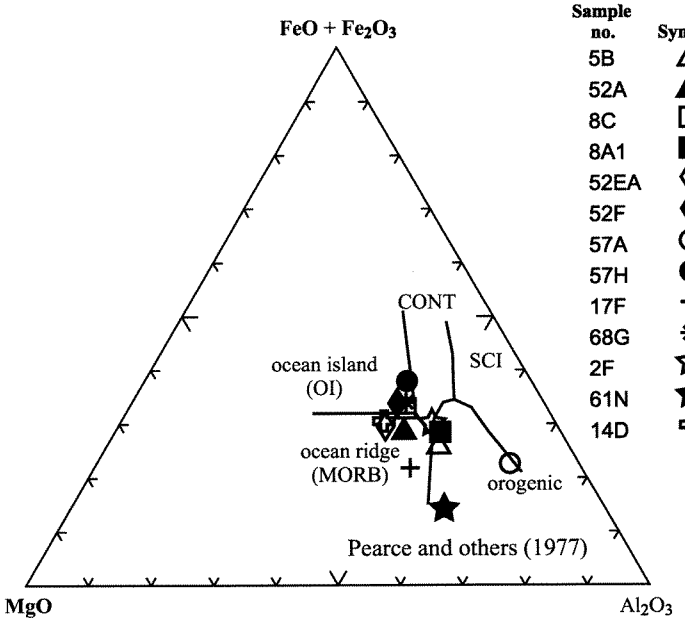


**Figure A3**

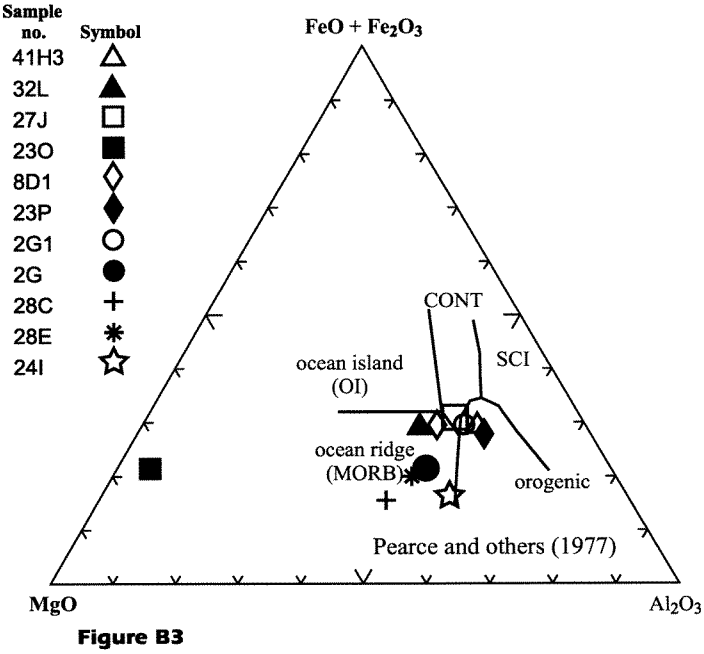


**Figure B3**

## Metabasalts

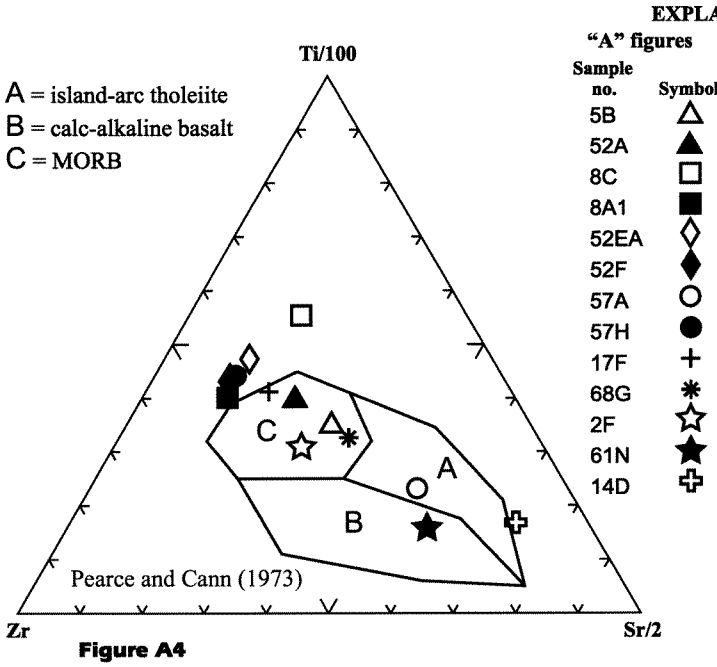


Figure A4

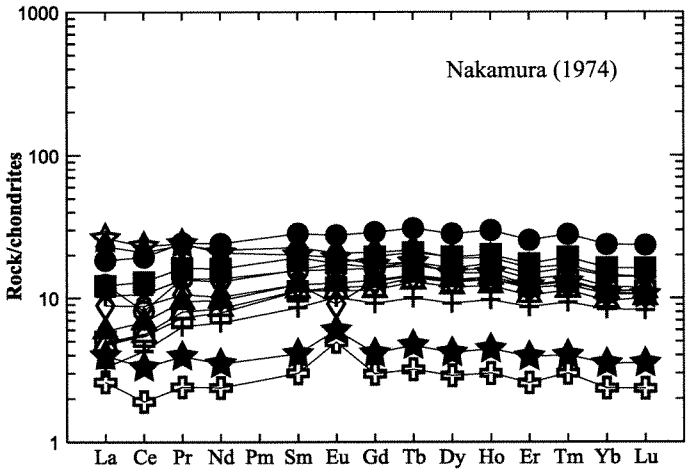


Figure A5

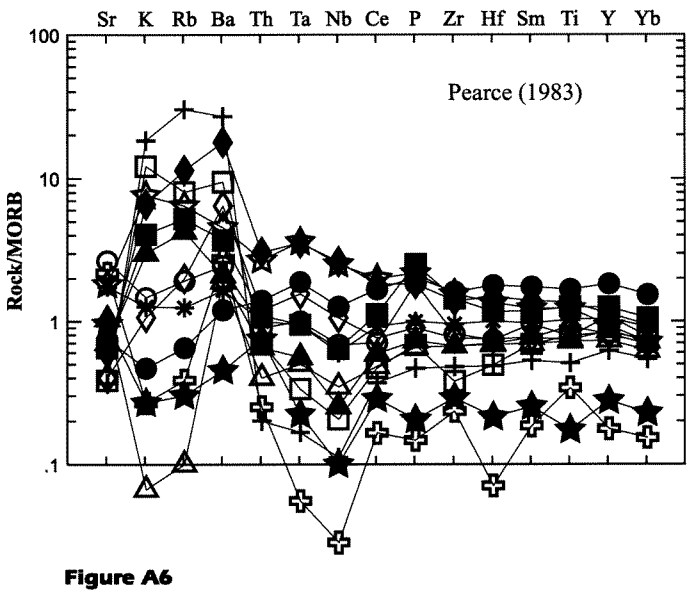


Figure A6

## Metagabbros, greenschists, ultramafites

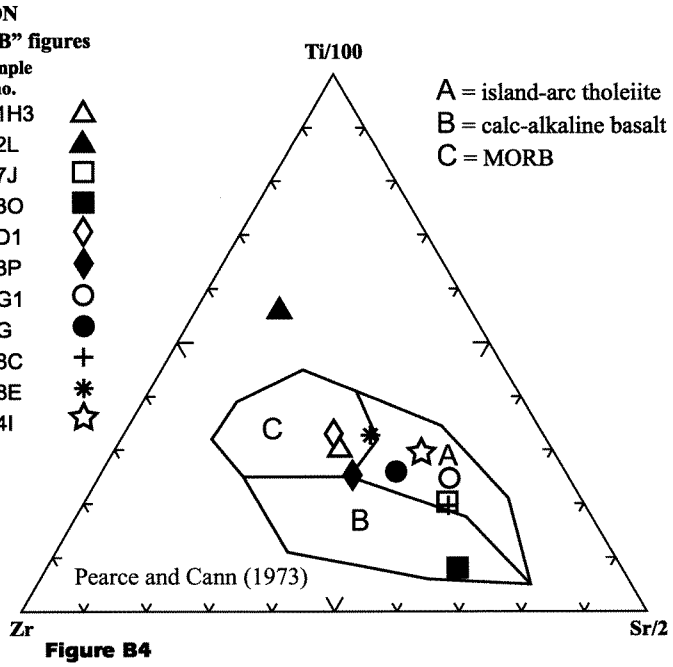


Figure B4

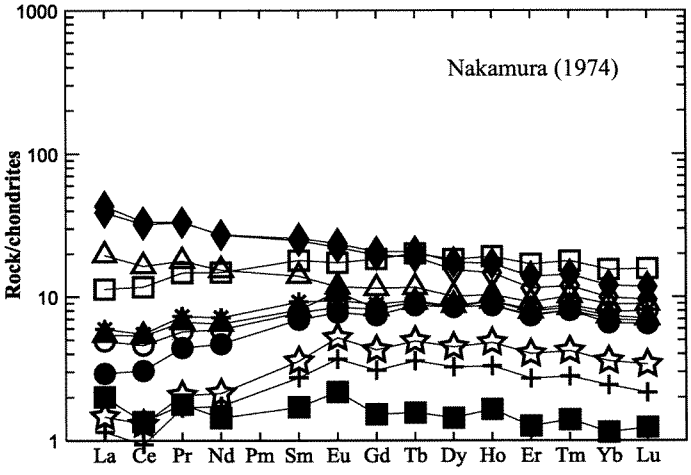


Figure B5

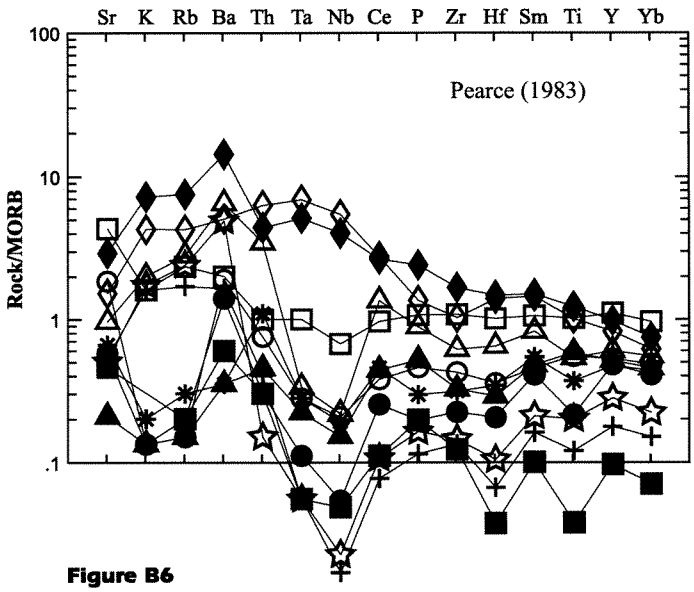


Figure B6

**Metabasalts**

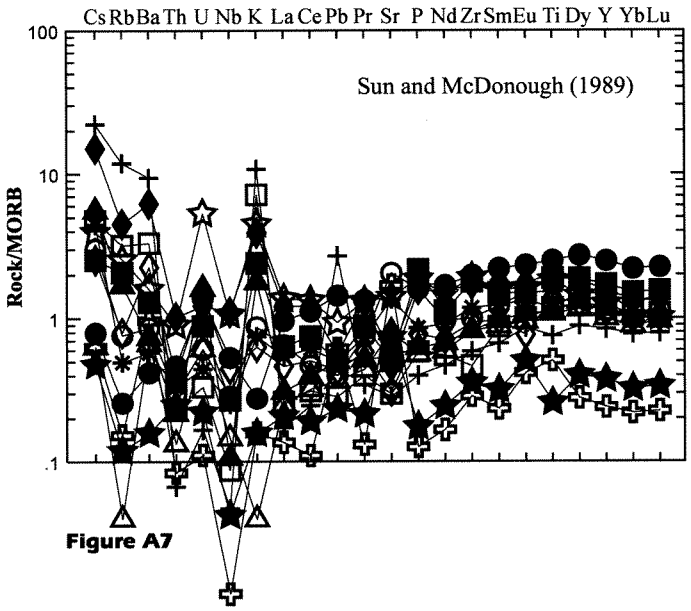


Figure A7

**Metagabbros, greenschists, ultramafites**

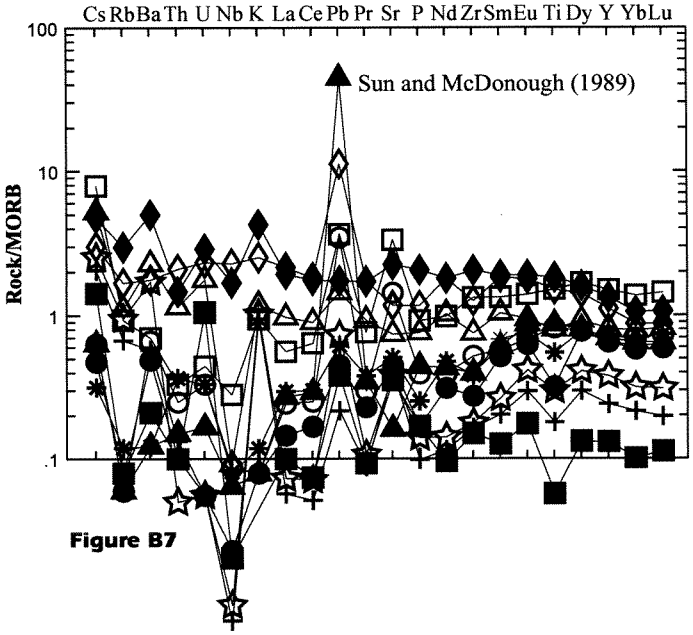


Figure B7

*See spidergram results tables for sample ranges for Figures A7, B7, A8, and B8.*

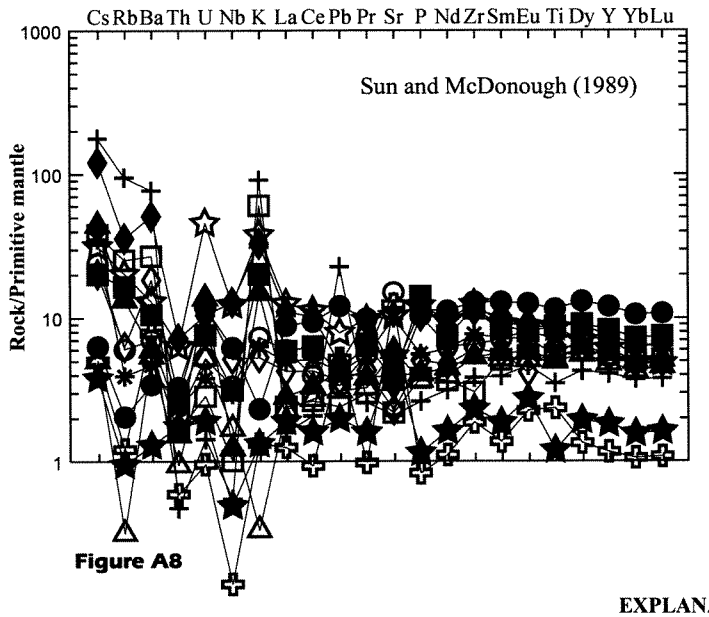


Figure A8

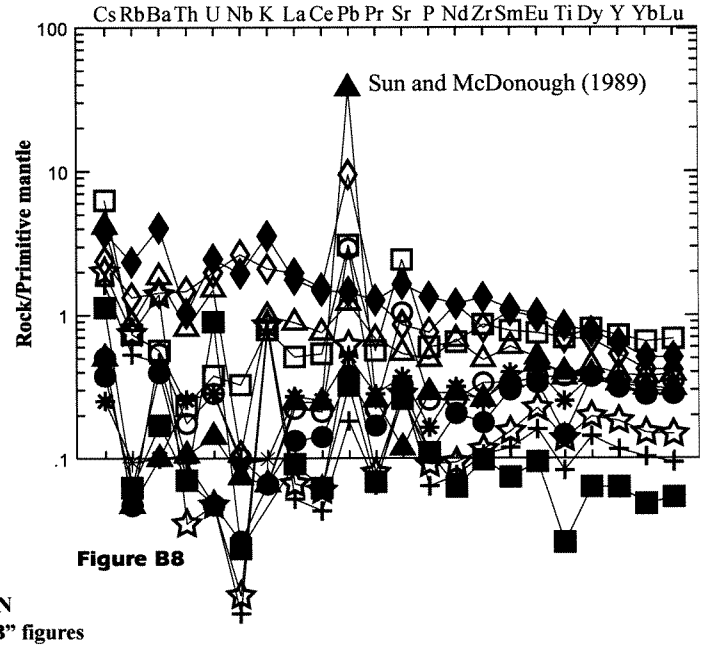


Figure B8

**EXPLANATION**

| "A" figures | | "B" figures | |
|---|---|---|---|
| Sample no. | Symbol | Sample no. | |
| 5B | △ | 41H3 | △ |
| 52A | ▲ | 32L | ▲ |
| 8C | □ | 27J | □ |
| 8A1 | ■ | 23O | ■ |
| 52EA | ◇ | 8D1 | ◇ |
| 52F | ◆ | 23P | ◆ |
| 57A | ○ | 2G1 | ○ |
| 57H | ● | 2G | ● |
| 17F | + | 28C | + |
| 68G | * | 28E | * |
| 2F | ☆ | 24I | ☆ |
| 61N | ★ | | |
| 14D | ✚ | | |

**Metabasalts**

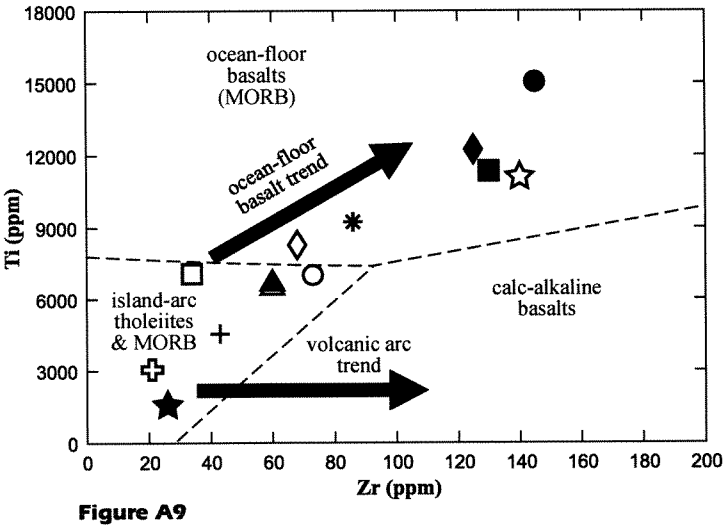


**Figure A9**

**Metagabbros, greenschists, ultramafites**

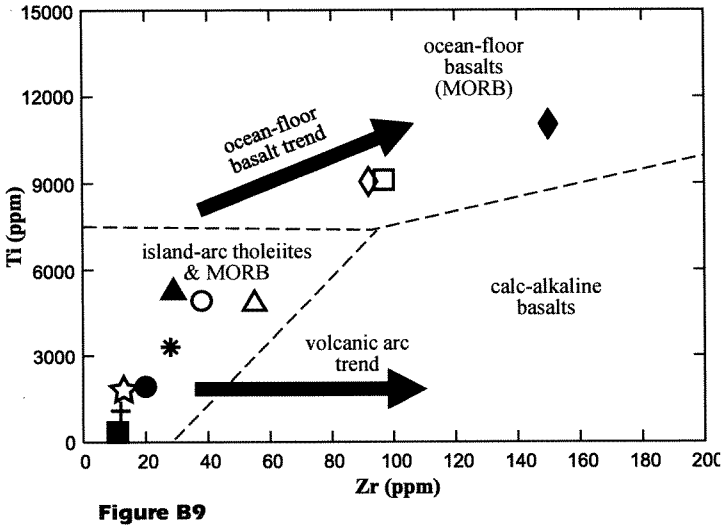


**Figure B9**

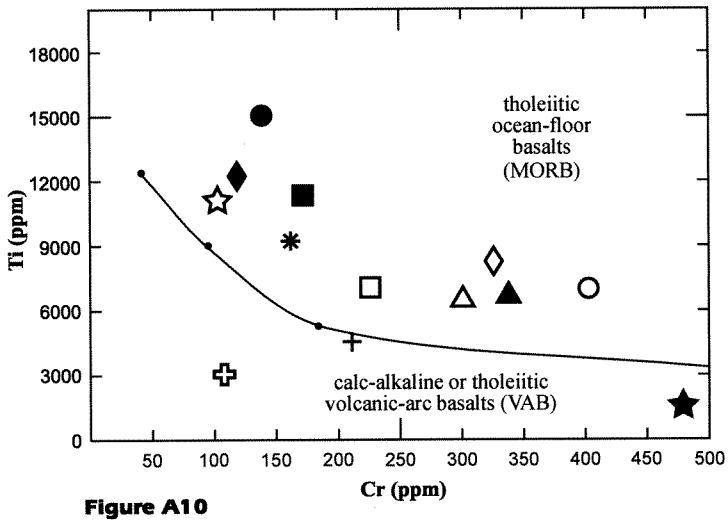


**Figure A10**

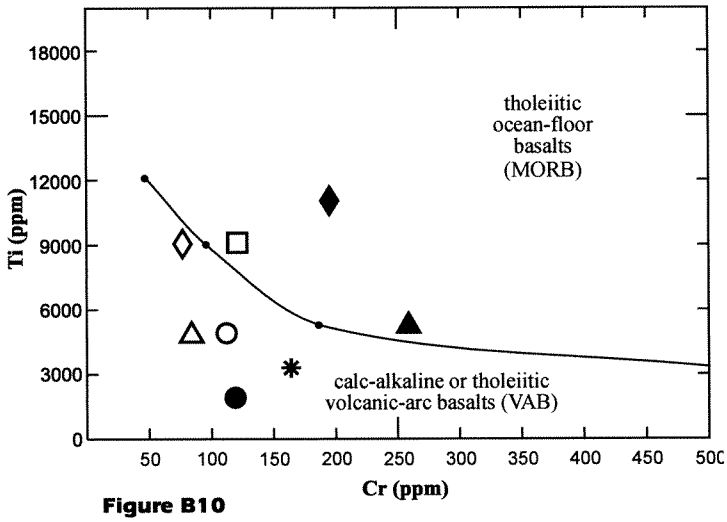


**Figure B10**

**EXPLANATION**

| "A" figures | | "B" figures | |
|---|---|---|---|
| Sample no. | Symbol | Sample no. | |
| 5B | △ | 41H3 | △ |
| 52A | ▲ | 32L | ▲ |
| 8C | □ | 27J | □ |
| 8A1 | ■ | 23O | ■ |
| 52EA | ◇ | 8D1 | ◇ |
| 52F | ◆ | 23P | ◆ |
| 57A | ○ | 2G1 | ○ |
| 57H | ● | 2G | ● |
| 17F | + | 28C | + |
| 68G | ✱ | 28E | ✱ |
| 2F | ☆ | 24I | ☆ |
| 61N | ★ | | |
| 14D | ✚ | | |

# Appendix 6. U-Pb zircon ages, this study

by Samuel A. Bowring and Kathaleen Davidek
Massachusetts Institute of Technology

## U-PB ZIRCON ISOTOPIC DATA AND APPARENT AGE (SINGLE GRAIN ANALYSES)

**Sample locations on Figure 3**

### 97-51H

| 97-51H fractions | Weight (mg) | U (ppm) | Pb (ppm) | $^{206}Pb^*/^{204}Pb$ | $^{208}Pb/^{206}Pb$ | $^{206}Pb/^{238}U$ | % err | $^{207}Pb/^{235}U$ | % err | $^{207}Pb/^{206}Pb$ | % err. | $^{206}Pb/^{238}U$ | $^{207}Pb/^{235}U$ | $^{207}Pb/^{206}Pb$ | corr. coef. | Pb (pg) | Blank (pg) |
|---|---|---|---|---|---|---|---|---|---|---|---|---|---|---|---|---|---|
| z3 | 0.0040 | 106.31 | 4.81 | 897.73 | 0.227 | 0.04101 | ( .26) | 0.30324 | ( .67) | 0.05363 | ( .59) | 259.1 | 268.9 | 355.4 | 0.486 | 1.3 | 1.3 |
| z2 | 0.0091 | 58.03 | 1.60 | 686.84 | 0.128 | 0.02697 | ( .29) | 0.21472 | ( .48) | 0.05775 | ( .36) | 171.5 | 197.5 | 520.2 | 0.670 | 1.4 | 1.4 |
| z1 | 0.0054 | 535.96 | 21.23 | 314.53 | 0.510 | 0.02621 | ( .35) | 0.18148 | ( .44) | 0.05021 | ( .25) | 166.8 | 169.3 | 204.8 | 0.823 | 16.3 | 3.7 |
| z9 | 0.0049 | 64.52 | 1.84 | 147.29 | 0.235 | 0.02574 | (1.50) | 0.17485 | (1.84) | 0.04926 | ( .99) | 163.9 | 163.6 | 160.2 | 0.842 | 4.1 | 4.1 |
| z11 | 0.0029 | 141.41 | 4.00 | 714.06 | 0.232 | 0.02565 | ( .29) | 0.17425 | ( .90) | 0.04927 | ( .81) | 163.3 | 163.1 | 160.6 | 0.466 | 1.0 | 1.0 |
| z13 | 0.0020 | 72.30 | 1.93 | 302.22 | 0.167 | 0.02555 | ( .70) | 0.17160 | (1.44) | 0.04872 | (1.19) | 162.6 | 160.8 | 134.5 | 0.563 | 0.8 | 0.8 |
| z12 | 0.0019 | 92.44 | 2.47 | 391.24 | 0.178 | 0.02533 | ( .53) | 0.17102 | ( .93) | 0.04897 | ( .73) | 161.3 | 160.3 | 146.3 | 0.629 | 0.8 | 0.8 |
| z14 | 0.0027 | 144.71 | 3.90 | 554.55 | 0.230 | 0.02449 | ( .38) | 0.16635 | ( .60) | 0.04927 | ( .45) | 155.9 | 156.2 | 160.8 | 0.667 | 1.1 | 1.1 |

| | $^{207}Pb/^{206}Pb$ | $^{206}Pb/^{238}U$ | $^{207}Pb/^{235}U$ |
|---|---|---|---|
| Weighted mean ages | 152.6 Ma ±33.0 Ma | 163.2 Ma ±0.4 Ma | 162.5 Ma ±3.5 Ma |
| % error (2-sigma) | 21.6% | 0.3% | 2.1% |
| Probability of fit = | 26% | 48% | 19% |
| based on an MSWD of | 1.35 | 0.73 | 1.66 |

### 97-32L

| 97-32L fractions | Weight (mg) | U (ppm) | Pb (ppm) | $^{206}Pb^*/^{204}Pb$ | $^{208}Pb/^{206}Pb$ | $^{206}Pb/^{238}U$ | % err. | $^{207}Pb/^{235}U$ | % err | $^{207}Pb/^{206}Pb$ | % err. | $^{206}Pb/^{238}U$ | $^{207}Pb/^{235}U$ | $^{207}Pb/^{206}Pb$ | corr. coef. | Pb (pg) | Blank (pg) |
|---|---|---|---|---|---|---|---|---|---|---|---|---|---|---|---|---|---|
| z2 | 0.0100 | 229.29 | 6.76 | 1437.64 | 0.281 | 0.02574 | (.15) | 0.17540 | (.22) | 0.04942 | (.16) | 163.8 | 164.1 | 168.0 | 0.689 | 2.7 | 2.7 |
| z5 | 0.0100 | 164.65 | 4.95 | 1410.73 | 0.308 | 0.02573 | (.15) | 0.17524 | (.22) | 0.04940 | (.16) | 163.7 | 164.0 | 167.0 | 0.703 | 2.0 | 2.0 |
| z4 | 0.0100 | 172.21 | 5.15 | 747.66 | 0.300 | 0.02574 | (.27) | 0.17512 | (.35) | 0.04935 | (.21) | 163.8 | 163.9 | 164.3 | 0.795 | 3.9 | 3.9 |

| | $^{207}Pb/^{206}Pb$ | $^{206}Pb/^{238}U$ | $^{207}Pb/^{235}U$ |
|---|---|---|---|
| Weighted mean ages | 166.8 Ma ±2.3 Ma | 163.8 Ma ±0.2 Ma | 164.0 Ma ±0.2 Ma |
| % error (2-sigma) | 1.4% | 0.1% | 0.1% |
| Probability of fit = | 48% | 88% | 74% |
| based on an MSWD of | 0.74 | 0.13 | 0.30 |

## SAMPLE DESCRIPTIONS

**See Appendix 5 for the geochemistry of these samples.**

### Helena–Haystack mélange metagabbroic greenstone (unit Jmv$_h$) (Sample 97-51H)

Rock quarry sample location. Light greenish gray, metagabbroic greenstone at the base of the Helena–Haystack mélange; occurs as a tens of meters thick body of homogeneous medium-grained, hypidiomorphic granular greenstone on Colony mountain east; locally protomylonitic to mylonitic near the underlying thrust contact with the Easton Metamorphic Suite; thrust-fault contact with the Easton suite locally defined by talc schist and serpentinite north of the quarry. Consists of 2 to 8 percent quartz, 20 to 40 percent plagioclase, 5 to 35 percent actinolite, 0 to 30 percent chlorite; 0 to 15 percent relict augite, 0 to 16 percent epidote, 0 to 15 percent pumpellyite, 0 to 6 percent titanite (sphene), and 0 to 1 percent opaque. Poorly to moderately recrystallized greenstone. Correlated with the Helena–Haystack mélange on the basis of the degree of recrystallization, inhomogeneous nature of the metamorphic fabric, association with ultramafite and metabasalts of mostly MORB geochemistry. Geochemistry of the body has both oceanic and island-arc intrusive geochemical signature (samples 2G and 2G1 from same rock quarry.)

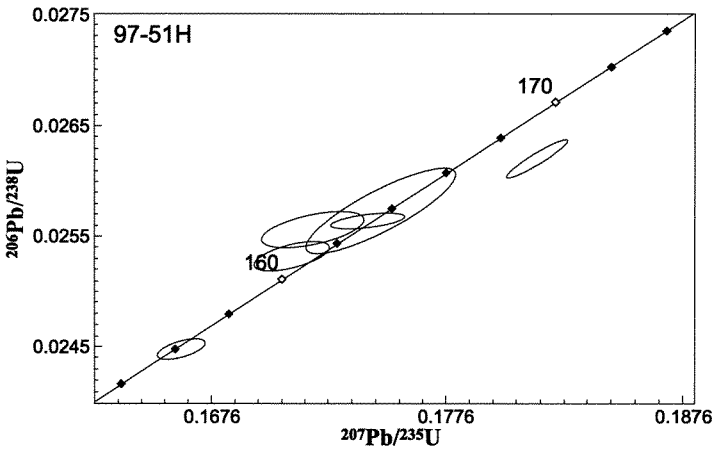

### Helena–Haystack mélange greenschist imbricate (unit Jmv$_h$) (Sample 97-32L)

Rock quarry sample location. Light olive-gray greenschist included as a thrust imbricate at the base of the Helena–Haystack mélange; occurs as a tens of meters thick body of homogeneous fine-grained greenschist on Anderson Mountain with pods of medium-grained greenschist. Consists of 15 percent quartz, 28 percent plagioclase; 30 percent Fe-chlorite; 4 percent stilpnomelane, 6 percent actinolite, 17 percent epidote, and minor probable pumpellyite. Well-recrystallized with a strong foliation and stretching lineation. Texturally granoblastic polygonal with localized zones of sutured quartz and plagioclase matrix. Serpentinite occurs at the base of the unit in at least two locations and is interpreted to be a klippe of metabasalt at the base of the Helena–Haystack mélange. Tentatively correlated with the Shuksan Greenschist on the basis of the degree of recrystallization relative to the metabasaltic greenstones of the Helena–Haystack mélange. Secondary correlation is with the metabasaltic greenstones of the Helena–Haystack mélange elsewhere in the study area.